

3D Analysis of Combined Extrusion-Forging Processes

**A THESIS SUBMITTED IN FULFILLMENT OF
THE REQUIREMENT FOR THE AWARD OF THE DEGREE**

OF

DOCTOR OF PHILOSOPHY

IN

MECHANICAL ENGINEERING

BY

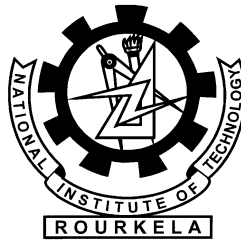
LAXMI NARAYAN PATRA

(ROLL NO. 508ME607)



**NATIONAL INSTITUTE OF TECHNOLOGY
ROURKELA - 769008, INDIA**

April - 2012



CERTIFICATE

This to certify that the thesis entitled “**3D Analysis of Combined Extrusion-Forging Processes** ” being submitted by **Laxmi Narayan Patra** for the award of the degree of Doctor of Philosophy (Mechanical Engineering) of NIT Rourkela, is a record of bonafide research work carried out by him under our supervision and guidance. Mr. Laxmi Narayan Patra has worked for more than three years seven months on the above problem at the Department of Mechanical Engineering, National Institute of Technology, Rourkela and this has reached the standard fulfilling the requirements and the regulation relating to the degree. The contents of this thesis, in full or part, have not been submitted to any other university or institution for the award of any degree or diploma.

Dr. Susanta Kumar Sahoo
Professor
Department of Mechanical
Engineering
NIT, Rourkela

Place: Rourkela
Date:

Dr. K. P. Maity
Professor & HOD
Department of Mechanical
Engineering
NIT, Rourkela

Place: Rourkela
Date:

ACKNOWLEDGEMENT

This thesis is a result of research that has been carried out at **National Institute of Technology, Rourkela**. During this period, I came across with a great number of people whose contributions in various ways helped my field of research and they deserve special thanks. It is a pleasure to convey my gratitude to all of them.

In the first place, I would like to express my deep sense of gratitude and indebtedness to my supervisors **Prof. S.K. Sahoo** and **Prof. K. P. Maity** for their advice, and guidance from early stage of this research and providing me extraordinary experiences throughout the work. Above all, they provided me unflinching encouragement and support in various ways which exceptionally inspire and enrich my growth as a student, a researcher.

I specially acknowledge **Prof. S.K. Sahoo** for his advice, supervision, and crucial contribution, as and when required during this research. His involvement with originality has triggered and nourished my intellectual maturity that will help me for a long time to come. I am proud to record that I had opportunity to work with an exceptionally experienced scientist like him.

I am grateful to Director, **Prof. S.K. Sarangi**, **Prof. R.K. Sahoo**, ex-Head of Mechanical Engineering Department, and **Prof. B.K. Nanda**, former Head of Mechanical Engineering Department, National Institute of Technology, Rourkela, for their kind support and concern regarding my academic requirements.

I express my thankfulness to the faculty and staff members of the Mechanical Engineering Department for their continuous encouragement and suggestions.

I am indebted to **Mr. Balaji Kumar Choudhury** for his support and co-operation which is difficult to express in words. The time spent with him will remain in my memory for years to come.

I thanks to Mr/s **Advanced Forming Technology Center (Regd.)** for their valuable cooperation during FEM analysis providing DEFORM[®]-3D software.

Thanks are also due to my co-scholars at **National Institute of Technology, Rourkela**, for their whole hearted support and cooperation during the duration of this work.

My parents deserve special mention for their inseparable support and prayers. They are the persons who show me the joy of intellectual pursuit ever since I was a child. I thank them for sincerely bringing up me with care and love.

The completion of this work came at the expense of my long hours of absence from home. Words fail me to express my appreciation to my wife **Sandhya Rani** and my son **Chandra Sekhar** for their understanding, patience and active cooperation throughout the course of my doctoral dissertation. I thank them for being supportive and caring.

Last, but not the least, I thank the one above all of us, the omnipresent **God**, for giving me the strength during the course of this research work.

Laxmi Narayan Patra

ABSTRACT

Combined extrusion-forging processes are now getting importance for its abilities to give improved material properties, high production rate and less material waste when compared with that produced by machining, casting or by assembling the individual parts produced by different manufacturing processes. In its simplest form of combined extrusion-forging process, a billet is forged by punch and dies with punch/die or both containing an opening for extrusion. This tooling arrangement permits the simultaneous lateral spread due to forging, and backward/forward extrusion or both forward and backward extrusion simultaneously through the die/punch opening(s). The flow pattern of the material is dependent on a number of factors, including the frictional conditions at the work piece/tooling interface; the geometry of the dies, particularly the size of the dies hole; the material type; and the percentage area reductions. Due to the complexity of the analysis, and because of the large number of process variables, it is difficult to estimate the forming force required to manufacture a given component. In this direction, the present work emphasizes on estimation of forming force for forward and forward-backward extrusion-forging process of regular shapes and different tooth spur gear shapes.

Though technological barriers exist, as in most manufacturing areas, it is important to overcome them by developing proper understanding of the process with related attributes. In this direction, present work emphasis on the forward and forward-backward extrusion-forging process analysis of different methodology applied to different section heads with circular shaft. Based on these guiding principles, the methodology applied are upper bound analysis (particularly reformulated spatial elemental rigid region (SERR) technique), finite element analysis (commercial package DEFORM[®]-3D codes), and experimentation.

The understandings generated in this work not only properly explain the complex material flow mechanism but also presents in detail the upper bound analysis. The results of UBA are well validated with that of finite element analysis and experimental results. The achievements realized from the present work can be summarized as follows:

- Experimental studies are carried out with a view to compare some of the theoretical results predicated using the upper bound method in general, modified

SERR technique in particular, with that obtained from the experiment. SERR technique is used to analysis the last stage of the combined extrusion forging process, which requires maximum load.

- A computational model for forward and forward-backward extrusion-forging process with and without considering friction is developed by incorporating all special features for all the section extrusions. Three formulations for forward extrusion-forging process and six formulations for forward-backward extrusion-forging processes are analyzed and the optimal solution for non-dimensional extrusion pressure is found out for further computation. The model is developed using FORTRAN code.
- Experiments are performed for triangle, square, pentagon, hexagon, 4-tooth, 6-tooth, 8-tooth and 12-tooth spur gear (involute profile and pressure angle $14\frac{1}{2}^\circ$) is form using flat / square dies. Both forward and forward-backward extrusion-forging processes are carried out.
- FEM based commercial package DEFORM[®]-3D code is used for finite element analysis of the processes.
- The results obtained from experimental investigation are found to be in good agreement with the similar one predicted by theoretical analysis using the proposed modified SERR technique and finite element analysis.

Keywords: Extrusion, Forging, Upper Bound Analysis, Spatial Elemental Rigid Region (SERR), Finite element,

Table of Contents

DOCTOR OF PHILOSOPHY	a
ACKNOWLEDGEMENT	i
ABSTRACT	iii
Table of Contents	v
List of Tables	x
List of Figures	xii
NOMENCLATURE	xix
ABBREVIATION	xxii
Introduction	1
1.1 Introduction	1
1.2 Existing Method of Manufacturing	2
1.3 Industry Demand and New Trend	3
1.4 Different Type of Conventional Dies	3
1.5 Extrusion-forging Process	4
1.5.1 Forward extrusion-forging process	4
1.5.2 Forward-backward extrusion-forging process	4
1.6 Research Objective	5
1.7 Thesis Outline	6
1.8 Closure	8
Literature Survey	9
2.1 Introduction	9
2.2 Slip-line Field Method	9
2.3 Slab-Method	11
2.4 Upper-Bound Analysis	14
2.4.1 Extrusion-forging process	20
2.4.2 SERR analysis	21
2.4.3 Gear shape extrusion	25
2.5 FEM Analysis	27
2.6 Closure	30
Upper Bound Techniques for Three Dimensional Metal Deformation	
Problems	32
3.1 Introduction	32
3.2 Mechanics of Metal Forming	34
3.2.1 Slab or Stress equilibrium method	35
3.2.2 Slip-line field theory	35
3.2.3 Limit analysis	35
3.2.3.1 Lower bound theorem	35
3.2.3.2 Upper bound theorem	36

3.3	General Techniques for deriving the Kinematically Admissible Velocity Fields in Three- Dimensional Metal Deformation Problems	36
3.3.1	The dual stream function method	37
3.3.2	The conformal transformation technique.....	37
3.3.3	The generalized velocity field technique	38
3.3.4	The SERR technique.....	39
3.4	Discretization of Deformation Zone in Section Extrusion	40
3.5	The Continuity Condition of a Discontinuous Velocity Field.....	41
3.6	Solution of a Plane Strain Problem.....	44
3.7	Closure.....	47

3D Analysis of Combined Extrusion-Forging Process for Round-Triangle-

Round Sections	48	
4.1	Introduction (Theoretical Analysis).....	48
4.2	SERR Method of Analysis.....	49
4.2.1	Forward extrusion-forging process	49
4.2.1.1	Single point formulation	54
4.2.1.2	Metal flow and satisfaction of continuity condition.....	64
4.2.1.3	Double point formulation	65
4.2.1.4	Triple point formulation	68
4.2.2	Forward-backward extrusion-forging process	71
4.3	Computation	72
4.4	Optimization Parameters	76
4.4.1	Forward extrusion-forging process	76
4.4.2	Forward-backward extrusion-forging process	76
4.5	Summary.....	77
4.5.1	Forward extrusion-forging process	77
4.5.2	Forward-backward extrusion-forging process	79
4.6	Introduction (Finite Element Analysis)	82
4.7	Formulation.....	83
4.7.1	Viscoplastic material formulation.....	83
4.7.2	Heat transfer formulation.....	84
4.7.3	Interface formulation	85
4.8	Pre-Processor	85
4.8.1	Simulation control.....	85
4.8.2	Materials	86
4.8.3	Object description	87
4.8.4	Inter-object relation.....	87
4.8.5	Movement control.....	88
4.8.6	Boundary condition.....	88
4.9	Simulation.....	88
4.10	Post-Processor.....	88
4.11	Summary.....	89
4.11.1	Forward Extrusion-forging process	89
4.11.2	Forward backward Extrusion-forging process.....	91
4.11.2.1	Mean stress and effective strain.....	91
4.12	Introduction (Experimental Analysis)	93
4.13	The Test Rig	94
4.14	Dies	103
4.15	Specimen.....	104

4.16	Experimental Procedure.....	107
4.17	Determination of Stress-strain Characteristics of Lead	110
4.18	Determination of Friction Factor	111
4.19	Summary.....	113
4.19.1	Forward extrusion-forging process	113
4.19.1.1	Die filling and flow pattern	114
4.19.2	Forward-backward extrusion-forging process	116
4.19.2.1	Flow pattern.....	117
4.20	Comparison of Results and Discussion	117
4.20.1	Forward extrusion-forging process	117
4.20.2	Forward-backward extrusion-forging process	119
4.21	Closure.....	120
4.21.1	Forward extrusion-forging process	120
4.21.2	Forward-backward extrusion-forging process	121

3D Analysis of Combined Extrusion-Forging Process for Round-Square-

Round Section.....	122	
5.1	Introduction.....	122
5.2	Theoretical Analysis.....	123
5.2.1	Summary.....	124
5.3	Finite Element Analysis of Forward Extrusion-Forging Process	126
5.4	Finite Element Analysis of Forward-Backward Extrusion-Forging Process.....	128
5.5	Experimental Analysis.....	129
5.5.1	Summary.....	132
5.6	Comparison of result and discussion	136
5.7	Closure.....	140
5.7.1	Forward extrusion-forging process	140
5.7.2	Forward-backward extrusion-forging process	140

3D Analysis of Combined Extrusion-Forging Process for Round-Pentagon-

Round Sections	141	
6.1	Theoretical Analysis	141
6.2	Finite Element Analysis.....	143
6.3	Experimental Analysis.....	146
6.3.1	Summary.....	150
6.3.1.1	Die filling and flow pattern	151
6.3.1.2	Flow pattern.....	154
6.4	Comparison of Results and Discussion	154
6.4.1	Forward extrusion-forging process	154
6.4.2	Forward-Backward Extrusion-Forging Process.....	157
6.5	Closure.....	158
6.5.1	Forward extrusion-forging process	158
6.5.2	Forward-backward extrusion forging process	158

3D Analysis of Combined Extrusion-Forging Process for Round-Hexagon-

Round Sections	160	
7.1	Theoretical Analysis	160
7.1.1	Forward extrusion-forging process	160
7.1.2	Forward backward extrusion-forging process	161
7.1.3	Summary.....	161

7.1.4	Forward-backward extrusion-forging process	162
7.2	Finite Element Analysis.....	163
7.2.1	Summary.....	163
7.2.1.1	Forward extrusion-forging process.....	163
7.2.1.2	Forward backward extrusion-forging process	164
7.3	Experimental Analysis.....	165
7.3.1	Summary.....	168
7.4	Comparison of Results and Discussion	172
7.4.1	Forward extrusion-forging process	172
7.4.2	Forward-backward extrusion-forging process	175
7.5	Closure.....	176
7.5.1	Forward extrusion-forging process	176
7.5.2	Forward-backward extrusion-forging process	176
3D Analysis of Combined Extrusion-Forging Process for Round Gear-Round		
Sections.....		177
8.1	Introduction (Theoretical Analysis).....	177
8.2	SERR Method of Analysis.....	178
8.2.1	Forward extrusion-forging process	178
8.2.2	Forward-backward extrusion-forging process	180
8.3	Computation	181
8.4	Summary.....	181
8.4.1	Forward extrusion-forging process	181
8.4.2	Forward-backward extrusion-forging process	182
8.5	Introduction (Finite Element Analysis)	183
8.6	Summary.....	183
8.6.1	Forward Extrusion-forging process	183
8.6.1.1	Mean stress and effective strain analysis.....	184
8.6.2	Forward backward extrusion-forging process	185
8.6.2.1	Mean stress and effective strain analysis.....	186
8.7	Introduction (Experimental Analysis)	187
8.8	Apparatus.....	187
8.8.1	Dies	187
8.8.2	Billet specification	187
8.9	Experimental Procedure.....	190
8.10	Summary.....	193
8.10.1	Forward extrusion-forging process	193
8.10.1.1	Die filling and flow pattern	195
8.10.2	Forward-backward extrusion-forging process	197
8.11	Comparison of Results and Discussion	200
8.11.1	Forward extrusion-forging process	200
8.11.1.1	Without considering friction.....	200
8.11.1.2	Considering friction.....	201
8.11.2	Forward-backward extrusion-forging	206
8.12	Clouser.....	207
8.12.1	Forward extrusion-forging process	207
8.12.2	Forward-backward extrusion-forging process	207
Executive Summary, Conclusions and Future Recommendations.....		208
9.1	Introduction.....	208

9.2	Summary of Findings	208
9.3	Contribution of the Research Work	209
9.4	Limitation of the Study	210
9.5	Scopes for future work.....	210
	REFERENCES	211
	Bio-data.....	223
	Published and Accepted Papers	224

List of Tables

Table 2.1. Important contribution in the area of SERR applied to square die:	22
Table 3.1 Summary of discontinuity lines and velocity vectors on their sides.....	45
Table 3.2 Summary of velocity discontinuities across the lines	47
Table 4.1 Global level of discretization	57
Table 4.2 Coordinates of points	58
Table 4.3 Equation of plane	59
Table 4.4 Velocity vector on both sides of the faces	60
Table 4.5 Equation of normal component of velocities	61
Table 4.6 Velocity discontinuity at the bonding face	62
Table 4.7 Global level of discretization schemes for double floating point formulation	67
Table 4.8 Global level of discretization schemes for triple floating point formulation	71
Table 4.9 Summary of subzones	77
Table 4.10 Summary of discretization schemes	78
Table 4.11 Summary of subzones	80
Table 4.12 Summary of discretization schemes	80
Table 4.13 Process parameter used in simulation	89
Table 4.14 List of components.....	95
Table 4.15 Computation of non-dimensional average extrusion pressure for forward extrusion-forging process	114
Table 4.16 Computation of non-dimensional average extrusion pressure for forward- backward extrusion-forging process	117
Table 4.17 Variation of non-dimensional extrusion pressure for different formulations without friction for forward extrusion-forging process.....	118
Table 4.18 Variation of non-dimensional extrusion pressure for different formulations for forward-backward extrusion-forging process.....	120
Table 5.1 Process parameter used in simulation	126
Table 5.2 Computation of non-dimensional average extrusion pressure for forward extrusion-forging process	133
Table 5.3 Computation of non-dimensional average extrusion pressure for forward- backward extrusion-forging process	135
Table 5.4 Variations of non-dimensional extrusion pressure for different formulations without friction for forward extrusion-forging process.....	137
Table 5.5 Comparison of non-dimensional average extrusion pressure without friction for forward-backward extrusion-forging process.....	139

Table 6.1 Computation of non-dimensional average extrusion pressure for forward extrusion-forging process	151
Table 6.2 Computation of non-dimensional average extrusion pressure for forward-backward extrusion-forging process	153
Table 6.3 Variation of non-dimensional extrusion pressure without friction for forward extrusion-forging process	155
Table 6.4 Comparison of non-dimensional average extrusion pressure without friction for forward-backward extrusion-forging process.....	158
Table 7.1 Computation of non-dimensional average extrusion pressure for forward extrusion-forging process	169
Table 7.2 Computation of non-dimensional average extrusion pressure for forward-backward extrusion-forging process	172
Table 7.3 Comparison of non-dimensional extrusion pressure without friction for forward extrusion-forging process	173
Table 7.4 Comparison of non-dimensional average extrusion pressure without friction for forward-backward extrusion-forging process.....	175
Table 8.1 Summary of discretization schemes for forward extrusion-forging process	181
Table 8.2 Computation of non-dimensional average extrusion pressure for forward extrusion-forging process of 4, 6, 8, 12-tooth spur gear	196
Table 8.3 Computation of non-dimensional average extrusion pressure for forward-backward extrusion-forging process of 4, 6, 8, 12-tooth spur gear.....	198
Table 8.4 Comparison of non-dimensional extrusion pressure without friction for forward extrusion-forging process of 4, 6, 8, 12-tooth spur gear.....	201
Table 8.5 Comparison of non-dimensional average extrusion pressure for forward-backward extrusion-forging process of 4, 6, 8, 12-tooth spur gear.....	206

List of Figures

Figure 1.1 Maximum tangential stresses of shafts	3
Figure 1.2 Different stages of forward extrusion forging process(Front half section).4	4
Figure 1.3 Different stages for forward-backward extrusion forging process	5
Figure 2.1 Slip-line fields by Prandl [2].....	10
Figure 2.2 Model of slab method used by Siebel [27]	12
Figure 2.3 Velocity field for axi-symmetric extrusion by Kudo [40]	15
Figure 3.1. (a) Johnson’s velocity field (b) Kudo’s velocity field	40
Figure 3.2. Discretization of a pyramid into tetrahedrons.....	40
Figure 3.3 Division of a prism into three tetrahedrons.....	41
Figure 3.4 A general surface separating two rigid regions.....	42
Figure 3.5 Plane strain extrusion problem.....	44
Figure 4.1 Front half section of the process (a) Forward extrusion-forging (b) Forward- backward extrusion-forging process	49
Figure 4.2 Dead metal zones in SERR formulation for extrusion of triangle-round section	51
Figure 4.3 Domain of interest G-B-O ₁ -O-b-6-7-a (one sixth of zone of deformation)	52
Figure 4.4 Extrusion velocity with number of sides of approximating polygon.....	52
Figure 4.5 one-sixth of the deformation zone (single point formulation)	53
Figure 4.6 one-sixth of the deformation zone (double point formulation).....	53
Figure 4.7 one-sixth of the deformation zone (triple point formulation)	54
Figure 4.8 Discretization of SFP deformation zone is divided into number subzones	55
Figure 4.9 Discretization of pyramidal subzones 11-2-9-10-3	56
Figure 4.10 Location of coordinates of different points.....	58
Figure 4.11 Interconnection of SERR blocks	65
Figure 4.12 Discretization of DFP deformation zone is divided into number subzones	66
Figure 4.13 Discretization of pyramid 2-11-5-6-12	67
Figure 4.14 Discretization of pyramid 12-2-9-10-3	68
Figure 4.15 Discretization of TFP deformation zone is divided into number subzones	69
Figure 4.16 Discretization of the prismatic subzone 12-2-9-13-3-10.....	70
Figure 4.17 Discretization of one floating point deformation zone is divided into number subzones.....	73

Figure 4.18 Discretization of three floating point deformation zone is divided into number subzones.....	73
Figure 4.19 Discretization of five floating point deformation zone is divided into number subzones.....	74
Figure 4.20 Discretization of seven floating point deformation zone is divided into number subzones.....	74
Figure 4.21 Discretization of nine floating point deformation zone is divided into number subzones.....	75
Figure 4.22 Discretization of eleven floating point deformation zone is divided into number subzones.....	75
Figure 4.23 Comparison of results for different formulation (N=24)	78
Figure 4.24 Comparison of results of different reduction with friction with punch travel	79
Figure 4.25 Comparison of results for different formulation (N=24)	81
Figure 4.26 Major input parameters for FEM simulation for extrusion-forging of the triangular head with circular shaft	82
Figure 4.27 Variation of punch load with punch travel.....	90
Figure 4.28 Mean stress and effective strain at particular reduction and punch movement for forward extrusion-forging process.....	90
Figure 4.29 Variation of punch load with punch travel.....	91
Figure 4.30 Mean stress and effective strain at particular reduction and punch movement for forward backward extrusion-forging process	92
Figure 4.31 Extrusion die Assembly	96
Figure 4.32 Container	97
Figure 4.33 Container sleeve.....	98
Figure 4.34 Container cover plate	99
Figure 4.35 Forging die holder.....	100
Figure 4.36 Extrusion die holder	101
Figure 4.37 Support/base plate.....	102
Figure 4.38 Punch.....	103
Figure 4.39 Triangular split type forging die	104
Figure 4.40 Triangular punch plates.....	105
Figure 4.41 Triangular backward extrusion die and cap	106
Figure 4.42 Testing plate	106
Figure 4.43 Extrusion dies	107
Figure 4.44 Photograph of INSTRON [®] 600KN machine with assembled setup.....	108
Figure 4.45 Extruded forward extrusion-forging triangular head shaped product...	109

Figure 4.46 Extruded forward-backward extrusion-forging triangular head shaped product	109
Figure 4.47 Stress-strain curve for lead.....	111
Figure 4.48 Theoretical calibration curve for standard ring (6:3:2).....	112
Figure 4.49 Variation of punch load with punch travel	113
Figure 4.50 Die filling at different punch movement.....	115
Figure 4.51 Flow pattern at different punch movement.....	115
Figure 4.52 Variation of punch load with punch travel.....	116
Figure 4.53 Flow pattern at 40.61% reduction and 28mm punch movement	117
Figure 4.54 Comparison of non-dimensional extrusion pressure without friction for forward extrusion-forging process	118
Figure 4.55 Variation of non-dimensional extrusion pressure with punch travel for forward extrusion forging process for different reduction.....	119
Figure 4.56 Comparison of non-dimensional average extrusion pressure without friction for forward-backward extrusion-forging process.....	120
Figure 5.1 Front half in section of the process (a) Forward extrusion-forging	122
Figure 5.2 Domain of interest G-B-O ₁ -O-b--a (one eight of zone of deformation). 123	
Figure 5.3 Variation of calculated extrusion velocity with the number of sides of approximating polygon	123
Figure 5.4 Comparison of results for different formulation (N=32)	125
Figure 5.5 Comparison of results for different formulation (N=32)	125
Figure 5.6 Variation of punch load with punch travel	127
Figure 5.7 Mean stress and effective strain at particular reduction and punch movement for forward extrusion-forging process of square section	127
Figure 5.8 Variation of punch load with punch travel	128
Figure 5.9 Mean stress and effective strain at particular reduction and punch movement for forward backward extrusion-forging process of square section	129
Figure 5.10 Square split type forging die	129
Figure 5.11 Square punch plate	130
Figure 5.12 Square backward extrusions die	130
Figure 5.13 Extruded forward extrusion-forging square head shaped product	131
Figure 5.14 Extruded forward-backward extrusion-forging square head shaped product	131
Figure 5.15 Variation of punch load with punch travel of experimental analysis of forward extrusion-forging process of square section.....	132
Figure 5.16 Die filling at different punch movement.....	133
Figure 5.17 Flow pattern at different punch movement.....	134

Figure 5.18	Experimental variation of punch load with punch travel.....	135
Figure 5.19	Flow pattern for forward-backward extrusion-forging process	136
Figure 5.20	Comparison of non-dimensional extrusion pressure without friction for forward extrusion-forging process	136
Figure 5.21	Variation of non-dimensional extrusion pressure with friction for forward extrusion forging process for different reduction.....	138
Figure 5.22	Comparison of non-dimensional average extrusion pressure without friction for forward-backward extrusion-forging process.....	139
Figure 6.1	Domain of interest A-O-B-O ₁ -a-b (one tenth of zone of deformation) .	141
Figure 6.2	Extrusion velocities with number of sides of approximating polygon.....	142
Figure 6.3	Comparison of results for different formulations (N=40).....	143
Figure 6.4	Comparison of results for different formulation (N=40)	143
Figure 6.5	Variation of punch load with punch travel	144
Figure 6.6	Mean stress and effective strain at particular reduction and punch movement for forward extrusion-forging process	144
Figure 6.7	Variation of punch load with punch travel	145
Figure 6.8	Mean stress and effective strain at particular reduction and punch movement for forward backward extrusion-forging process.....	146
Figure 6.9	Pentagon split type forging die.....	147
Figure 6.10	Pentagon punch plate	147
Figure 6.11	Pentagon backward extrusions die	148
Figure 6.12	Extruded forward extrusion-forging pentagonal head shaped product.	149
Figure 6.13	Extruded forward-backward extrusion-forging pentagonal head shaped product	149
Figure 6.14	Variation of punch load with punch travel of experimental analysis ...	150
Figure 6.15	Die filling at different punch movement.....	152
Figure 6.16	Flow pattern at different punch movement.....	152
Figure 6.17	Variation of punch load with punch travel of experimental analysis ...	153
Figure 6.18	Flow pattern at 28mm of punch travel	154
Figure 6.19	Comparison of non-dimensional extrusion pressure without friction for forward extrusion-forging process	155
Figure 6.20	Variation of non-dimensional extrusion pressure with friction for forward extrusion forging process for different reductions	156
Figure 6.21	Comparison of non-dimensional extrusion pressure without friction for forward-backward extrusion-forging process	157
Figure 7.1	Domain of interest A-O-B-O ₁ -a-b (one tenth of zone of deformation) ..	160
Figure 7.2	Extrusion velocities with number of sides of approximating polygon.....	161

Figure 7.3 Comparison of results for different formulation without friction (N=48)	162
.....	162
Figure 7.4 Comparison of results for different formulation	162
Figure 7.5 Variation of punch load with punch travel	163
Figure 7.6 Mean stress and effective strain at particular reduction and punch movement for forward extrusion-forging process	164
Figure 7.7 Variation of punch load with punch travel	164
Figure 7.8 Mean stress and effective strain at particular reduction and punch movement for forward backward extrusion-forging process	165
Figure 7.9 Hexagon split type forging die	166
Figure 7.10 Hexagon punch plate	167
Figure 7.11 Hexagon backward extrusions die	167
Figure 7.12 Extruded forward extrusion-forging triangular head shaped product	168
Figure 7.13 Extruded forward-backward extrusion-forging hexagon head shaped product	168
Figure 7.14 Variation of punch load with punch travel of experimental analysis	169
Figure 7.15 Die filling at different punch movement	170
Figure 7.16 Flow pattern at different punch movement	171
Figure 7.17 Variation of punch load with punch travel of experimental analysis	172
Figure 7.18 Comparison of non-dimensional extrusion pressure without friction for forward extrusion-forging process	173
Figure 7.19 Variation of non-dimensional extrusion pressure with friction for forward extrusion forging process for different reduction	174
Figure 7.20 Comparison of non-dimensional extrusion pressure without friction for forward-backward extrusion-forging process	175
Figure 8.1 Cavity formed by the dead metal zone for 12-tooth spur gear (a) forward and (b) forward-backward extrusion-forging process	177
Figure 8.2 Domain of interest A-O-B-O ₁ -a-b (one twelfth of zone of deformation)	178
.....	178
Figure 8.3 Deformation zone with single-point formulation	179
Figure 8.4 Deformation zone with double-point formulation	179
Figure 8.5 Deformation zone with triple-point formulation	180
Figure 8.6 Deformation zone of 12-tooth gear (one twenty-fourth subzone) with nine floating point formulation	180
Figure 8.7 Comparison of non-dimensional extrusion pressure with percentage area reduction for different tooth gear	182
Figure 8.8 Comparison of optimal results for different tooth gear	182
Figure 8.9 Variation of punch load with punch travel for different tooth gears	183

Figure 8.10 Mean stress and effective strain at particular reduction and punch movement for forward extrusion-forging process.....	184
Figure 8.11 Variation of punch load with punch travel of four, six, eight and twelve tooth spur gear fem simulation	185
Figure 8.12 Mean stress and effective strain at particular reduction and punch movement for forward-backward extrusion-forging process	186
Figure 8.13 4-tooth gear split type forging die	188
Figure 8.14 6-, 8-, 12- tooth gears forging dies.....	188
Figure 8.15 4-tooth spur gear punch plate.....	189
Figure 8.16 6-, 8-, 12-tooth spur gears punch plate	189
Figure 8.17 4-tooth gear backward extrusions die	190
Figure 8.18 6-, 8-, 12-tooth gears backward extrusions dies	190
Figure 8.19 Extruded forward extrusion-forging 4-tooth gear head shaped product	191
Figure 8.20 Extruded forward extrusion-forging 6-tooth gear head shaped product	191
Figure 8.21 Extruded forward extrusion-forging 8-tooth gear head shaped product	191
Figure 8.22 Extruded forward extrusion-forging 12-tooth gear head shaped product	192
Figure 8.23 Extruded forward-backward extrusion-forging 4-tooth gear head shaped product	192
Figure 8.24 Extruded forward-backward extrusion-forging 6-tooth gear head shaped product	192
Figure 8.25 Extruded forward-backward extrusion-forging 8-tooth gear head shaped product	193
Figure 8.26 Extruded forward-backward extrusion-forging 12-tooth gear head shaped product	193
Figure 8.27 Variation of punch load with punch travel of experimental analysis of four, six eight and twelve tooth spur gear.....	194
Figure 8.28 Die filling at different position of punch travel	195
Figure 8.29 Flow pattern at different punch movement.....	195
Figure 8.30 Variation of punch load with punch travel of experimental analysis for forward-backward extrusion of four, six, eight and twelve tooth spur gear shape.....	197
Figure 8.31 Die filling at different position of punch travel (a comparison between FEA and experimental analysis)	199

Figure 8.32 Comparison of flow pattern between FEM and experiment at different punch travel movement.....	199
Figure 8.33 Comparison of non-dimensional extrusion pressure without friction for forward extrusion-forging process of 4, 6, 8, 12-tooth spur gear	200
Figure 8.34 Variation of non-dimensional extrusion pressure with friction for forward extrusion forging process of 4-tooth spur gear for different reductions	202
Figure 8.35 Variation of non-dimensional extrusion pressure with friction for forward extrusion forging process of 6-tooth spur gear for different reductions	203
Figure 8.36 Variation of non-dimensional extrusion pressure with friction for forward extrusion forging process of 8-tooth spur gear for different reductions	204
Figure 8.37 Variation of non-dimensional extrusion pressure with friction for forward extrusion forging process of 12-tooth spur gear for different reductions	205
Figure 8.38 Comparison of non-dimensional extrusion pressure for forward-backward extrusion-forging process of 4, 6, 8, 12-tooth spur gear	206

NOMENCLATURE

English symbols (in alphabetical order)

A	Area of a triangle
A_b, A_e	Area of the billet and product cross section
A_i	Area of the i^{th} face of the tetrahedral rigid region
A_x, A_y, A_z	X-, Y-, Z-projections of triangle in space
a	Half width of the product
B	Length of side of the triangle section
c	Overall width of product cross section
d	Overall length of product cross section
F, G	Functions of die cavity parameters
H, L	Optimization parameters
i, j, k	Unit vectors along the axis of a Cartesian co-ordinate frame
J	Upper bound energy consumption
J_1	Internal power dissipated due to plastic deformation
J_2	Power for shear deformation against velocity discontinuity
J_3	Frictional power dissipated at tool/work interface
J_{min}	Minimum value of J
J_{Si}	Power of shear deformation on the plane S,
L	Height/length of deformation zone
m	friction factor on the die surface
M	Height of the floating point on the extrusion axis from origin

\hat{n}	Unit vector normal to a surface
P_{av}	Average extrusion pressure
R	Shaft radius/Radius of extruded shaft
N	Number of sides of approximating polygon
s	Length of each side of the approximating polygon
S_i	i^{th} surface of velocity discontinuity
S_{Di}	i^{th} interface of tool/work
t_1, t_2	Relevant widths in section dimensions
V	Velocity vector in general
V_o	Volume of deformation zone
V_1, V_2	Velocity vectors on both sides of a surface
V_k	Velocity vector in tensor notation
ΔV	Velocity discontinuity
$\Delta V/S_i$	Velocity discontinuity across the i^{th} surface
$\Delta V/S_{Di}$	Velocity discontinuity across the surface S_{Di}
$\Delta V/i$	Velocity discontinuity across the i^{th} face
V_b, V_p	Billet and product velocity
V_{1n}, V_{2n}	Components of V_1 and V_2 along \hat{n}
V_x, V_y, V_z	Component of velocity in Cartesian coordinates
W	Half width of the billet
x, y, z	Axes of general Cartesian coordinates
σ_o	Yield stress in uniaxial tension or compression

f	Function representing the equation of a planer surface
ε_{ij}	Components of strain rate tensor
k	Yield stress in simple shear
$\varepsilon_{xx}, \varepsilon_{yy}, \varepsilon_{zz}$	Strain rate components (direct)
$\varepsilon_{xy}, \varepsilon_{yz}, \varepsilon_{zx}$	Strain rate components (shear)
ζ, η, Z	Transformed co-ordinate system
ψ_1, ψ_2	Dual stream functions
θ	Internal angle of the polygon

ABBREVIATION

DFP	Double Floating Point
DMZ	Dead Metal Zone
DPF	Double Point Formulation
DFP	Double Floating Point
DZ	Deformation Zone
FEM	Finite Element Method
FEA	Finite Element Analysis
PERR	Plainer Elementary Rigid Region
SERR	Spatial Elementary Rigid Region
SFP	Single Floating Point
SPF	Single Point Formulation
TFP	Triple Floating Point
TPF	Triple Point Formulation

1.1 Introduction

Many exogenous factors lead to modify the existing method of product design and exploited for sustenance of firms in a competitive environment. Among them, the introduction of new materials, technologies for reducing design and manufacturing lead time, services and the attention paid to the end user requirements are critical to gain an edge over competitors. The emphasize on reduction of product development time, better quality product, fewer chances of failure have a pro-found influence on manufacturing processes and result in the birth of new technique and methodology of the production process. Metal forming processes in general and extrusion and/or forging in particular, get importance for their abilities to give improved material properties, high production rate and less material waste when compared with that produced by machining, casting or by assembling the individual parts produced by different manufacturing processes. Depending on the direction of the punch movement and the direction of the material flow, extrusion process is classified into three basic types, named as a forward (direct) extrusion, backward (indirect) extrusion and radial/lateral extrusion. In addition to the basic extrusion operation, there are some combined extrusion processes in which two (or more) basic extrusion processes and/or forging processes occur simultaneously.

Extrusion-forging is a bulk metal forming operation in which the cross-section area of the billet is reshaped and changed into a certain shape by forcing it through a narrow path called extrusion die and obtaining a desired shape at the end of the billet or at other locations by filling the forging die cavity. A variety of regular/irregular cross-sections and complex shape can be achieved by this process. This process has a definite advantage over other production processes used to manufacture complicated sections having re-entrant corners. Large reduction achieved even at high strain rates has made this process is one of the fastest growing metals working methods.

Because of the large forces required in extrusion, most metals are extruded hot where the deformation resistance of metal is low. However, cold extrusion is possible for many metals and has become an important commercial process. The reaction of the extrusion billet with the container and die results in high compressive stress that effectively reduces cracking of materials during the primary breakdown from the

ingot. This is an important reason for increased utilization of extrusion on the working of metals difficult to form; like stainless steel, nickel based alloys and other high-temperature materials.

The variables influencing an extrusion process are: (i) percentage of area reduction, (ii) dies geometry, (iii) product geometry, (iv) speed of extrusion, (v) billet temperature, and (vi) lubrication between the die and extruding material. In an industrial application, the above parameters should be suitably optimized to achieve the best results. The ram speed and temperature have a major influence on plastic properties of the billet material, and their effect can be studied by choosing a suitable constitutive equation.

1.2 Existing Method of Manufacturing

In the present manufacturing practice, the components are produced separately and assembled by means of keys, snap rings, inference fit, or welding process, etc. The assembly process is used because of (i) ease of mass production, (ii) interchangeability, (iii) cost effective and (iv) maintainability. Major drawbacks of the present method of manufacturing are:

- (i) Corrosion: The shaft corrodes or welds to the gear or splines, making it difficult or impossible for the user to remove it for further maintenance.
- (ii) Keyway Cost: Fitting and cutting a keyway on a solid shaft an added expense.
- (iii) Deformation: The keyway is the only item that transmits torque. Fatigue stress can occur over time, depending on the application. For correct installation, a key of sufficient length and must ensure a proper fit between the key and the keyway. Otherwise, the keyway may experience plastic deformation that produces a loose fit, especially on reversing applications.
- (iv) Tapped Hole: To secure the shaft inside the gear reducer and to prevent axial movement, the end of the shaft should contain a tapped hole, which is an extra expense.
- (v) Limited sizes: Keyed shafts are usually available in only one or two diameters. Alternate bores require a special shaft (expensive).
- (vi) Maximum tangential stress: Maximum tangential stress approaches a value twice as great as that for a solid disk over a hollow disk which cause stress concentration and failure at the shaft gear junction. (Figure 1.1)

- (vii) Backlash: Because of the air gap around the key, a keyed shaft has an inherently higher backlash than a keyless shaft.

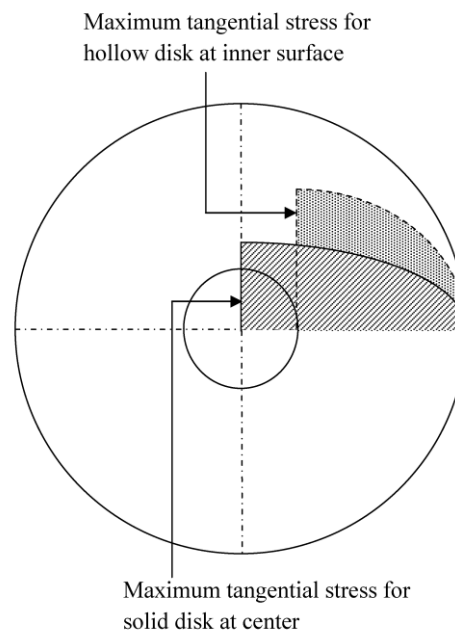


Figure 1.1 Maximum tangential stresses of shafts

1.3 Industry Demand and New Trend

In general, gears, splines, triangular, rectangular, pentagonal, and hexagonal shaped machine elements mostly used to transmit load & torque by rotating generally at high speed. Therefore, there is an industrial demand to produce these parts with high strength with narrow tolerances, improved mechanical properties, high production rate and less material waste. Forming gear like element rather than cutting has all the above advantages with greater utilization of the raw material and high productivity. The major advantage of metal forming processes (i.e., extrusion, forging and combined extrusion-forging processes) is to avoid machining, casting and assembling. As high precision and high-capacity presses (for mass production) are available it can be utilized for the forming processes. Post-processing of products in case of forming gears is also easy and cost effective.

1.4 Different Type of Conventional Dies

The different types of conventional dies used in extrusion are; (i) Square dies (ii) Tapper or linearly converging dies and (iii) Curved or mathematically contoured dies. From the point of view of economy, square dies are preferably used where the reduction in load is the prime concern as in the extrusion of materials which are hard and

difficult to form. For common engineering materials, a square (flat) or a wedge-shaped die will probably be more economical since these dies are easier to manufacture.

1.5 Extrusion-forging Process

1.5.1 Forward extrusion-forging process

In this combined forward extrusion-forging process round/sectioned shafts with different shaped (triangular, square, pentagon, hexagon, gear) heads at one end are formed. The entire process can be divided into three stages as shown in Figure 1.2. In the first stage, extrusion and upsetting take place simultaneously until the deformed material begins to make contact with the die wall. In the second stage, extrusion and forging take place simultaneously until filling of the forging die cavity. In this stage, the flow of metal is restricted by the boundary wall of the forging die. In the last stage, the deformation in the head part is completed, and only steady state extrusion takes place. It is evident from the experiments (detail description is given in subsequent sections) that the last stage of the process requires maximum load and a steady state extrusion of product (shaft) takes place. This steady state maximum load is very much important for die design. The present theoretical analyses focus on this last stage steady state extrusion of the round shaft from shaped billet that already filled the forging die cavity.

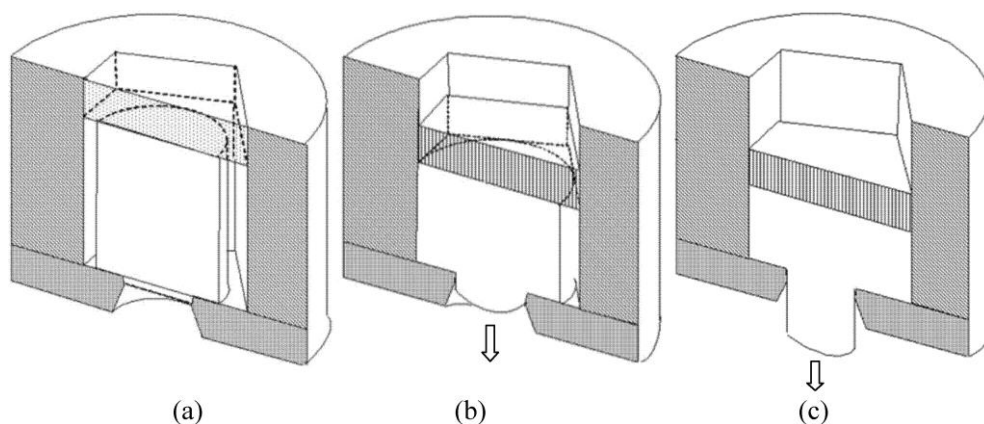


Figure 1.2 Different stages of forward extrusion forging process(Front half section)

1.5.2 Forward-backward extrusion-forging process

In this combined forward-backward extrusion-forging process round shaft with different shaped (triangular, square, pentagon, hexagon, gear) heads at different location other than ends are formed. This process (Figure 1.3) follows similar stages as forward extrusion-forging process. In comparison to previous one, instead of forward extrusion both forward and backward extrusion takes place simultaneously.

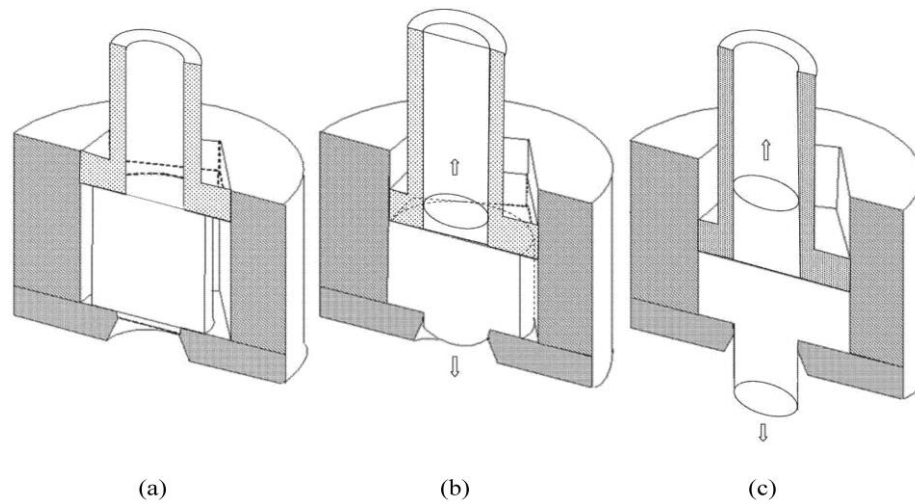


Figure 1.3 Different stages for forward-backward extrusion forging process
(Front half section)

1.6 Research Objective

Though technological barriers exist, as in most manufacturing areas, it is important to overcome them by developing proper understanding of the process with related attributes. In this direction, next chapter (Chapter 2) explains the various efforts directed to improving the industrial demand and different methodology applied to plastic deformation. The exhaustive literature review reveals that forward and forward-backward extrusion-forging process is least explored out of different extrusion and forging processes. In this direction, present work emphasis on the forward and forward-backward extrusion-forging process analysis of different methodology applied to different section heads with circular shaft.

Based on these guiding principles, the objectives of present research can be summarized as follows:

- To replace ‘Thumb rules’ or ‘designer’s intuition’ base design, which are still prevalent in the industry, by a methodical analysis process when installing and deciding on the capacity of a machine/ equipment/tool/die and production of complex parts.
- To find out a class of kinematically admissible discontinuous velocity fields based on reformulated spatial elemental rigid region (SERR) technique, and then to examine it so as to identify the velocity field giving the lowest upper-bound. The optimum velocity field is then used to compute the upper-bound extrusion pressure for various area reductions.

- Finite element analysis using commercially available plastic deformation analysis package software to examine the validation of the proposed reformulated SERR model.
- Design and fabrication an experimental setup for forward and forward-backward extrusion-forging of different sections so as to examine the validation of the proposed reformulated SERR model.

1.7 Thesis Outline

The remainder of this thesis is organized as follows:

Chapter 2: Literature review

Includes a literature review to provide a summary of the base of knowledge already available involving the types of metal forming analysis, and types of extrusion processes.

Chapter 3: Upper bound technique for three dimensional metal deformation problems

Include a description of the metal forming analysis, types of available solutions and brief description and application of SERR technique.

Chapter 4: 3D analysis of combined extrusion-forging process for round-triangle-round sections

This chapter deals with the extrusion-forging of the triangular head with a circular shaft for both forward and forward-backward extrusion process. A kinematically admissible discontinuous velocity field based on reformulated spatial elemental rigid region (SERR) technique is proposed. Upper bound extrusion pressure is computed. The upper bound extrusion pressure is validated by commercially available finite element analysis software DEFORM[®]-3D and exhaustive experiments.

Chapter 5: 3D analysis of combined extrusion-forging process for round-square-round sections

This chapter deals with the extrusion-forging of the square head with the circular shaft for both forward and forward-backward extrusion process. A kinematically admissible discontinuous velocity field based on reformulated spatial elemental rigid region (SERR) technique is proposed. Upper bound extrusion pressure is computed. The upper bound extrusion pressure is validated by finite element analysis and experiments.

Chapter 6: 3D analysis of combined extrusion-forging process for round-pentagon-round sections

This chapter deals with the extrusion-forging of the pentagonal head with circular shaft for both forward and forward-backward extrusion process. A kinematically admissible discontinuous velocity field based on reformulated spatial elemental rigid region (SERR) technique is proposed. Upper bound extrusion pressure is computed. The upper bound extrusion pressure is validated by finite element analysis and experiments.

Chapter 7: 3D analysis of combined extrusion-forging process for round-hexagon-round sections

This chapter deals with the extrusion-forging of the hexagonal head with the circular shaft for both forward and forward-backward extrusion process. A kinematically admissible discontinuous velocity field based on reformulated spatial elemental rigid region (SERR) technique is proposed. Upper bound extrusion pressure is computed. The upper bound extrusion pressure is validated by finite element analysis and experiments.

Chapter 8: 3D analysis of combined extrusion-forging process for round-spur gear - round sections

This chapter deals with the extrusion-forging of 4-tooth, 6-tooth, 8-tooth and 12-tooth spur gear head with a circular shaft for both forward and forward-backward extrusion process. A kinematically admissible discontinuous velocity field based on reformulated spatial elemental rigid region (SERR) technique is proposed. Upper bound extrusion pressure is computed. The upper bound extrusion pressure is validated by commercially available finite element analysis and experiments.

Chapter 9: Conclusions

The conclusion and scope for future work are given in this part of the thesis.

1.8 Closure

This chapter provides the insight into various past developments in the area of combined extrusion-forging process for manufacturing of rotating component with integrated shaft. The chapter also outlines:

- Drawbacks of existing method of manufacturing and highlights the industrial demands with new trends.
- The advantage of square dies over other types is summarized.
- Both forward and forward-backward extrusion-forging processes are described.

Considering the objective of present work a review of the exhaustive literature survey is presented in the next chapter.

2.1 Introduction

One of the current challenges faced by the manufacturing industry is to produce component of high strength, resistance to fatigue, heat, corrosion and low production cost. Forming is one such process, which has the additional advantage of greater utilization of raw materials and high productivity apart from above advantage. Among all forming processes extrusion-forging is a process where difficult to produce shapes, can be formed with higher mechanical properties and net shape production can be achieved.

The experimental works on plastic deformation and metal forming started in France by Colomb and Tresca as per Osakada [1]. In the early 20th century the research on plastic deformation flourished in German. Towards the 2nd half of the 20th century analysis of the metal forming process was developed and efficiently used all over the world. Many researchers contribute remarkable findings towards the field of plasticity.

Various approximation methods have been devised depending upon the assumption and approximation, order of complexity and availability to predict final results. Some most well-known solution methods are:

1. Slip-line field analysis
2. Slab or stress equilibrium method
3. Upper-bound analysis
4. Finite element analysis

2.2 Slip-line Field Method

Prandtl [2] presented an analysis of plane strain indentation of flat punch into a rigid plastic solid body as shown in Figure 2.1. He assumed a rigid-perfectly plastic material without work hardening but with a pressure sensitive flow stress (Mohr's yield criterion). By solving the equilibrium equation, he constructed a series of lines having directions parallel to the maximum shear stress (Figure 2.1). He correctly obtained the indenting pressure for a material with shearing flow stress k without pressure sensitivity as:

$$p = 2k \left(1 + \frac{\pi}{2} \right) \quad (2.1)$$

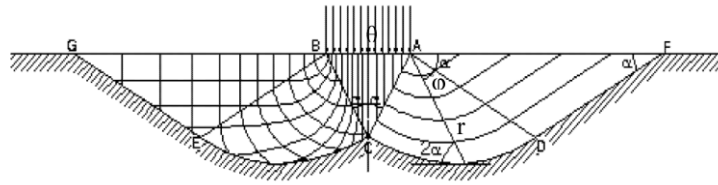


Figure 2.1 Slip-line fields by Prandl [2]

Hencky [3] derived a general theorem of stress state for slip-line field. He concluded that a statically admissible stress field which satisfies the equilibrium equation, yield condition and boundary force is not always correct; because the velocity field associated with the stress state may not satisfy the volume constancy or may lead to negative energy consumption. Geiringer [4] derived an equation in relation to the velocity field by considering the incompressibility condition in plastic deformation and the relation between strain rate and velocity. Hill [5] and Prager and Hodge [6] presented the systematic approach of slip-line field theory. Prager's introduction of hodograph or velocity diagram simplifies the handling of slip-line solution and removed the prior difficulties. Johnson et al. [7] have analyzed the extrusion process with plain strain deformation using slip-line field technique by neglecting the elastic strains, work hardening, temperature and strain rate effects. This method is highly successful in clearly defining the rigid and plastic zones and explained the strain history as observed in a grid deformation test besides predicting the extrusion pressure with reasonable accuracy. The slip-line field technique was adopted by Johnson [8, 9], Johnsons and Mellor [10], Dodeja and Johnson [11], A.P.Green [12] and W.A.Green [13] to predict solutions for extrusion through different die geometry. However, with the development of series method of construction by Ewing[14], Matrix method by Collins[15] slip-line field technique could be successfully applied to a number of mixed boundary value problems [16, 17, 18, 19]. Bacharach and Samanta [20] presented a numerical method for slip-line field analysis of rigid perfectly plastic material, which analysis metal forming operation as constructed optimization problem. They develop the solution for the extrusion through curved dies with zero exit angles and non-zero entrance angle using the proposed method and computed the extrusion pressure with respect to reduction with other parameters. Das and Maity [21] computed the mean extrusion and die pressure

for a number of dies geometry by varying different parameter using slip-line field for wedge shaped dies. The finding was, the mean extrusion pressure increases with increasing of corresponding die angle “ α ” and form factor for the transit field. The optimal die angle increases with the increase in reduction and friction factor. Attempts have also been made to incorporate work hardening in the slip-line field analysis [22]. This method has remained confined to plain strain and plain stress deformation of rigid and perfectly plastic materials with a few axisymmetric solutions [23, and 24]. Das and Johnson [25] have suggested a slip-line field solution for end extrusion through square dies with slipping friction at the work piece die interface. The variation of the mean steady extrusion pressure with reduction has been computed in these fields. Recently, Abrinia and Mossuleh [26] reported a three-dimensional solution for metal forging using an appropriate load estimation method based on the slip-line field theory.

During the 1950’s to 80’s, many slip-line field solutions were proposed for extrusion, forging, rolling, drawing and metal cutting. Since slip-line field solution method provides the stress state in the deforming material, it is effectively used, although its plane strain assumption makes the method unrealistic.

2.3 Slab-Method

Siebel [27] presented the analysis for forging assuming a thin area (slab) to make equilibrium equation. In the case of compression of a cylinder of diameter d and height $2h$ shown in Figure 2.2 , he considered a dx in layer of a thickness dx and a height same as the cylinder, and made equilibrium of forces acting to the layer. When yield stress is Y and friction coefficient is μ , he derived the average contacting pressure \bar{p} as:

$$\bar{p} = Y \left[1 + \frac{1}{3} \mu \left(\frac{d}{h} \right) \right] \quad (2.2)$$

In the case of present slab method, the average pressure is calculated to be

$$\bar{p} = 2Y \left(\frac{h}{\mu d} \right)^2 \left\{ \exp \left(\frac{\mu d}{2h} \right) - \frac{\mu d}{2h} - 1 \right\} \cong Y \left[1 + \frac{1}{3} \mu \left(\frac{d}{h} \right) \right] \quad (2.3)$$

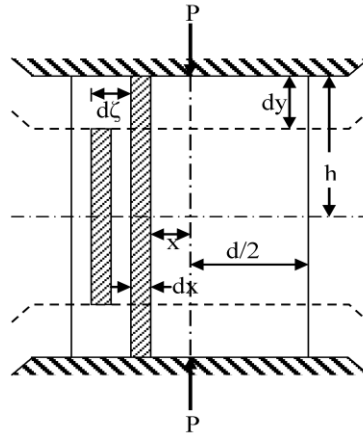


Figure 2.2 Model of slab method used by Siebel [27]

The equation (2.2), identical to the Siebel's solution, is an approximation of the equation (2.3), when $\mu d / h$ is enough smaller than 1.0. Siebel numerically calculated the average pressures for some typical cases of forging, and discussed the way to apply the result to backward extrusion. Soon after the Siebel's work, many researchers extend as well as Siebel continue to analyze various processes. Since the analyzed results are mathematically expressed, they are effectively used in the industry [28, 29]. In the 1950s in the USA and UK, and in the 1960s in Japan, automation of strip rolling in the steel industry began, and many engineers studied and improved the theories in the industry.

Kaneko et al. [30] applied the slab method to the backward extrusion of high density polyethylene (HDPE) with various extrusion ratios at room temperature. The work hardening of polymers at room temperature is more extensive than metal. This characteristic is considered on the result of tension test of a biaxial tensioned HDPE sheet by forging between opposite punch. A good agreement is obtained between the theory and the experiment. Shichun et al. [31] applied the modified slab method to predict the forming defect. The critical condition for the corner-cavity formation during backward extrusion is derived and concluded that the critical relative thickness of the bottom of the billet for corner-cavity formation decreases with an increase in the reduction in area. Chitkara and Aleem [33] developed a generalized slab method for analysis of the extrusion of axi-symmetric bi-metallic tubes through the profiled shaped dies and over profile shaped mandrels. An experimental investigation into forward extrusion of bi-metallic tubes made of cp aluminum and hc copper was also carried out and the resultant non-dimensional extrusion pressures, flow patterns and

characteristic deformation modes observed and found reasonable good agreement with theoretical calculation. Hsu and Tzou [34] derived and compared the formulations of double-layer clad sheet compression forming based on the upper bound and the slab methods. In their analysis effects of various compression conditions such as the clad thickness ratio, the shear yield stress ratio, the frictional factor ratio, the ratio of width thickness, and the friction factor on the compression characteristics are found by the two methods. The comparison between the two methods with compression force is performed in order to realize the feasibility of the two analytical models. Bakhshi-Jooybari et al. [35] proposed a combined upper bound and slab method for estimating the deformation load for cold rod extrusion of aluminum and lead in an optimum curved die profile. The experimental results validate the finite element results that obtained by commercially available finite element software, ABAQUS[®]. It was illustrated that the extrusion load in the optimum curved die during the deformation is considerably less than that in the optimum conical die. Ghoshchi et al. [36] proposed a new slab method formulation which could be applied to three-dimensional problems in metal forming. A parametric slab has been considered in this analysis, and the force balance on the slab was carried out to obtain equilibrium equations in terms of these parameters. The parameters, in fact, are related to the geometry of the final extruded shape, the die and the material flow regime assumed in the formulation. The new formulation tested for forward extrusion of a square cross section. The effect of reduction of area, frictional conditions and other process parameters on the extrusion pressure was investigated. The theoretical results obtained are validated with that of experimental. They concluded that the new slab method of analysis gave reasonable results for the problem analyzed, and that it could be applied to other bulk metals forming processes such as rolling, wire drawing and forging. Kamble and Nandedkar [37] investigated an analytical slab method taking into account the effect of material properties, friction and heat transfer at die/material interface, press ram speed, flash dimensions, forging geometry, and billet and die temperature. The method is modified for the flow stress variation with temperature and empirical flash dimensions based on the experimental investigation. They validated this reported modifications in slab method's results by conducting experiments and found the variations within 10% variation.

2.4 Upper-Bound Analysis

The upper bound method provides an approximate forming load which is never lower than the exact value. Because of this, the load calculated by this method is safe in selecting the forming machines and designing the tools or dies, and thus this method has been used practically. From the relation between velocity and strain rate, the associated strain rate distribution can be determined in deforming region. With a kinematically admissible velocity field, which satisfies the condition of volume constancy and the velocity boundary condition, together with the flow stress value of the material, energy dissipation rate and overestimation forming load higher or equal to the correct values are obtained. This is guaranteed by a limit theorem for rigid-plastic material. The upper bound theorem was introduced by Hill [38] in 1950 together with other bounding theorems.

Let us consider a simple plane-strain case that a rigid-perfectly plastic body with a shearing flow stress k is deformed by external force T through a tool moving with a velocity v . A kinematically admissible velocity field only with velocity discontinuous lines S_d with sliding velocity v^* is assumed. The upper bound theorem states:

$$Tv = \sum \int_s |v^*| dS_d \quad (2.4)$$

Where the left side is the correct working rate and the right side is the energy dissipation rate for the plastic deformation along the velocity discontinuities. This inequality means that the energy dissipation rate of the right side is greater or equal to the correct value of the left side. The upper bound value of the forming load T is obtained by dividing the calculated value of right side with v .

In 1951, Green [39] applied the theorem to the plane-strain compression between smooth plates, and compared the result with that of slip-line field method. While a slip-line field requires a long time to draw, a kinematically admissible field with only velocity discontinuity lines can be constructed easily with the help of hodograph, and gives a reasonably good result.

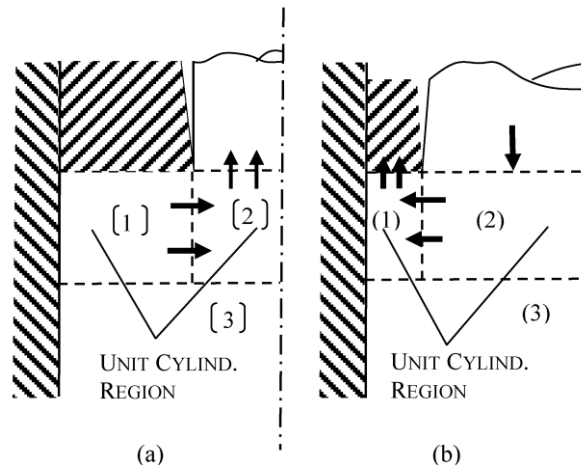


Figure 2.3 Velocity field for axis-symmetric extrusion by Kudo [40]

(a) and (b) are two proposed hypothetically unit

In 1960, H. Kudo [40] proposed a method for applying the upper bound method to axis-symmetric forging and extrusion. He divided the axis-symmetric billet into several hypothetical units, and derived mathematical expressions of velocity in the units by satisfying the condition of volume constancy and the surface velocities to be consistent with those of the neighboring units and the tool surfaces as demonstrated in Figure 2.3.

Kudo [41] first presented a new upper-bound approach to calculate the load required for plastic deformation. To facilitate the calculation of good upper bounds, the concept of a unit region is introduced. He showed that the upper-bound approach method proposed by him seems to offer a fairly accurate and simple means in analysing plane-strain forging problems. Upper bound solutions for plain-strain and axisymmetric extrusion has been proposed by Johnson [42], Johnson and Kudo [43], Adie and Alexander [44] and Avitzur [45]. Johnson, Kudo and Alexander used discontinuous velocity fields with triangular rigid regions to compute the extrusion load, while Avitzur proposed a continuous spherical velocity field throughout the deforming region to compute the plastic strains and work done. In all the case, the material was assumed to be rigid and perfectly plastic, and the effect of work hardening was not taken into account.

Work hardening and strain rate effects has been taken into account in the viscoplasticity method [46] in which the deformation of square grid, imposed on the major plane of metal flow, was analyzed to determine the stress and strain history in the deformation region. However, the usefulness of this method is limited by the fact

that the theoretical solution is dependent on experimental deformation of grid pattern. The above difficulty was eliminated to a certain extent by the flow-function method of analysis developed by Shabaik and Thomsen [47] in which the stream lines were predicted by determining the value of the flow function. The method makes use of the finite difference and relaxation techniques with an iterative procedure to compute the value of the flow function. But, due to the difficulties encountered in the determination of the flow function, application of this method has been restricted to the plain strain problems only.

The first attempt for developing a general method of analysis for three dimensional metal forming problems was made by Hill [48]. In this method, a class of velocity fields is assumed. The most suitable velocity field that nearly satisfies the statically requirements is then selected by using the virtual work principle for continuum. Hill [48] applied this method to determine the spread in flat bar rolling and forging. Hwang et al. [49] analyzed an analytical model for complex rolling of sandwich sheets. Effects of various rolling conditions such as the flow stress ratio and initial thickness ratio of the raw sheets, total thickness reduction, etc., upon the bonding factors such as the bonding length, mean contact pressure, and the relative sliding distance at the interface as well as the newly generated surface ratio is analyzed. Through the comparisons, the proposed mathematical model is verified with that of experiments and the characteristics of the bonding behavior at the roll gap during complex rolling of sandwich sheets are manifested. Chitkara and Aleen [50] extended the generalized upper bound technique of their previously published paper to analyze the problem of bi-metallic tube extrusions through the profile shaped dies and mandrel combinations. Theoretical results of mean extrusion pressures obtained from the generalized upper bound analysis are compared with those obtained earlier by the generalized slab method of analysis. A few salient observations during the experimental investigations carried out in the forward extrusion of bi-metallic tubes made of highly conductive copper and commercially pure aluminum are also given, and the results are commented upon. Chitkara and Bhutta [51] presents some typical results of an experimental investigation into the dynamic heading of triangular, hexagonal, and octagonal shaped heads, each at one end of the initially solid cylindrical rod-type specimens made of tellurium lead and commercially pure aluminum, which were clamped at the other end in each case. The results of die load–

die movement curves obtained, and were compared with those estimated from a modified simple upper bound analysis that takes account of the inertia forces of the un-deformed material. Comparison of the dynamic heading results with those observed from similar quasi-static cases suggests that though the dynamic heading loads were, in general, 20–40% higher than the similar quasi-static loads, the estimated dynamic forging loads employing the modified upper bound analysis taking account of the inertia, showed good correlations with the experimental results.

Celik and Chitkara [53] investigate the optimum shape for the extrusion dies of non-symmetric U- and I-shaped sections that yield the lowest upper-bound for a given reduction in area, die length, off-centric positioning and frictional conditions. For this purpose, a computer program was developed. Computations were carried out for various cases, and some of the results compared with the experimental verifications. Curvature of the extruded product and simulated deforming grid patterns were also predicted and compared. The theoretical predictions were observed to be in good agreement with the experimental results. Gordon et al. [54] has developed an upper bound model for extrusions through spherical dies. The velocity field, strain rate field and power terms were determined. The model indicates that the required extrusion pressures for a spherical die are higher than those for an “equivalent” conical die. They conclude the reason for the increase is the higher values for the internal power of deformation. The upper bound model that has been developed can be easily extended to other die shapes with the appropriate substitution for the die surface function. Darani and Ketabchi [55] in his work have investigated the material flow in extrusion of “L” section by an upper bound method. The results show that material in its plastic flow selects the path which needs minimum energy, so an optimum Limason shapes (somewhat heart shape comes from mathematical formula $r = 1 + \cos(\theta)$), intermediate section appears between the initial and exit sections. In flat face die extrusion process of non-axisymmetrical “L” section, intermediate section appears between initial round section and final “L” section. He observed that the experimental results of metal flow pattern, has a very important role in determining the energy of the whole process. The optimum intermediate Limason shape will minimize the process energy, without which the process energy will be double. Simulated metal flow pattern is comparable with experimental results.

Deformation of the material during a 90° equal-channel angular extrusion (ECAE) process is analyzed using upper-bound theorem by Altan et al [56]. The model findings include the effect of friction between the sample, and the die walls, radius of the inner corner of the dies and the dead metal zone on the deformation patterns during ECAE. In their study, the deformation model that includes the friction between the sample, and the die walls, the radius of the inner corner of the die and the dead metal zone effect on the deformation region in ECAE is proposed. Eivani and Taheri [57] analyzed the deformation of material in equal channel angular extrusion (ECAE) process with outer curved corner using an upper bound solution. The effects of die angle, friction between the sample and the die walls, and the angle of the outer curved corner, on the extrusion pressure are all considered in the analysis. They found that the extrusion pressure decreases with increasing both the die angle and the outer curved corner angle and increases with increasing the friction coefficient. Moreover, a good agreement is found between the predicted and experimental results of extrusion pressure relating to two dies of different outer curved corner angles used in ECAE tests of an aluminum alloy, AA 6070.

Ajiboye and Adeyemi [59] investigated the effects of die land on the extrusion pressures experimentally and theoretically. The effects of extrusion pressure due to the ironing effect, resulting from frictional forces within the die land region are analyzed by the upper bound method. The extrusion pressure contributions due to the die land evaluated theoretically and practically, are found to increase with die land length for any given percentage reduction and also increase with increasing percentage die reductions at any given die land length. There is a good agreement between theory and experiment on the extrusion pressures evaluated. For the purpose of designing for suitable extrusion dies to extrude lead material, they recommended that the die land length should be chosen equal to or greater than 0.6 of the billet diameter for small work pieces and with die exit clearance angles less than 10° , so as to extrude lead products with negligible bend or curvature. Ajiboye and Adeyemi [59] also analyzed the effect of die land lengths on the extrusion pressure increases with increasing complexity of die opening's geometry with, I-shaped section giving the highest extrusion pressure followed by T-shaped section, rectangular, circular-shaped die openings with square section die opening, giving the least extrusion pressure for any given die reduction at any given die land lengths. Ajiboye [60] presented Upper

bound elemental technique (UBET) for prediction of extrusion pressure in the three-dimensional forward extrusion process. Using square/rectangular billets, the study of the effect of die land length has been extended for the evaluations of extrusion pressures to extrude sections such as circular, square and rectangular shaped sections with power of deformation due to ironing effect on the die land taken into account. The extrusion pressure contributions due to the die land evaluated theoretically for these shaped sections considered are found to increase with die land lengths for any given percentage reduction and also increase with increasing percentage die reductions at any given die land length. The effect of die land lengths on the extrusion pressures increases with complexity of die openings geometry with rectangular section giving the highest extrusion pressure followed by circular with square section die opening, giving the least extrusion pressure for any given die reduction at any given die land lengths. They concluded that the proper choice of die land length is imperative if excessive pressure buildup at the emergent section is to be avoided so as to maintain good quality and metallurgical structure of the extrude products.

Yang et al. [61] proposed a new method of die surface representation, using blending function and Fourier series expansion, by which smooth transitions of die contour from the die entrance to the die exit are obtained. The flow patterns as well as the upper-bound extrusion pressures are obtained on the basis of the derived velocity field. Experiments are carried out for aluminum alloys at room temperature for a rounded square section and an elliptic section. In order to visualize the plastic flow, the grid-marking technique is employed. The theoretical predictions both for extrusion load and deformed pattern are in good agreement with the experimental results. Bakhshi-Jooybari [62] presented a friction model for the extrusion process and shown that the model works very well for cold extrusion of aluminum in dry conditions, but not suitable for hot extrusion of lubricated steel. Onuh et al. [63] has made an experimental investigation on the effects of extrusion ratio, die angle, loading rate on the quality of the extrusion products, extrusion pressures and flow pattern for cold extrusion of aluminium and lead alloys having shapes of inner circle section with four symmetrical projections. The radius of curvature for both extruded lead and aluminium alloys and the average hardness value of the extruded products along the projections and along the circumferential solid positions are found to increase with area reduction, and marginally with the increase of load rates. They

found that the non-dimensional specific coring pressure and maximum extrusion pressure are minimum at an die angle of 90^0 , which is ideal for die design to minimize extrusion pressure and increase die life. A three-dimensional solution for the extrusion of sections with larger dimensions than the initial billet or container is presented by Abrinia and Makaremi [64]. A generalized kinematically admissible velocity field was formulated using the upper bound theorem. Extrusion of shapes such as square and rectangle were considered for which kinematically admissible velocity fields were obtained. The finite element simulation was used to assist the theoretical analysis with regards to the material flow and filling of the die cavity. Based on the analytical results, extrusion dies for the rectangular sections were designed and manufactured and experiments were carried out. The results of the tests showed that the dies performed very well and complete filling of the die cavity and a successful extruded profile was observed. Sinha, et al. [65] describes the procedure for the design of a multi-hole extrusion process. They observed that in the case of the multi-hole extrusion, ram force is always lesser (about two-third) than in the case of the single-hole extrusion. Thus, the multi-hole extrusion process can become a productive process for the mass production of small sized components.

2.4.1 Extrusion-forging process

Brayden and Monaghan [66] present an analytical approach to investigate the deformation during an extrusion/forging operation. The method of analysis is based on the upper-bound technique for which the necessary velocity fields were obtained from a series of experimental tests. The resulting upper-bound expressions provide a systematic approach to load and stress evaluation form during an extrusion/forging process. Vickery and Monaghan [67] present results obtained from an experimental and analytical investigation of a combined forging-extrusion process applied to an axisymmetric component. They established that the forging-extrusion process consisted of three distinct stages. A number of upper-bound expressions were derived to account for: the energy required for plastic deformation; to overcome friction; and to account for shearing on surfaces of internal velocity discontinuities; during each stage. Very good agreement was achieved between predicted upper-bound values for the forging pressure ratio, P/σ , and those determined experimentally. Lee et al. [68] used UBET to analysis the forward and backward extrusion of hexagonal- and trochoidal shaped wrench bolts. A new kinematically admissible velocity field is

proposed to determine the forming load, the extruded length and the deformation pattern with respect to the punch travel. Experiments are carried out in order to validate the upper bound results and good agreement was achieved. Similar analyses are carried out by Hwan et al. [69] for polygonal and trochoidal headed bars from solid cylindrical billets. Yamin et al. [70] conducted a series of experiments of cup-rod combined extrusion processes to study the impact of deformation temperature and the lubrication to the plastic properties of magnesium alloy (AZ61A). Narayanasamy et al. [71] investigated extrusion-forging during cold upsetting using a suitable die for aluminium alloy (H9-6063) solid cylinders subjected to different approaching angles namely, 35°, 45°, 50° and 60°, 8mm and 10mm initial protrusion heights. During the experiments, three geometries such as barreled cylinder, truncated cone part and protruded part or extruded parts were observed. A relationship has been established between the approaching angle and protrusion height and relationship among various height strains and stress ratio parameters. Narayanasamy et al. [72] has carried out an experimental investigation of aluminium alloy billets during extrusion-forging using different lubricants. It is observed that the protrusion height increases with the increase in the approaching angle for a given extrusion load. The relationship among the various bulge parameters namely the hoop stress, the hydrostatic stress and the stress ratio parameters are also established.

2.4.2 SERR analysis

Gatto and Giarda [73] first proposed a three dimensional kinematic model by limit analysis for plastic deformation, denoted by SERR (Spatial Elementary Rigid Region). In this analysis, the volume of the solid was thought to of as made up of rigid polyhedral, with the plastic deformation localized on the faces of the same spatial figure, but which are allowed to glide over another whilst maintain contact. This scheme is a generalization of the model used in the limit analysis of plain plastic deformation. They analyze the characteristic of some spatial figures, which were considered as particularly useful in partitioning the space in the limit analysis of certain three-dimensional plastic deformation. Other contributions using SERR approach are summarized in Table 2.1.

Table 2.1. Important contribution in the area of SERR applied to square die:

Year	Author/ Reference	Title	Summary
1985	Kar et al. [75]	Upper Bound Analysis of Extrusion of Square Sections Using Square Dies	The spatial elementary rigid regions (SERR) technique of Gatto and Giarda [73] is reformulated to render it suitable for analysis of extrusion through square dies. Using this, the non-dimensional extrusion pressures for various reductions are computed for extruding square bars through square dies. Results are compared with the experimental data of Chitkara and Adeyemi [74] and with the slip line field solution of Das and Banerjee for plane strain extrusion.
1996	Sahoo et al. [76]	Upper Bound Analysis of Extrusion of Hexagonal Section Bars from Rectangular Billets through the Square Dies	The reformulated SERR technique is applied for analysis of extrusion of hexagonal bars from square/ rectangular billets through the square dies. Non-dimensional extrusion pressure at various area reductions has been computed for the different billet aspect ratio. The results are compared with the slip line field solution of the equivalent plane strain condition and found satisfactory.
1997	Kar and Sahoo [77]	Application of the SERR Technique to the Analysis of Extrusion of Section from Round Billets	The SERR technique is applied for extrusion of square bars from round billet. The circular section of round billet is approximated by a regular polygon of equal area and the number of sides of the polygon is progressively increased until convergence of the extrusion pressure is achieved.
1997	Sahoo et al. [78]	SERR Technique for Extrusion of Triangular Section Bars from	The authors have developed an analytical method based on the upper-bound theory to investigate the extrusion of triangular section bars from square/rectangular billets through the square dies by using SERR (Spatial Elementary Rigid Region) technique. The non-dimensional extrusion pressure at various area reductions is computed for different billet aspect ratios

		Square/Rectangular Billets through Square Dies	assuming unequal dead metal height at corner points by using SERR technique. The results have been computed with the slip line field solution of the equivalent plane-strain condition.
1998	Sahoo et al. [79]	Upper-bound analysis of the extrusion of a bar of channel section from square / rectangular billets through square dies	The extrusion of bars of channel section from square or rectangular billets through a rough square dies has been presented by an upper-bound analysis. A class of kinematically admissible discontinuous velocity fields, based on the reformulated SERR technique, is calculated and the lowest upper-bound is identified. They also computed the upper-bound extrusion pressure for various area reductions and three points' formulations. The triple point formulation gives the lowest upper-bound to the non-dimensional average extrusion pressure for the extruding channel section bar.
2000	Kar et al. [80]	Upper bound analysis for Extrusion of T-section Bars from Square Billets Through Square Dies	Upper bound analysis of extrusion of T-section bars from square billets through the square dies using the modified SERR (Spatial Elementary Rigid Region) technique is carried out. Optimized values of the non-dimensional average extrusion pressure at various area reductions and three formulations (single-point, double-point and triple-point) have been computed and compared with experimental results. It seems that the SERR technique as reformulated provides a useful tool for the analysis of extrusion of sections with re-entrant corners. There is a good agreement between computed and experimental results.
2000	Sahoo [81]	Comparison of SERR analysis in extrusion with experiment.	The author has carried out experimental work to compare some of the theoretical results predicted using SERR analysis. Experiments are performed for hexagon, channel, triangle and cross-type sections from rectangular billets using square dies. The upper-bound analysis of extrusion of different sections through square dies can be carried out by using proposed discontinuous velocity field. The theoretical results are compared with experimental non-dimensional mean extrusion pressure and it is found to within 14% variation.

Sahoo et al. [82] has analyzed the extrusion of hexagon-section bars from round billets through linearly converging dies. It is found that, the optimal dies-geometry (the equivalent semi-cone angle) can be obtained for different reductions of the area and friction conditions for reasonable upper-bound extrusion pressures. This can be extended to obtain the solution of generalized problems of non-axisymmetric extrusion or drawing through converging dies. Sahoo and Kar [83] have investigated the drawing of hexagon section bars from round billets through the straightly converging dies. The SERR technique is eminently suitable for analyzing drawing/extrusion of sections having re-entrant corners. The approximation of the curved surface to planer surfaces and the three-dimensional nature of the problem give higher value, which can be minimized by increasing the number of sides of the polygon and the number of floating points. It can be concluded that for the limited purposes, the present technique can be extended to obtain the solution for generalized non-axisymmetric drawing or extrusion through converging dies. Sahoo [84] applied Upper Bound Theory (SERR technique) for investigation of non-axisymmetric extrusion of T-section bar from round billet through a straight taper die. Computation for the upper bound pressure is carried out for various process variables such as area reduction, die angle and interface friction. The theoretical results are compared with experiments and found to be well within engineering tolerance. Sahoo et al. [85] has analyzed the spatial elementary rigid region (SERR) technique for extrusion of the section having re-entrant corners and the extrusion of triangular section bars from round billets through linearly converging dies. The circular cross-section of the round billet is approximated by a regular polygon of equal area and the number of sides of the approximating polygon is progressively increased until convergence of the extrusion pressure is achieved. Sahoo et al. [86] investigate an upper bound solution for the extrusion of channel section from round billet through the taper die. The rigid-perfectly plastic model of the material is assumed, and the spatial elementary rigid region (SERR) technique is presented for which the kinematically admissible velocity field is found out by minimizing the plastic dissipation of power. The comparison made with prior experimental results shows that the present solution can predict reasonable upper bound extrusion pressure.

2.4.3 Gear shape extrusion

Chitkara and Bhutta [87] analysis based on an upper bound elemental technique is presented for the incremental forging of a near-net shaped splined rotor shaft-type component formed using a cylindrical rod-type specimen. The experimental investigation consists: prediction of working pressures and observations of deformation modes during progressive forging of tellurium-lead specimens of different aspect (length to diameter) ratios into spline shaped components and compared with those predicted theoretically. There was good agreement between theoretical and experimental results. The forging of spur gear has been analyzed by the upper-bound method by Choi et al. [88]. The tooth profile consists of an involute curve and a circular arc shapes fillet. A kinematically admissible velocity field has been proposed. It can be seen from their experimental result that an axisymmetric deformation zone exists. The fractional radius obtained by the analysis increases with increasing of the number of teeth and increases abruptly near the final filling up stage. Good agreement was found between the predicted values of the forging load, and those obtained from the experimental results. Chitkara and. Bhutta [89] presents the results of an experimental investigation carried out in quasi-static incremental upset-forging of spur gear forms around the periphery of initially solid cylindrical billets, the outer radius of each of which was of the same size as the radius of the dedendum circle of the spur gear to be forged. The punch or die used was of the same size and shape and had the same number of teeth at its circumference as that in the female stationary die and correspond to the shape and size of the gear to be forged in each case. For the analysis, an upper bound elemental technique was applied to forging spur gear forms having the actual profile teeth around its circumference each with the pressure angle of $14\frac{1}{2}^{\circ}$. The results of theoretical investigations presented here are confirmed with experiments and are compared with the upper bound analysis. Closed-die forging of external spline gear forms is analyzed by Chitkara and Kim [90] using an upper bound elemental energy method. The kinematically admissible velocity field for the three-dimensional deformation was obtained on the assumption that the profiled surface of the tooth was straight but tapered. The upper bound to the deforming load necessary and the deformed configurations are predicted using integration of the formulation of energy expressions, which were obtained from the presented velocity fields. The theoretical results compared with the experimental

ones. Experiments were carried out on plasticine as model material at room temperature where the talcum powder was used as a lubricant. Two different forging methods denoted here as A, viz. a side extrusion method and B, an upset forging method was considered in their analysis. The investigation revealed that the analytical method B predicts a reduced forging load and improved configuration better than method A for the forged products. Cho et al. [91] investigated on closed-die forging of spur gears, of which the shape of the fillet is a straight line in the radial direction, by the upper-bound method. A kinematically admissible velocity field has been proposed. An involute curve has been introduced to represent the tooth profile of the forging die. It was found that forging load or average relative pressure was dependent, predominantly on the number of teeth. Precision forging is an important manufacturing procedure of spline and spur gear forms. It has advantages of improved strength, good tolerance, saving billet material, dispensing with the cutting, etc. Hsu [92] proposed a mathematical model using an upper bound method for forging of spur gear forms and spline to investigate the plastic deformation behavior of billet within the die cavity. The material of solid billet was assumed as rigid-plastic and the shape of the tooth profile was accounted for the mathematical modeling of the kinematically admissible velocity field assumed for the plastic zone. The non-uniform velocity was employed for simulating the inhomogeneous deformation and the effect of barreling during the forging. Using the model, various effects of forming parameter such as the friction factor, reduction, the number of teeth, etc. upon the non-dimensional forging pressure, forging force and barreling of the spur gear forms and spline were analyzed systematically and the results compared with those of other researcher's analytical and experimental work. It was shown that the present modeling of the process improves knowledge of the process design performance for the precision forging of spur gear form and spline. Altinbalik and Can [93] investigated the lateral extrusion of splines in terms of the load requirements and die filling. The upper bound method has been employed to investigate the load requirement for different process parameters, to this effect; kinematically admissible velocity fields have been developed. The experiment has been carried out using solid lead billets with two different diameters. The theoretical prediction of forming load is compared with experimental results. The predicted load values are higher than the experimental values during the tooth formation period but lower than the experimental values during the corner filling

stage. Metal flow in the tooth region is not uniform and barreling occurs due to frictional resistance between the work piece, and the die gap surface.

2.5 FEM Analysis

The finite element method (FEM) was developed for elastic analysis of airplane structure in the 1950s. In this method a plate was divided into many hypothetical elements, and equations of equilibrium at nodal points were made. Since the equations were linear in terms of the nodal displacements, they were suitable to be solved by the matrix method using digital computers, which just became to be usable in some limited research facilities in the USA. In 1967 Zienkiwicz and Cheung published a book entitled “The finite element method in structural and continuum mechanics” [94], in which the method explained in detail with the software written in FORTRAN language. Referring to this book, many groups in the world began to develop software because digital computers had become usable in many countries. The elastic-plastic FEM was developed as an extension of elastic FEM. In 1967, Marcal (Brown University) and King [95] published a paper of elastic-plastic analysis of plate specimen with a hole in which the development of plastic zone. In 1967, Hayes and Marcal [95] presented a paper of the usage of the FEM for optimizing the upper bound method of a plane stress problem. In the case of the plane stress problem, the stress state could be calculated from the optimized velocity field, but this was not true for other cases. In the late 1980s the rigid-plastic finite element method was expanded to three dimensional problems and was installed in commercial software. Maccarini et al. [97] correlating some relevant data obtained from the experimental with the theoretical results using FEM, the authors offer the solution to some plastic deformation processes expressing the frictional tangential stress on the upset surface as a function of the friction coefficient in order to find a solution consistent with the adherence existing between die and piece. A rezoning (i.e., a mesh reassembling) is introduced whenever either relevant changes in constraint conditions or geometrical non-conformability of the elements take place. Within the limits of the experimental tests performed (reverse extrusion and extrusion forging) they conclude that the FEM method integrated with the reasoning reassembling procedure offers a powerful tool for the evaluation of both the actual deformed shape and the compression force. Cold forging need for quick product and process design. Process simulation can assist the forging designer in establishing and optimizing process variables and die design. Cold

forging involves typically several preforming (sequence) operations and fractures are often a limiting factor due to severe deformation during cold forging. Die stress is potentially very high causing dies failure and die deflection should be considered to satisfy forging tolerance requirements. Oh et al. [98] demonstrate the capabilities of the DEFORM[®] system for automatic mesh generation and remeshing which is an essential feature for industrial applications. The design of the complex cold forging process has been mainly achieved based on experience and trial and error. Development of the process simulation technology enables a designer to study and even optimize the cold forging process on a computer before actual tryout which reduces process design cost and time. Meidert [99] in their analysis, using two modeling techniques, finite element (FE) based numerical modeling and physical modeling with plasticine, presented a process for tool design in cold forging. A strategy has been developed to allow successful 2D FE modeling of bevel gear forging. The results from the process simulation are then used as load input data for a punch stress analysis. It is, thus, possible to modify the punch geometry in order to reduce the punch stresses. Physical modeling is then applied to verify the results of the 2D FE simulations. Reinikainen et al. [100] in their research work studied the finite-element simulation of various axisymmetric extrusion processes applied to copper using both flat-faced and converging dies with two frictional conditions. The extrusion was assumed to be isothermal and under plane strain condition. It was found that the results of the FEM simulation agreed well with the laboratory experimental results. Knoerr et al. [101] summarizes some of the industrially relevant research results obtained by FEM analysis, including the prediction of flow-induced defects, precision forging of aluminum alloys, investigation of a suck-in type extrusion defect, forging of bevel gears, stress analysis of forging dies, and development of a new test to evaluate lubrication in cold forging. Kim et al. [102] summarizes the results of industrially relevant "work-in-progress" research with the FEM systems. Their investigation includes: a new tool design for cross groove inner race for a constant velocity joint, the flashless forging of an aluminum connecting rod, design of cold forgings and forming sequences, die wear in warm forging extrusion, and simulations of a connecting rod, blade coining, and wire drawing of shapes. They conclude that in order to facilitate finite-element simulations and to make this design technique more economical, automatic meshing and remeshing, as well as optimization of the mesh-density distribution, are necessary. Wu and Hsu [103] studied the influences of

various die shapes on extrusion and forging deformation using the finite element method. The effects of draft angle and the fillet radius on extrusion load, the boss height, the flange width, strain are studied. Experiments using two sets of dies with different shapes have been performed, the results being in accordance with the FEM analysis of the deformation mode. The results of the influence of the die shape on the flow deformation in this study could be expanded to the design of a more complicated pre-forging die and the planning of the forming process. Cho et al. [104] investigated the process design of a forward and backward extruded axi-symmetric part. The important factors in the cold forging of an intricate part are the shape of the initial billet, number of stages of operations, as well as the shape of the pre-form. Numerical simulation of the cold forging operation has been carried out using the commercial finite element software. The design criteria for the operation are the forming load, defect-free geometrical filling of the dies and sound distribution of strain in the final product. The numerical simulation result was confirmed to be good in agreement with experimental results. Zhou et al. [105] attempts to explore the possibilities of using the updated lagrangian approach to simulate the aluminium extrusion process both in the transient state and in the steady state. It was conducted to reveal the non-steady characteristics of the process of extruding complete billet with an L/D ratio of 4 into a solid cross shaped profile. Yang and Lee [106] use finite element analysis software, MARC[®], to simulate the process for a subject material undergoing equal channel angular extrusion (ECAE), as well as calculating the strain conditions. It was concluded that for a single ECAE pass simulation, influential factors are channel angles and joining. Fang et al. [107] investigate the effect of steps in the die pocket on metal flow to produce two chevron profiles with unequal thicknesses through two-hole dies, by means of 3D FEM simulation of extrusion in the transient state. The results showed that the pocket step could be effectively used to balance the metal flow. Extrusion experiments validated the predictions of metal flow, extrusion temperature and the pressure required for extrusion through the pocket dies with different designs. 3D FEM was demonstrated to be a powerful tool in optimizing die design and decreasing the number of trial extrusion runs. Farhoumand and Ebrahimi [108] present the analysis of forward-backward-radial extrusion process. Finite element method has been used to investigate the effect of geometrical parameters such as die corner radius and gap height as well as process condition such as friction on the

process. ABAQUS[®] software is also used by many researchers for finite element simulations. The finite element results are compared with experimental data in terms of forming load and material flow in different regions. Hardness distribution in longitudinal cross-section of the product is also used to verify strain distribution obtained from finite element analysis. The comparison between the theoretical and the experimental results show good agreement. The relation between hardness and strain value is compatible with previous work of the authors. Qamar [109] investigates the effect of shape complexity on the dead metal zone (DMZ) and metal flow through cold extrusion experiments and finite element simulations on some solid profiles. Experiments were performed using flat-face dies of different complexities and different billet materials. 2D and 3D finite element simulations were carried out. One significant conclusion is that currently existing definitions of extrusion shape complexity cannot satisfactorily explain the variations in DMZ size under different conditions. Factors such as die profile symmetry and extrusion ratio may play significant roles in the formation of DMZ and distortion of metal flow through the die. Jafarzadeh and Zadshakoyan [110] present numerical and experimental study of spline production with an injection forging process, in terms of load requirement and material flow. A three-dimensional finite element model has been developed to analyze the effect of initial billet diameter, number of spline teeth, and die corner radius of the required forging load, pattern of material flow, and effective strain distribution. Also, a series of experimental tests has been carried out using solid commercial lead billets with two different billet diameters and three different die cavities (two, three, and six teeth). The results obtained using the numerical solutions were compared with the experimental data for each case study and good agreement was observed. Both the simulation and experimental results highlight the major role of the above-mentioned parameters on the required forming load and material flow pattern. It has been shown that the initial billet diameter and the number of spline teeth have significant effects on the forming load. Although, the die corner radius has little effect on the required forming load, it is an important factor in forming the material flow pattern and strain distribution.

2.6 Closure

Present chapter highlights the importance of metal forming processes and its past developments. For the sake of simplicity, it is divided into five main sections and

three subsections. Section 2.1 focused on the brief history and birth of metal forming processes. Section 2.2 describes some of the pioneer's noble gift to the field of metal forming. Different researchers proposed the slip-line field method for different practical application such as extrusion, rolling, drawing and metal cutting. A good number of research works were reported during 1950s to 70s using this technique. Section 2.3 reviews the literature on the slab-method applied to metal forming process. In the 1950s in the USA and UK, and in the 1960s in Japan [1], automation of the strip rolling in steel industry began, and many engineers studied and enriched these theories in the industry. Section 2.4 reviews the detail literature on upper-bound theory applied to the extrusion process. Mainly, extrusion processes are achieved either through converging dies or square dies. Emphasize is given to the square dies extrusion process in present work. Sub-section 2.3.1 focused on extrusion of gear like elements. Section 2.4 reviewed with the finite-element analysis of different section extrusion through different shapes dies. Commercially available Finite element analysis software packages, due to its flexibility and versatility, are becoming popular among the researchers.

From the reviewed papers, it is observed that, a good number of works are reported on extrusion for the different sections from cylindrical billet. Very few works were reported on the extrusion-forging process and gear like element extrusion. Sahoo et. al. [80,81,82,83,85] present a discontinuous kinematically velocity field to analysis the extrusion of non-symmetric sections, no attempt has been made till now to adopt this technique to the combined extrusion-forging process. The present work attempts to fill this gap and gives a sincere effort to extend this technique for combined extrusion-forging of different head shapes. The results are also validated with that of experimental and finite element analysis.

Upper Bound Techniques for Three Dimensional Metal Deformation Problems

3.1 Introduction

For many metals working operations, exact solutions for the load to cause unconstrained plastic deformation are either non-existent or too difficult to compute. Accordingly, means have been sought whereby this load can be established approximately. Two such approximate methods have found extensive application in the analysis of quasi-static metal forming process, viz., the upper bound (over estimation of load), and the lower bound (under estimation of load) techniques. Attention has been consolidated on obtaining upper bounds to the yield point load, since, in metal forming processes, over-estimate constitutes a safe load. This technique has played a dominant role in the analysis of three-dimensional metal deformation process. Because it gives a complete solution to the problem consists of an equilibrium stress field and the associated velocity field satisfying the deformation occurs even with the rigid-plastic assumption and does not violate the yield criterion in the rigid region. Besides, other available analytical techniques such as Hill's [38] general method is usually not suitable to deal with problems involving complex geometries.

The upper bound solution is constructed on a kinematically admissible velocity field. A velocity field that satisfies the compatibility, flow rule and the velocity boundary conditions both in the rigid as well as the plastic zones is known as kinematically admissible velocity field. When the admissible velocity field is determined, upper bound to the deformation load is estimated from virtual work principle by equating the rate of external work done to the rate of energy dissipated.

For a continuum deforming plastically in contact with a die, the rate of energy dissipated, J , is given by the relation

$$J = J_1 + J_2 + J_3 \quad (3.1)$$

where,

J_1 = internal power dissipated due to plastic deformation,

J_2 = power for shear deformation against the velocity discontinuities, and

J_3 = frictional power dissipated at the tool/work interface.

For a material obeying Levy-Misses flow rule, the internal power J_1 is given by

$$J_1 = \frac{2\sigma_0}{\sqrt{3}} \int_v \sqrt{\frac{1}{2} \dot{\varepsilon}_{ij} \dot{\varepsilon}_{ij}} dv \quad (3.2a)$$

Where,

σ_0 = yield stress in uniaxial tension, and

ε_{ij} = strain rate tensor defined as,

$$\varepsilon_{ij} = \frac{1}{2} \left[\frac{\partial V_i}{\partial V_j} + \frac{\partial V_j}{\partial V_i} \right] \quad (3.2b)$$

Here, V_i and V_j represent the velocity components in Cartesian coordinates. Evidently, the internal power is computed by integrating Von-Misses work equation [33] over the total volume V_0 .

The power of shear deformation J_2 , along the velocity discontinuity surface S_i in the deformation zone is given by

$$J_2 = \frac{\sigma_0}{\sqrt{3}} \int_{S_i} |\Delta V|_{S_i} dS_i \quad (3.3a)$$

Finally, the friction power J_3 , dissipated at the tool/work piece interface is determined from the relation,

$$J_3 = \frac{m\sigma_0}{\sqrt{3}} \int_{S_{D_i}} |\Delta V|_{S_{D_i}} dS_{D_i} \quad (3.3b)$$

where, m is the friction factor and $|\Delta V|_{S_i}$ and $|\Delta V|_{S_{D_i}}$ are the magnitude of velocity discontinuity at the surfaces S_i and S_{D_i} respectively.

The power J , calculated from equation (3.1), will be exact when the kinematically admissible velocity field postulated for the forming process under consideration is the actual one. But, if it is different from the actual, equation (3.1) yields an upper bound to the power necessary for the forming operation in question. This is precisely the upper bound method as suggested by Hill [38] for a rigid-perfectly plastic material.

This chapter highlights the various techniques normally employed to derive kinematically admissible velocity fields in case of three-dimensional metal deformation problems. While such techniques for plane-strain problems are well established [119, 43, 45] similar procedures for three-dimensional problems are relatively recent. Sahoo et al [80,81,84,85] proposed a kinematic velocity field for analysis the extrusion of different sections from rectangular and cylindrical billet. The present work aims to extend this technique to combined extrusion-forging process. The following section briefly presents the construction process of the kinematically admissible velocity fields by this technique in general.

3.2 Mechanics of Metal Forming

The theory of plasticity is the formulation of the mathematical relationship of stress and strain in plastically deforming solid (metals). The governing equations for the solution of the mechanics of plastic deformation of rigid-plastic materials must satisfy equilibrium equations, stress-strain relations, yield criterion, compatibility equations, boundary condition on stress, and boundary condition on the velocity and volume constancy. As the strain involved in the plastic deformation process is very large, it is usually possible to neglect elastic strain and consider only the plastic strain (rigid-plastic region). The strain hardening is also neglected to formulate the analysis simpler.

In most cases, the unknowns for the solution of a quasi-static plastic deformation process are six stress component and three strain rate. The governing equations are three equilibrium equations, the yield condition and six stress strain relations derived from flow rule. The boundary conditions are prescribed in terms of velocity and traction. Along the tool-die interface the velocity component is prescribed in the direction normal to the interface and the traction is specified by the frictional stress in the tangential direction.

Since it is difficult to obtain a complete solution that satisfies all the governing equations, various approximation methods have been devised depending upon the assumption and approximation, order of complexity and availability to predict final results. Some most well-known solution methods are:

1. Slab or stress equilibrium method
2. Slip-line field analysis,

3. Limit analysis,
4. Weighted residual technique,
5. Finite element method.

3.2.1 Slab or Stress equilibrium method

The slab method of solution assumes that the stresses on a plane or spherical surface perpendicular to the direction of flow are principal directions. The stress values are fixed on a plane. A slab straight or curved of infinitesimal thickness is selected parallel to this plane at any arbitrary in the deformed metal. A force balance is made on this slab that will result in a differential equation of static equilibrium condition. The differential equation is then put into an integral form with boundary conditions. The boundary conditions determine the forming forces.

3.2.2 Slip-line field theory

This method is developed to analyses non-homogenous plane strain deformations of a rigid-perfectly plastic isotropic solid. In this method the velocity and stresses lie in a plane and does not vary with respect to the third co-ordinate axis. The solution consists of a number of maximum and minimum constant shear lines that form a network of lines which are right angles wherever they intersects in the plastic flow field. These shear lines satisfy static equilibrium, yield condition and a possible flow field everywhere in the plastic zone of metal. Slip-line patterns can often be obtained from the stress and the yield conditions.

3.2.3 Limit analysis

The exact load or force calculation for plastic flow of metals is often difficult. Exact solution requires the both stress equilibrium and geometrical self-consistent flow patterns of flow that satisfy throughout the deforming body. Limit theorem permits force calculations which provide values that are known to be either lower or higher than the actual force.

3.2.3.1 Lower bound theorem

Lower bound solution will give a load predication that is less than or equal to the exact load cause a body to experience full plastic deformation. The lower bound is associated with the principle of maximum work. The stress field that describes the stress distribution within the deforming region should be continuous, obey the

equation of equilibrium, satisfy the surface traction and obey the yield criterion. If these entire requirements are met than the stress field is called statically admissible stress field. It states that among all statically admissible stress fields the actual one maximizes the deformation load. So the theorem is a safe calculation in the design of structures that are not intended to deform plastically.

3.2.3.2 Upper bound theorem

An upper bound solution will give a load predication that is greater than or equal to the exact load cause a body to experience full plastic deformation. The upper bound is also associated with the principle of maximum work, but in the point of view of strain. It states that among all kinematically admissible velocity fields the actual one minimize the deformation load. A kinematically admissible velocity should satisfy the continuity equation, velocity boundary condition and volume constancy condition. In metal forming operations, it is of greater interest to predict a force that will cause the body to deform plastically to produce the desired shape change. Upper bound analysis focus upon satisfying a yield criterion and assuring the shape changes are geometrically self-consistent.

3.3 General Techniques for deriving the Kinematically Admissible Velocity Fields in Three- Dimensional Metal Deformation Problems

Numbers of techniques have been reported to find out kinematically admissible velocity fields for three-dimensional metal forming problems. These are,

1. The Dual stream Function Method,
2. The Conformal Transformation Technique,
3. The Generalized Velocity Field Technique, and
4. The SERR Technique.

The first three techniques mentioned above lead to continuous velocity fields in the deformation region where the velocity at any point is described by a continuous function of the space coordinates, whereas, the last method leads to a discontinuous velocity field.

The following sections outline the salient features of these techniques and their limitations.

3.3.1 The dual stream function method

For ideal fluid flow in three dimensions, Yih [32] suggested the use of two stream functions in place of one as in the case of two-dimensional flow. Each stream function represents a class of surfaces called stream surfaces. The line of intersection of two stream surfaces, one taken from each class, is the three-dimensional stream line. Nagpal [116] used these dual stream functions to determine kinematically admissible velocity fields for different three-dimensional plastic flow problems.

Let $\Psi_1(x, y, z)$ and $\Psi_2(x, y, z)$ be two continuous functions. These two can be treated as a pair of dual stream functions if they satisfy the boundary conditions on velocity. The three velocity components are then given as

$$V_x = \left(\frac{\partial \Psi_2}{\partial y} \right) \left(\frac{\partial \Psi_1}{\partial z} \right) - \left(\frac{\partial \Psi_1}{\partial y} \right) \left(\frac{\partial \Psi_2}{\partial z} \right) \quad (3.4a)$$

$$V_y = \left(\frac{\partial \Psi_2}{\partial z} \right) \left(\frac{\partial \Psi_1}{\partial x} \right) - \left(\frac{\partial \Psi_1}{\partial z} \right) \left(\frac{\partial \Psi_2}{\partial x} \right) \quad (3.4b)$$

$$V_z = \left(\frac{\partial \Psi_2}{\partial x} \right) \left(\frac{\partial \Psi_1}{\partial y} \right) - \left(\frac{\partial \Psi_1}{\partial x} \right) \left(\frac{\partial \Psi_2}{\partial y} \right) \quad (3.4c)$$

When the velocity field is generated through equations (3.4a, 3.4b and 3.4c), becomes kinematically admissible since the continuity condition is implicitly satisfied. The only limitation of this procedure is that it may be extremely difficult to find dual stream functions when the section shape is complex or when it involves re-entrant corners.

3.3.2 The conformal transformation technique

In ideal fluid flow problem in three dimensions, the equation of a stream line is given by

$$\frac{dx}{V_x} = \frac{dy}{V_y} = \frac{dz}{V_z} \quad (3.5)$$

By finding a transformation function that transforms an intermediate section in the deformation zone along the axis into a unit square (or circle), it can be stated as

$$\frac{dx}{F(x, y, z)} = \frac{dy}{G(x, y, z)} = \frac{dz}{1} \quad (3.6)$$

Functions F and G depend upon the parameters of the section geometry which are functions of x, y and z. Comparing equations (3.5) and (3.6) we get,

$$\frac{V_x}{F(x, y, z)} = \frac{V_y}{G(x, y, z)} = \frac{V_z}{1} \quad (3.7)$$

The axial velocity component V_z is found by applying the continuity condition (or volume constancy condition) to the deformation zone. Thus,

$$V_x = \frac{A_b V_b}{A(z)} \quad (3.8)$$

Where,

A_b, V_b = billet cross-section area and billet velocity respectively, and

$A(z)$ = cross-sectional area of the die cavity at any point on z-axis.

Hence, velocity components V_x and V_y can be calculated using equation (3.8).

The present method is similar to the dual stream function method (section 3.3.1) in the sense that in either case the velocity at any point in the deformation zone is calculated from the corresponding equation to the stream line through that point. But this method is more versatile and can deal with problems involving relatively complex geometries for which dual stream functions may be very difficult to guess. With all its advantages, however, its application is limited to only such sections where the product shape is similar to that of billet. Hence, it is more suitable for polygonal sections with axial symmetry (sections that can be inscribed in a circle) but may lead to considerable difficulties when dealing with sections with re-entrant corners.

3.3.3 The generalized velocity field technique

The Conformal Mapping Technique discussed in the preceding section suffers from three basic limitations. Firstly, for a mapping function to exist, the sectional symmetry must be maintained throughout the deforming region. Further, the surfaces of velocity discontinuity at entry and exit must be assumed planar and the velocity across any intermediate section in the deforming zone must be assumed constant so that it can be calculated from the continuity condition. Hence, the conformal mapping technique can be applied only to limited problems.

When the billet and the product shapes are dissimilar, section symmetry does not exist in the deforming region. Such a situation is encountered when a polygonal shape is extruded from a round billet. To deal with such problems, Yang and his associates [61] have recently proposed a method in which the velocity at any point in the deformation zone is expressed as a general function of the space coordinates. The proposed method has none of the limitations of the conformal mapping technique and has been used to analyze extrusion of clover and regular polygonal sections from round billets. The method is also suitable for predicting intermediate shapes of the die profile when extrusion is carried out with the help of converging dies. However, this method is tedious and involves a considerable amount of computation for prediction of upper bound load.

3.3.4 The SERR technique

The SERR (spatial elementary rigid region) technique as a method for analyzing three-dimensional metal deformation problems was first proposed by Gatto and Giarda [73]. The distinguishing feature of this technique is that the deformation zone is discretized into rigid regions thus providing a discontinuous velocity field in the deformation zone.

In a plane strain situation, the velocity in a rigid region is determined when its components along two mutually perpendicular directions are known. Thus, the problem involves only two unknowns and two equations are necessary to determine the unknowns considering the mass continuity condition on any two faces bounding this rigid region. Hence, the planar elementary rigid region is always a triangle and this has formed the basis for the construction of the well-known velocity fields by Johnson and Kudo [43] for plane strain extrusion (Figure 3.1(a) and (b)). In a three-dimensional deformation problem, however, the spatial velocity in a rigid zone has three unknown components and their determination necessitates the setting up of three equations from the mass continuity condition. Thus, the spatial elementary rigid region for a three-dimensional deformation problem is tetrahedral in shape. This is the basis of the SERR technique as proposed by Gatto and Giarda [73].

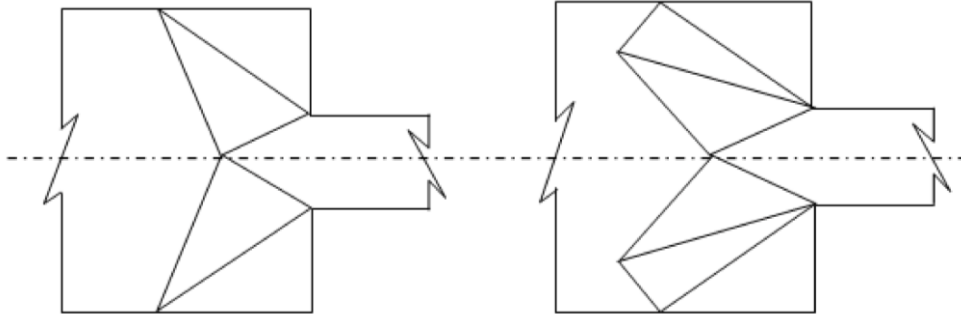


Figure 3.1. (a) Johnson's velocity field (b) Kudo's velocity field

The above investigators analyzed the extrusion of square sections through wedge shaped dies with the help of the SERR technique. They also suggested methods by which complex geometrical shapes like prism and pyramids can be discretized into elementary tetrahedrons. The limitation of this technique appears to be that it can be applied only when the deformation zone is bounded by planar faces.

3.4 Discretization of Deformation Zone in Section Extrusion

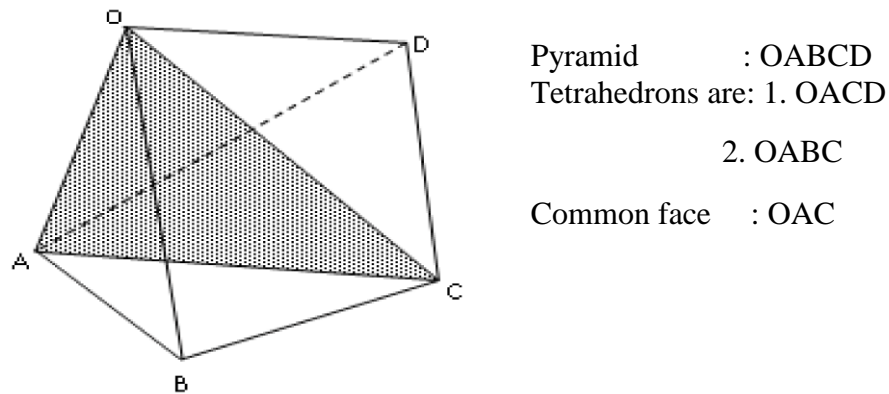


Figure 3.2. Discretization of a pyramid into tetrahedrons

The deformation zone in section extrusion may consist of simply a pyramid or a combination of pyramids and prisms (as in case of extrusion of sections having re-entrant corners). A pyramid can be discretized into two tetrahedrons (Figure 3.2). These two tetrahedral regions have two internal velocity vectors (one for each region) having six spatial components and the exit velocity can be represented by a single component by suitably choosing a coordinate frame. When the inlet velocity for this pyramidal zone is prescribed, there are seven unknown velocity components to be determined to establish the velocity field. Thus seven equations are necessary and sufficient to determine the velocity field. Further, two tetrahedrons of a pyramidal region have a

common face amounting to seven independent bounding faces. On applying the continuity condition, a set of seven equations is generated which contain the unknown velocity components enumerated above. On solving this set of seven velocity equations, a unique velocity field is determined. In a similar fashion, a prism can be discretized into three tetrahedrons with ten independent bounding faces that can generate a set of ten velocity equations for establishing the corresponding velocity field. The discretization of a prism into tetrahedrons is shown in Figure 3.3. When a deformation zone consists of a combination of pyramids and prisms, their discretization into tetrahedrons and subsequently application of continuity condition to all the independent bounding faces, generate a system of determinate velocity components.

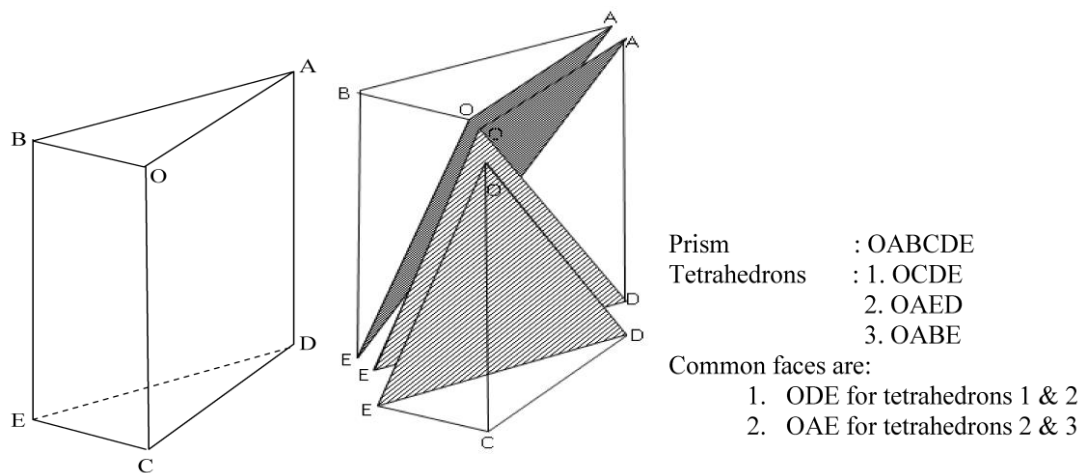


Figure 3.3 Division of a prism into three tetrahedrons

3.5 The Continuity Condition of a Discontinuous Velocity Field

As described in the previous section, in the SERR technique, the deformation zone is envisaged to consist of tetrahedral rigid blocks and each block separated from other by planes of velocity discontinuity. Each rigid block has its own internal velocity vector consistent with the bounding conditions. If there are N rigid blocks, then the number of unknown internal velocity vectors is also N and there by $3N$ spatial velocity components. The velocity at entry to the deformation zone (the billet velocity) is normally known. The exit velocity (product velocity) is assumed to unidirectional (coincide with extrusion axis, i.e., z -axis of the proposed coordinate system) and has a single component. Therefore, the total number of unknown velocity components in the global level is $3N+1$. The unknown velocity components can be determined if an equal number of equations is generated. This is done by applying the mass continuity

condition to the bounding faces of all the tetrahedral rigid blocks taken together. The set of velocity equations so generated becomes consistent and can be determined only if the SERR blocks are tetrahedral in shape, where the number of triangular bounding faces is $3N+1$.

To illustrate the application of the above principles, let the equation of the i^{th} bounding face in the assembly of tetrahedrons be

$$\phi(x, y, z) \equiv a_{i1}x + a_{i2}y + a_{i3}z + 1 = 0 \quad (3.9)$$

The coefficients, a_{i1} , a_{i2} and a_{i3} can be determined by specifying the coordinates of the three vertices of the concerned triangular face. Then the unit normal vector to this face is given by the relation

$$\hat{n} = \frac{\nabla\phi}{|\nabla\phi|} \quad (3.10)$$

Figure 3.4 shows a surface separating two spatial regions with \vec{V}_1 and \vec{V}_2 as the velocity vectors on both sides. The components of these two vectors normal to the separating surface ϕ are given by the following equations:

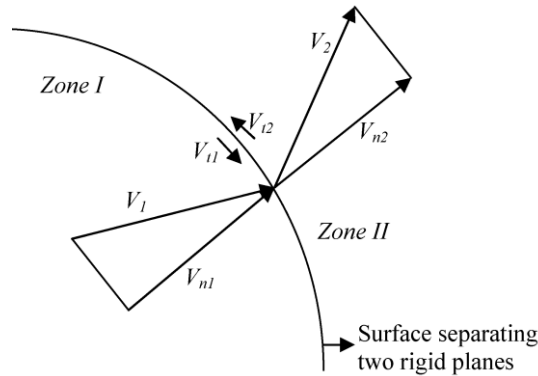


Figure 3.4 A general surface separating two rigid regions

$$V_{n1} = \hat{n}\vec{V}_1 = \frac{\Delta\phi}{|\Delta\phi|}.\vec{V}_1 \quad (3.11)$$

$$V_{n2} = \hat{n}\vec{V}_2 = \frac{\Delta\phi}{|\Delta\phi|}.\vec{V}_2 \quad (3.12)$$

If A and ρ denote the area of the surface segment and the material density respectively, then $A\rho V_{n1}$ and $A\rho V_{n2}$ are the mass flow rates across the surface segment taken from both sides. Applying the mass continuity condition and equating V_{n1} and V_{n2} gives

$$\Delta\phi\vec{V}_1 = \Delta\phi\vec{V}_2 \quad (3.13)$$

It may be noted that the regions on both sides of the surface ϕ (Figure 3.4) are rigid if \vec{V}_1 and \vec{V}_2 are constant vectors, i.e., when the equation (3.13) is linear. The linearity of equation (3.13) is assured when the surface ϕ is a plane. Thus the bounding faces of the spatial elementary rigid regions can only be planar. Some of these bounding faces may lie on the die surface (or, the dead metal surface in case of square die), or on planes of symmetry. Since no material flow occurs across such faces, equation (3.13) takes the following form:

$$\Delta\phi\vec{V}_1 = 0 \quad (3.14)$$

The equation of each of the triangular faces can be determined when the coordinates of the three vertices are specified. Then the velocity equations can be formed by applying the mass continuity condition either in the form of equation (3.13) or (3.14) as applicable. The velocity of material in the zones I and II are V_1 and V_2 respectively are not identical. The components of velocity in the normal and tangential direction of the surface are, V_{n1} , V_{n2} and V_{t1} , V_{t2} . The normal velocity V_{n1} should be equal to V_{n2} for the continuity of the material. The tangential velocity V_{t1} and V_{t2} need not be equal. The difference is called the velocity discontinuity ΔV and is given as follows:

$$\Delta V = V_{t1} - V_{t2} \quad (3.15)$$

Such equations are formulated for each of faces bounding the rigid regions to give a determinate set of equations. This set of equations, when solved, generates the velocity components in the rigid regions constituting the deformation zone. For a plane strain problem the above solution is conveniently carried out graphically by the hodograph method [43, 45,119]. For a three-dimensional problem involving complex geometry, however, such a method will be extremely tedious and a digital computer has to be used to generate the velocity vectors in the deformation zone. The basic advantage in formulating the equations (3.13) and (3.14) based on continuity condition is that the

solution to the velocity equations can be carried out conveniently by numerical computation.

3.6 Solution of a Plane Strain Problem

The method of solution elucidated in the previous section is illustrated taking the example of a plane strain extrusion process. The geometry of the process is shown in Figure 3.5 for a rough square/flat die. Dead metal zones ABC and DEF are formed on both sides of the extrusion axis. Only one half of the deformation zone, consisting of the triangle ABO, is considered for this analysis. Thus, this triangle is a single planar elementary rigid region is bounded by lines AB, BO and OA which are also lines of velocity discontinuity. Since the extrusion axis is presumed to coincide with x-direction, the billet and product velocity vectors have only one component each. It may be noted that a and W are known parameters, being the half widths of the product and the billet respectively. L , the distance of the floating point O from the midpoint of the die orifice and H , the overall length of the deformation zone along the extrusion axis are two unknowns. These two variables are to be selected such that the power of deformation becomes minimum i.e., L and H are the variables with respect to which deforming power is minimized.

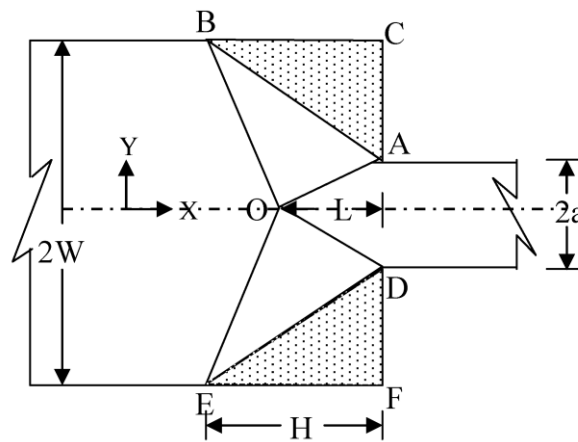


Figure 3.5 Plane strain extrusion problem

In terms of the coordinates of the vertices, the equations of the three bounding lines are given by

$$\text{Line AB: } \frac{W-a}{H}x + y - a = 0 \quad (3.16a)$$

$$\text{Line BO: } \frac{W}{H-L}x + y - \frac{W.L}{H-L} = 0 \quad (3.16b)$$

$$\text{Line OA: } \frac{a}{L}x + y - a = 0 \quad (3.16c)$$

When the billet velocity V_b is known, there are three unknown velocity components, i.e., V_p , the product velocity, and V_x and V_y the x- and y-components of the velocity vector in the elementary rigid region.

The line AB (Figure 3.5) is the limiting line for the dead metal zone. Material enters the deformation zone across line BO and the product leaves the deformation zone through line AB. Table 3.1 describes these lines and the velocity vectors corresponding to both sides of each line.

Table 3.1 Summary of discontinuity lines and velocity vectors on their sides

Lines and their equations	Side 1	Velocity vector on side 1	Side 2	Velocity vector on side 2
AB = $(W-a)x/L + y - a = 0$	Deformation zone	$\hat{i}V_x + \hat{j}V_y$	Dead metal zone	0
BO = $Wx/(H-L) + y - WL/(H-L) = 0$	Deformation zone	$\hat{i}V_x + \hat{j}V_y$	Billet	$\hat{i}V_b$
OA = $ax/L + y - a = 0$	Deformation zone	$\hat{i}V_x + \hat{j}V_y$	Product	$\hat{i}V_p$

Employing the mass continuity condition (equations 3.13 and 3.14 appropriately), velocity equations are given by

$$\frac{W-a}{H}V_x + V_y = 0 \quad (3.17a)$$

$$\frac{W}{H-L}V_x + V_y = \frac{W}{H-L}V_b \quad (3.17b)$$

$$\frac{-a}{L}V_x + V_y = \frac{a}{L}V_p \quad (3.17c)$$

On solving this set of linear equations the velocity vectors obtained are

$$V_x = \frac{HWW_b}{Ha + LW - aL} \quad (3.18a)$$

$$V_y = \frac{-(W-a)WV_b}{Ha + LW - aL} \quad (3.18b)$$

$$V_p = \frac{WV_b}{a} \quad (3.18c)$$

Since the elementary region is rigid, the strain rate tensor in this region is zero. Therefore the power for internal deformation J_1 , is zero. Further, the deformation zone is separated from the die surface by the dead metal zone and, as such, there is no relative motion between the two. Therefore, there is no dissipation of power due to the friction at the die faces ($J_3 = 0$). Thus the power consumed for deformation is dissipated only along the lines of velocity discontinuity. Hence in this case, equation (3.1) reduces to

$$J = J_2 \quad (3.19)$$

In the present analysis, all the lines of velocity discontinuity separate the rigid regions. Hence the absolute values of the velocity discontinuities at each line are constant. If S_{AB} , S_{BO} and S_{OA} denote the lengths of the line segments AB, BO and OA respectively and $|\Delta V|_{AB}$, $|\Delta V|_{BO}$ and $|\Delta V|_{OA}$ represents the corresponding absolute values of the velocity discontinuities, then total deformation power can be expressed as

$$J = \frac{\sigma_0}{\sqrt{3}} \left[|\Delta V|_{AB} S_{AB} + |\Delta V|_{BO} S_{BO} + |\Delta V|_{OA} S_{OA} \right] \quad (3.20)$$

Table 3.2 describes the absolute values of the velocity discontinuities across the lines. The lengths of the corresponding line segments, calculated using the coordinates of the points A, B and O, are also mentioned. The upper bound to the deforming power can be calculated from equation (3.20) using the values of velocity discontinuities and lengths of the line segments.

The upper bound so obtained can be optimized with respect to the parameters H and L and the minimum upper bound J_{\min} , to the deforming power can be obtained corresponding to this velocity field. The average extrusion pressure, non-dimensionalized by σ_o , can then be calculated from the equation

$$\frac{P_{av}}{\sigma_o} = \frac{J_{\min}}{WV_b \sigma_o} \quad (3.21)$$

It may be noted here that the solution is similar to that presented by Johnson [43, 45,119] using the hodograph method. This solution is given here only as a demonstration of the PERR technique which is the two-dimensional representation of the reformulated SERR technique.

Table 3.2 Summary of velocity discontinuities across the lines

Line	Velocity discontinuity	Length
<i>AB</i>	$\sqrt{\left(\frac{WHV_b}{Ha + LW - aL}\right)^2 + \left(\frac{W(W - a)V_b}{Ha + LW - aL}\right)^2}$	$\sqrt{H^2 + (W - a)^2}$
<i>BO</i>	$\sqrt{\left(\frac{WHV_b}{Ha + LW - aL} - V_b\right)^2 + \left(-\frac{W(W - a)V_b}{Ha + LW - aL}\right)^2}$	$\sqrt{(H - L)^2 + W^2}$
<i>OA</i>	$\sqrt{\left(\frac{WHV_b}{Ha + LW - aL} - \frac{W}{a}V_b\right)^2 + \left(-\frac{W(W - a)V_b}{Ha + LW - aL}\right)^2}$	$\sqrt{a^2 + L^2}$

3.7 Closure

Present chapter highlights the importance of the upper bound theorem and gives a simple example for 2D application. The prime constraint for the upper-bound solution is to find a kinematically admissible velocity field for the three-dimensional configuration under consideration. A number of techniques have been proposed to generate kinematically admissible velocity fields for such analysis. These include the dual stream function, conformal transformation technique and generalized velocity field. These velocity fields are continuous in the sense that the velocities are expressed as a continuous function in the plastic flow zones. The discontinuous velocity field that envisaged the plastic zone to be composed of spatial element rigid region is proposed by Gatto and Giarda [73], with suitable modification can be easily applied to the analysis of extrusion of polygonal sections with or without re-entrant corner.

In the next chapter upper bound concept with modified SERR technique is applied to study the combined extrusion-forging process for round-triangle-round sections.

3D Analysis of Combined Extrusion-Forging Process for Round-Triangle-Round Sections

I. THEORETICAL ANALYSIS

4.1 Introduction (Theoretical Analysis)

Upper bound solution for extrusion of round to triangular sections from circular billets using straight or curved converging dies has received the attention of many investigators. An approximate solution to the problem was first proposed by Basily and Sansome [111] who derived a kinematically admissible velocity field for the square section by assuming a triangular element of the billet section at entry to be transformed into a corresponding triangular element at exit. Juneja and Prakash [112] have proposed solutions for extrusion of polygonal sections from similar shaped billets using conventional spherical velocity field. The limitation of the above methods was that these lacked generality and therefore, could not be applied for arbitrary shape billet or product or combined processes.

General analytical procedures for deriving kinematically admissible velocity fields for the above class of problems have been suggested by Nagpal and Altan [113] (using the concept of dual stream function) and by Yang and Lee [114] (using conformal mapping technique). Both these techniques, however, were again limited to problems where the billets and the product area of similar shape so that section similarity is maintained throughout the deforming region. Sahoo et al, [85] analysis the extrusion of triangular section bars from round section through linearly converging dies. In most of the cases square or linearly converging dies are used. From the point of view of economy and easy of manufacture square dies are preferred where the reduction in load is the prime concern as in the extrusion of materials which are hard and difficult to form.

The present chapter proposes an upper bound solution for forward extrusion-forging of the triangular section head with the circular shaft through the square dies from round section billets and forward-backward extrusion-forging of circular shaft with triangular section head in between. Figure 4.1 shows the front half section of the process. Considering the observations made by Hill [115], Johnson [8], and Green [13], dead metal zones have been assumed to cover the die faces and the upper bound loads have been computed using the proposed discontinuous velocity fields. The discontinuous

velocity fields have been obtained by discretizing the deformation zone into tetrahedral blocks using the reformulated SERR technique (explained in chapter 3).

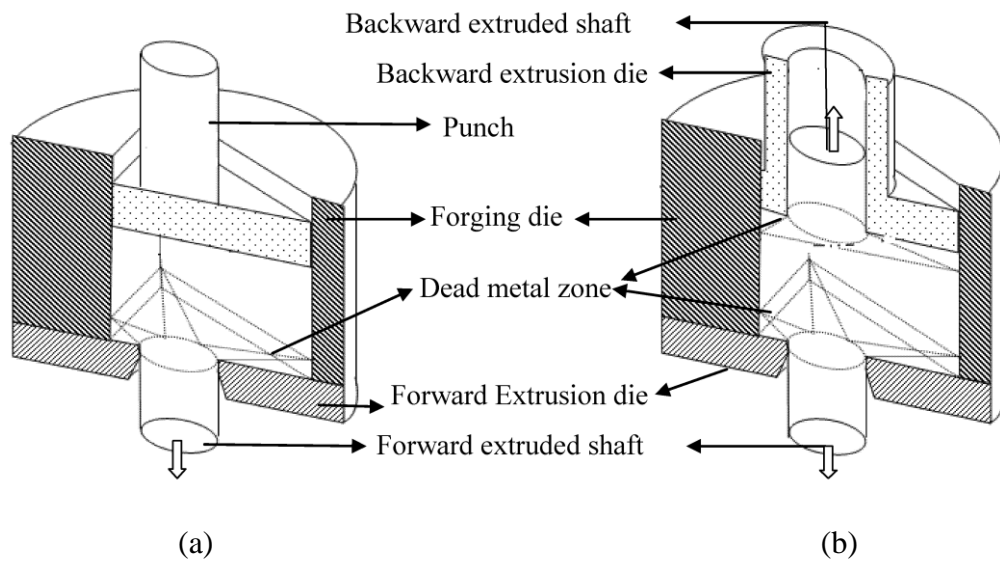


Figure 4.1 Front half section of the process (a) Forward extrusion-forging (b) Forward- backward extrusion-forging process

Assumptions made in the present analysis are:

1. The material is isotropic, homogeneous, rigid plastic and obeys the Von-Mises yield criterion.
2. Material is incompressible.
3. The die and punch are rigid and not deformed.
4. Elastic deformation is small compared to the plastic deformation and therefore neglected.
5. Frictional shear stress is expressed by a constant friction factor “ m ”.
6. The centroid of the die aperture lies on the billet axis.
7. Dead metal zones are formed on the sides of the die orifice.
8. Backward extrusion velocity is proportional to forward extrusion velocity and the proportionality factor is considered here as one optimizing parameter.

4.2 SERR Method of Analysis

4.2.1 Forward extrusion-forging process

The proposed SERR technique is used here to analyze the last stage of the combined extrusion forging process, which requires maximum load. In the brief discussion presented in chapter 3 it is pointed out that in the SERR method of analysis

the deformation zone is discretized into elementary rigid regions thus leading to a discontinuous velocity field. It is further stated that when these rigid regions are in the shape of tetrahedrons, a determinate set of equations are obtained (by application of the continuity conditions to the individual faces defining the rigid regions) from which the velocity components in each rigid region can be calculated.

In the present analysis, it is assumed that the centroid of the die aperture lies on the billet axis. This assumption is necessary so that the product remains straight as it comes out of the die orifice [52]. The die face being rough; it is further assumed that dead metal zones form on all sides of the orifice as shown in Figure 4.2. The dead metal zones are proposed in this manner so that a deformation cavity is formed in which the triangular section of the billet gradually forms into the circular sections of the product. It is appropriate to mention here that the dead metal zones are a part of the proposed velocity field (being zones of zero velocities), and the upper bound theorem admits any velocity fields as long as it is kinematically admissible. The cavity formed by the dead metal zones, called the domain of interest hereafter, is shown in Figure 4.3 for one-sixth of the deformation geometry of triangular section with equal side lengths (because of its symmetry about three planes with respect to billet cross-section).

The SERR technique can be applied where there are planner boundaries. Hence, the curved surface is to be replaced by planner surfaces so as to accommodate the SERR analysis. To approximate the circular cross-section of the shaft into a regular polygon, the cross-sectional area of the approximate polygon is maintained equal. This condition is enforced through the relation:

$$\pi R^2 = N \frac{1}{4} s^2 \cot\left(\frac{1}{2} \theta\right) \quad (4.1)$$

Where, R is the shaft radius, N is number of sides of approximating polygon, s is the length of each side of the approximating polygon and θ is the internal angle of the polygon.

Analyses are made by an increasing number of sides of approximating polygon for different reductions. It is found that at 24 numbers of sides of approximating polygon the upper bound results (calculated extrusion velocity, w.r.t. unit billet velocity) are closer to the theoretical extrusion velocity (as per area reduction) for this analysis. Further increasing the numbers of sides of the approximating polygon, there is a negligible change in results (Figure 4.4). Following the principles laid down in reference

[76, 116, 117], the subzones of deformation are delineated in the domain of interest by taking suitably located floating points (an arbitrary point in the domain of interest named here as a floating point since its location is not a priori known). Three formulations are considered, which are acknowledged as one, two and three floating points respectively. For single floating point formulation, an arbitrary point is taken on the extrusion axis. For double point formulation, two floating points are taken in the domain of interest, one on the extrusion axis as before and the second on the plane of symmetry at an arbitrary position. Finally, in the triple-point formulation, three floating points are taken, one on extrusion axis, second one on the plane of symmetry and the third in an arbitrary position in the domain of interest. Figure 4.5 (point 11 is the floating point), Figure 4.6 (point 11 and 12 are the two floating points) and Figure 4.7 (point 11, 12 and 13 are the three floating points) refer to the single, double and triple point formulation respectively.

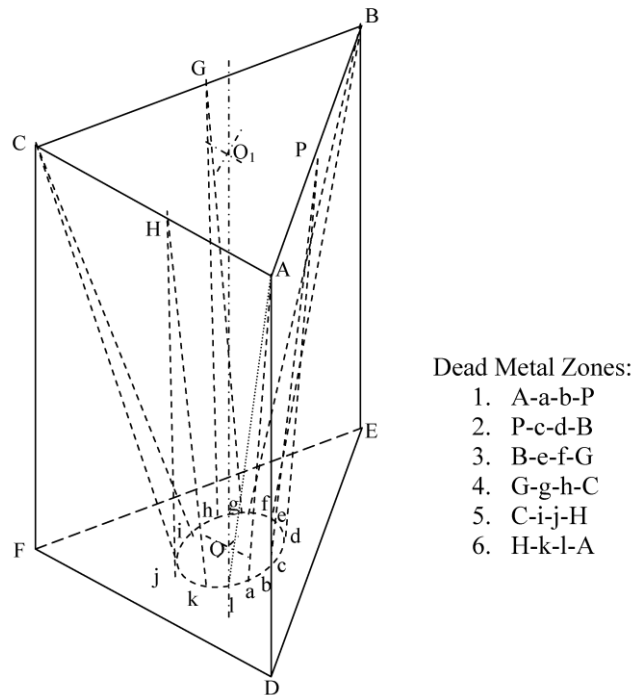


Figure 4.2 Dead metal zones in SERR formulation for extrusion of triangle-round section

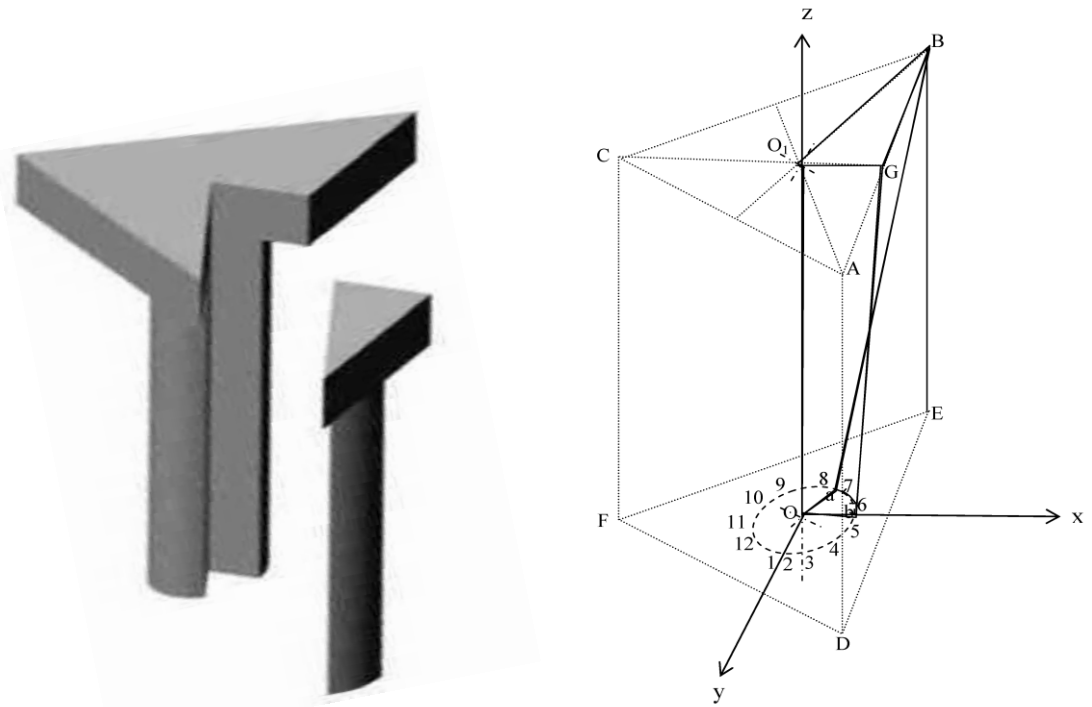


Figure 4.3 Domain of interest G-B-O₁-O-b-6-7-a (one sixth of zone of deformation)

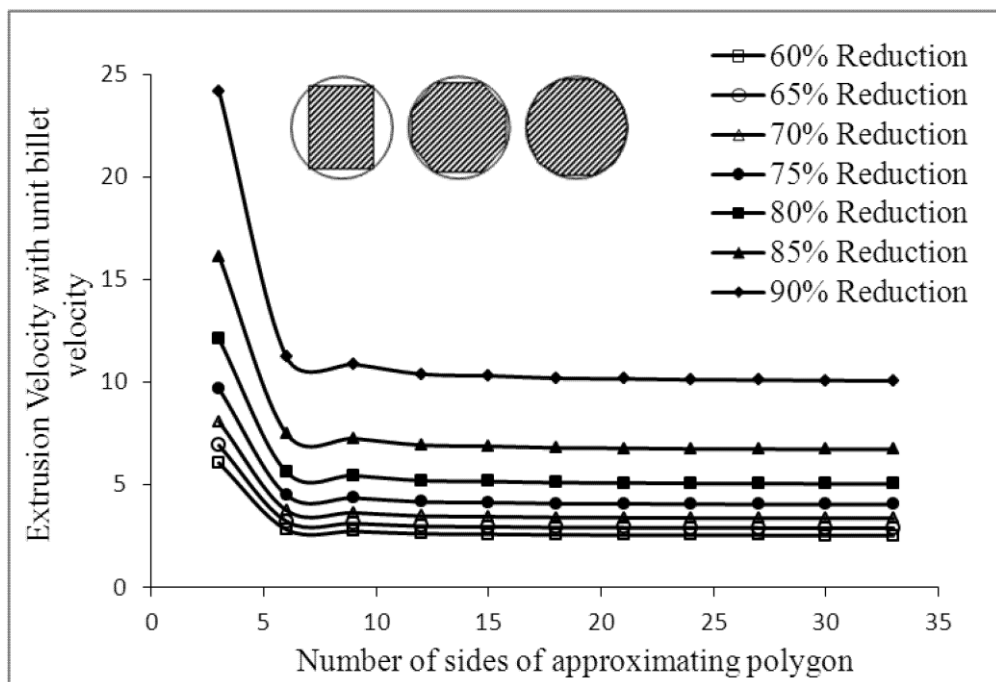
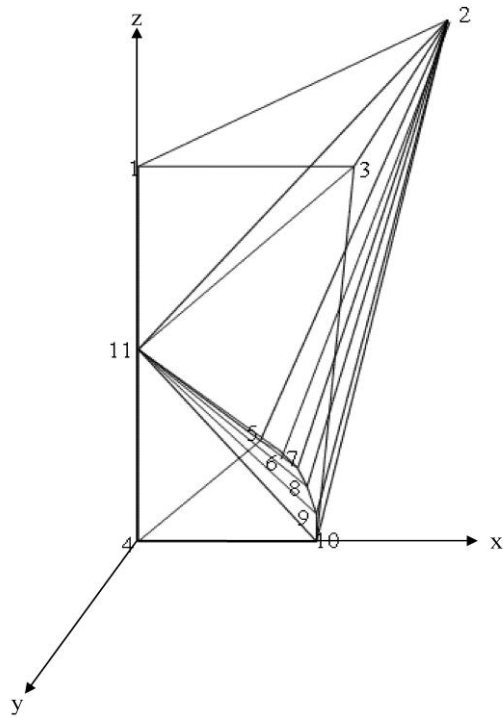


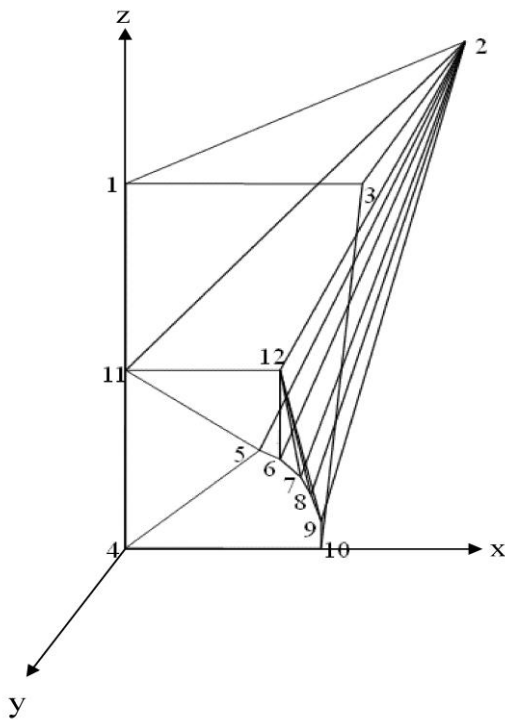
Figure 4.4 Extrusion velocity with number of sides of approximating polygon



Subzones:

1. Pyramid : 11-2-9-10-3
2. Tetrahedrons : 5-2-11-6
6-2-11-7
7-2-11-8
8-2-11-9

Figure 4.5 one-sixth of the deformation zone (single point formulation)



Subzones:

1. Pyramids : 2-11-15-6-12
12-2-9-10-3
2. Tetrahedrons: 6-2-12-7
7-2-12-8
8-2-12-9

Figure 4.6 one-sixth of the deformation zone (double point formulation)

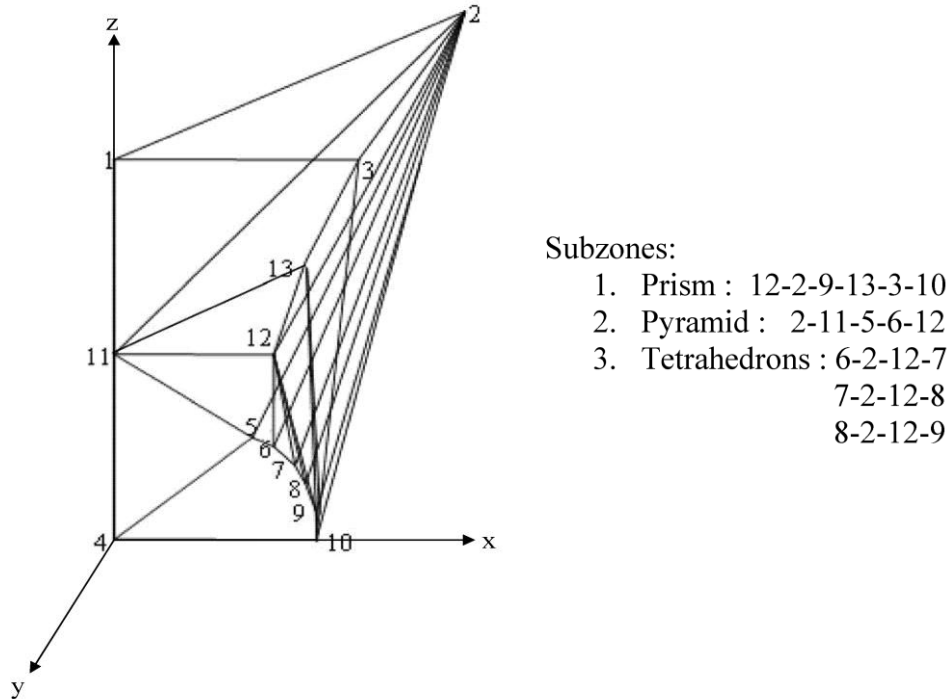


Figure 4.7 one-sixth of the deformation zone (triple point formulation)

4.2.1.1 Single point formulation

As mentioned earlier, since the triangular section (with equal length of sides) has symmetry about the three axes, only one-sixth of the extrusion geometry may be considered as the domain of interest for the analysis. Figure 4.5 shows the one-sixth of the die cavity along with the pertinent coordinate frame. The deformation zone is delineated by joining the corner points of the entry and exit to a point on the extrusion axis (known as floating point), which is in analogy with the plane strain case. By this process, the deformation zone is divided into five subzones (Figure 4.8), four tetrahedrons (5-2-11-6, 6-2-11-7, 7-2-11-8, and 8-2-11-9) and one pyramid (11-2-9-10-3). Each pyramid can be subdivided into two tetrahedrons in two different ways. The two different ways of discretization for pyramid 11-2-9-10-3 is shown in Figure 4.9. Hence, the deformation zone can be subdivided into six tetrahedrons in 2 different ways (Table 4.1).

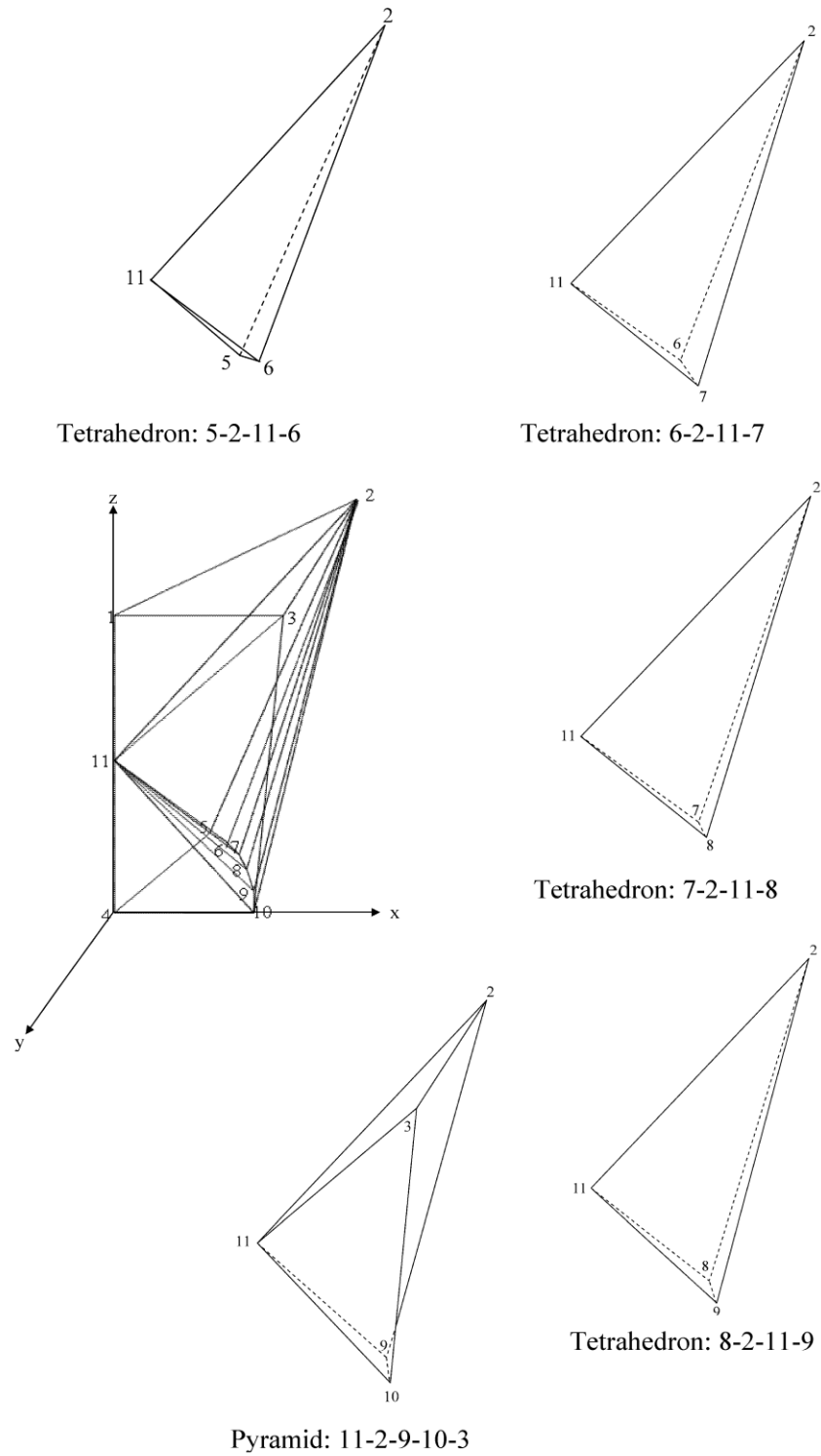


Figure 4.8 Discretization of SFP deformation zone is divided into number subzones

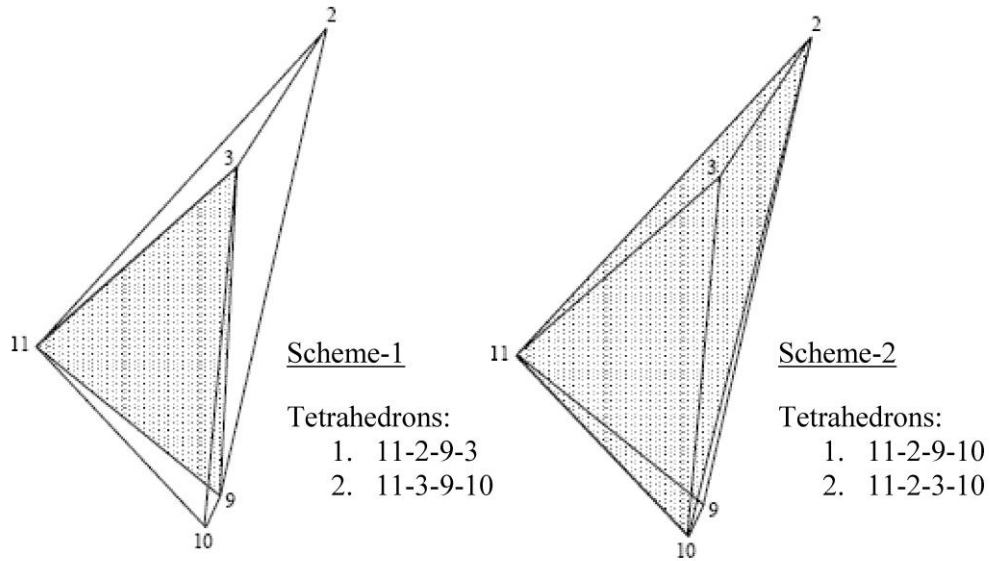


Figure 4.9 Discretization of pyramidal subzones 11-2-9-10-3

Four tetrahedrons with and two tetrahedrons of pyramid 11-2-9-10-3 (for scheme-1 11-2-9-3 & 11-3-9-10 and for scheme-2 11-2-9-10 & 11-2-3-10) are constituted six tetrahedrons in total. Each tetrahedron contains four triangular faces. Therefore, six tetrahedrons contain 24 triangular faces/planes, out of which five are common planes, for two conjugative tetrahedrons. Finally, we got nineteen triangular planes for the deformation zone. The tetrahedrons are being rigid; each has a constant internal velocity vector. The internal velocities are $\vec{V}_1, \vec{V}_2, \vec{V}_3, \dots, \vec{V}_6$. When resolve into respective three components along the Cartesian coordinate axes, $\vec{V}_1, \vec{V}_2, \vec{V}_3, \dots, \vec{V}_6$ have 18 components. The billet and product velocities, \vec{V}_b and \vec{V}_e , are along axial direction (z-axis) and, therefore, can consider to have one velocity component each. With a given billet velocity \vec{V}_b , there are nineteen unknown velocity components including \vec{V}_e . When the mass continuity condition is applied to all the nineteen bonding faces of this six tetrahedron, nineteen equations are obtained. These nineteen equations, forming a determinate set, solved simultaneously to give all the unknown velocity components.

Table 4.1 Global level of discretization

Global Scheme of discretization	Discretization Scheme for pyramid	Deformation zone (tetrahedrons)	Number of planes	Planes	Type of planes
		5-2-11-6	4	2-5-6 11-5-2 11-6-2 11-5-6	Dead metal zone Plane of symmetry Internal plane Exit plane
		6-2-11-7	4	11-6-2 11-7-2 2-6-7 11-6-7	Common plane Internal plane Dead metal zone Exit plane
		7-2-11-8	4	11-7-2 11-8-2 2-7-8 11-7-8	Common plane Internal plane Dead metal zone Exit plane
		8-2-11-9	4	11-8-2 11-9-2 2-8-9 11-8-9	Common plane Internal plane Dead metal zone Exit plane
Scheme - 1	11-2-9-10-3	9-2-11-3	4	11-9-2 11-9-3 9-2-3 11-3-2	Common plane Internal plane Dead metal zone Entry Plane
		9-2-11-10	4	11-9-2 11-10-3 9-10-3 11-9-10	Common plane Plane of symmetry Dead metal zone Exit plane
Scheme - 2	11-2-9-10-3	11-2-9-10	4	11-2-10 11-2-9 9-10-2 11-9-10	Common plane Internal Plane Dead metal zone Exit plane
		11-2-3-10	4	11-2-10 11-3-10 2-3-10 11-2-3	Common plane Plane of symmetry Dead metal zone Entry plane

As an illustration, nineteen faces, i.e. 11-5-2, 11-6-2, 11-5-6, 2-5-6, 2-6-7, 11-7-2, 11-6-7, 2-7-8, 11-8-2, 11-7-8, 2-8-9, 11-9-2, 11-8-9, 9-2-3, 11-9-3 11-3-2, 9-10-3, 11-9-10, and 11-10-3, for pyramid 11-2-9-10-3 for scheme-1 can be considered. Table 4.2 gives the co-ordinates of the points 1, 2, 3, 4, 5, 6, 7, 8, 9, 10 and 11. Figure 4.10 gives

the location of the coordinates for better understanding. Using these coordinates, the equations of the planes containing the nineteen faces under consideration can be determined as shown in Table 4.3. Considering the mass continuity condition, the normal components on both sides of each face must be equal. Table 4.4 illustrates the velocity vectors on both sides of the nineteen faces under consideration. Equating the normal components of velocities on both sides of each face under consideration, a set of nineteen equations are obtained, which are given in Table 4.5.

Table 4.2 Coordinates of points

Points	X-coordinate	Y-coordinate	Z-coordinate
1	0.0	0.0	L
2	0.29B	0.5B	L
3	0.29B	0.0	L
4	0.0	0.0	0
5	0.86R	0.5R	0
6	0.79R	0.61R	0
7	0.61R	0.71R	0
8	0.38R	0.92R	0
9	0.13R	0.99R	0
10	R	0.0	0
11	0.0	0.0	M

Where, R is the radius of the extruded shaft, B is the length of side of the triangle section, M is the height of the floating point on the extrusion axis from origin; L is the height/length of the deformation zone.

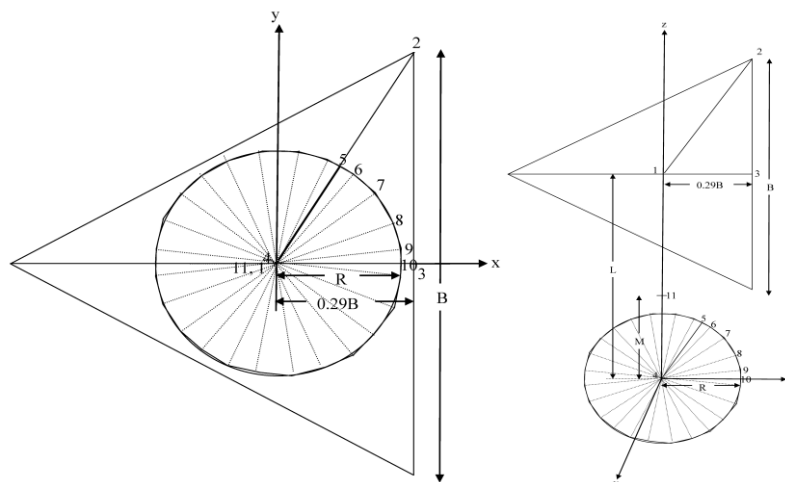


Figure 4.10 Location of coordinates of different points

Table 4.3 Equation of plane

Tetrahedrons	Planes	Equation of planes
5-2-11-6	5-6-2	$(0.5BL-0.61RL)x + (-0.07L)y + (0.61RB-0.52R^2-0.145B^2)z + (0.5246R^2L-0.395RLB) = 0$
	11-5-2	$(0.5BL)x + (0.86RM-0.29BM-0.86RL)y + (0.43RB-0.145B^2)z + (0.145B^2M-0.43BRM) = 0$
	11-6-2	$(0.61RL-0.61RM+0.5BM)x + (0.79RM-0.29BM-0.79RL)y + (0.2181RB)z + 0.2181BRM = 0$
	11-5-6	$(0.5BM+0.61RM)x + (0.07RM)y + (0.5246R^2-0.395RB)z + (-0.5246R^2M+0.395RMB) = 0$
6-2-11-7	2-6-7	$(0.1RL)x + (0.18RL)y + (0.1888R^2-0.119BR)z + (-0.1888R^2L) = 0$
	11-7-2	$(0.71RL-0.71RM+0.5BM)x + (0.61RM-0.29BM-0.61RL)y + (0.4331R^2-0.2059B)z + (-0.0991BRM) = 0$
	11-6-7	$(1.32RM)x + (0.18RM)y + (0.1888R^2)z + (-0.1888R^2M) = 0$
7-2-11-8	2-7-8	$(1.63RL)x + (0.23RL)y + (0.2914R^2-0.1759BR)z + (-0.2914R^2L) = 0$
	11-8-2	$(0.92RL-0.92RM+0.5BM)x + (0.38RM-0.29BM-0.38RL)y + (-0.0768RB)z + (0.0768RBM) = 0$
	11-7-8	$(0.21RM)x + (0.23RM)y + (0.2914R^2)z + (-0.2914R^2M) = 0$
	2-8-9	$(0.07RL)x + (0.25RL)y + (0.2475R^2-0.1453BR)z + (-0.26551RL) = 0$
8-2-11-9	11-9-2	$(0.99RL-0.99RM+0.5BM)x + (0.13MR-0.29BM-0.13RL)y + (-0.2221RB)z + (0.2221BRM) = 0$
	11-8-9	$(0.07RM)x + (0.25MR)y + (0.2566R^2)z + (-0.2566R^2M) = 0$
	9-2-3	$(0.5BL)x + (0.0)y + (0.065RB-0.145B^2)z + (-0.065RBL) = 0$
9-2-11-3	11-9-3	$(0.99RL-0.99RM)x + (0.13RM-0.29MB-0.13RL)y + (-0.2871RMB)z + (0.2871RBM) = 0$
	11-3-2	$(0.5BM-0.5BL)x + (0.0)y + (0.145B^2)z + (-0.145B^2M) = 0$
9-2-11-10	9-10-3	$(0.99RL)x + (-0.87RL)y + (0.2871RB-0.99R^2)z + (0.99R^2L-0.2871R^2) = 0$
	11-9-10	$(-0.99MR)x + (-0.87MR)y + (-0.99MR)z + 0.99MR = 0$
	11-10-3	$(0.0)x + (MR-0.29BM-RL)y + (0.0)z + (0.0) = 0$

Table 4.4 Velocity vector on both sides of the faces

Face	Velocity vector on one side	Velocity vector on other side
5-6-2	$\vec{V}_1 = \hat{i}V_{1x} + \hat{j}V_{1y} + \hat{k}V_{1z}$	0
11-5-2	$\vec{V}_1 = \hat{i}V_{1x} + \hat{j}V_{1y} + \hat{k}V_{1z}$	$\vec{V}_1 = \hat{i}V_{1x} + \hat{j}V_{1y} + \hat{k}V_{1z}$
11-6-2	$\vec{V}_1 = \hat{i}V_{1x} + \hat{j}V_{1y} + \hat{k}V_{1z}$	$\vec{V}_2 = \hat{i}V_{2x} + \hat{j}V_{2y} + \hat{k}V_{2z}$
11-5-6	$\vec{V}_1 = \hat{i}V_{1x} + \hat{j}V_{1y} + \hat{k}V_{1z}$	$\vec{V}_e = \hat{k}V_e$
2-6-7	$\vec{V}_2 = \hat{i}V_{2x} + \hat{j}V_{2y} + \hat{k}V_{2z}$	0
11-7-2	$\vec{V}_2 = \hat{i}V_{2x} + \hat{j}V_{2y} + \hat{k}V_{2z}$	$\vec{V}_3 = \hat{i}V_{3x} + \hat{j}V_{3y} + \hat{k}V_{3z}$
11-6-7	$\vec{V}_2 = \hat{i}V_{2x} + \hat{j}V_{2y} + \hat{k}V_{2z}$	$\vec{V}_e = \hat{k}V_e$
2-7-8	$\vec{V}_3 = \hat{i}V_{3x} + \hat{j}V_{3y} + \hat{k}V_{3z}$	0
11-8-2	$\vec{V}_3 = \hat{i}V_{3x} + \hat{j}V_{3y} + \hat{k}V_{3z}$	$\vec{V}_4 = \hat{i}V_{4x} + \hat{j}V_{4y} + \hat{k}V_{4z}$
11-7-8	$\vec{V}_3 = \hat{i}V_{3x} + \hat{j}V_{3y} + \hat{k}V_{3z}$	$\vec{V}_e = \hat{k}V_e$
2-8-9	$\vec{V}_4 = \hat{i}V_{4x} + \hat{j}V_{4y} + \hat{k}V_{4z}$	0
11-9-2	$\vec{V}_4 = \hat{i}V_{4x} + \hat{j}V_{4y} + \hat{k}V_{4z}$	$\vec{V}_5 = \hat{i}V_{5x} + \hat{j}V_{5y} + \hat{k}V_{5z}$
11-8-9	$\vec{V}_4 = \hat{i}V_{4x} + \hat{j}V_{4y} + \hat{k}V_{4z}$	$\vec{V}_e = \hat{k}V_e$
9-2-3	$\vec{V}_5 = \hat{i}V_{5x} + \hat{j}V_{5y} + \hat{k}V_{5z}$	0
11-9-3	$\vec{V}_5 = \hat{i}V_{5x} + \hat{j}V_{5y} + \hat{k}V_{5z}$	$\vec{V}_6 = \hat{i}V_{6x} + \hat{j}V_{6y} + \hat{k}V_{6z}$
11-3-2	$\vec{V}_5 = \hat{i}V_{5x} + \hat{j}V_{5y} + \hat{k}V_{5z}$	$\vec{V}_b = \hat{k}V_b$
9-10-3	$\vec{V}_6 = \hat{i}V_{6x} + \hat{j}V_{6y} + \hat{k}V_{6z}$	0
11-9-10	$\vec{V}_6 = \hat{i}V_{6x} + \hat{j}V_{6y} + \hat{k}V_{6z}$	$\vec{V}_e = \hat{k}V_e$
11-10-3	$\vec{V}_6 = \hat{i}V_{6x} + \hat{j}V_{6y} + \hat{k}V_{6z}$	$\vec{V}_6 = \hat{i}V_{6x} + \hat{j}V_{6y} + \hat{k}V_{6z}$

where, i, j, k are unit vectors along the axis of a Cartesian co-ordinate frame

Table 4.5 Equation of normal component of velocities

Tetrahedrons	Planes	Equation of equating normal component of velocities on both sides of each face
5-2-11-6	5-6-2	$(0.5BL-0.61RL)V_{1x} + (-0.07L)V_{1y} + (0.61RB-0.52R^2-0.145B^2)V_{1z} = 0$
	11-5-2	$(0.5BL)V_{1x} + (0.86RM-0.29BM-0.86RL)V_{1y} + (0.43RB-0.145B^2)V_{1z} = 0$
	11-6-2	$(0.61RL-0.61RM+0.5BM)V_{1x} + (0.79RM-0.29BM-0.79RL)V_{1y} + (0.2181RB)V_{1z} = (0.61RL-0.61RM+0.5BM)V_{1x} + (0.79RM-0.29BM-0.79RL)V_{1y} + (0.2181RB)V_{1z}$
6-2-11-7	11-5-6	$(0.5BM+0.61RM)V_{1x} + (0.07RM)V_{1y} + (0.5246R^2-0.395RB)V_{1z} = (0.5246R^2-0.395RB)V_e$
	2-6-7	$(0.1RL)V_{2x} + (0.18RL)V_{2y} + (0.1888R^2-0.119BR)V_{2z} = 0$
7-2-11-8	11-7-2	$(0.71RL-0.71RM+0.5BM)V_{2x} + (0.61RM-0.29BM-0.61RL)V_{2y} + (0.4331R^2-0.2059B)V_{2z} = (0.71RL-0.71RM+0.5BM)V_{2x} + (0.61RM-0.29BM-0.61RL)V_{2y} + (0.4331R^2-0.2059B)V_{2z}$
	11-6-7	$(1.32RM)V_{2x} + (0.18RM)V_{2y} + (0.1888R^2)V_{2z} = (0.1888R^2)V_e$
8-2-11-9	2-7-8	$(1.63RL)V_{3x} + (0.23RL)V_{3y} + (0.2914R^2-0.1759BR)V_{3z} = 0$
	11-8-2	$(0.92RL-0.92RM+0.5BM)V_{3x} + (0.38RM-0.29BM-0.38RL)V_{3y} + (-0.0768RB)V_{3z} = (0.92RL-0.92RM+0.5BM)V_{3x} + (0.38RM-0.29BM-0.38RL)V_{3y} + (-0.0768RB)V_{3z}$
9-2-11-10	11-7-8	$(0.21RM)V_{3x} + (0.23RM)V_{3y} + (0.2914R^2)V_{3z} = (0.2914R^2)V_e$
	2-8-9	$(0.07RL)V_{4x} + (0.25RL)V_{4y} + (0.2475R^2-0.1453BR)V_{4z} = 0$
9-2-11-3	11-9-2	$(0.99RL-0.99RM+0.5BM)V_{4x} + (0.13MR-0.29BM-0.13RL)V_{4y} + (-0.2221RB)V_{4z} = (0.99RL-0.99RM+0.5BM)V_{4x} + (0.13MR-0.29BM-0.13RL)V_{4y} + (-0.2221RB)V_{4z}$
	11-8-9	$(0.07RM)V_{4x} + (0.25MR)V_{4y} + (0.2566R^2)V_{4z} = (0.2566R^2)V_e$
9-2-11-3	9-2-3	$(0.5BL)V_{5x} + (0.0)V_{5y} + (0.065RB-0.145B^2)V_{5z} = 0$
	11-9-3	$(0.99RL-0.99RM)V_{5x} + (0.13RM-0.29MB-0.13RL)V_{5y} + (-0.2871RMB)V_{5z} = (0.99RL-0.99RM)V_{5x} + (0.13RM-0.29MB-0.13RL)V_{5y} + (-0.2871RMB)V_{5z}$
9-2-11-10	11-3-2	$(0.5BM-0.5BL)V_{5x} + (0.0)V_{5y} + (0.145B^2)V_{5z} = (0.145B^2)V_e$
	9-10-3	$(0.99RL)V_{6x} + (-0.87RL)V_{6y} + (0.2871RB-0.99R^2)V_{6z} = 0$
9-2-11-10	11-9-10	$(-0.99MR)V_{6x} + (-0.87MR)V_{6y} + (-0.99MR)V_{6z} = (-0.99MR)V_e$
	11-10-3	$(0.0)V_{6x} + (MR-0.29BM-RL)V_{6y} + (0.0)V_{6z} = 0$

Table 4.6 Velocity discontinuity at the bonding face

Tetrahedrons	Planes	Velocity Discontinuities at bonding faces
5-2-11-6	5-6-2	$ \Delta V _1 = [V_{1x}^2 + V_{1y}^2 + V_{1z}^2]^{1/2}$
	11-5-2	$ \Delta V _2 = 0$
	11-6-2	$ \Delta V _3 = [V_{1x} - V_{2x}^2 + V_{1y} - V_{2y}^2 + V_{1z} - V_{2z}^2]^{1/2}$
	11-5-6	$ \Delta V _4 = [V_{1x}^2 + V_{1y}^2 + V_{1z} - V_e^2]^{1/2}$
6-2-11-7	2-6-7	$ \Delta V _5 = [V_{2x}^2 + V_{2y}^2 + V_{2z}^2]^{1/2}$
	11-7-2	$ \Delta V _6 = [V_{2x} - V_{3x}^2 + V_{2y} - V_{3y}^2 + V_{2z} - V_{3z}^2]^{1/2}$
	11-6-7	$ \Delta V _7 = [V_{2x}^2 + V_{2y}^2 + V_{2z} - V_e^2]^{1/2}$
7-2-11-8	2-7-8	$ \Delta V _8 = [V_{3x}^2 + V_{3y}^2 + V_{3z}^2]^{1/2}$
	11-8-2	$ \Delta V _9 = [V_{3x} - V_{4x}^2 + V_{3y} - V_{4y}^2 + V_{3z} - V_{4z}^2]^{1/2}$
	11-7-8	$ \Delta V _{10} = [V_{3x}^2 + V_{3y}^2 + V_{3z} - V_e^2]^{1/2}$
8-2-11-9	2-8-9	$ \Delta V _{11} = [V_{4x}^2 + V_{4y}^2 + V_{4z}^2]^{1/2}$
	11-9-2	$ \Delta V _{12} = [V_{4x} - V_{5x}^2 + V_{4y} - V_{5y}^2 + V_{4z} - V_{5z}^2]^{1/2}$
	11-8-9	$ \Delta V _{13} = [V_{4x}^2 + V_{4y}^2 + V_{4z} - V_e^2]^{1/2}$
9-2-11-3	9-2-3	$ \Delta V _{14} = [V_{5x}^2 + V_{5y}^2 + V_{5z}^2]^{1/2}$
	11-9-3	$ \Delta V _{15} = [V_{5x} - V_{6x}^2 + V_{5y} - V_{6y}^2 + V_{5z} - V_{6z}^2]^{1/2}$
	11-3-2	$ \Delta V _{16} = [V_{5x}^2 + V_{5y}^2 + V_{5z} - V_b^2]^{1/2}$
9-2-11-10	9-10-3	$ \Delta V _{17} = [V_{6x}^2 + V_{6y}^2 + V_{6z}^2]^{1/2}$
	11-9-10	$ \Delta V _{18} = [V_{6x}^2 + V_{6y}^2 + V_{6z} - V_e^2]^{1/2}$
	11-10-3	$ \Delta V _{19} = 0$

The above equations are solved to determine the nineteen velocity components. The solution can be obtained algebraically or with the help of a digital computer using a suitable subprogram for matrix inversion. The velocity discontinuities at the nineteen bounding faces are given in Table 4.6.

When the coordinates of the three vertices of a triangle in space are (x_1, y_1, z_1) , (x_2, y_2, z_2) and (x_3, y_3, z_3) , then the area of the triangle A , is given by the relation,

$$A = \left(A_x^2 + A_y^2 + A_z^2 \right)^{1/2} \quad (4.1)$$

where,

$$A_x = \frac{1}{2} \left[y_1 z_2 - y_2 z_1 + y_2 z_3 - y_3 z_2 + y_3 z_1 - y_1 z_3 \right] \quad (4.1a)$$

$$A_y = \frac{1}{2} \left[x_1 z_2 - x_2 z_1 + x_2 z_3 - x_3 z_2 + x_3 z_1 - x_1 z_3 \right] \quad (4.1b)$$

$$A_z = \frac{1}{2} \left[x_1 y_2 - x_2 y_1 + x_2 y_3 - x_3 y_2 + x_3 y_1 - x_1 y_3 \right] \quad (4.1c)$$

Using the above equations, the areas of the bounding faces can be calculated. Then the deformation power, consisting of only the powers of shear deformation at the planes of velocity discontinuity, may be determined using the relation,

$$J = \frac{\sigma_0}{\sqrt{3}} \sum_{n=1}^{n=N} |\Delta V|_n A_n \quad (4.2)$$

where,

N = total number of bonding faces, and

$|\Delta V|_n$ = velocity discontinuity at the n^{th} face whose area is A_n

If, A_b is the area of the billet cross section and P_{av} is the extrusion pressure, the external power supplied will be $P_{av} V_b A_b$. Equating it with upper bound power, the non-dimensional average extrusion pressure can be expressed as

$$\frac{P_{av}}{\sigma_0} = \frac{J}{A_b V_b \sigma_0} \quad (4.3)$$

where, σ_0 is the average yield strength of the material.

The non-dimensional average extrusion pressure, P_{av}/σ_0 , can be calculated using equation 3.16(a-c) and optimized with respect to L and M, the two adjustable parameters of the deformation zone.

4.2.1.2 Metal flow and satisfaction of continuity condition

Detailed explanation of the metal flow and the relation existing among the various internal velocity vectors, the pyramidal subzone 11-2-9-10-3 is isolated from the domain of interest of single floating point formulation as illustrated in Figure 4.8. The discretization of the pyramidal subzone into two tetrahedrons according to a particular scheme is shown in Figure 4.11. In tetrahedron 9-2-11-3, the face 11-3-2 is the entry plane through which billet admitted to the deformation zone. So the internal velocity vector is related to billet velocity when equation (3.13) is applied to this face. The billet velocity vector is in the z-axis direction. The face 9-2-3 is a dead metal plane admitting no mass flow in a direction normal to itself. Hence the internal velocity vector should remain parallel to this face. These conditions are enforced by taking the right-hand side of equation (3.13) equal to zero. Finally, the plane 11-9-3 is an internal plane separating the first and second SERR blocks of the subzone under consideration. Thus, the internal velocity vector of the first tetrahedron is related to that of the second by applying equation (3.13) to that face. Continuing in this way, the internal velocity vector of the previous tetrahedron (8-2-11-9) is related to that of the first tetrahedron (9-2-11-3) of the first considered pyramidal subzone by applying equation (3.13) to the connecting face 11-9-2. In this manner, all internal velocity vectors are interrelated through the application of equation (3.13) to different faces of all the SERR blocks in the global system. In the second tetrahedron (9-2-11-3) the face 11-10-3 lies on a plane of symmetry, hence the internal velocity vector of this SERR block is also parallel to the plane 2-6-9. These conditions are enforced by taking the right-hand side of the equation (3.13) equal to zero. The face 11-9-10 is one of the planes through which the bullet's exit the deformation zone. So the internal velocity vector is related to billet velocity when equation (3.13) is applied to this face.

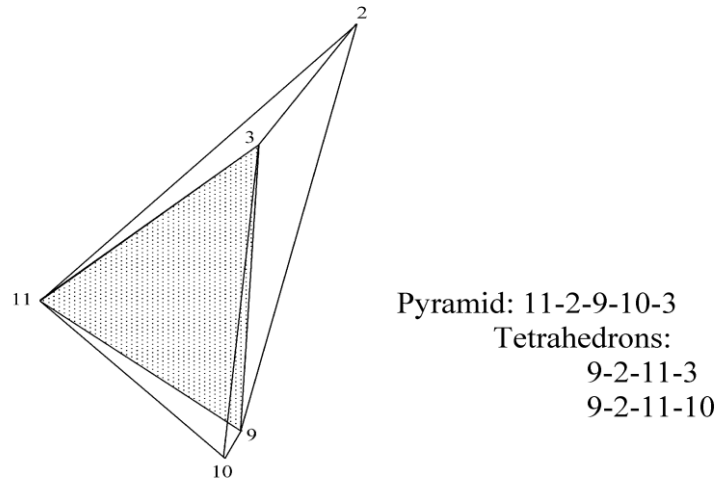
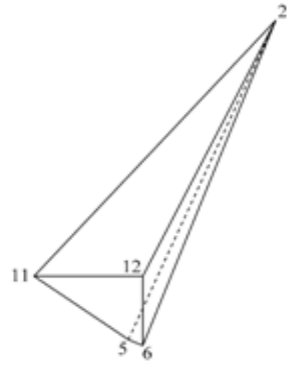


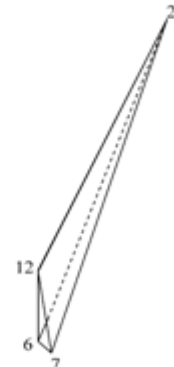
Figure 4.11 Interconnection of SERR blocks

4.2.1.3 Double point formulation

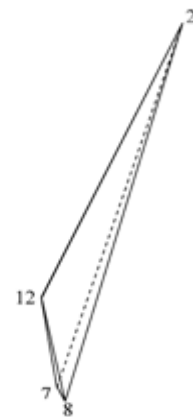
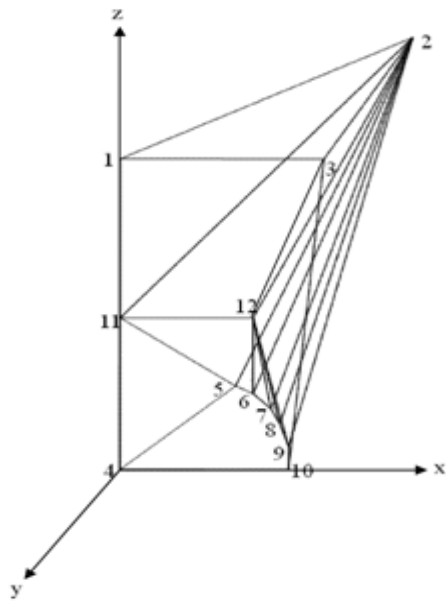
As shown in Figure 4.6 two floating points are taken for this formulation; first is point 11 on the extrusion axis and second one being point 12 on the plane of symmetry 1-3-10-4. As illustrated in Figure 4.12, the double point formulation leads to two pyramidal (2-11-5-6-12, 12-2-9-10-3) and three tetrahedral (6-2-12-7, 7-2-12-8, 8-2-12-9) subzones. A single pyramid can be discretized in two different ways. So, two pyramids can be discretized in four different ways as shown in Figure 4.13 and Figure 4.14. The detail scheme of discretization is summarized in Table 4.7. There are seven tetrahedrons and four global schemes of discretization. All these subzones are interconnected and have common triangular faces. Thus, the basic SERR blocks in their totality have 22 bounding faces for DPF. As all these bounding faces are triangular in shape, by applying equation (3.13) we can get 22 velocity equations for this formulation. When these equations are solved, equal number of velocity components can be obtained and be used for the further calculation purpose as explained in previous section 4.2.1.



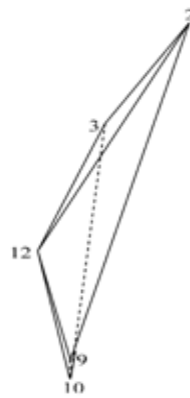
Pyramid: 2-11-5-6-12



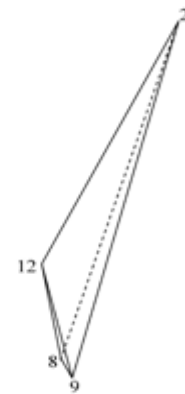
Tetrahedron: 6-2-12-7



Tetrahedron: 7-2-12-8



Pyramid: 12-2-9-10-3



Tetrahedron: 8-2-12-9

Figure 4.12 Discretization of DFP deformation zone is divided into number subzones

Table 4.7 Global level of discretization schemes for double floating point formulation

Global Scheme of discretization	Descritization Scheme for		Deformation zone (tetrahedrons)
	Pyramid 2-11-5-6-12	Pyramid 12-2-9-10-3	
1	1	1	2-11-12-6, 6-2-12-7, 8-2-12-9, 12-2-10-9, 2-11-6-5, 7-2-12-8, 12-2-9-3,
2	1	2	2-11-12-6, 6-2-12-7, 8-2-12-9, 12-3-10-9, 2-11-6-5, 7-2-12-8, 12-2-10-3,
3	2	1	2-12-6-5, 6-2-12-7, 8-2-12-9, 12-2-10-9, 2-12-5-11, 7-2-12-8, 12-2-9-3,
4	2	2	2-12-6-5, 6-2-12-7, 8-2-12-9, 12-3-10-9, 2-12-5-11, 7-2-12-8, 12-2-10-3

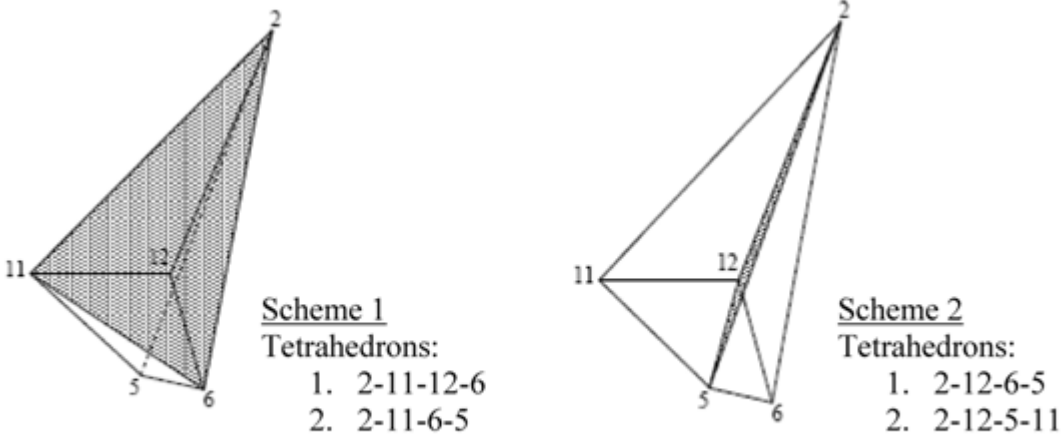


Figure 4.13 Discretization of pyramid 2-11-5-6-12

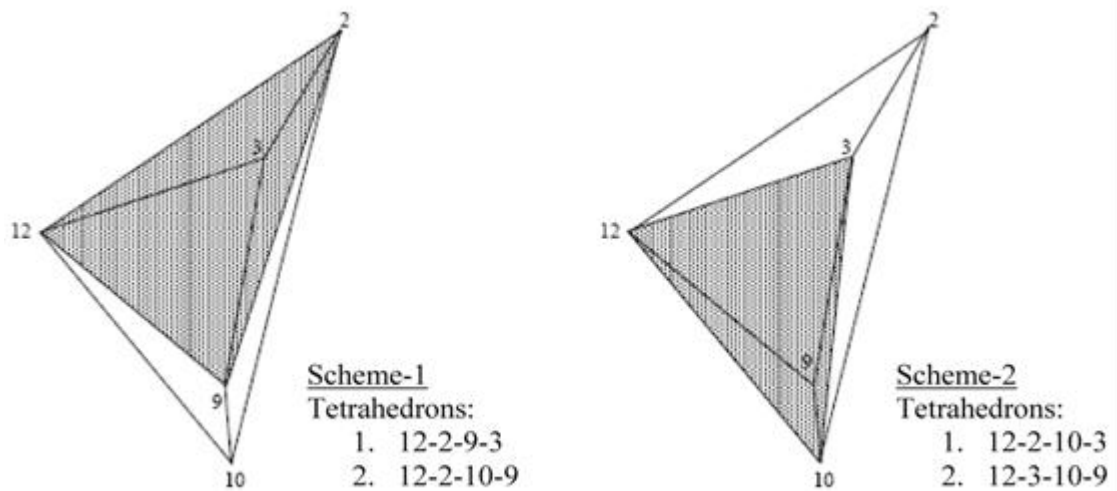
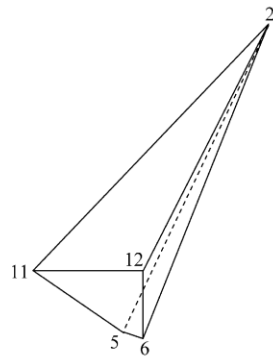


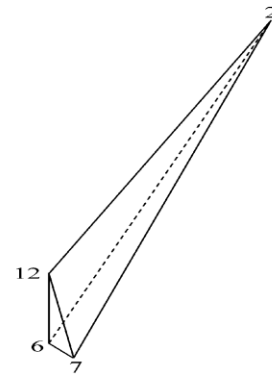
Figure 4.14 Discretization of pyramid 12-2-9-10-3

4.2.1.4 Triple point formulation

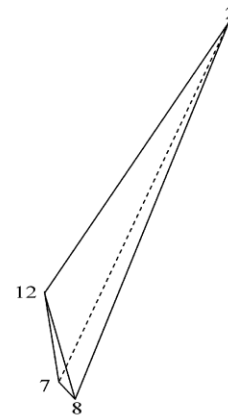
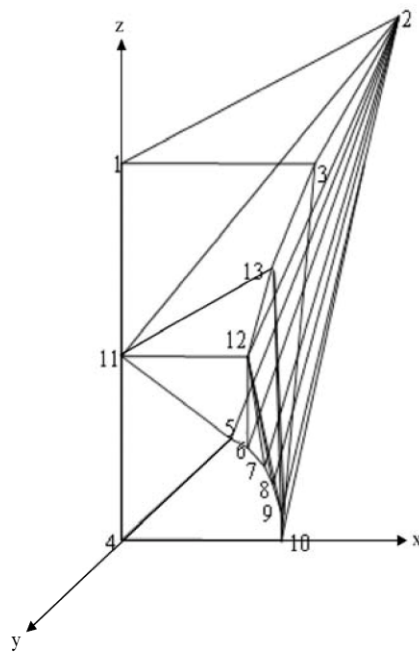
As shown in Figure 4.7 three floating points are taken in this formulation; first is point 11 on the extrusion axis and second one being point 12 on the plane of symmetry 1-3-10-4 and the third one being point 13 in the domain of interest. As illustrated in Figure 4.15, the triple point formulation leads to one pyramidal (2-11-5-6-12), three tetrahedral (6-2-12-7, 7-2-12-7, 8-2-12-9) subzones and one prismatic (12-2-9-13-3-10) subzones. Pyramid (2-11-5-6-12) can be discretized in two different ways as shown in Figure 4.13. The prism (12-2-9-13-3-10) can be discretized in six different ways as shown in Figure 4.16. The detail scheme of discretization is summarized in Table 4.8. A single pyramid can be subdivided into two tetrahedrons in two different ways and a prism can be subdivided into three tetrahedrons in six different ways. Hence, there are eight tetrahedrons and twelve global schemes of discretization. All these subzones are interconnected and have common triangular faces. Thus, the basic SERR blocks in their totality have 25 bounding faces for TPF. As all these bounding faces are triangular in shape, by applying equation (3.13) we can get 25 velocity equations for this formulation. When these equations are solved, equal number of velocity components can be obtained and be used for the further calculation purpose as explained in previous section 3.2.1.



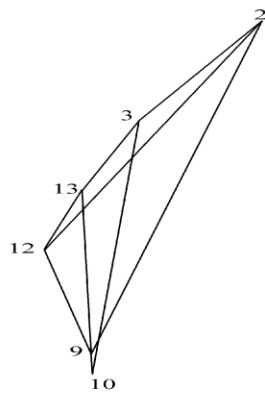
Pyramid: 2-11-5-6-12



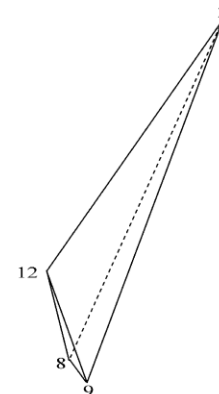
Tetrahedron: 6-2-12-7



Tetrahedron: 7-2-12-8

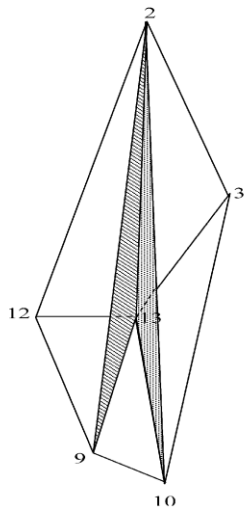


Prism: 12-2-9-13-3-10



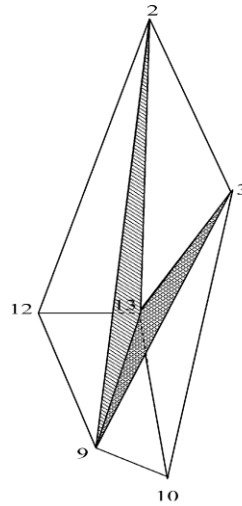
Tetrahedron: 8-2-12-9

Figure 4.15 Discretization of TFP deformation zone is divided into number subzones



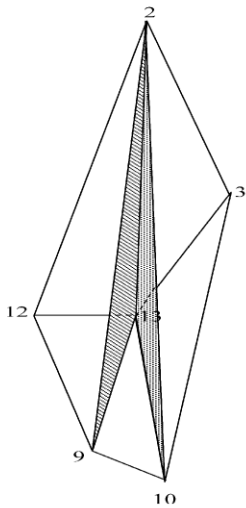
Scheme 1

- Tetrahedrons:
1. 13-9-12-2
 2. 13-3-10-9
 3. 13-9-2-3



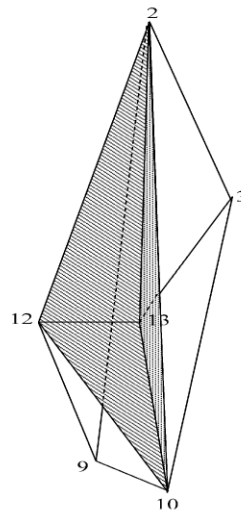
Scheme 2

- Tetrahedrons:
1. 13-9-12-2
 2. 13-3-10-2
 3. 13-9-10-2



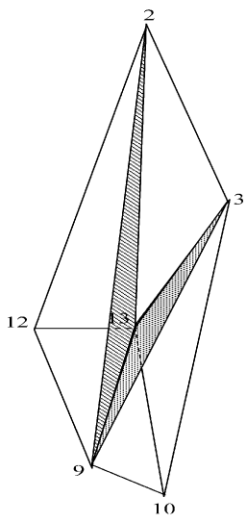
Scheme 3

- Tetrahedrons:
1. 13-2-3-10
 2. 2-10-12-13
 3. 2-10-9-11



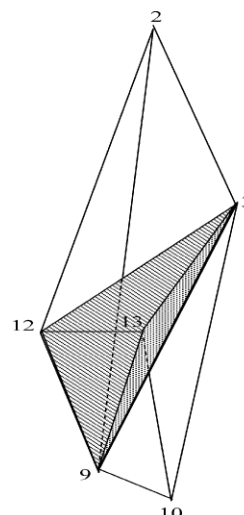
Scheme 4

- Tetrahedrons:
1. 13-2-3-10
 2. 2-13-9-12
 3. 2-13-10-9



Scheme 5

- Tetrahedrons:
1. 13-3-10-9
 2. 9-12-2-13
 3. 9-13-2-3



Scheme 6

- Tetrahedrons:
1. 13-3-10-9
 2. 9-12-3-13
 3. 9-12-2-3

Figure 4.16 Discretization of the prismatic subzone 12-2-9-13-3-10

Table 4.8 Global level of discretization schemes for triple floating point formulation

Global Scheme of discretization	Discretization Scheme for			Deformation zone (tetrahedrons)
	Pyramid: 2-11-5-6-	Prism: 12-2-9-13-3-10		
1	1	1	1	2-11-12-6, 7-2-12-8, 13-3-10-9, 2-11-6-5, 8-2-12-9, 13-9-2-3, 6-2-12-7, 13-9-12-2,
2	1	1	2	2-11-12-6, 7-2-12-8, 13-3-10-2, 2-11-6-5, 8-2-12-9, 13-9-10-2, 6-2-12-7, 13-9-12-2,
3	1	2	1	2-11-12-6, 7-2-12-8, 2-10-12-13, 2-11-6-5, 8-2-12-9, 2-10-9-11, 6-2-12-7, 13-2-3-10,
4	1	2	2	2-11-12-6, 7-2-12-8, 2-13-9-12, 2-11-6-5, 8-2-12-9, 2-13-10-9, 6-2-12-7, 13-2-3-10,
5	1	3	1	2-11-12-6, 7-2-12-8, 9-12-2-13, 2-11-6-5, 8-2-12-9, 9-13-2-3, 6-2-12-7, 13-3-10-9,
6	1	3	2	2-11-12-6, 7-2-12-8, 9-13-3-13, 2-11-6-5, 8-2-12-9, 9-12-2-3, 6-2-12-7, 13-3-10-9,
7	2	1	1	2-12-6-5, 7-2-12-8, 13-3-10-9, 2-12-5-11, 8-2-12-9, 13-9-2-3, 6-2-12-7, 13-9-12-2,
8	2	1	2	2-12-6-5, 7-2-12-8, 2, 2-12-5-11, 8-2-12-9, 6-2-12-7, 13-9-12-2,
9	2	2	1	2-12-6-5, 7-2-12-8, 10, 2-12-5-11, 8-2-12-9, 6-2-12-7, 13-2-3-
10	2	2	2	2-12-6-5, 7-2-12-8, 10, 2-12-5-11, 8-2-12-9, 6-2-12-7, 13-2-3-
11	2	3	1	2-12-6-5, 7-2-12-8, 9, 2-12-5-11, 8-2-12-9, 6-2-12-7, 13-3-10-
12	2	3	2	2-12-6-5, 7-2-12-8, 9, 2-12-5-11, 8-2-12-9, 6-2-12-7, 13-3-10-

4.2.2 Forward-backward extrusion-forging process

The discretization of the forward-backward extrusion-forging process of the triangular head with a circular shaft on both face side is analyzed by the same procedure as follows in the forward extrusion-forging process. Six formulations are considered, which are acknowledged as one, three, five, seven, nine and eleven numbers of floating points respectively. It is observed that nine numbers of floating point formulation give the optimal solution Figure 4.17 to Figure 4.22 visualize the discretization of one-sixth

of the deformation zone with a different floating point formulation for forward-backward extrusion-forging process.

4.3 Computation

A comprehensive computational model is developed incorporating all special features of the proposed cross section as explained in section 4.2. The solution process consists of the following steps:

- (a) Determination of the coefficients of equations representing the plane containing bounding faces of the tetrahedral blocks.
- (b) Determination of the coefficients of the velocity equations (Table 4.5) by applying mass continuity conditions to the respective faces
- (c) Find out the magnitudes of the velocity discontinuities (Table 4.6) by numerically solving equations of Table 4.5 using Gauss-Jordan algorithm with column pivoting [85]. This solution also determines the exit velocity, which serves as a check on computation since exit velocity can be independently calculated using the billet velocity and the area reduction.
- (d) Computation of the deformation work by equation (4.2) and the normalized extrusion pressure by equation (4.3).
- (e) Optimization of the normalized extrusion pressure with respect to optimizing parameters (length of the deformation zone and coordinates of the floating point) using a multivariate unconstrained optimization routine [121].

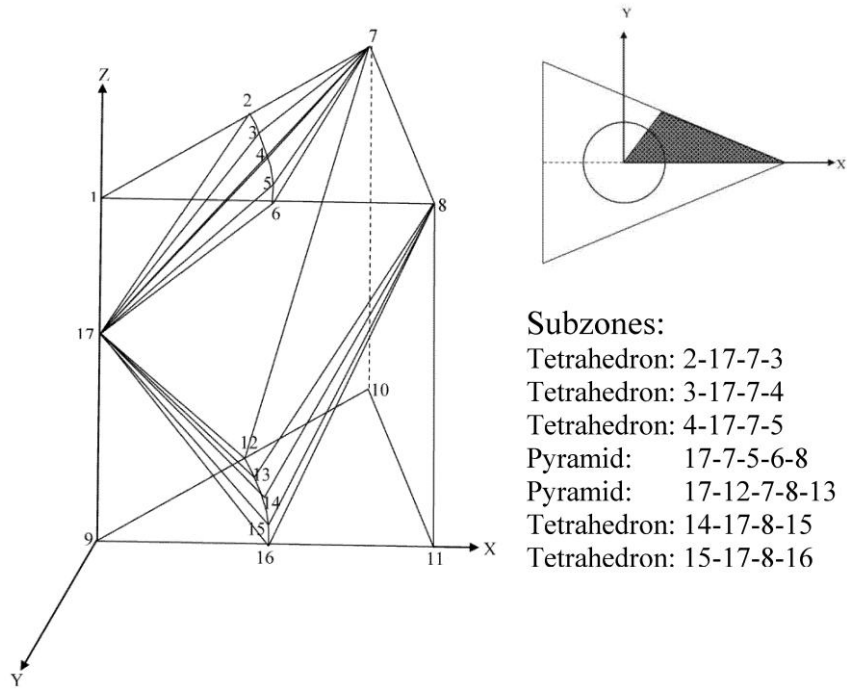


Figure 4.17 Discretization of one floating point deformation zone is divided into number subzones

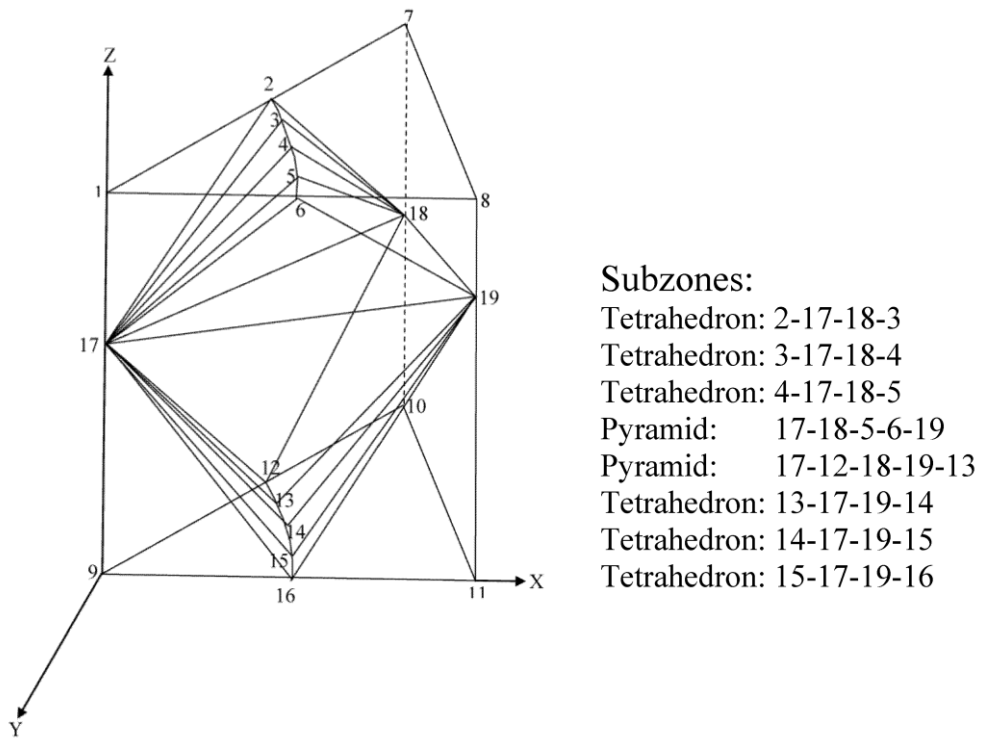


Figure 4.18 Discretization of three floating point deformation zone is divided into number subzones

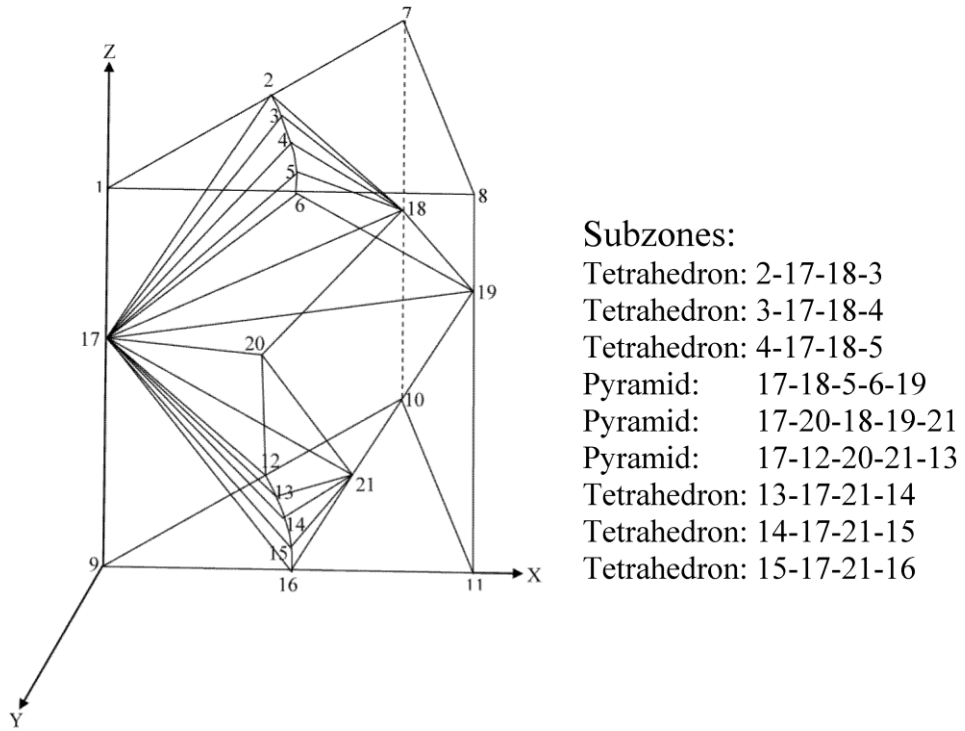


Figure 4.19 Discretization of five floating point deformation zone is divided into number subzones

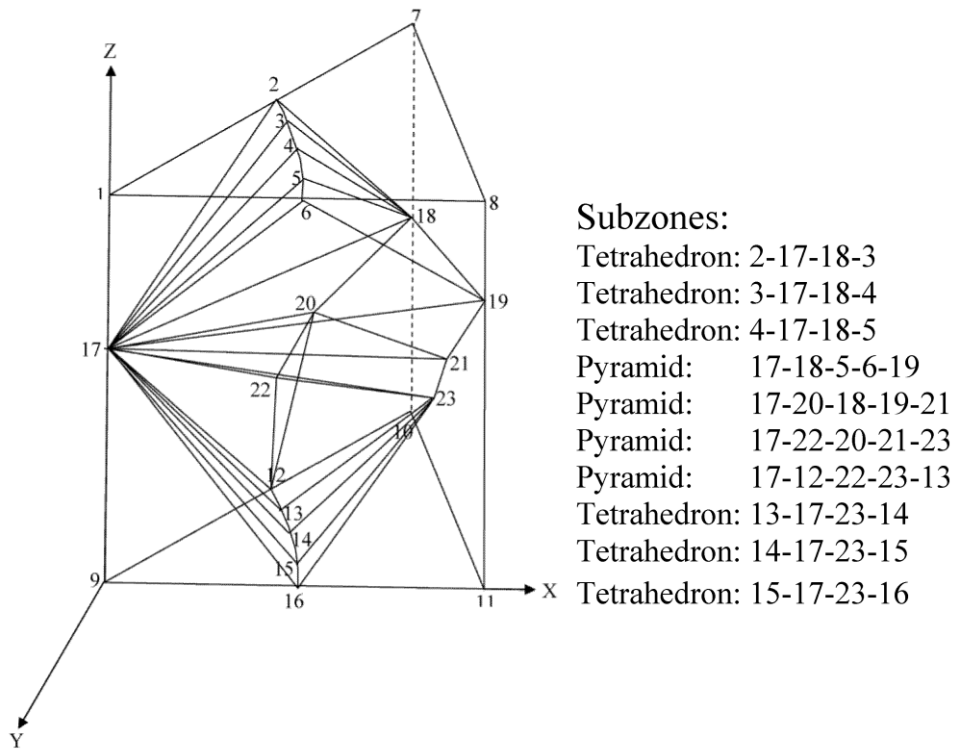


Figure 4.20 Discretization of seven floating point deformation zone is divided into number subzones

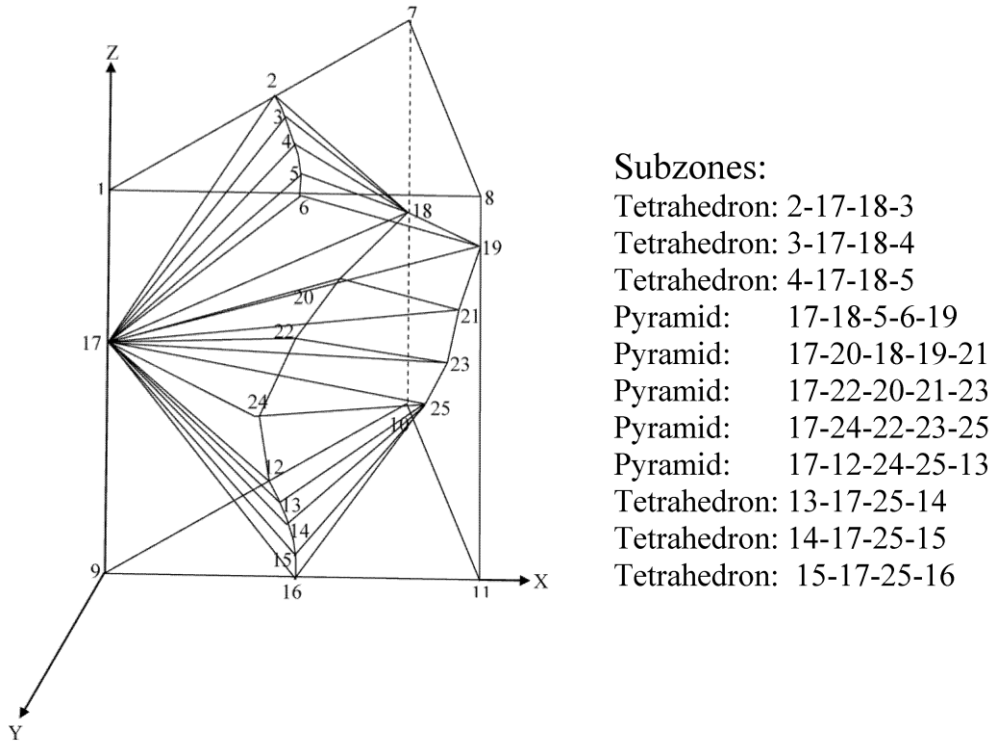


Figure 4.21 Discretization of nine floating point deformation zone is divided into number subzones

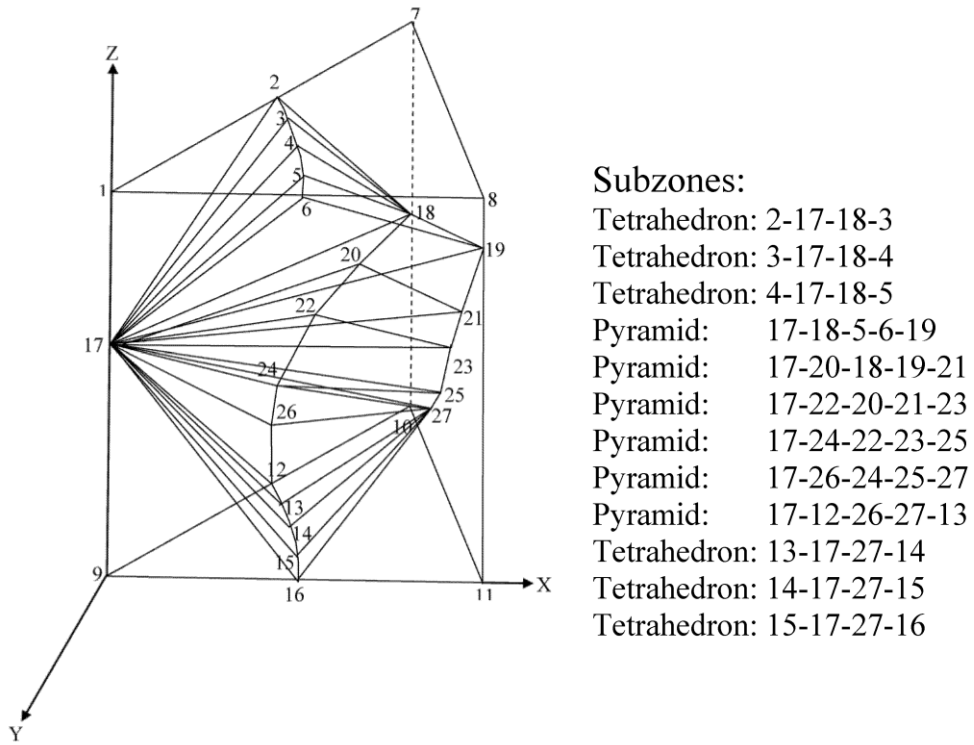


Figure 4.22 Discretization of eleven floating point deformation zone is divided into number subzones

4.4 Optimization Parameters

4.4.1 Forward extrusion-forging process

For the single point formulation (SPF), the floating point lies on the extrusion axis. Thus, it has one unknown coordinate. Further, the height of the dead metal zone (the z-coordinate of the point of intersection of the dead metal faces and the container wall) is an unknown parameter. These two unknown quantities serve as the optimization parameters to minimize the extrusion pressure for this formulation.

In case of the double point formulation (DPF), there are two floating point; one on the extrusion axis and the other one on one of the plane of symmetry and as such, has two unknown coordinates. The height of the deformation zone is another unknown parameter. Thus, the number of unknown parameters in this case is four, and they serve as the optimizing parameters for this formulation.

Similarly, in case of triple point formulation (TPF), there are three floating point; one on the extrusion axis, second one on the planes of symmetry and third one at an arbitrary location in the extrusion cavity. The height of the deformation zone is another unknown parameter. Thus, the total number of optimization parameters for this formulation is seven.

Computational model is developed for computing the non-dimensional average extrusion pressure. Among the three point's formulations and different combination of schemes, the optimum solution is identified. The whole process is analyzed the last stage of the combined extrusion forging process which require maximum load and steady state extrusion starts. To know the effect of friction non-dimensional extrusion pressure is calculated with punch movement as billet length decreases in this steady state stage.

4.4.2 Forward-backward extrusion-forging process

For forward-backward extrusion-forging process, one, three, five, seven, nine and eleven floating point formulations are formulated. Out of these above formulations nine floating point formulation gives the optimum result.

For the one floating point formulation (1FP), the floating point lies on the extrusion axis. Thus, it has one unknown co-ordinate. Further, the height of the dead metal zone (the z-coordinate of the point of intersection of the dead metal faces and the container wall) is an unknown parameter. Also, the proportionality between forward and

backward extrusion velocity is considered here as one optimizing parameter. These three unknown quantities serve as the optimization parameters to minimize the extrusion pressure for this formulation. Similarly, three floating point formulation (3FP), five floating point formulation (5FP), seven floating point formulation (7FP), nine floating point formulation (9FP) and eleven floating point formulation (11FP) has four, nine, thirteen, seventeen and twenty one variables respectively, which serve as the optimization parameters to minimize the extrusion pressure for these formulations.

4.5 Summary

4.5.1 Forward extrusion-forging process

Table 4.9 summarizes the zone of interest into different subzones. Computations are carried out for all the two global discretization schemes of single-point formulation, and the scheme gives the least upper bound energy is identified. The discretized deformation zone corresponding to the least upper bound is named here as optimum configuration. The optimum configuration in case of double point formulation is similarly determined testing all four schemes. The optimum configuration in case of triple point formulation is also similarly determined testing all 12 schemes (discretization details are summarized in Table 4.10. Figure 4.23 gives the comparison of the computed results of the three formulations for their respective optimal configurations. It is obvious from the Figure 4.23 that the double-point formulation gives the best results. Therefore, this formulation only is used for further computation and comparison.

Table 4.9 Summary of subzones

Type of subzones	Formulation		
	Single point	Double point	Triple point
Prism			12-2-9-13-3-10
Pyramid	11-2-9-10-3	2-11-5-6-12, 12-2-9-10-3	2-11-5-6-12
Tetrahedron	5-2-11-6, 6-2-11-7, 7-2-11-8, 8-2-11-9	6-2-12-7, 7-2-12-8, 8-2-12-9	6-2-12-7, 7-2-12-8, 8-2-12-9

Table 4.10 Summary of discretization schemes

Item	Single Point Formulation	Double Point Formulation	Triple Point Formulation
Subzones	1 Pyramid, 4 Tetrahedrons	2 Pyramids, 3 Tetrahedron	1 Prism, 1 Pyramid, 3 Tetrahedrons
Total No. of SERR blocks	6	7	8
No. of discretization schemes	2 X 1=2	2 X 2 =4	6 X 2=12
Total No. of triangular faces	19	22	25
No. of Velocity Component	6x3=18for SERR + 1 at exit velocity, total=19	7 x 3=21 for SERR + 1 at exit velocity, total=22	8 x 3=24 for SERR + 1 at exit velocity, total=25

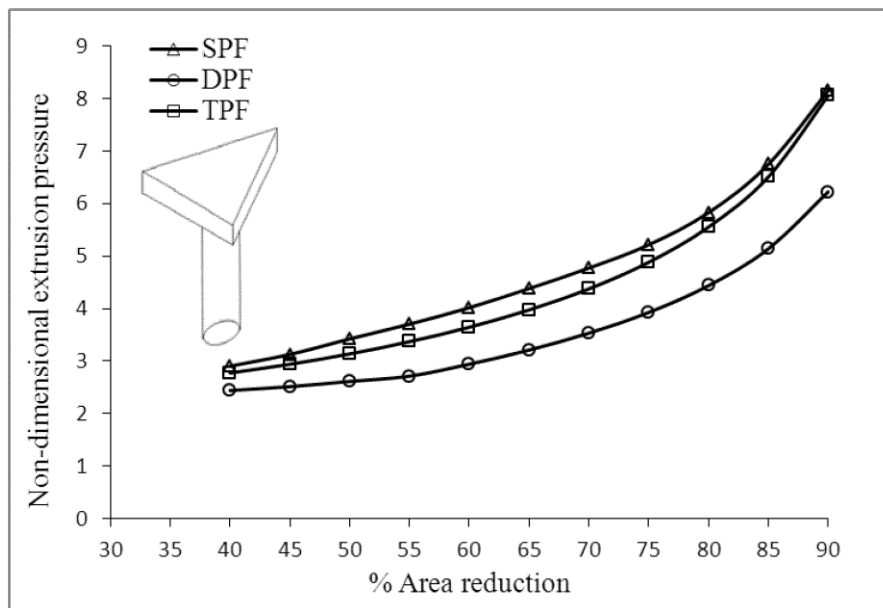


Figure 4.23 Comparison of results for different formulation (N=24)

When forging process completed and only steady state extrusion process takes place, the billet touches the whole die surface. With further punch travel the billet length reduces, decreasing the frictional resistance and thereby lessening the punch load. Figure

4.24 gives the punch load with punch travel for different reduction taking friction ($m=0.23$, found out by experiment described in section 4.18) into account.

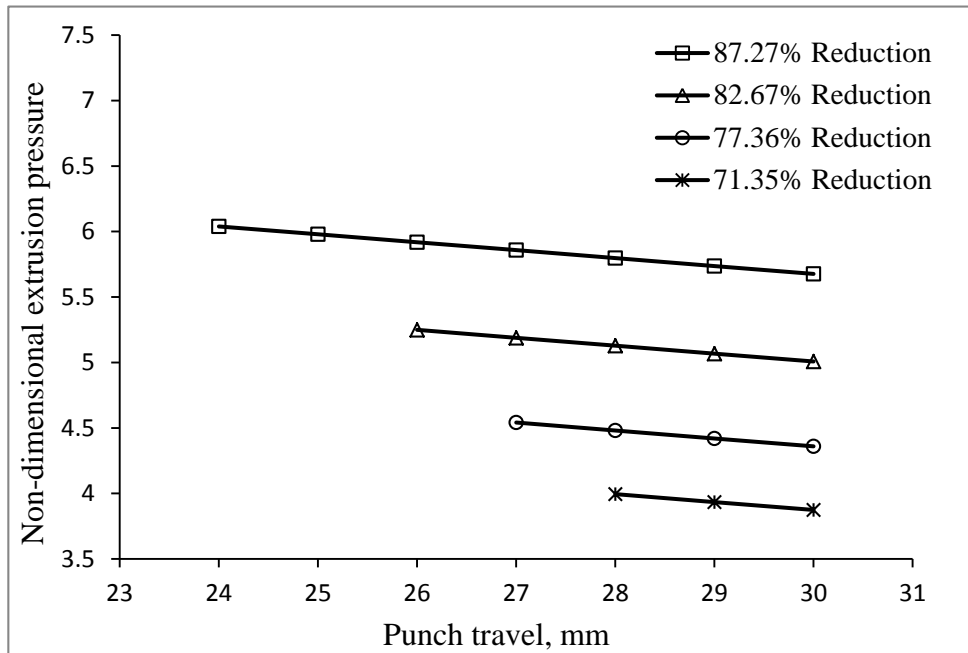


Figure 4.24 Comparison of results of different reduction with friction with punch travel

4.5.2 Forward-backward extrusion-forging process

Assumptions made for present analysis are:

1. The material is isotropic, homogeneous, rigid plastic and obeys the Von-Mises yield criterion.
2. The material is incompressible.
3. The die and punch are rigid and not deformed.
4. Elastic deformation is small compared to the plastic deformation and therefore neglected.
5. Frictional shear stress is expressed by a constant friction factor “ m ”.
6. The centroid of the die aperture lies on the billet axis.
7. Dead metal zones are formed on the sides of the die orifice.
8. Backward extrusion velocity is proportional to forward extrusion velocity and the proportionality factor is considered here as one optimizing parameter.

Table 4.11 summarizes the zone of interest into different subzones. Computations are carried out for all the global discretization schemes of one, three, five, seven, nine and eleven and the scheme gives the least upper bound energy is identified. The discretization scheme summarizes in Table 4.12. The discretized deformation zone corresponding to the least upper bound, named as optimum configuration. Figure 4.25 gives the comparison of the computed results of the six formulations for their respective optimal configurations. It is obvious from the Figure 4.25 that the three-point formulation gives the best results. Therefore, this formulation only is used for further computation and comparison.

Table 4.11 Summary of subzones

Type of Subzones	Formulation					
	1-floating point	3-floating point	5-floating point	7-floating point	9-floating point	11-floating point
Prisms						
Pyramids	17-7-5-6-8 17-12-7-8-13	17-18-5-6-19 17-12-18-19-13	17-18-5-6-19 17-20-18-19-21 17-12-20-21-13	17-18-5-6-19 17-20-18-19-21 17-22-20-21-23 17-12-22-23-13	17-18-5-6-19 17-20-18-19-21 17-22-20-21-23 17-24-22-23-25	17-18-5-6-19 17-20-18-19-21 17-22-20-21-3 17-24-22-23-5 17-12-14-15-13 17-12-14-15-3
Tetrahedrons	2-17-7-3 3-17-7-4 4-17-7-5 13-17-8-14 14-17-8-15 15-17-8-16	2-17-7-3 3-17-7-4 4-17-7-5 13-17-19-14 14-17-19-15 15-17-19-16	2-17-7-3 3-17-7-4 4-17-7-5 13-17-21-14 14-17-21-15 15-17-21-16	2-17-7-3 3-17-7-4 4-17-7-5 13-17-21-14 14-17-21-15 15-17-21-16	2-17-18-3 3-17-18-4 4-17-18-5 13-17-25-14 14-17-25-15 15-17-25-16	2-17-18-3 3-17-18-4 4-17-18-5 13-17-27-14 14-17-27-15 15-17-27-16

Table 4.12 Summary of discretization schemes

Items	1FP	3FP	5FP	7FP	9FP	11FP
Subzones	2 Pyramids, 6 Tetrahedrons	2 Pyramids, 6 Tetrahedrons	3 Pyramids, 6 Tetrahedrons	4 Pyramids, 6 Tetrahedrons	5 Pyramids, 6 Tetrahedrons	6 Pyramids, 6 Tetrahedrons
Total No. of SERR blocks	10	10	12	14	16	18
No. of discretization schemes	$2 \times 2 = 4$	$2 \times 2 = 4$	$2 \times 2 \times 2 = 8$	$2 \times 2 \times 2 \times 2 = 16$	$2 \times 2 \times 2 \times 2 \times 2 = 32$	$2 \times 2 \times 2 \times 2 \times 2 \times 2 = 64$
Total No. of triangular faces	31	31	37	43	49	55
No. of Velocity Component	$10 \times 3 = 30$ for SERR + 1 at exit velocity, total=31	$10 \times 3 = 30$ for SERR + 1 at exit velocity, total=31	$12 \times 3 = 36$ for SERR + 1 at exit velocity, total=37	$14 \times 3 = 42$ for SERR + 1 at exit velocity, total=43	$16 \times 3 = 48$ for SERR + 1 at exit velocity, total=49	$18 \times 3 = 54$ for SERR + 1 at exit velocity, total=55
No of optimizing parameters	3	4	9	13	17	21

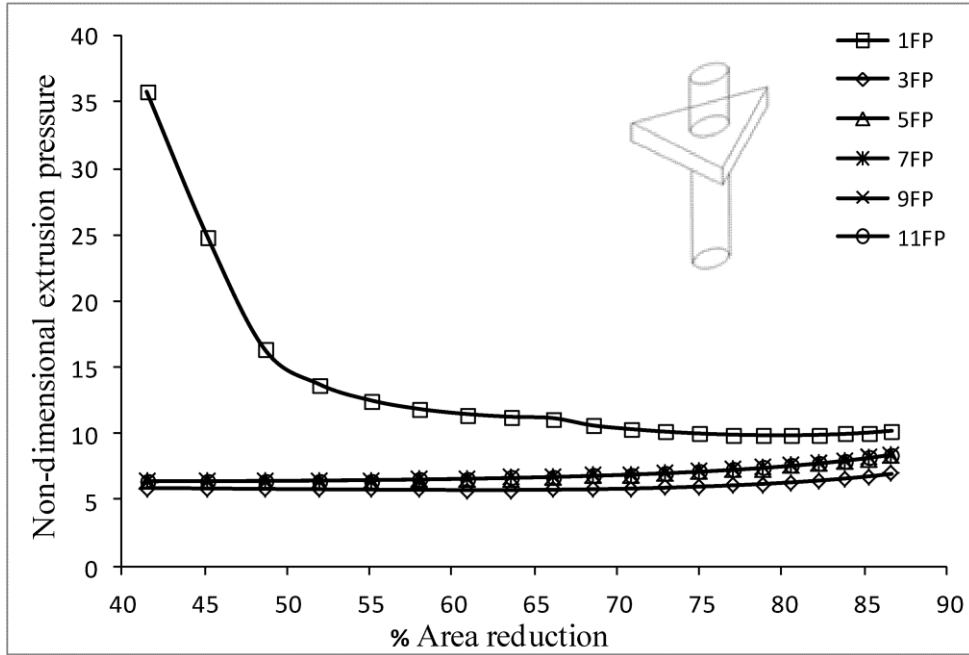


Figure 4.25 Comparison of results for different formulation (N=24)

II. FINITE ELEMENT ANALYSIS

4.6 Introduction (Finite Element Analysis)

Traditionally, the metal forming process that produces an acceptable product has been accomplished by extensive previous experience and an expensive and time consuming cycle of trials, evaluations and redesign. Such a traditional forming design approach is rapidly being replaced by more efficient computer simulation. Today, computer modeling is routinely used by industry for fast evaluation and optimization of forming processes before any actual physical trial. There are various metals forming analysis software that can realistically simulate material forming processes. Among them, DEFORM[®]3D is one, which is popular among the researchers and industries. Major input requisite for simulation is listed below Figure 4.26.

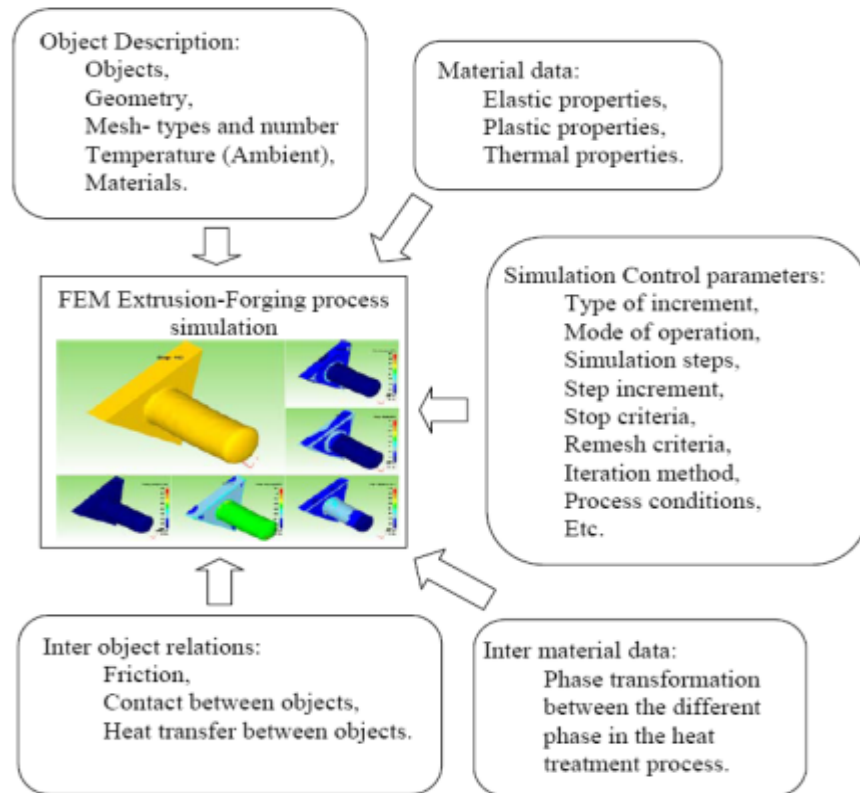


Figure 4.26 Major input parameters for FEM simulation for extrusion-forging of the triangular head with circular shaft

Total system consists of three major components

- (i) Per-processor: Design to establish the input conditions of the forming process analysis.

- (ii) Simulation: According to input data the finite element simulation performs the numerical calculations to solve the problem.
- (iii) Post-processor: A post-processor for reading the database files from the simulation engine and displaying the results graphically and for extracting numerical data. The postprocessor is used to view simulation data after the simulation has been run. The postprocessor features a graphical user interface to view geometry, field data such as strain, temperature, and stress, and other simulation data such as die loads. The postprocessor can also be used to extract graphic or numerical data for use in other applications.

4.7 Formulation

4.7.1 Viscoplastic material formulation

In the present analysis, focus to be placed on cold forming conditions. A rigid-viscoplastic material formulation is used for the work piece. The governing equations [118] that have to satisfy during the extrusion-forging process are:

$$\text{Equilibrium conditions: } \sigma_{ij,j} = 0 \quad (4.4)$$

$$\text{Compatibility condition: } \dot{\varepsilon}_{ij} = \frac{1}{2}(v_{i,j} + v_{j,i}) \quad (4.5)$$

$$\text{Constitutive relations: } \sigma'_{ij} = \frac{2\bar{\sigma}}{3\bar{\varepsilon}} \varepsilon_{ij} \quad (4.6)$$

$$\text{Incompressibility condition: } \dot{\varepsilon}_{kk} = 0 \quad (4.7)$$

$$\text{Boundary conditions: } \sigma_{ij}n_j = \bar{F}_i \text{ on } S_f, \quad v_i = \bar{v}_i \text{ on } S_v \quad (4.8)$$

The field equations given above can solved by a variational principle expressed as

$$\delta\phi = \int_V \bar{\sigma} \delta\dot{\varepsilon} dV + \int_V k \dot{\varepsilon}_{kk} \delta\dot{\varepsilon}_{mm} dV + \int_{S_f} \bar{F} \delta v_i dS = 0 \quad (4.9)$$

where, σ_{ij} = Stress component,

$\dot{\varepsilon}_{ij}$ = Strain rate component,

v_i = Velocity component,

σ'_{ij} = deviatoric stress component,

i, j and k for 3D problem vary from 1 to 3 and the repeated subscript means summations.

In the above equation, V is the billet volume, S_v the velocity surface, \bar{F} the traction (frictional) stress and k is a large positive constant to penalize volume change. The variational function can be converted to non-linear algebraic equations by utilizing the FEM discretization procedure. The solution of non-linear equations can be obtained by the Newton-Raphson method.

In the isotropic rigid-viscoplastic material model, flow stress is a function of effective strain, effective strain rate and temperature as:

$$\bar{\sigma} = f(\bar{\varepsilon}, \dot{\bar{\varepsilon}}, T) \quad (4.10)$$

where, $\bar{\sigma}$, $\bar{\varepsilon}$, $\dot{\bar{\varepsilon}}$, are effective stress, effective strain and effective strain rate, respectively.

4.7.2 Heat transfer formulation

Temperature plays an important role in forming operation since the material properties, such as flow stress, are highly dependent on temperature. The rigid-viscoelastic material model coupled a heat-transfer model (the temperature distribution of work piece, tooling and ambient surrounding) expressed by the following equation:

$$(kT_{,i})_{,i} + \dot{r} - (\rho c_p T) = 0 \quad (4.11)$$

Where, T is temperature, k denotes thermal conductivity, \dot{r} the heat generation rate, ρ the specific density, c_p is the specific heat and $(,)$ is used for differentiation. The first term represents the heat transfer rate, the second term represents the rate of heat generation in the deforming billet due to plastic deformation, and the third term represents the internal energy generation rate.

$$\dot{r} = \alpha \rho \dot{\varepsilon} \quad (4.12)$$

where, \dot{r} is the heat generation efficiency, α represents the fraction of mechanical energy converted into heat and is usually assumed to be 0.9. The energy balance equation can be rewritten, by using weighted residual method as:

$$\int_V k T_{,i} \partial T_{,i} dV + \int_V \rho c_p \dot{T} \partial T dV - \int_V \alpha \bar{\sigma} \dot{\bar{\varepsilon}} T dV - \int_S q_n \partial T dS = 0 \quad (4.13)$$

Where, q_n is the heat flux normal to the boundary surface. In general, q_n includes the convection heat loss and radiation heat loss to the environment, the friction heat gain due to movement between the dies and the work pieces, and the heat loss or gain through contact with colder or hotter object. The temperature distribution of both the work piece and the die can be obtained readily by solving the above energy balance equation.

4.7.3 Interface formulation

In the interface formulation, an interaction between the work piece and dies during metal forming operations is incorporated. The contact conditions can be mathematically described by:

$$v \cdot n = 0, \quad t = 0 \quad (4.14)$$

where, v and t are the velocity and traction vectors, respectively, n is a unit normal to the contact surface, and (\cdot) indicates the discontinuity amount across the contact boundary. Moreover, the traction in the tangential direction should satisfy the frictional law. The interface formulation between the work piece and rigid dies is relatively simple. In order to simulate more complicated forming operations, such as canned extrusion, pack rolling, and hot isostatic pressing, the interface formulation should be capable of handling the contact conditions between the deforming bodies. The interface conditions given in equation (4.14) can be expressed in variational form as:

$$\int_S K_t \Delta v_n \delta \Delta v_n dS + \int_S t_s \delta \Delta v_s dS = 0 \quad (4.15)$$

Where, Δv_n is a penetrating velocity in the normal direction, Δv_s sliding velocity in the tangential direction, and t_s traction representing frictional stress. Here K_t is a large positive constant to penalize the penetration.

4.8 Pre-Processor

4.8.1 Simulation control

In this simulation SI unit convention, langrangian incremental type and deformation mode of simulation are followed. Deformation mode, simulates the deformation due to mechanical, thermal, or phase transformation effects. The primary die is the punch plate for which stopping and stepping criteria are defined. Stopping is terminating the simulation when the distance between reference points on two objects/dies reaches the specified distance. Stopping distance are in conjunction with the

reference points. Solution step size or stepping criteria can be controlled by time step or by displacement of the primary die. If the stroke per step is specified, the primary die will move the specified amount in each time step. The total movement of the primary die will be the displacement per step multiplied by the total number of steps. In this simulation die displacement method of stepping criteria is chosen. During the simulation, extensive deformation of plastic objects may cause elements in those object meshes to become so distorted that the mesh is no longer usable (negative Jacobian). To continue a simulation after a mesh has become unusable, the object must be remeshed. Remeshing is the process of replacing a distorted mesh with a new undistorted mesh and interpolating the field variables (strain, velocity, damage, and temperature, etc.) from the old mesh to the new mesh. The interference depth controls the initiation of a remeshing procedure based on the depth of interference between a slave object and a master object. The depth of interference is the depth an element edge of the slave object crosses the surface of a master object. The object to be remeshed must be a slave object, in this simulation billet. The interference depth parameter should be used with extremely sharp corners where the corner radius is nearly the same size as the adjacent element edge length. The remesh depth should be set to roughly half of the element edge length. Too large an interference depth may cause excess volume loss. Too small a value may cause too many remeshings, leading to slow run times and excessive interpolation error. Here relative interference depth 0.7 and global remeshing is considered, where in every element of the old mesh gets replaced with the new mesh elements, followed by interpolation. New Local meshing functionality allows several options to control the element size and quality. The iteration controls specify criteria the FEM solver uses to find a solution at each step of the problem simulation. Conjugate-Gradient solver and direct iteration are opted. Convergence problems are well suited for Conjugate-Gradient. The processing condition's menu contains information about the process environment, and constants related to general solution behavior. Appropriate constant values are automatically set SI units.

4.8.2 Materials

The material model used in this study was isotropic and rigid-perfectly plastic. The material chosen is commercially available lead. Stress required for deformation (flow stress) is generally given as a function of plastic strain, strain rate and temperature. With some equations or user subroutines, additional factors such as grain size or carbon

content may be included. The flow stress governing equation is followed by the equation (4.10). The numerical value of flow stress is 0.023kN/mm² (from experiment). The chemical composition is analysis on SEM. Depending upon the composition, the elastic, plastic and thermal property's data are taken from [123].

4.8.3 Object description

In this simulation triangular shape forging die and different percentage reduction extrusion dies are together form the bottom die. A triangular shape punch plate is considered as primary die or top die. These are considered as rigid objects and made of non-deformable materials. The rigid objects are modeled in solid modeling software and STL files are imported for simulation during defining the geometry. The plastic object is the billet/work piece and cylindrical in shape. The geometry of the billet is generated by using Geo Primitive options for 3D forming. Tetrahedral shape, 25000 numbers of initial elements and finer internal mesh were generated for billet. Ambient temperature is considered for the simulation.

4.8.4 Inter-object relation

The purpose of inter-object relations is to define how the different objects in a simulation interact with each other. All objects which may come in contact with each other through the course of the simulation must have a contact relation defined. This includes an object having a relationship to it if self-contact occurs. It is very important to define these relationships correctly for a simulation to model a forming process accurately. The critical variables to be defined between contacting objects are:

- Friction factor: 0.23 (from ring test, described in section 4.18).
- Interface heat transfer coefficient: The interface heat transfer coefficient specifies the coefficient of heat transfer between two objects in contact. This can be specified as a constant or a function of time or interface pressure. The interface heat transfer coefficient is generally a complex function determined by the interface pressure, amount of sliding, and interface temperature. If this table is available, item is entered as a table. If no data is available, value 0.004(English) or 11 (SI, system defined default value) is considered which gives reasonable results.
- Contact relation.
- Separation criterion (The separation criteria define how the nodes at inter object interface will behave when acted upon by a tensile force. The default setting will

cause normal separation when the contacting node experiences a tensile force or pressure greater than 0.1 considered in this case).

4.8.5 Movement control

Movement controls can be applied to rigid objects and boundary nodes of meshed objects. The surface defined by these nodes can be thought of as a "rigid surface". During the simulation, the constrained nodes will move synchronously in the speed and direction defined by the movement controls i.e., translational motion. Mechanical press with $-z$ direction movement of ram at a speed of 1mm/min was opted. Total forging stroke 30mm is chosen which is equal to the top die displacement.

4.8.6 Boundary condition

The top die or punch movement is only in $-z$ direction. There was no movement of bottom die.

4.9 Simulation

When all requisite data are given in the pre-processor steps the simulation system checks for any missing data and generates a database. The simulation starts and initiates a series of operations to run the simulation and generate new meshes as necessary. Run-time information will be written to the ProblemId.MSG and ProblemId.LOG files. Execution information, including convergence information for each step and simulation error messages, can be found in the .MSG file. Information on simulation and remeshing, execution times, and fatal errors can be found in the .LOG file or in the command window where DEFORM was executed from.

4.10 Post-Processor

Post processor with a variety of features and graphics allows engineers to check the model results and present them in a way to understand the model results in an efficient manner. The post-processor is used to view and extract data from the simulation results in the database file. All results steps which were saved by the simulation engine are available in the post-processor. Information which is available from the post-processor includes:

- Deformed geometry, including tool movements and deformed mesh at each saved step.

- Contour plots: Line or shaded contours display the distribution of any state variables, including stress, strain, temperature, damage, and others.
- Vector plots: displacement and velocity vectors indicate magnitude and direction of displacement or velocity for every node at each step throughout the process.
- Graphs of key variables such as press loads, volumes, and point tracked state variables.
- Point tracking to show how material moves and plots of state variables at these points.
- Flow net showing material flow patterns on a uniform grid. Generally a very good predictor of grain flow patterns in the finished part.
- State variables can be tracked between any two points and plotted in a graph format. The state variables can either follow the boundary or linearly between the points.
- A histogram plot of any state variable can be made to view the distribution of any given state variable throughout a body.

4.11 Summary

4.11.1 Forward Extrusion-forging process

The process parameters used in this simulation is summarized in Table 4.13. Five different area reduction dies (87.24%, 82.63%, 77.31%, 71.28% and 64.55% reductions) are used in this series of experiments. The dies and punch plate used for simulation was same as that of experimental sets. Figure 4.27 gives comparison of punch load with punch movement for different percentage area reductions.

Table 4.13 Process parameter used in simulation

Billet length	40mm
Billet diameter	30mm
Billet temperature	Ambient
Ram speed	1mm/min
Friction factor	0.23
Flow stress	0.0233kN/mm ²

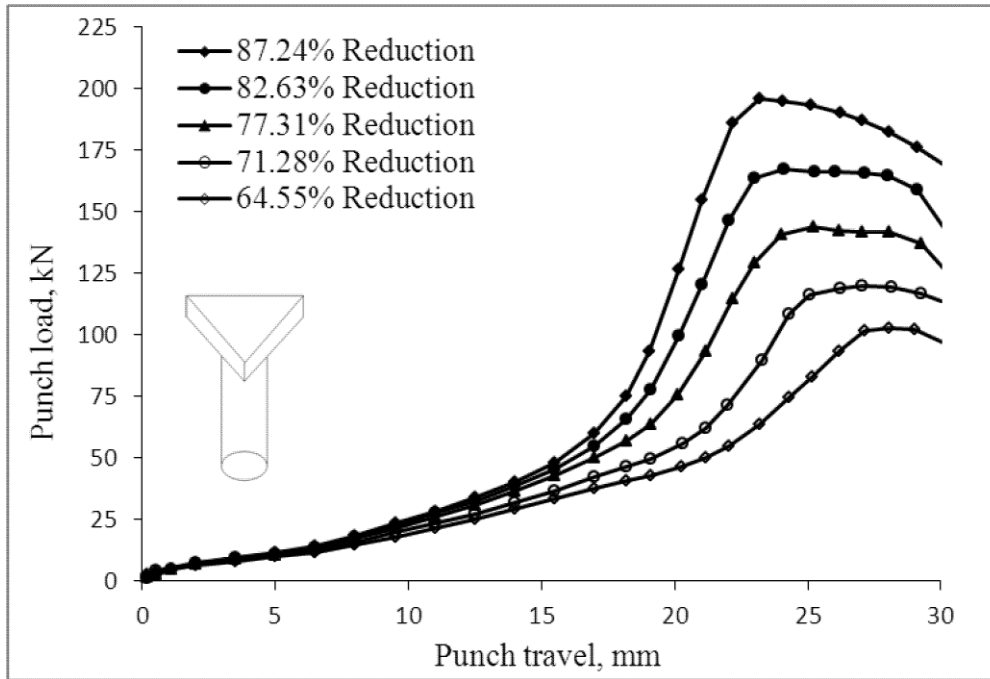


Figure 4.27 Variation of punch load with punch travel

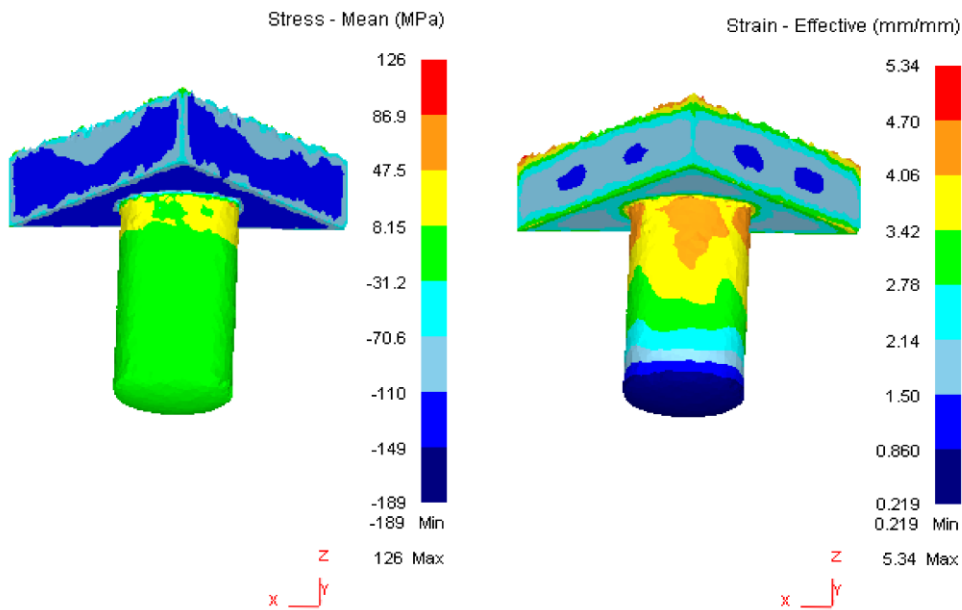


Figure 4.28 Mean stress and effective strain at particular reduction and punch movement for forward extrusion-forging process

Figure 4.28 shows the mean stress distribution and effective strain in terms of solid profile for the reduction of 77.31; at a ram speed of 1mm/min and ram displacement of 25mm. for forward extrusion-forging process. The positive stress signifies the tensile component of stress. From the figure it is observed that just after the

die land the material attain a maximum tensile stress. At the die land the stress is found 0.031kN/mm^2 which is around the flow stress of the material chosen. Maximum compressive stresses reaches near die walls. It is observed that there is a large stress concentration ($0.0278 - 0.0342\text{kN/mm}^2$) round the die entrance. The effective strain is more immediate after the extrusion through flat die and gradually decreases.

4.11.2 Forward backward Extrusion-forging process

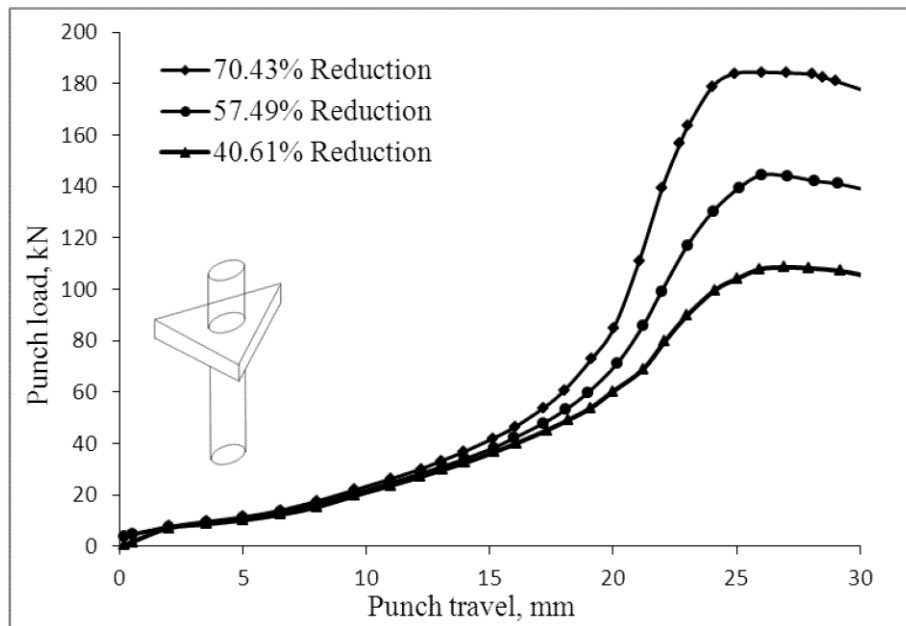


Figure 4.29 Variation of punch load with punch travel

Three different area reduction dies (70.43%, 57.49% and 40.61% reduction) are used in this series of experiments. The dies and punch plate used for simulation was same as that of experimental sets. Figure 4.29 gives comparison of punch load with punch movement for different percentage area reductions.

4.11.2.1 Mean stress and effective strain

Figure 4.30 shows the mean stress distribution and effective strain in terms of solid profile for the reduction of 77.31%, at a ram speed of 1mm/min and ram displacement of 25mm for forward-backward extrusion forging process. The positive stress signifies the tensile component of stress. From the figure it is observed that just after the die land the material attain a maximum tensile stress. At the die land the stress is found 0.031kN/mm^2 which is around the flow stress of the material chosen. Maximum compressive stresses reach near die walls. From the figure it is observed that there is a large stress concentration ($0.0278 - 0.0342\text{kN/mm}^2$) round the die entrance. Because of

severe deformation, the effective strain is more immediately after the extrusion through flat die and gradually decreases afterwards.

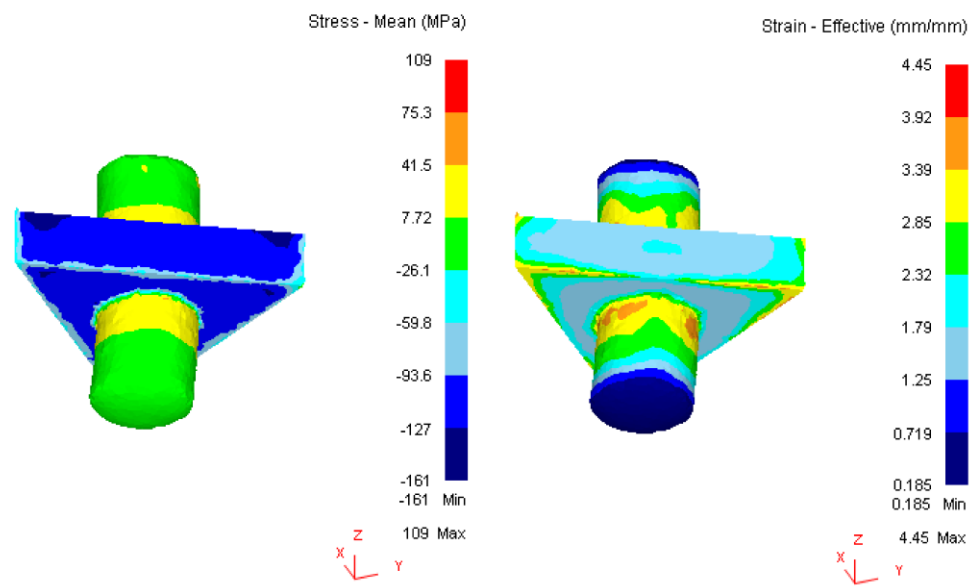


Figure 4.30 Mean stress and effective strain at particular reduction and punch movement for forward backward extrusion-forging process

III. EXPERIMENTAL ANALYSIS

4.12 Introduction (Experimental Analysis)

In the theoretical analysis, idealized assumptions are invariably made concerning the nature of the deformation and material properties. Therefore, before adopting the theoretical results, their suitability needs to be verified experimentally. A number of experimental studies on plain strain and axisymmetric extrusion using symmetric and asymmetric dies have been carried out in the past by different investigators. An exhaustive list of such work has been given by Johnson and Kudo [43]. The main objective of these studies has been either to compare the theoretically predicated extrusion load with the experimental value [11, 46, 118], or to compare predicated stream lines with those obtained by deformation of a square grid or to compare the die filling at different stages. Measurement of container wall pressure has also been carried out by Frisch and Thomson [46] and Kudo [120] while the effect of tool geometry on mean extrusion pressure has been studied by Dodeja and Jonson [11].

Although a lot of studies have been carried out on plain strain and axisymmetric extrusion, countable work has been reported on extrusion of section with re-entrant corners. Johnson [122] performed a series of tests on different section bars using circular billets of pure and tellurium lead. He also studied the effect of punch speed on extrusion load. Experimental investigation on extrusion of square, triangle and elliptic sections from round bars using stream lined dies have been reported by Yang et al. [61]. Recently, Sahoo [81] compare the experimental result with that of theoretical for different sections using square dies from square billet. However, very few authors have compared the experimental results with those predicted by theoretical analysis.

In the present investigation, experimental studies are carried out with a view to compare the experimental results with the theoretical ones obtained from proposed method of analysis, and finite element analysis obtained from commercially available FEM software. Experiments are performed on an INSTRON® 600KN Universal testing machine (maximum capacity of 600kN) for extrusion-forging of round-triangle-round sections using square dies. Commercially available lead is used for above mentioned purpose. An extrusion-forging setup for laboratory experimentation is designed and fabricated.

4.13 The Test Rig

The experimental setup used in the present series of test is shown in Figure 4.31. The apparatus consists of seven parts, namely; the container, the extruding punch, the forging die holder, extruding die holder, support plate, a series forging dies and different reduction extruding dies. The details' lists of components are given in below in Table 4.14. The container (140mm diameter and 100mm length) is made of EN31 steel, and having a cylindrical chamber (50mm ϕ and 100mm length). This is accomplished first by turning the outer diameter and drilling the inner chamber (having tolerance of $\pm .01$ mm) using wire cut EDM. The detail dimensions are given in Figure 4.32. Four numbers of Allen's screw holes are made on both flat faces. Inner faced holes are used for bolting the whole assembly and outer holes are used to hold firmly the cover plate. A container sleeve (Figure 4.33), insert for container, outer diameter match with the inner diameter of the container. The inner diameter of the sleeve matches the diameter of the punch rod. Its function is to guide the punch rod through it and avoid bulging of the punch rod. By changing the sleeve, we can use a different diameter punch for the different purpose. To avoid back slip of the sleeve from the container during experimentation container cover (Figure 4.34) is used. Similar processes are followed for manufacturing of the forging die holder (Figure 4.35), extrusion die holder (Figure 4.36). A support plate (Figure 4.37) made up of EN8 steel is used in this set up for supporting the uneven surfaces of the assembly. Generally, during experimentation, back flow of material through the punch, bulging of punch rod due to excessive back pressure sticks the punch with the sleeve and removal of punch is difficult. For easy removal of punch (Figure 4.38), punch is made up two parts; first one is punch rod and another one is the punch rod holder which is assembled by Allen's screw.

Table 4.14 List of components

SL. NO.	DESCRIPTION	QTY.	MATERIAL	SIZE	REMARK
1	COVER PLATE	1	EN8	Ø140x10	HRc 45-48
2	CONTAINER	1	EN31	Ø140x100	HRc 45-48
3	CONTAINER SLEEVE	1	EN31	Ø50x100	HRc 45-48
4	DIE HOLDER	1	EN31	Ø140x50	HRc 45-48
5	EXTRUSSION DIE HOLDER	1	EN31	Ø140x30	HRc 45-48
6	SUPPORT PLATE	1	EN8	Ø160x20	HRc 45-48
7	PUNCH-1	1	D2	Ø30x150	HRc 50-55
8	PUNCH-2	1	D2	Ø30x180	HRc 50-55
9	PUNCH ROD HOLDER	2	D2	Ø160x25	HRc 50-55
10	TESTING PLATE	2	D2	Ø130x30	HRc 50-55
11	TRIANGULAR SPLIT DIE	01 Set	D2	VARIABLES	HRc 50-55
12	SQUARE SPLIT DIE	01 Set	D2	VARIABLES	HRc 50-55
13	PENTAGON SPLIT DIE	01 Set	D2	VARIABLES	HRc 50-55
14	HEXAGON SPLIT DIE	01 Set	D2	VARIABLES	HRc 50-55
15	GEAR SHAPE SPILT DIE	04 Set	D2	VARIABLES	HRc 50-55
16	EXTRUSSION DIE SPLIT TYPE	04 Set	D2	Ø60x20	HRc 50-55
17	COUNTER SHINK SCREW	4	EN31	M8x15	
18	ALLEN SCREW	1	EN31	M8x30	
19	ALLEN SCREW	1	EN31	M8x35	
20	ALLEN SCREW	4	EN31	M10x105	

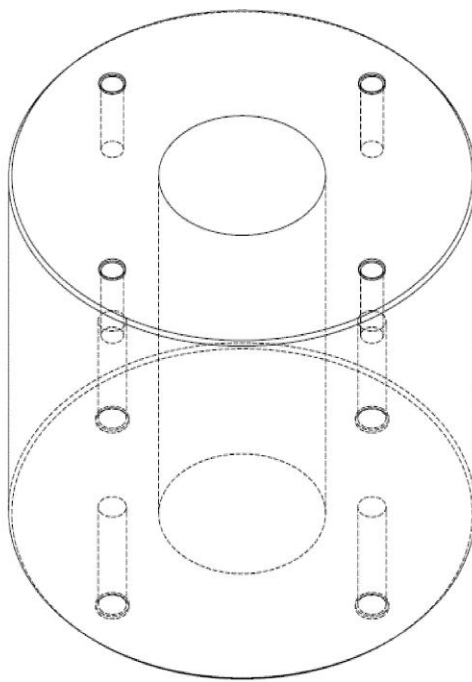
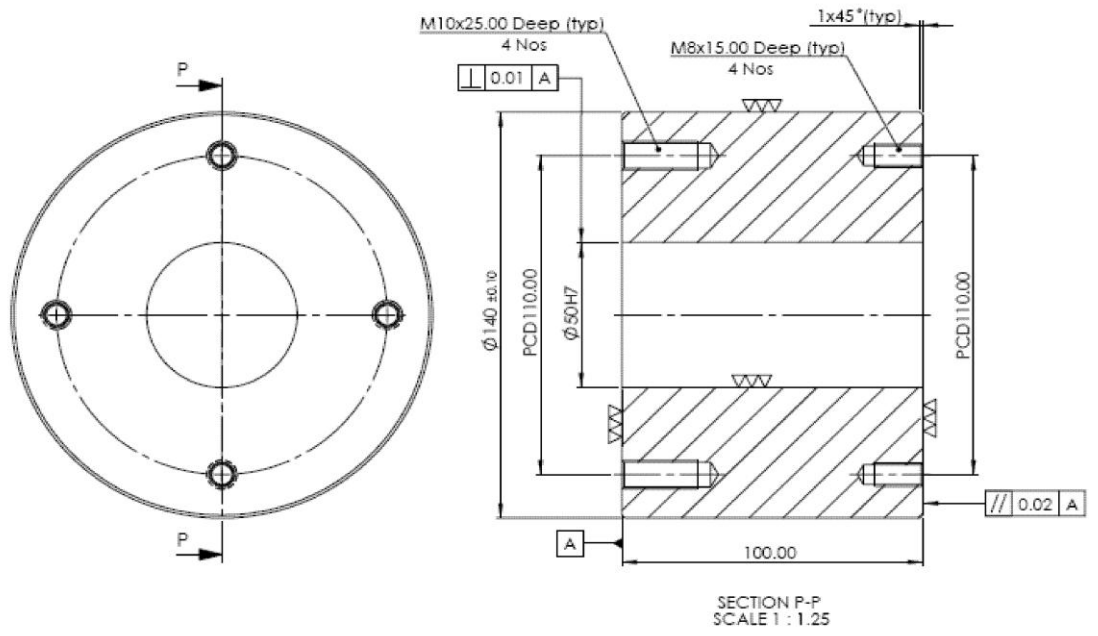


Figure 4.32 Container

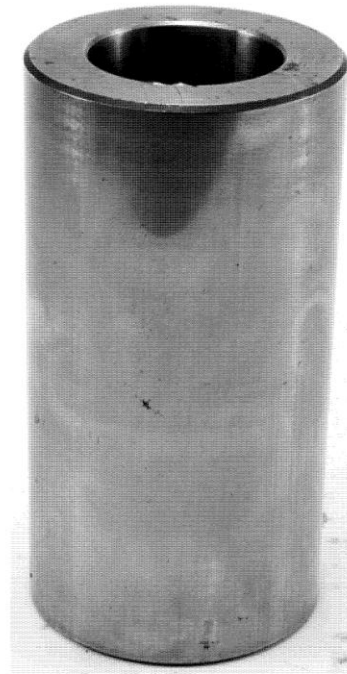
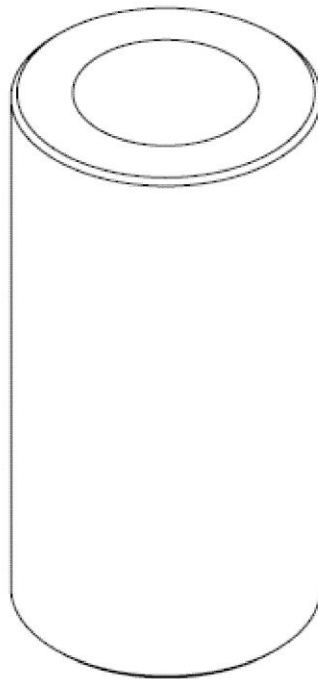
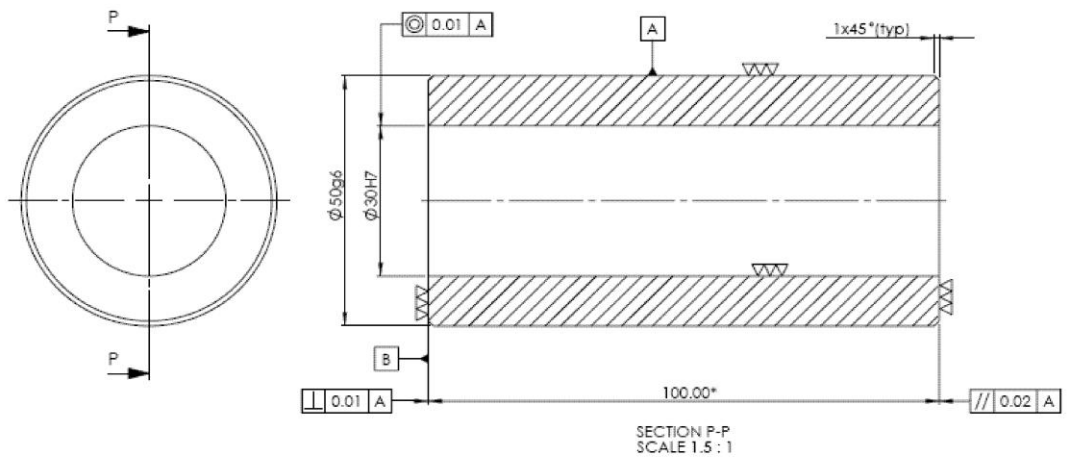


Figure 4.33 Container sleeve

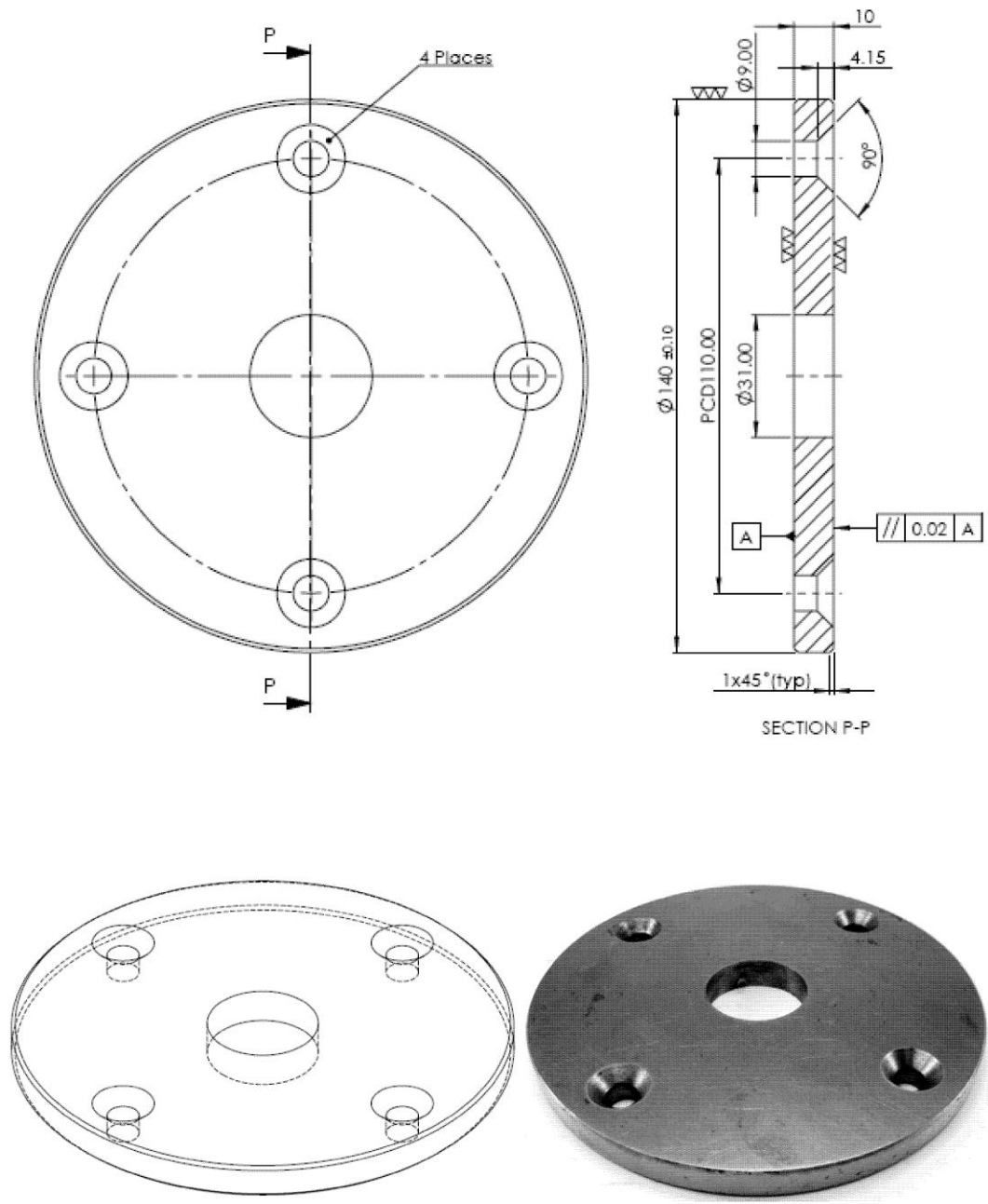


Figure 4.34 Container cover plate

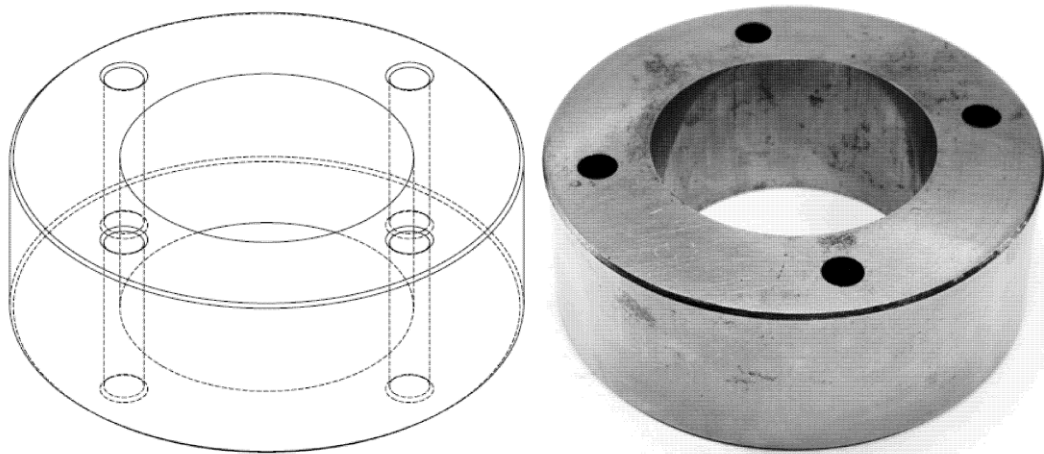
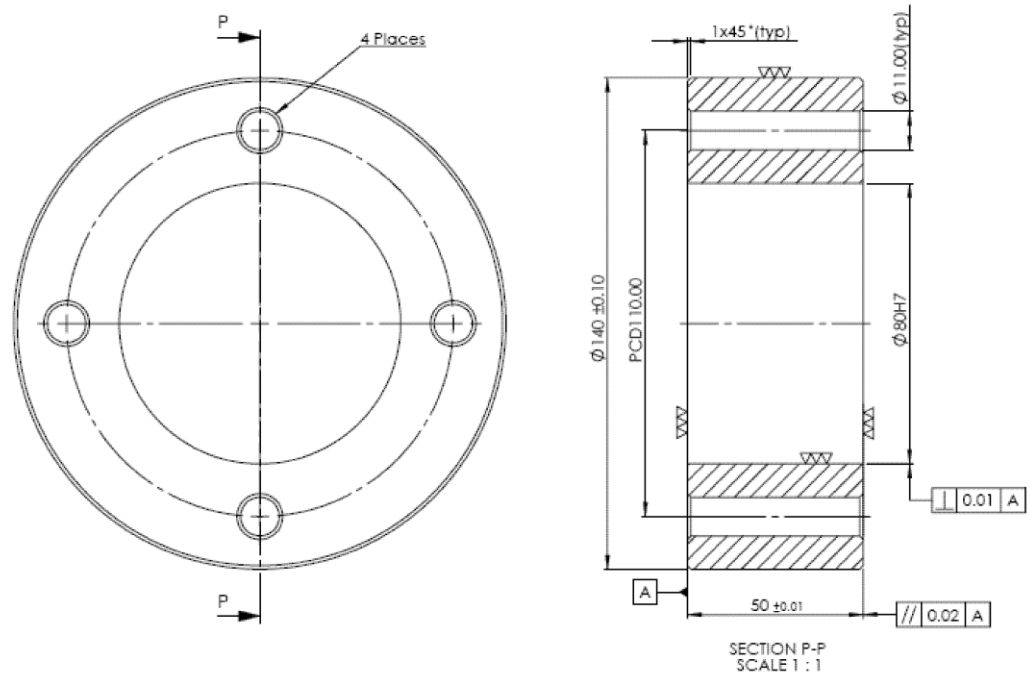


Figure 4.35 Forging die holder

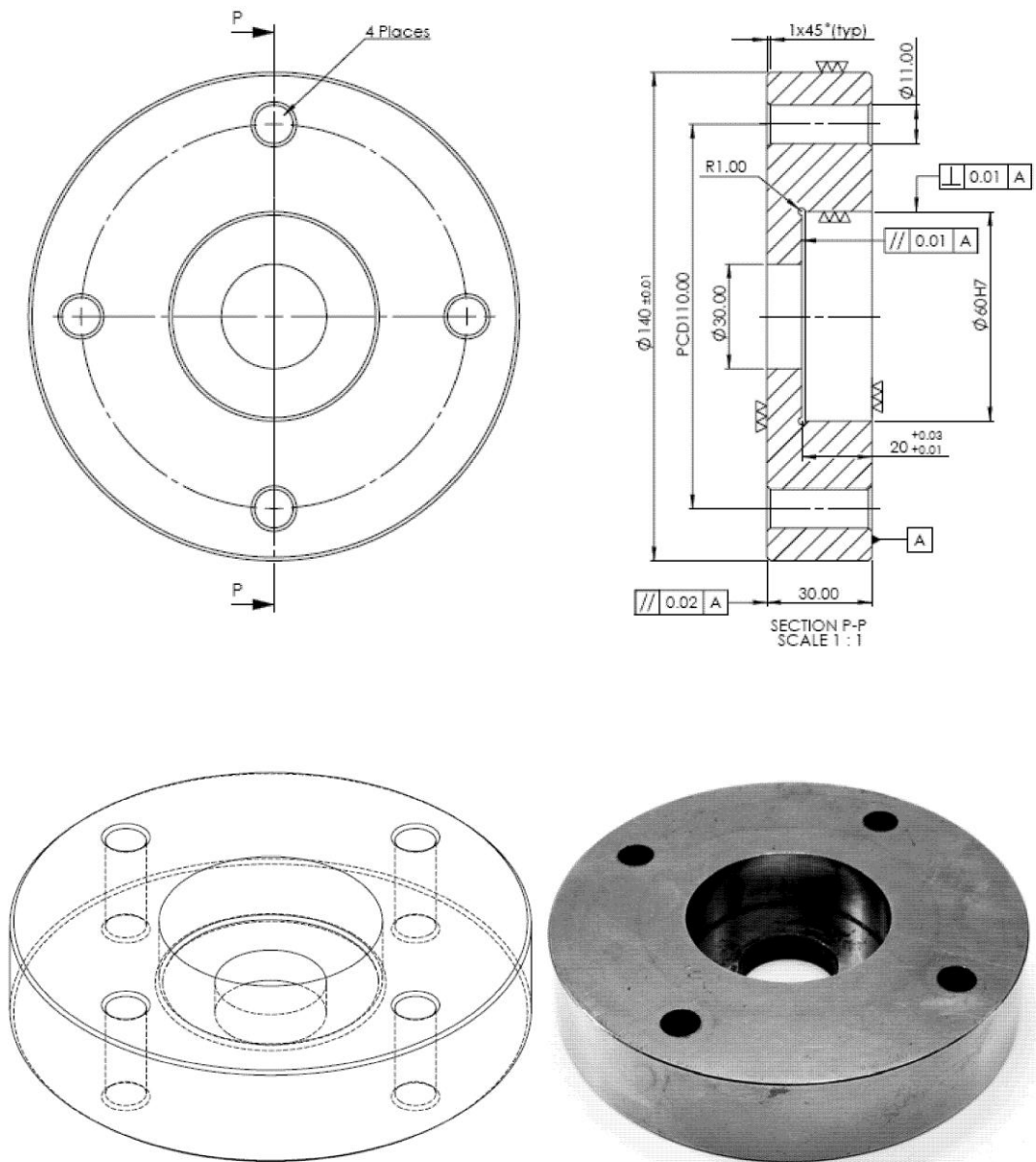


Figure 4.36 Extrusion die holder

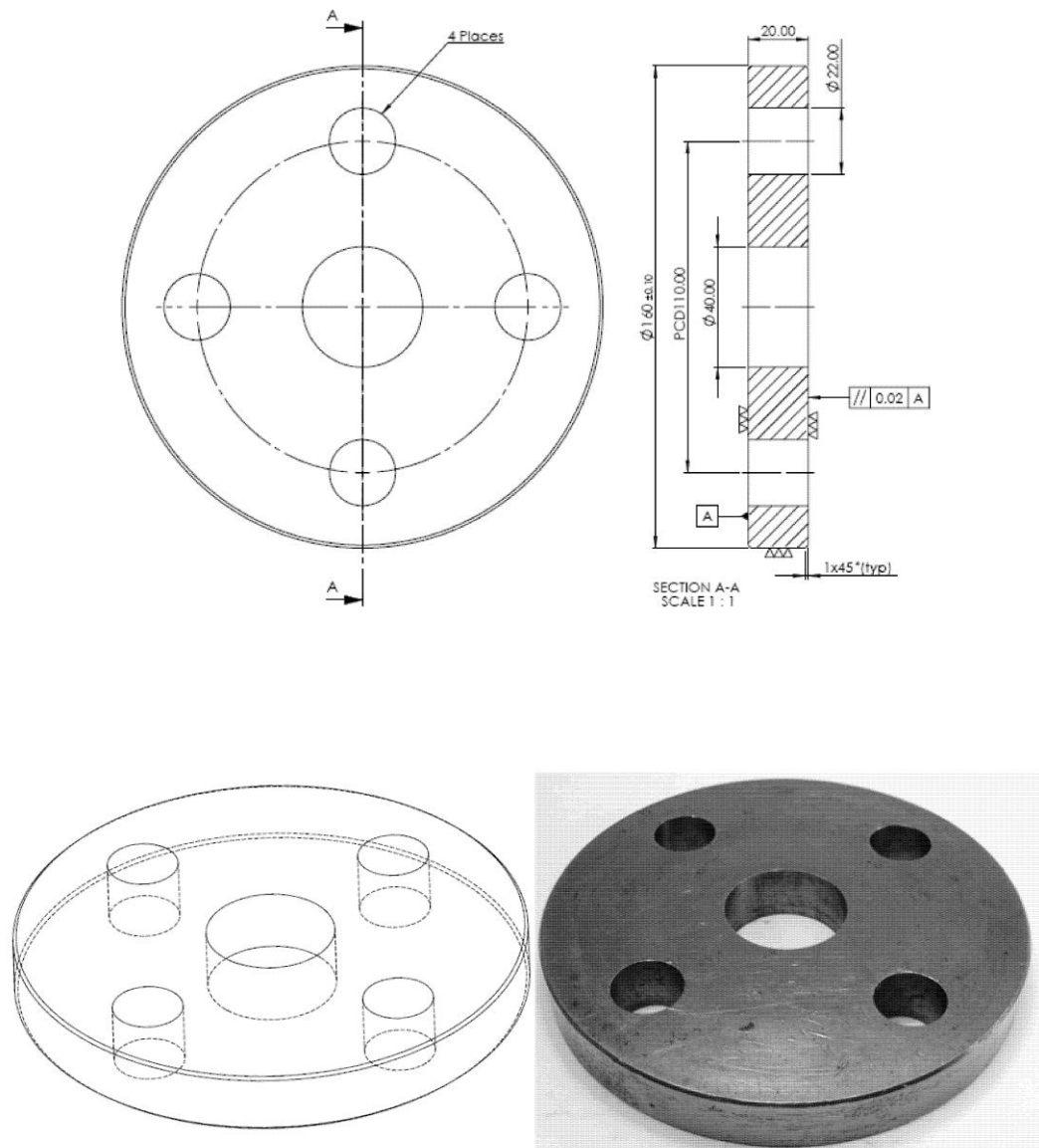


Figure 4.37 Support/base plate

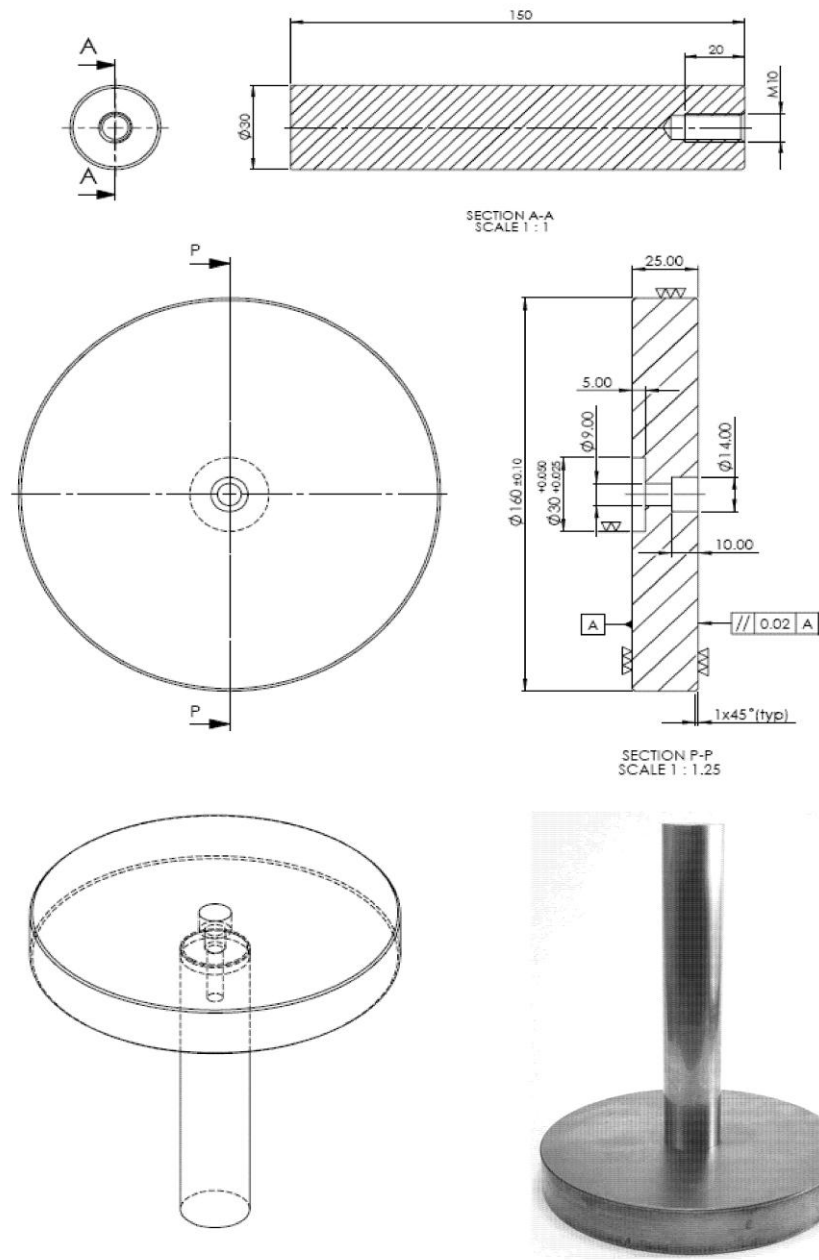


Figure 4.38 Punch

4.14 Dies

The forging and extrusion dies are made of two split halves for easy removal of product after extrusion cycles. These dies are manufactured from D2 steel, hardened up to HRc 50-55. The die halves are produced by wire cut EDM from rectangular stack. The inner surface of the dies are maintained the specified surface roughness by finishing operations. The orifices are located in such a way that the respective centers

of the gravity lie on the assembled setup axis. The extrusion dies openings are relieved by ten degrees to avoid interference of the extruded product with the die exist for all reductions. Extrusion die land is taken as 3mm for all reductions. Five sets of forward extrusion die (at different reduction in the area), and three sets of forward-backward extrusion die are employed for experimentation. The details of the forging die and extrusion dies are presented in Figure 4.39-4.41. A set of flat cylindrical blocks (Figure 4.42) is produced so that the flat surfaces of the blocks are finished to that accuracy that the forging dies inner surface attained. This is to archive the flow stress, friction factor in lubricated condition that of the forging dies.

4.15 Specimen

All the experiments are conducted with commercially available lead (96.29% by weight, results obtained from SEM test), as working material. The lead specimens are casted in the green sand mold to the required diameter cylindrical blocks from ingots. The specimens are then finished to size by turning using kerosene as cutting fluid. All specimens before experimentation are annealed in the boiling water for a period of two hours. For this series of experiment the specimens are cylindrical in shape of 30mm diameter and 40mm height. These dimensions are so chosen that the cylindrical specimens should accommodate in the triangular cavity of the forging die.

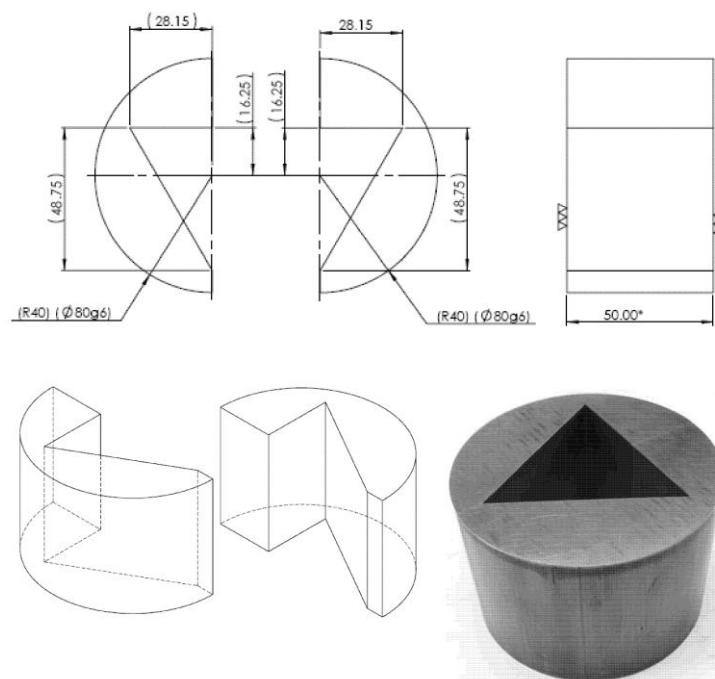


Figure 4.39 Triangular split type forging die

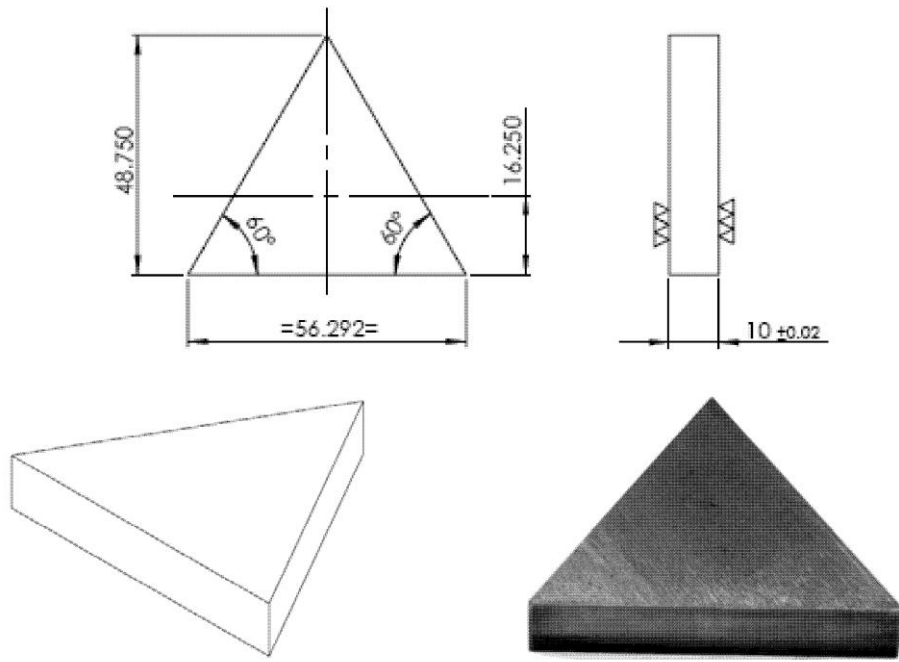
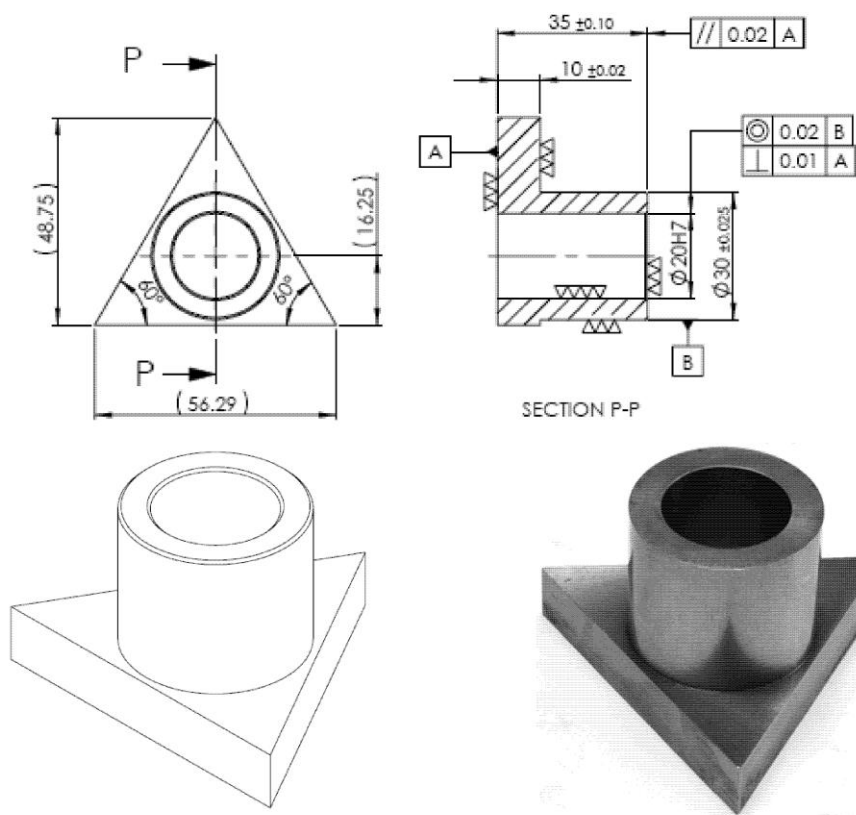


Figure 4.40 Triangular punch plates



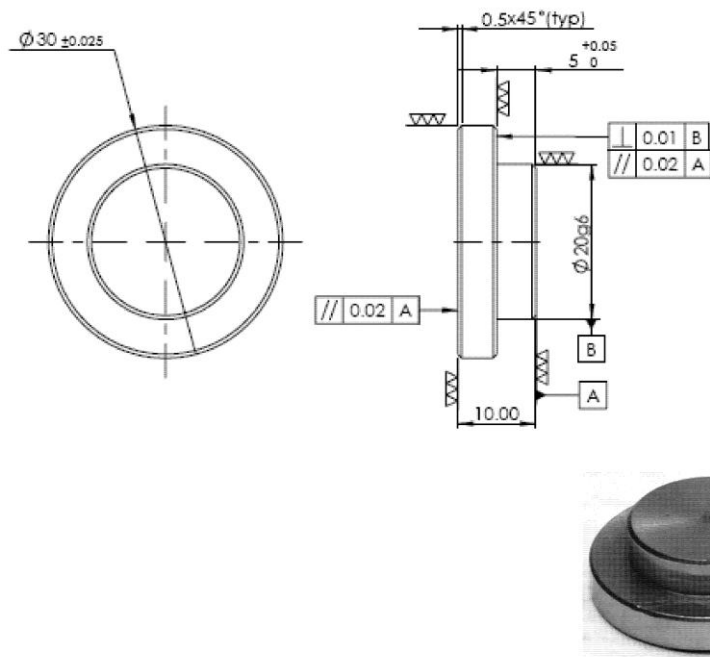


Figure 4.41 Triangular backward extrusion die and cap

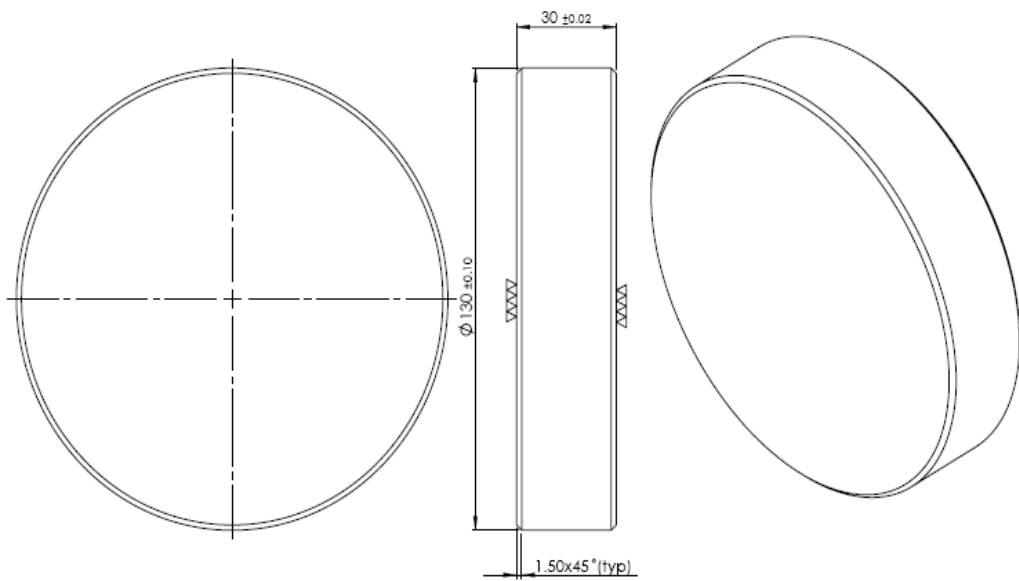
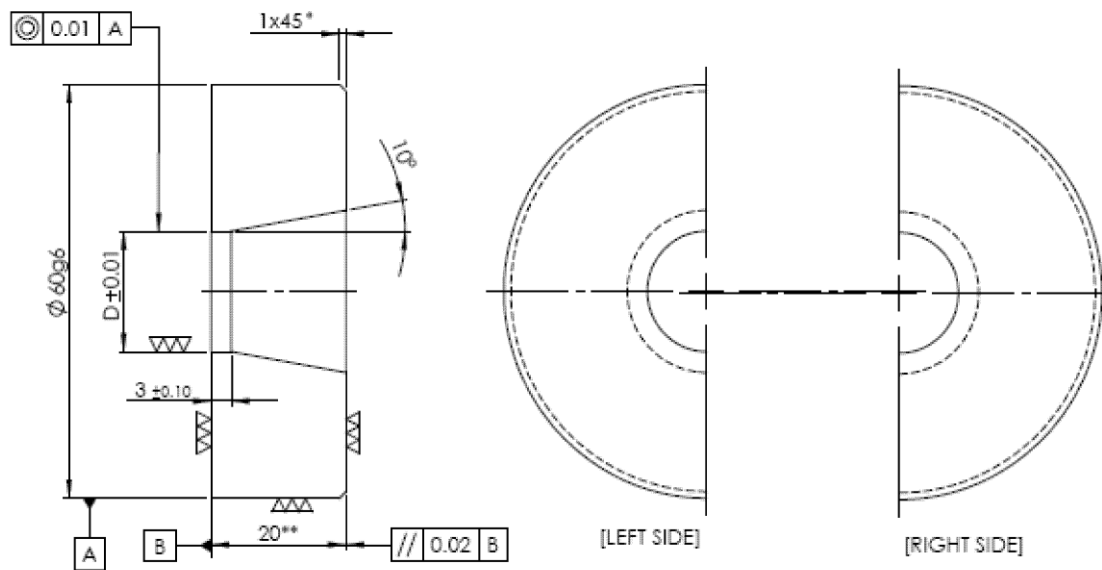


Figure 4.42 Testing plate



DIE DIA.	TYPE I	TYPE II	TYPE III	TYPE IV	TYPE V
D	15mm	17.5mm	20mm	22.5mm	25mm

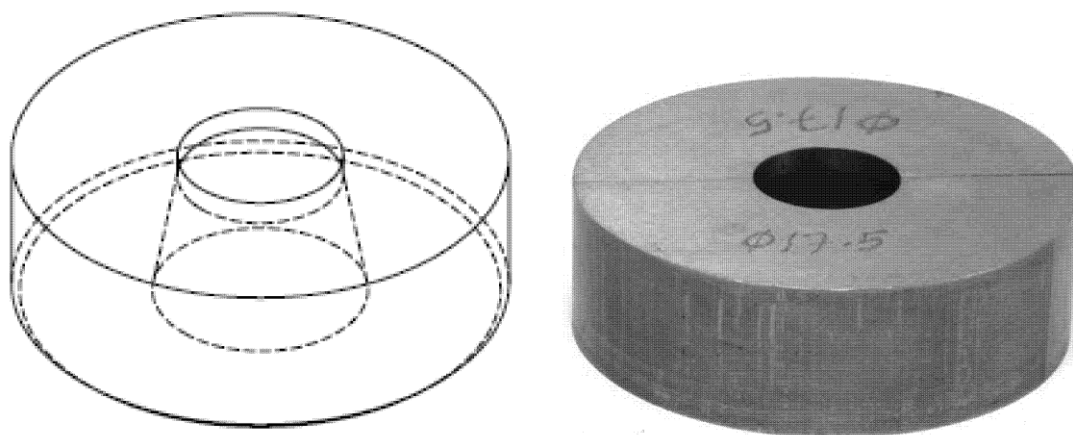


Figure 4.43 Extrusion dies

4.16 Experimental Procedure

The die-sets, the die holder and the inside faces of the extrusion chamber are cleaned with carbon tetrachloride before starting the tests to degrease the total setup. The two halves of the forging and extrusion die sets are then push fitted into their respective die holder. The inner surfaces of the dies and outer surfaces of the specimen are smeared lubricated using lithium based grease (commercially available

SKF LGMT 3IN1 general purpose grease). The prepared specimen is placed inside the cavity of the forging die and the total assembly is perfectly made by screwing the four alloy's bolts. The specimen is so placed inside the forging die cavity so that the axis of the billet lies on the assembled setup axis and machine axis. The full assembly is then placed on the lower table of the universal testing machine (Figure 4.44 (INSTRON® 600KN)) having maximum capacity of 600kN. The punch is then

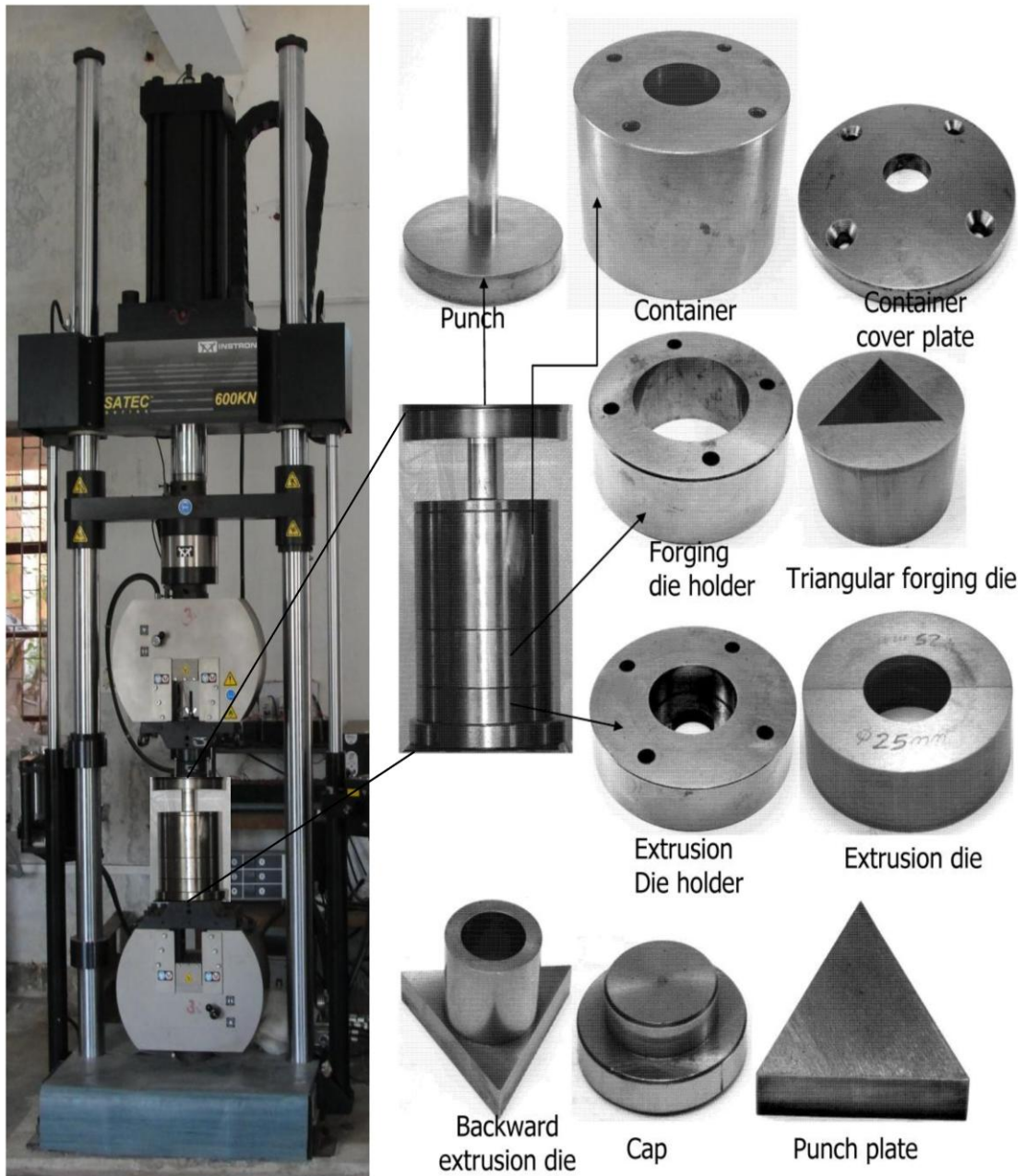


Figure 4.44 Photograph of INSTRON® 600KN machine with assembled setup

inserted into its position. After centering the apparatus under the machine lower table, the machine is started and the extrusion process is continued. To avoid rate affect the movement of the punch being adjusted to approximately 1 mm per minute. Punch load is recorded at every 30sec of punch travel. Extrusion is continued until the specified punch movement reaches. At this point, the machine is stopped, and the test is terminated. For our experiments, product head thickness is 10mm. The die holder is separated from the extrusion chamber after the experiment, and finally the die halves with the extruded product are pressed out from the die holder. Experiments were conducted for all reductions and for both forward and forward-backward extrusion forging process. Figure 4.45 and Figure 4.46 gives the product photograph of forward and forward-backward extrusion forging process.

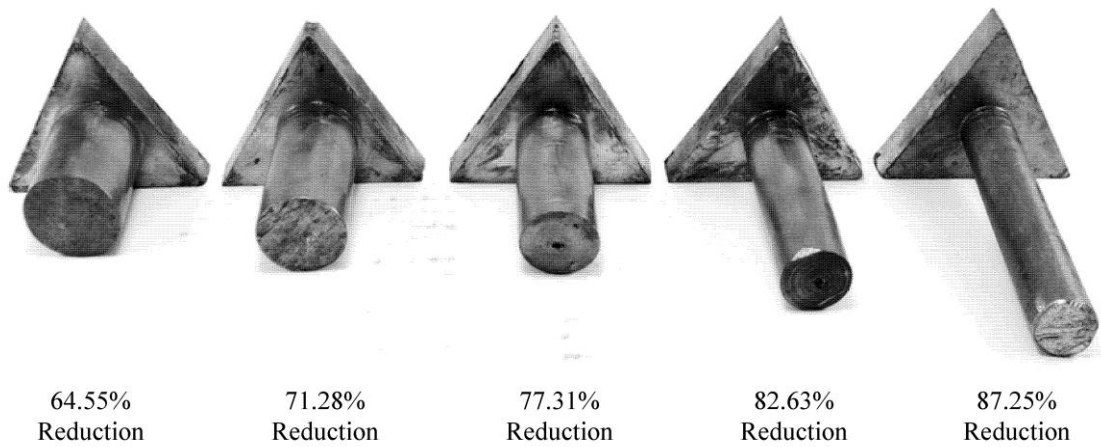


Figure 4.45 Extruded forward extrusion-forging triangular head shaped product

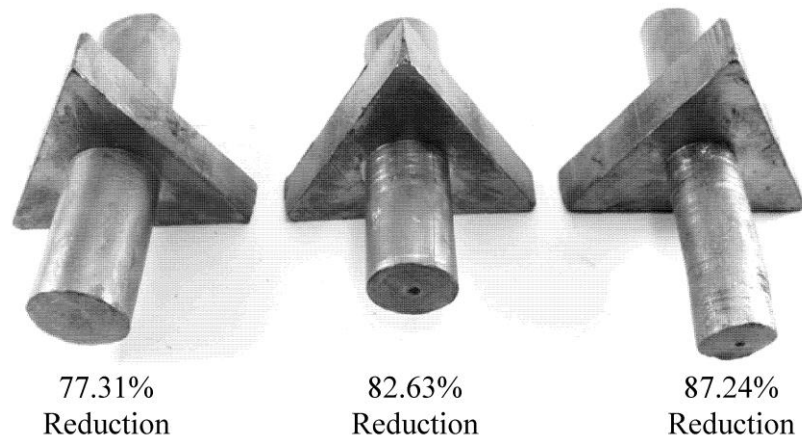


Figure 4.46 Extruded forward-backward extrusion-forging triangular head shaped product

4.17 Determination of Stress-strain Characteristics of Lead

In order to plot the stress-strain diagram, a cylindrical specimen of lead of 30 mm diameter and 45 mm length is machined from casted billet. The specimen had oil grooves turned on both ends to entrap lubricant during the compression process. After annealing the specimen in boiling water for two hours, its ends were adequately lubricated with grease and tested in uniaxial compression on the INSTRON[®]- 600KN hydraulic pressing machine. The compression rate is 1mm/min, is same that adopted for extrusion test. The compressive load is recorded at every 0.5 mm of punch travel. After compressing the specimen to about 10 mm, it was taken out from the sub-press, re-machined to the cylindrical shape of diameter 30mm with the oil grooves again turned on both ends and tested in compression. This process continues until the specimen was reduced to about 15 mm. The stress-strain diagram of lead obtained in this manner is shown in Figure 4.47.

To determine the uniaxial yield stress of the billet material for any given reduction R , the corresponding strain imparted to the billet material during the extrusion process must be known to the priori. For the same reduction, the strain imparted to the billet during the extrusion process is always higher than that imparted to the billet during compression because of the redundant work done during the extrusion process. Following the principles laid by Johnson and Mellor [119], the above strain in the present case was calculated from the empirical relation,

$$\bar{\epsilon} = 0.8 + 1.5 \ln \left(\frac{1}{1-R} \right) \quad (4.16)$$

Where, R is the fractional reduction. The average stress of the extruded billet was then calculated by dividing the area under the stress-strain curve with the corresponding value of the abscissa. The magnitude of the strain calculated from the equation (4.16) and the magnitude of the average yield stress σ_0 for different reductions determined in the above manner.

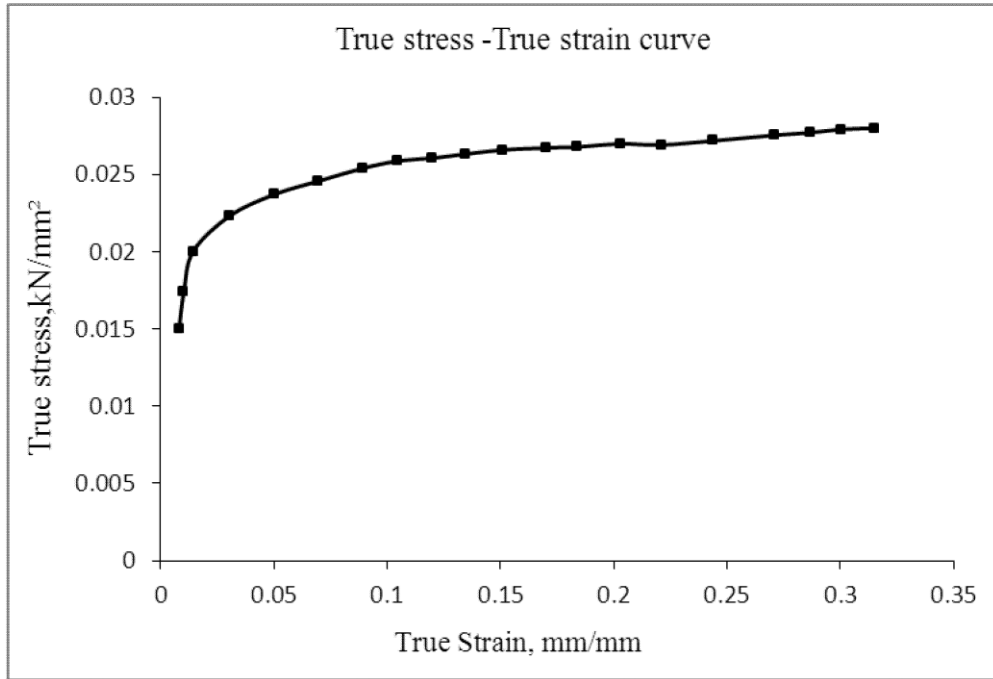


Figure 4.47 Stress-strain curve for lead

4.18 Determination of Friction Factor

In the metal forming process friction plays an important role. The metal flow is caused by the pressure transmitted from the dies to the deforming work piece. Therefore, the friction condition at the material/die interface greatly influences metal flow. In our experimentation, experiments are carried out at the lubricated condition. Therefore, analyses are made for lubricating conditions. In this ring test, a flat ring shape specimen having OD: ID: Thickness ratios 6:3:2 is considered. The dimensions of the ring used are 45:22.5:15 mm (outside diameter: inside diameter: thickness). To estimate accurate friction between die inner surface and the billet material two flat plates (Figure 4.42) having the same surface condition that of internal surface of dies are equipped. The prepared ring is compressed to a fixed percentage of thickness and after every compression, internal diameter is measured. To obtain the magnitude of the friction factors, the internal diameter of the compressed ring must be compared with the various available standard theoretical calibration curve of the friction factors, m . From the Figure 4.48, we found that for lubricated condition, friction factor is 0.23.

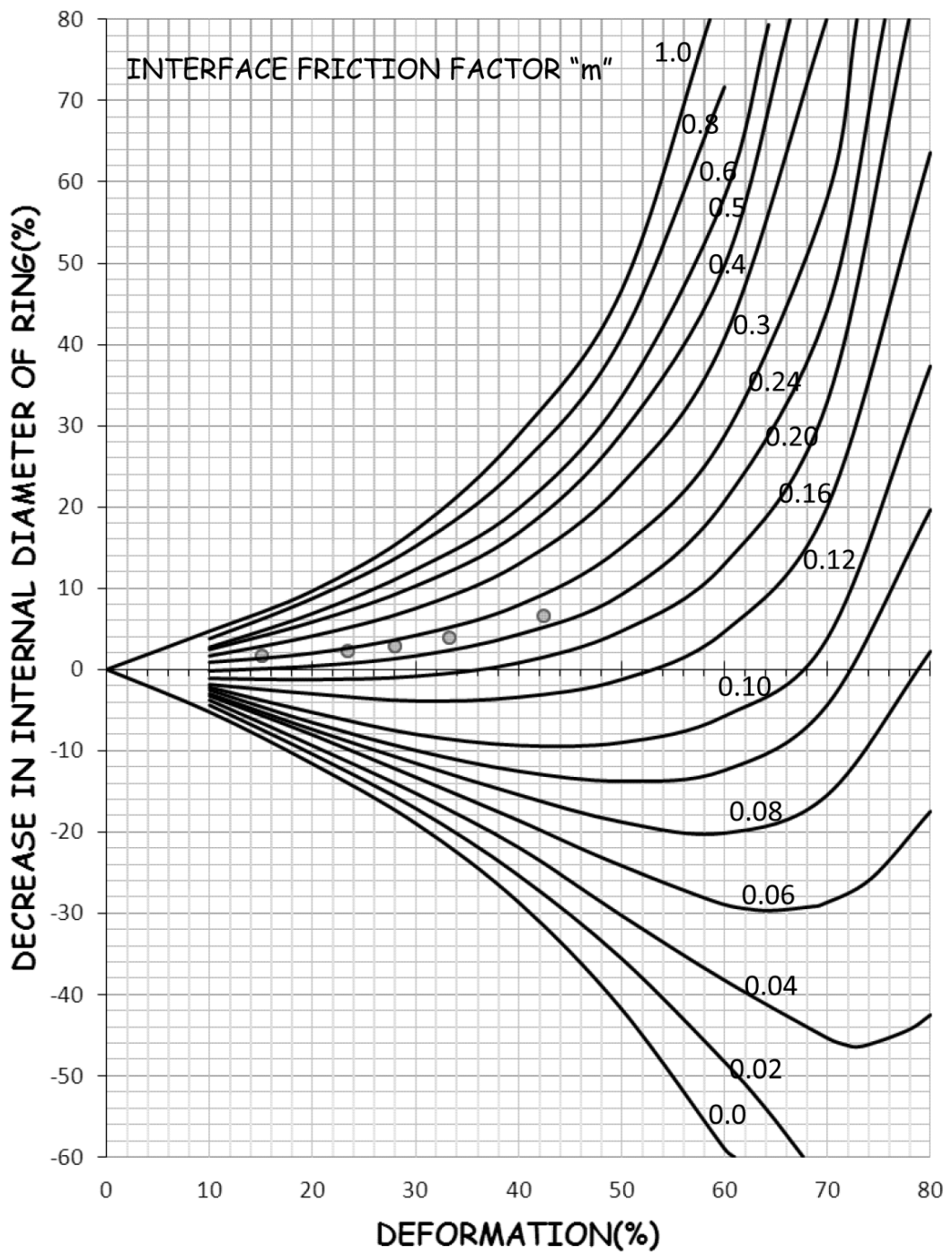


Figure 4.48 Theoretical calibration curve for standard ring (6:3:2)

4.19 Summary

4.19.1 Forward extrusion-forging process

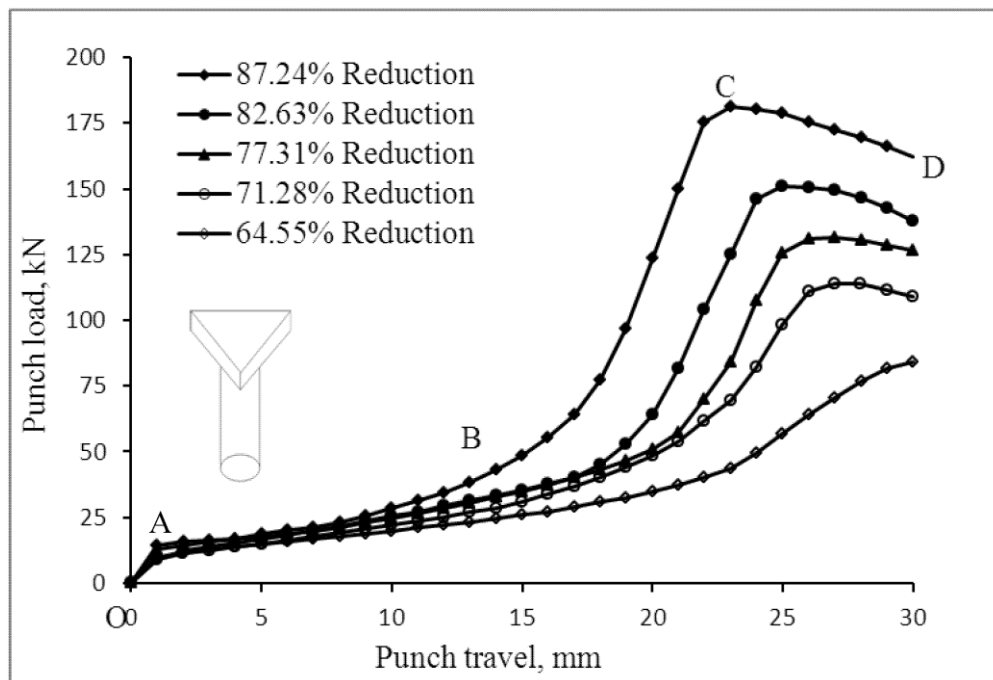


Figure 4.49 Variation of punch load with punch travel

Experiments are carried out for forward extrusion-forging process. Five different area reduction dies (87.24%, 82.63%, 77.31%, 71.28% and 64.55% reductions) are used to investigate the process. Figure 4.49 represents the variation of punch load with punch travel. Referring to the above diagram, it is seen that the whole process consists of four major stages: namely (i) a coining stage in which initial compression (O to A) of the billet takes place. The second stage refers to the forging stage (A to B) where the billet forged till it touches the die wall. In this stage load increase slowly with respect to punch movement. In the third stage die corners are filled up (B to C), where the maximum load reaches. In this stage there is an increase in load with respect to punch movement followed by a steep rise. There is no fixed distinguish region of the load-moment curve for die filling/ corner filling stages. Above all the process simultaneous extrusion process is accomplished. After the die completely filled, in the fourth stage (C to D) the steady-state extrusion process takes place. There is a drop in load in this stage due to continuous decrease of billet length thereby decreasing the frictional force between billet and extrusion chamber. However, the drop in load from the peak value is found to be

minimal, which may be due to adequate lubrication between the billet and the extrusion chamber.

The load corresponding to the peak load, where steady state extrusion starts, considered as the extrusion load and is tabulated in the Table 4.15. This table provides the value of the mean extrusion pressure P_{av} , the value of the uniaxial yield stress in compression σ_o , and the non-dimensional mean extrusion pressure P_{av}/σ_o .

Table 4.15 Computation of non-dimensional average extrusion pressure for forward extrusion-forging process

% Reduction	Extrusion load(kN)	P_{av} MPa	σ_o MPa	P_{av}/σ_o (Experiment)	P_{av}/σ_o (Theoretical)
87.24	180.154	129.83	23.45	5.536	5.680
82.63	151.087	108.88	23.50	4.633	4.788
77.31	131.232	94.57	23.55	4.016	4.183
71.28	113.989	82.15	23.60	3.481	3.651
64.55	84.264	60.72	23.65	2.568	3.201

4.19.1.1 Die filling and flow pattern

Figure 4.50 shows the complete process at different punch movement, for forward extrusion-forging process, for both FEM simulations and experiment at 77.31% reduction and at particular intervals of punch movement. It explains that combined extrusion-forging process takes place till the die cavity is completely filled. After that only pure extrusion process takes place.

As an illustration, Figure 4.51 shows the photograph of the flow pattern for a 77.31% reduction of forward extrusion-forging process at different punch movement for both in FEM and experimental. The grid line distortion indicates that the process utilizes the maximum amount of redundant work to create flanges of the triangle.

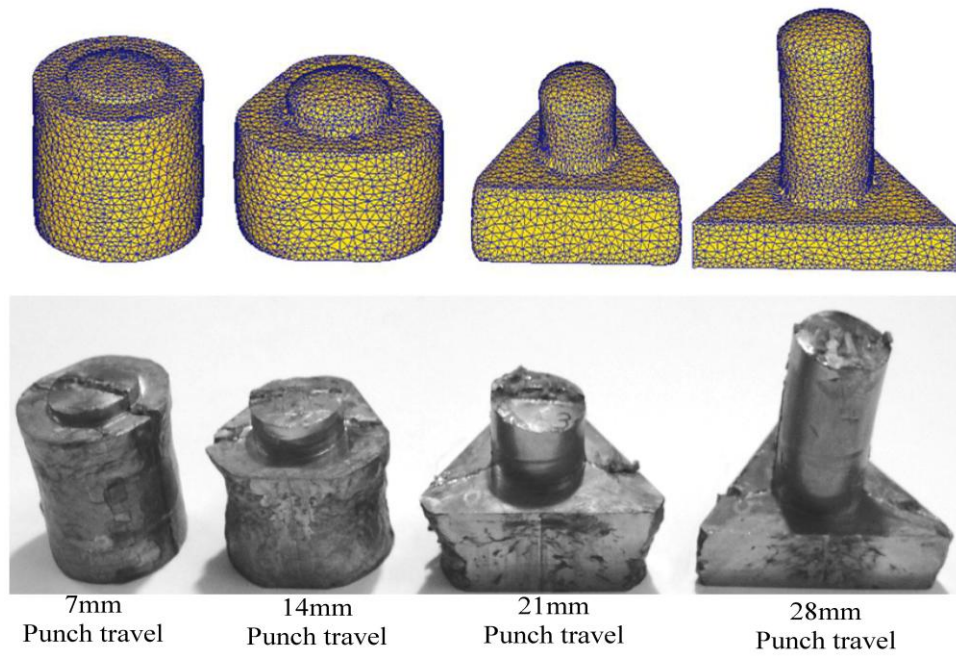


Figure 4.50 Die filling at different punch movement

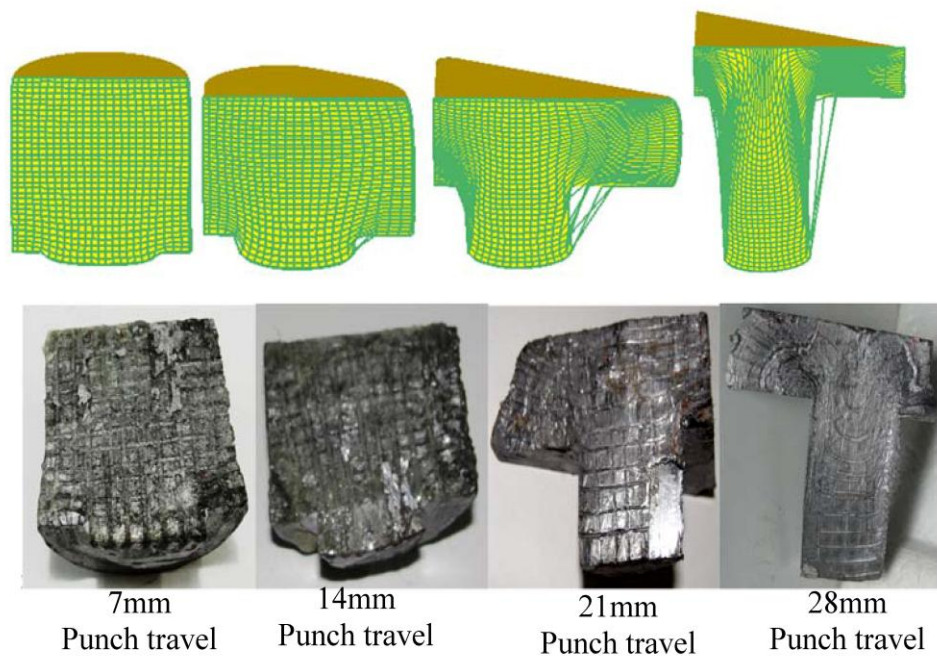


Figure 4.51 Flow pattern at different punch movement

4.19.2 Forward-backward extrusion-forging process

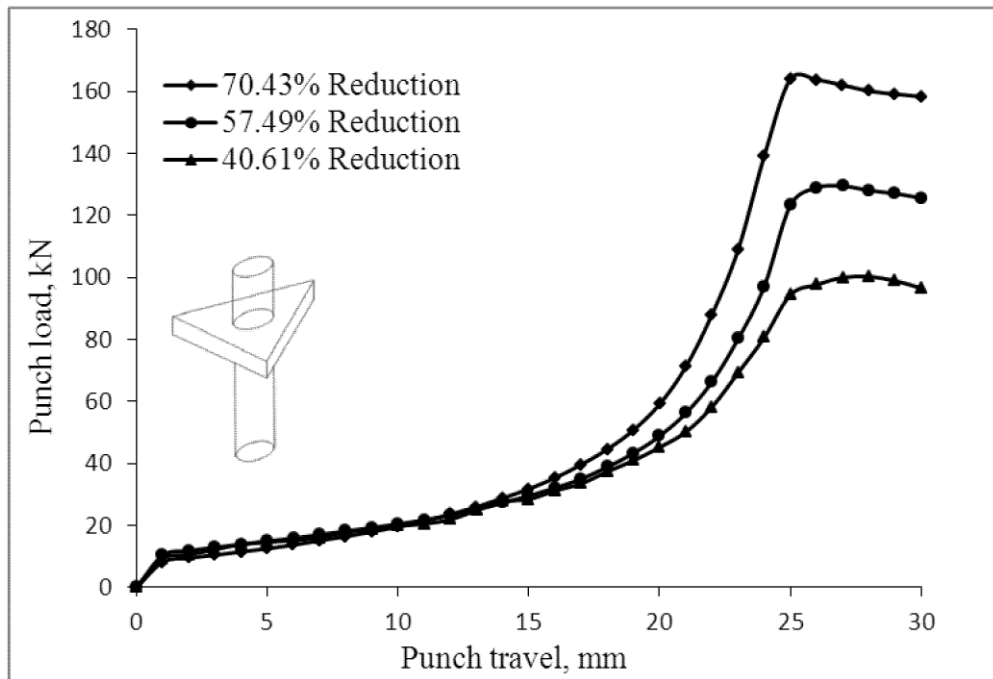


Figure 4.52 Variation of punch load with punch travel

Experiments are carried out for forward extrusion-forging process. Three different area reduction dies (70.43%, 57.49% and 40.61% reduction) are used for forward-backward extrusion-forging process. Figure 4.52 represents the punch load with punch travel. It is seen that the whole process consists of four principal stages: namely (i) a coining stage in which initial compression (O to A) of the billet takes place. The second stage refers to the forging stage (A to B) where the billet forged till it touches the die wall. In this stage load increase slowly with respect to punch movement. In the third stage die corners are filled up (B to C), where the maximum load reaches. In this stage there is an increase in load with respect to punch movement followed by a steep rise. There is no fixed distinguish region of the load-moment curve for die filling/ corner filling stages. Above all the process simultaneously forward and backward extrusion process is accomplished. After the die completely filled, in the fourth stage (C to D) the steady-state extrusion process takes place for both forward and backward directions. The load corresponding to the peak load, where steady state extrusion starts, considered as the extrusion load and is tabulated in the Table 4.16. This table provides the value of the mean extrusion pressure P_{av} , the value of the uniaxial yield stress in compression σ_0 , and the non-dimensional mean extrusion pressure P_{av}/σ_0

Table 4.16 Computation of non-dimensional average extrusion pressure for forward-backward extrusion-forging process

% Reduction	Extrusion load(kN)	P_{av} MPa	σ_o MPa	P_{ave}/σ_o (Experiment)	P_{ave}/σ_o (Theoretical)
70.43	155.97	130.47	23.605	5.53	5.82
57.49	142.43	125.87	23.697	5.31	5.74
40.61	131.28	124.09	23.807	5.21	5.70

4.19.2.1 Flow pattern

As an illustration, Figure 4.53 shows the photograph of the flow pattern for a 40.61% reduction of forward-backward extrusion-forging process at the 28mm punch movement for both in FEM and experimental. The grid line distortion indicates that the process utilizes the maximum amount of redundant work to create flanges of the triangle.

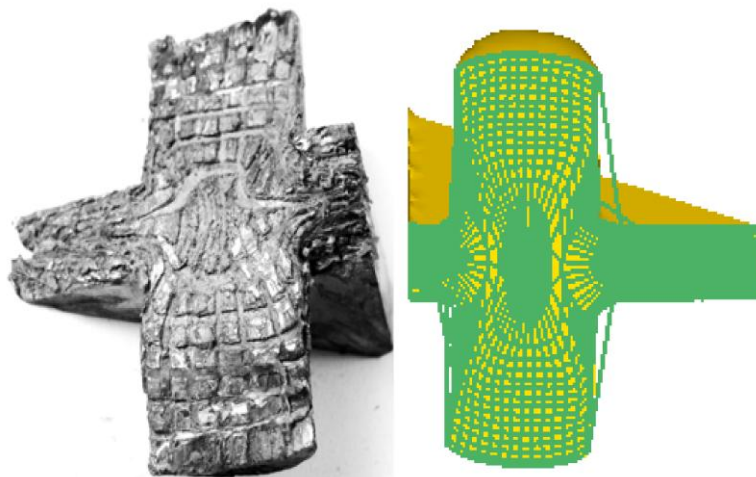


Figure 4.53 Flow pattern at 40.61% reduction and 28mm punch movement

4.20 Comparison of Results and Discussion

4.20.1 Forward extrusion-forging process

The comparison between proposed upper bound analyses, finite element analysis and experimental analysis are shown in Figure 4.54. It is observed from Table 4.17 that the difference between UBA and FEA are within 13.00%, whereas the difference between UBA and experimental results are within 5.00%. As in case of 64.55% reduction the die filling is not completed within the prescribed punch

movement so the percentage differences are of higher values. The results seem to confirm the suitability of the proposed technique for the combined extrusion-forging processes studied in the present work.

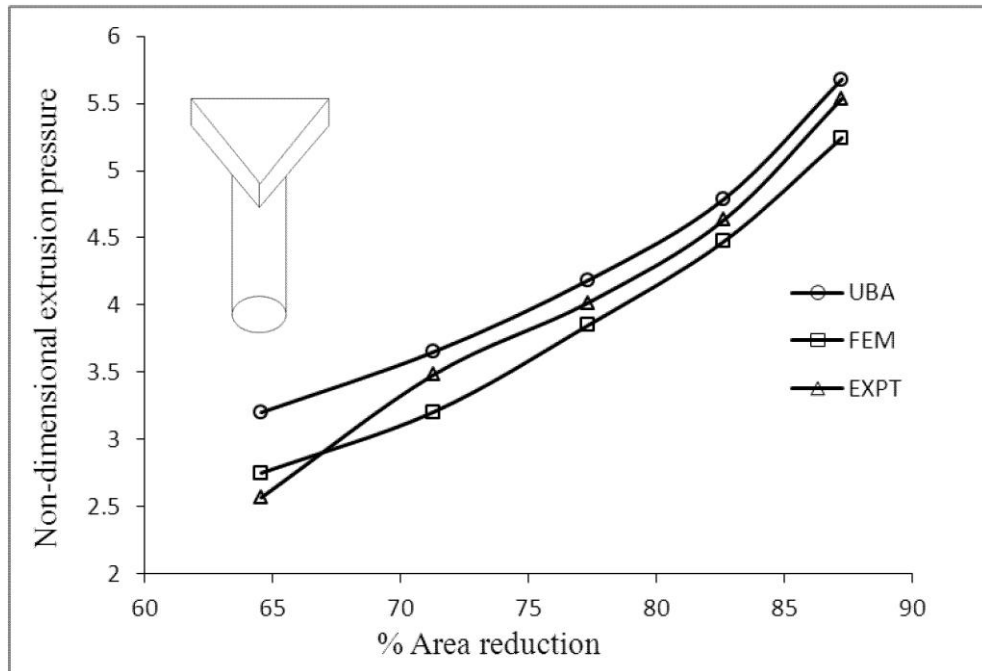


Figure 4.54 Comparison of non-dimensional extrusion pressure without friction for forward extrusion-forging process

Table 4.17 Variation of non-dimensional extrusion pressure for different formulations without friction for forward extrusion-forging process

% Reduction	% Difference UBA-FEA	% Difference UBA-EXPT
87.24	7.65	2.53
82.63	6.57	3.23
77.31	7.99	3.99
71.28	12.23	4.66
64.55	14.07	19.79

Figure 4.55 shows the variation of the punch load obtained by proposed SERR technique with the advance of the punch and its comparison with experiment and finite element analysis. It is observed that in this case the die filling and extrusion takes place simultaneously till the forging process is completed, followed by only

extrusion. It is found that the FEM results are higher than experimental results limited to 12%, which is very close to that of proposed SERR technique.

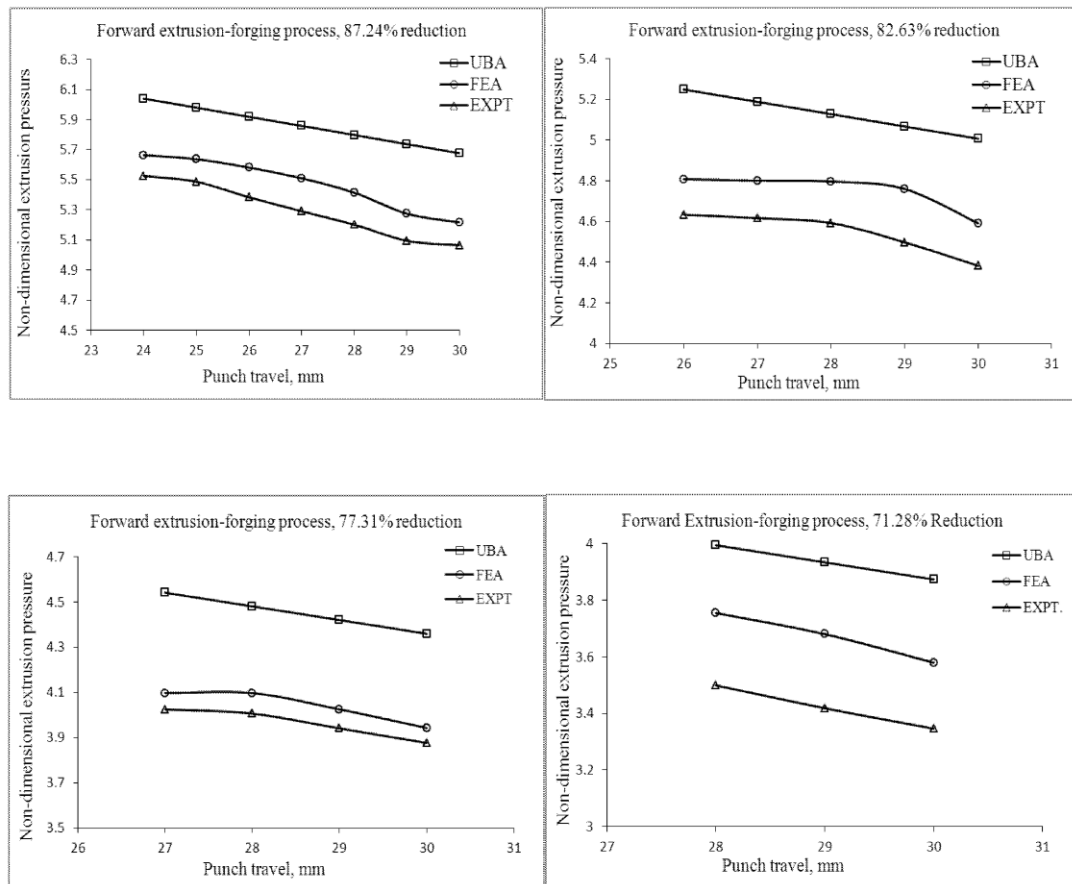


Figure 4.55 Variation of non-dimensional extrusion pressure with punch travel for forward extrusion forging process for different reduction

4.20.2 Forward-backward extrusion-forging process

The comparison between proposed upper bound analyses, finite element analysis and experimental analysis are shown in Figure 4.56. It is observed from Table 4.18 that the difference between UBA and FEA are within 5.0%, whereas the difference between UBA and experimental results are within 9.0%. It indicates that the proposed method of analysis is also suitable for the forward-backward combined extrusion-forging process.

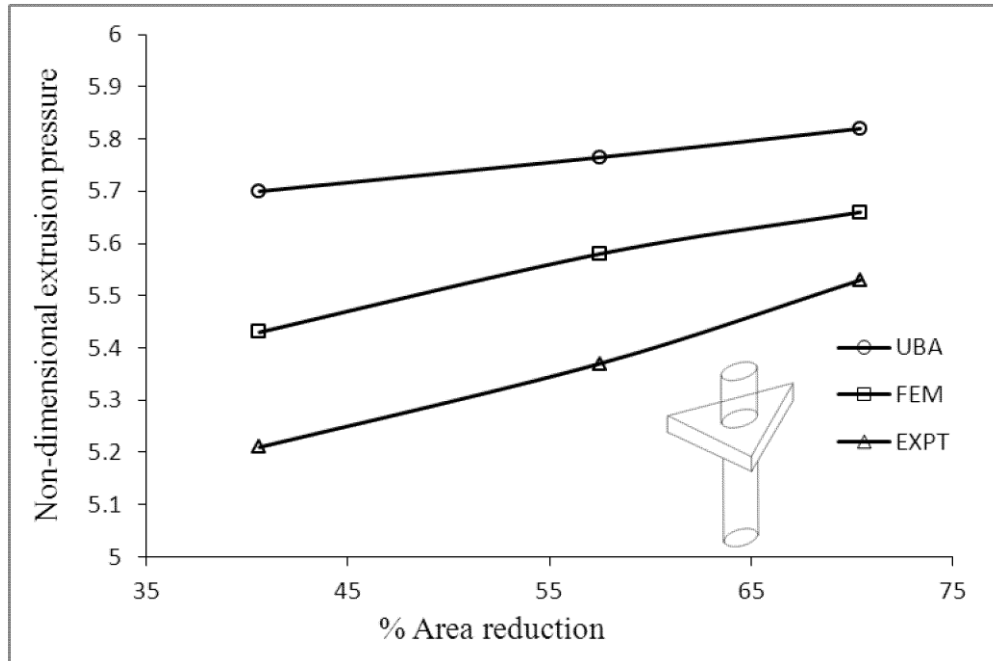


Figure 4.56 Comparison of non-dimensional average extrusion pressure without friction for forward-backward extrusion-forging process

Table 4.18 Variation of non-dimensional extrusion pressure for different formulations for forward-backward extrusion-forging process

% Reduction	% Difference UBA-FEM	% Difference UBA-EXPT
70.43	4.51	5.06
57.49	2.84	7.48
40.61	4.62	8.50

4.21 Closure

4.21.1 Forward extrusion-forging process

1. The experimental non-dimensional extrusion pressure P_{av}/σ_o , agrees with the theoretical value computed with the help of proposed SERR technique to within 7% of the range of reduction studied. The results validate and convey the suitability of the proposed technique for the combined extrusion-forging process.
2. Among the three SERR formulation carries out in this study, double-point formulation gives the lowest upper bound to the extrusion pressure for the square

section. . It is evident that by increasing the floating point, more than the optimized number, we may incorporate more redundancy (long flow path).

3. The obtained variation of punch load with respect to stroke by proposed technique is also well validated with FE analysis and experiment. It is also observed that with the increase of reduction variation of FE analysis with experimental results increases marginally with the addition of redundant work.
4. The experimental die filling and flow pattern agrees with the FEM analysis.
5. The proposed upper-bound analysis using discontinuous velocity field (modified SERR technique) provides a better method of analysis for this type of section extrusion.

4.21.2 Forward-backward extrusion-forging process

1. The experimental non-dimensional extrusion pressure P_{av}/σ_0 , agrees with the theoretical value computed with the help of proposed SERR technique to within 10% of the range of reduction studied.
2. Among the six SERR formulation carries out in this study, three-point formulation gives the lowest upper bound to the extrusion pressure for the extrude section.
3. The obtained variation of punch load with respect to stroke by proposed technique is also well validated with FE analysis and experiment.
4. The experimental flow pattern agrees with the FEM analysis.
5. The proposed upper-bound analysis using discontinuous velocity field (modified SERR technique) provides a better method of analysis for this type of section extrusion.

3D Analysis of Combined Extrusion-Forging Process for Round-Square-Round Section

5.1 Introduction

The present chapter provides the upper bound solutions for extrusion-forging of the square section head with the circular shaft through the square dies from round section billets. Analyses are made for both forward and forward-backward extrusion-forging process for different reductions. Figure 5.1 shows the front half in section of the process. The dead-metal zones are proposed in this manner so that a deformation cavity is formed in which the square section of the billet gradually forms into the round section of the product. The dead metal zones have been assumed to cover the die faces and the upper bound loads have been computed using discontinuous velocity fields. The discontinuous velocity fields have been obtained by discretizing the deformation zone into tetrahedral blocks using the reformulated SERR technique.

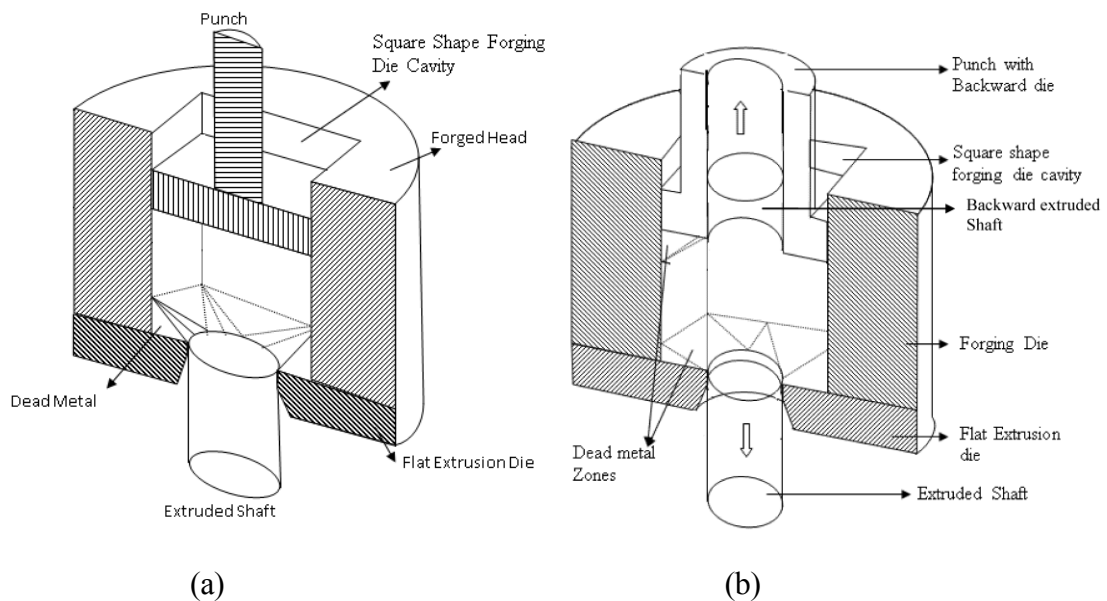


Figure 5.1 Front half in section of the process (a) Forward extrusion-forging

(b) Forward-backward extrusion-forging process

5.2 Theoretical Analysis

Following the same procedure described in section 4.2.1 one eighth of the deformation zone (Figure 5.2) is considered for the square section (because of its symmetry about four planes with respect to billet cross-section). The circular cross-section of the shaft is approximated by a 32 sided regular polygon (Figure 5.3).

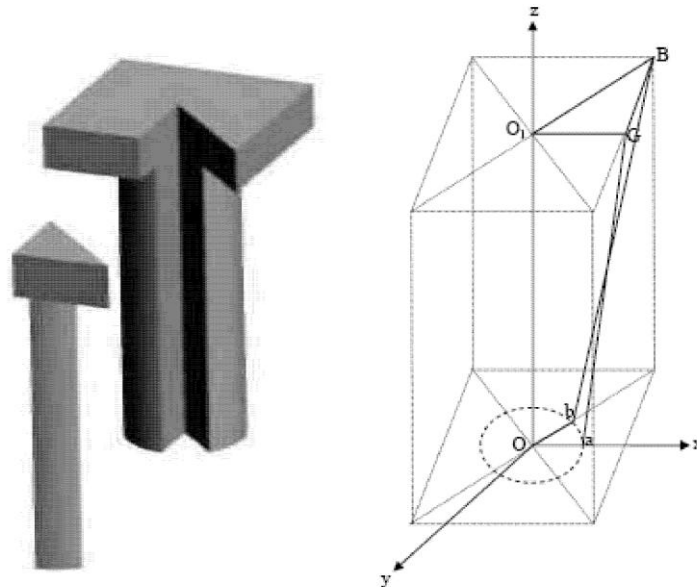


Figure 5.2 Domain of interest G-B-O₁-O-b--a (one eighth of zone of deformation)

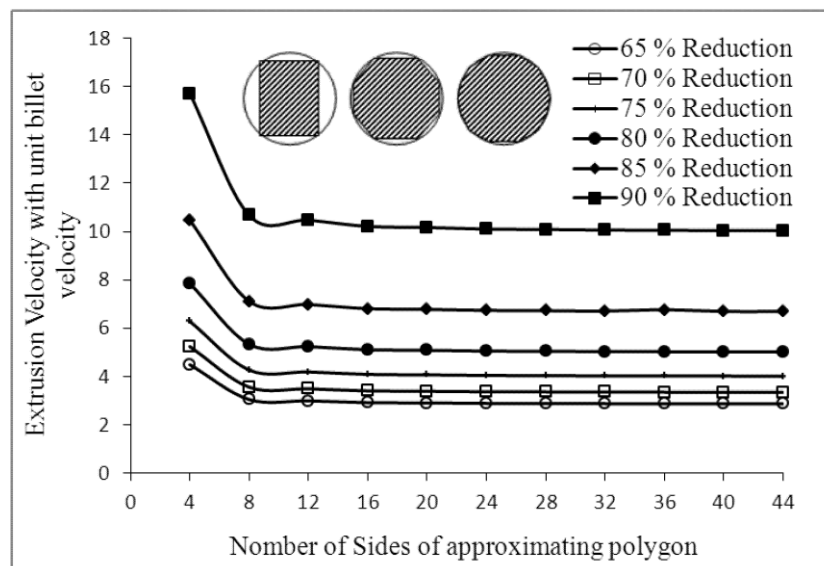


Figure 5.3 Variation of calculated extrusion velocity with the number of sides of approximating polygon

The subzones of deformation are delineated in the domain of interest by taking suitably located floating points (an arbitrary point in the domain of interest named here as a floating point since its location is not a priori known). Following the same procedure explained in previous chapter three formulations are considered, which acknowledge one, two and three floating point respectively. For single floating point formulation, an arbitrary point is taken on the extrusion axis. For double point formulation two floating points are taken in the domain of interest, one on the extrusion axis as before and the second on the plane of symmetry at an arbitrary position. Finally, the triple-point formulation, three floating points are taken, one on the extrusion axis, the second on the plane of symmetry and the third in an arbitrary position in the domain of interest.

The discretization of the forward-backward extrusion-forging process of the square elements with circular shaft on both faces of the element is analyzed on the same procedure as followed by the forward extrusion-forging process. Six formulations are considered, which acknowledge one, three, five, seven, nine and eleven numbers of floating points respectively.

A comprehensive computational model (using FORTRAN code) for forward and forward-backward extrusion-forging process with and without considering friction is developed by incorporating all special features of the proposed cross section. Three formulations for forward extrusion-forging process and six formulations for forward-backward extrusion-forging process is considered.

5.2.1 Summary

Computations for all floating point formulations are carried out and optimal configuration are considered. Figure 5.4 gives the comparison of the computed results for optimal configurations of forward extrusion-forging processes. It is obvious from the Figure 5.4 that the double-point formulation gives the best results. Therefore, this formulation only is used for further computation and comparison.

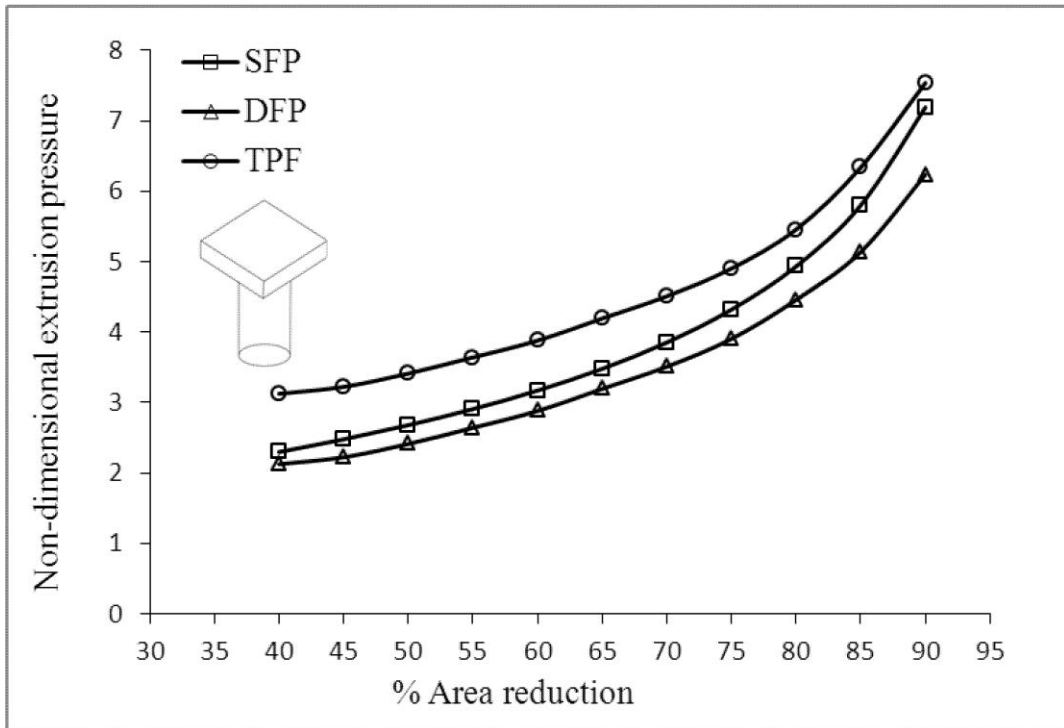


Figure 5.4 Comparison of results for different formulation (N=32)

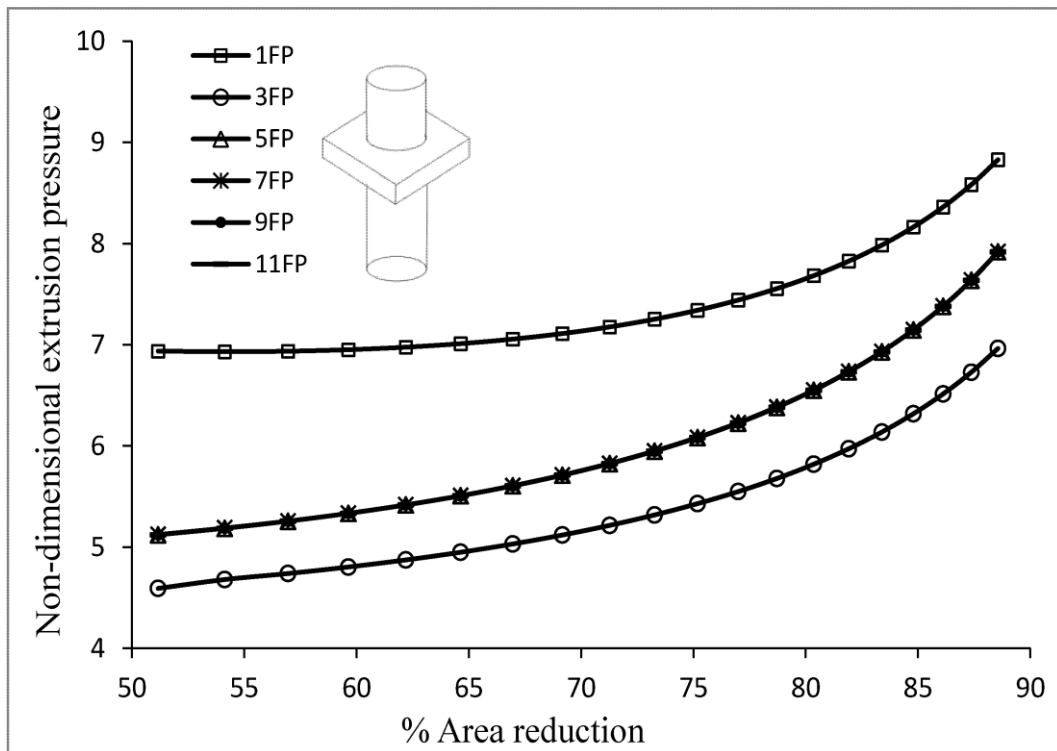


Figure 5.5 Comparison of results for different formulation (N=32)

Figure 5.5 summarize the non-dimensional extrusion pressure of one, three, five, seven, nine and eleven floating point formulations optimal results for forward-backward extrusion-forging process.. Out of this formulation, three floating point formulation gives optimum result and is used for further computation and comparison. It is observed from the graph that increasing the number of floating point after five floating there is a negligible change in the computed value. So, five, seven, nine eleven floating point computed results seem to overlap on the graph.

5.3 Finite Element Analysis of Forward Extrusion-Forging Pocess

The process parameters used in this simulation are summarized in Table 5.1. Five different area reduction dies (88.96%, 84.97%, 80.37%, 75.15% and 69.32% reduction) for forward extrusion-forging are used in this series of experiments. The dies, and punch plate used for simulation was same as that of experimental sets.

Figure 5.6 gives comparison of punch load with ram movement for different percentage area reductions for forward extrusion-forging process..

Table 5.1 Process parameter used in simulation

Billet length	40mm
Billet diameter	35mm
Billet temperature	Ambient
Ram speed	1mm/min
Friction factor	0.23
Flow stress	0.0233kN/mm ²

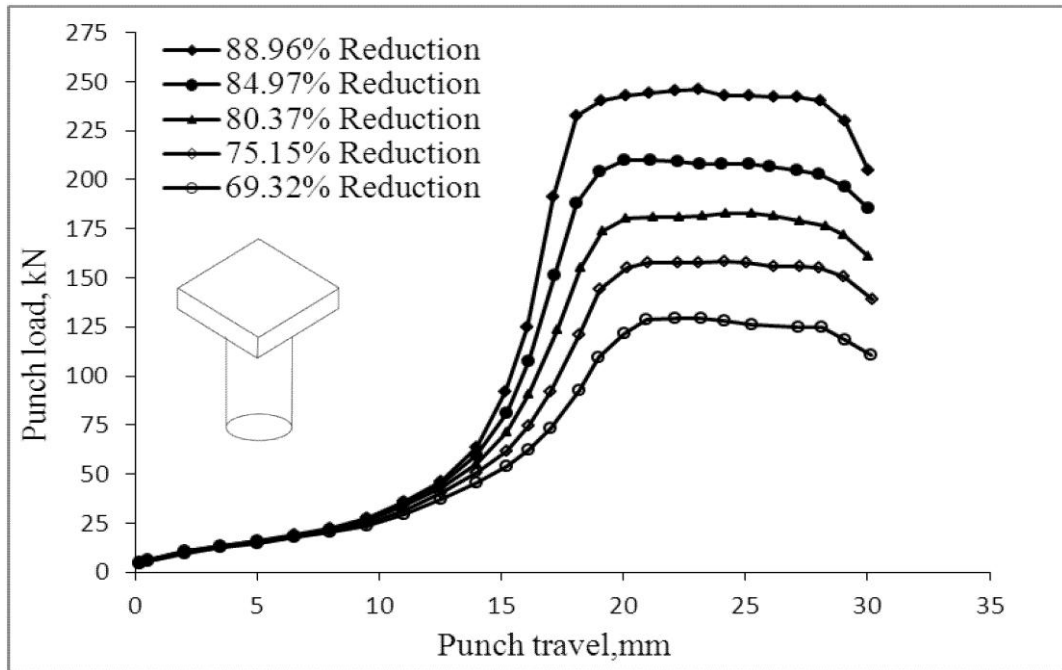


Figure 5.6 Variation of punch load with punch travel

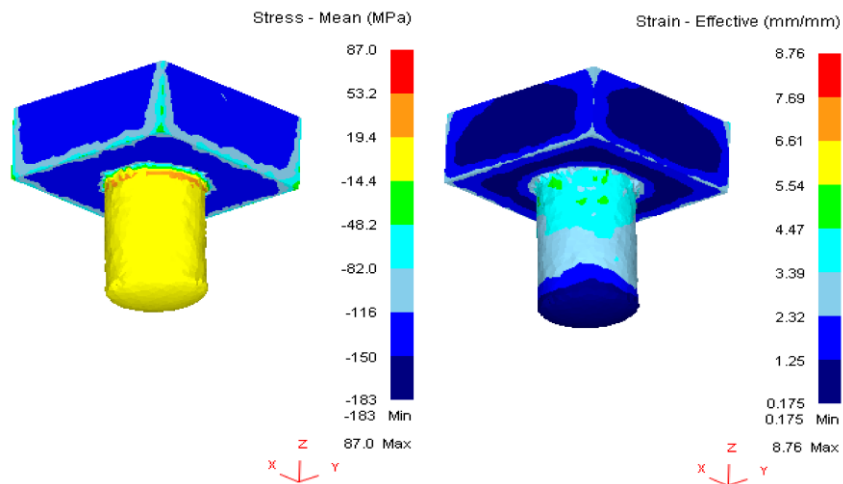


Figure 5.7 Mean stress and effective strain at particular reduction and punch movement for forward extrusion-forging process of square section

Figure 5.7 shows the mean stress distribution and effective strain in terms of solid profile for the reduction of 80.37%; at a ram speed of 1mm/min and ram displacement of 20 mm for forward extrusion-forging process. The positive stress signifies the tensile component of stress. From the figure it is observed that at the die land and near die walls the material attains a maximum compressive stress. The

effective strain is large immediate after the extrusion through flat die and gradually decreases.

5.4 Finite Element Analysis of Forward-Backward Extrusion-Forging Process

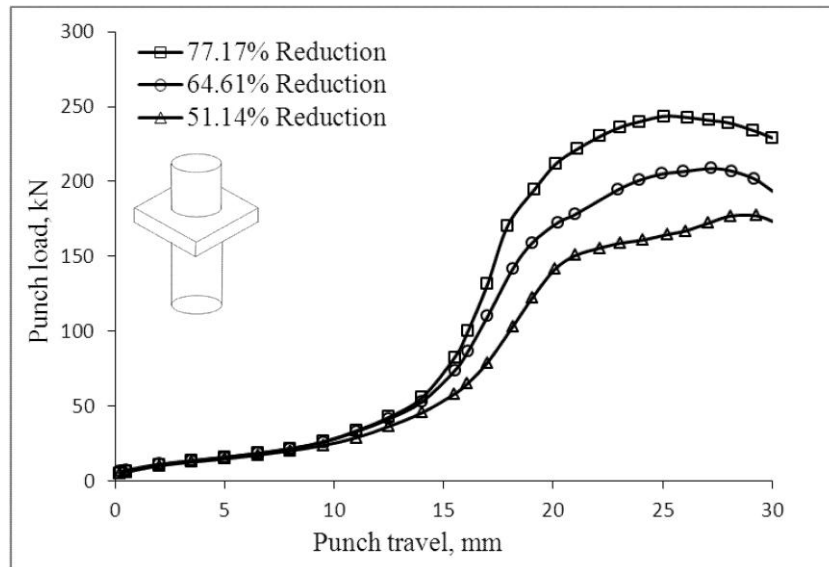


Figure 5.8 Variation of punch load with punch travel

Three different area reduction dies (75.17%, 64.61% and 51.14% reduction) for forward-backward extrusion-forging process are used in this series of experiments. The dies and punch plate used for simulation was same as that of experimental sets. Figure 5.8 gives comparison of load with ram movement for different percentage area reductions.

Figure 5.9 shows the mean stress distribution and effective strain in terms of solid profile for the reduction of 51.14%, at a ram speed of 1mm/min and ram displacement of 25mm for forward-backward extrusion forging process. The positive stress signifies the tensile component of stress. At the die land higher compressive stresses reach near die walls. From the figure it is observed that there is a large stress concentration (0.0797 – 0.0341kN/mm²) round the die entrance. The effective strain is large after the extrusion through flat die and gradually decreases.

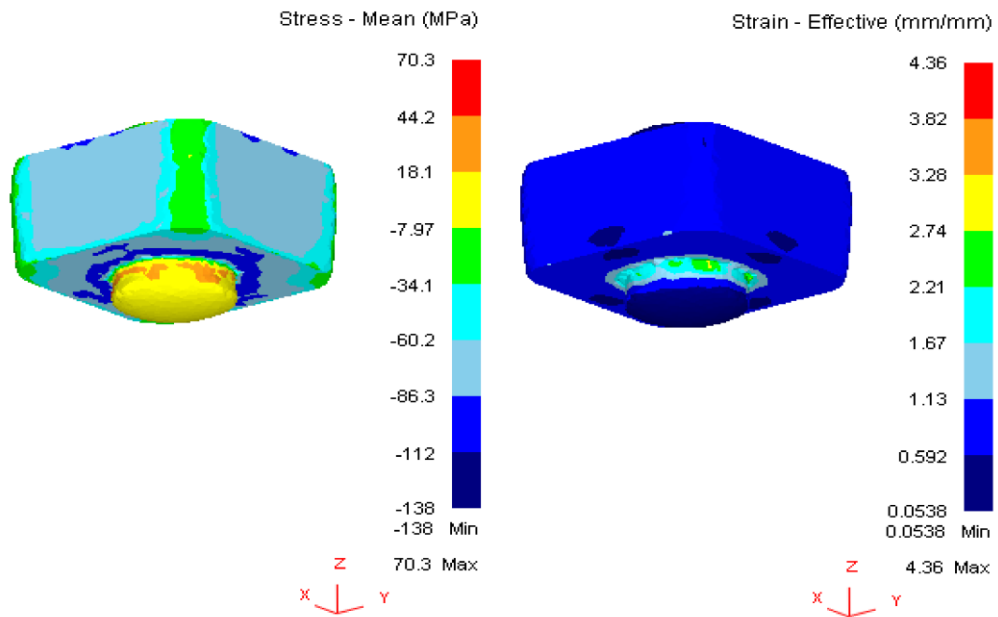


Figure 5.9 Mean stress and effective strain at particular reduction and punch movement for forward backward extrusion-forging process of square section

5.5 Experimental Analysis

Experiments are carried out for both forward and forward-backward extrusion-forging process. Commercially available lead is used for above mentioned purpose. An extrusion-forging setup for laboratory experimentation is designed and fabricated. The details of the forging die and extrusion dies are presented in Figures 5.10 - 5.12. As described in section 4.16 experiments are conducted for both forward (Figure 5.13) and forward-backward (Figure 5.14) extrusion-forging process.

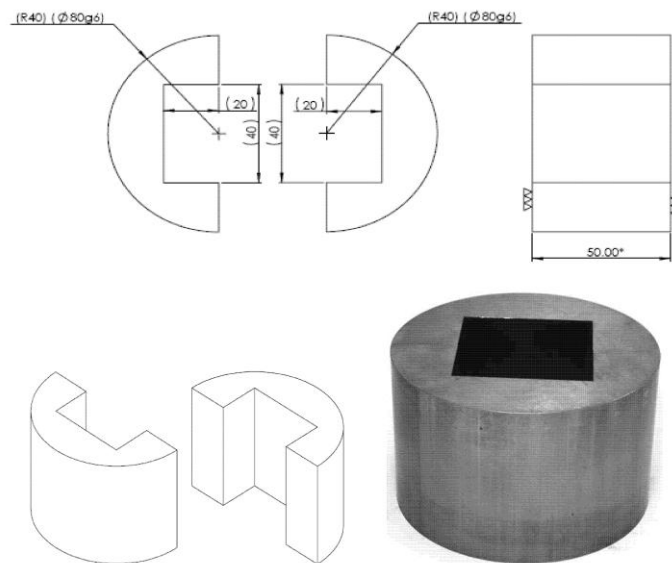


Figure 5.10 Square split type forging die

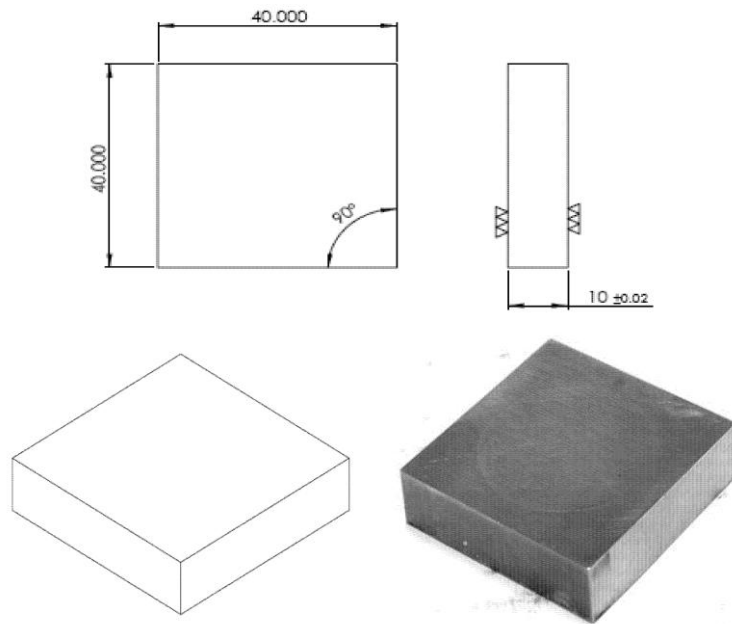


Figure 5.11 Square punch plate

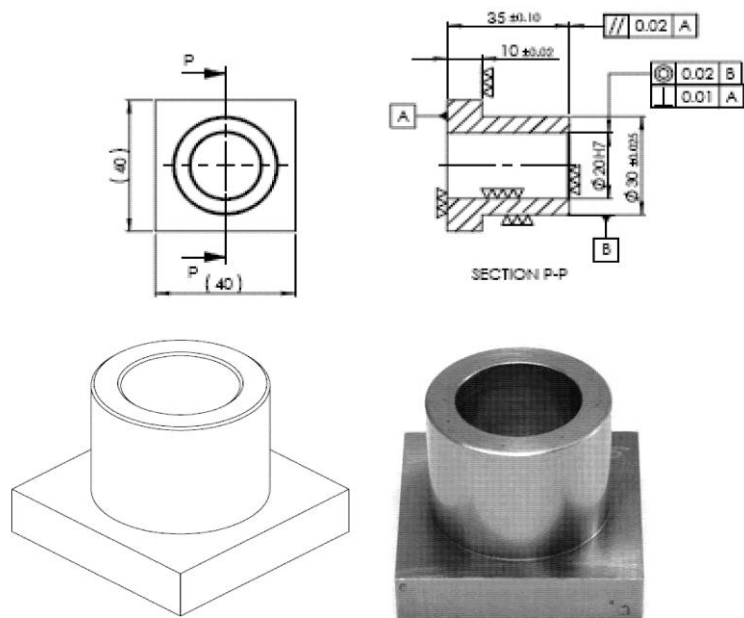


Figure 5.12 Square backward extrusions die

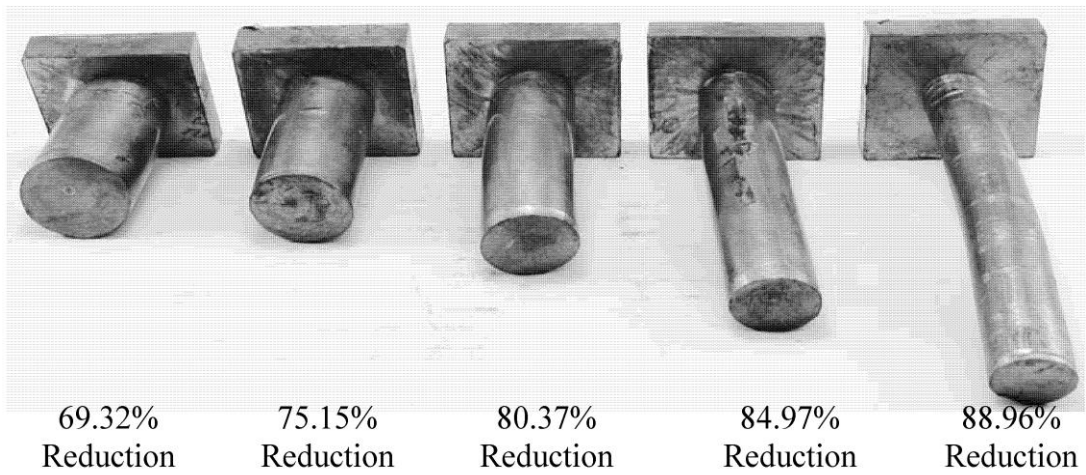


Figure 5.13 Extruded forward extrusion-forging square head shaped product

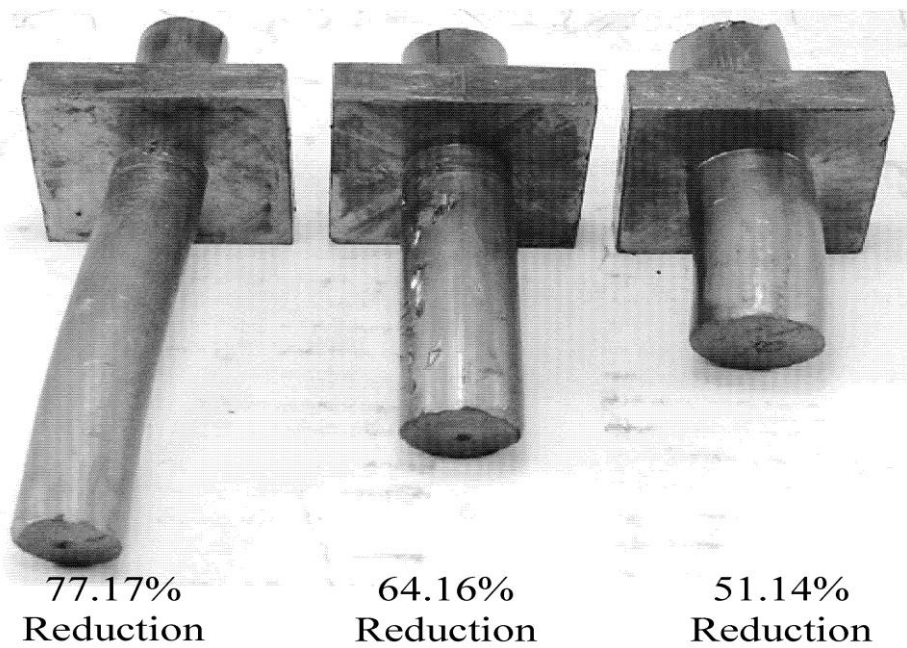


Figure 5.14 Extruded forward-backward extrusion-forging square head shaped product

5.5.1 Summary

Experiments are carried out for forward extrusion-forging process. Five different percentage area reduction dies (88.96%, 84.97%, 80.37%, 75.15% and 69.32% reduction) are used for forward extrusion-forging.

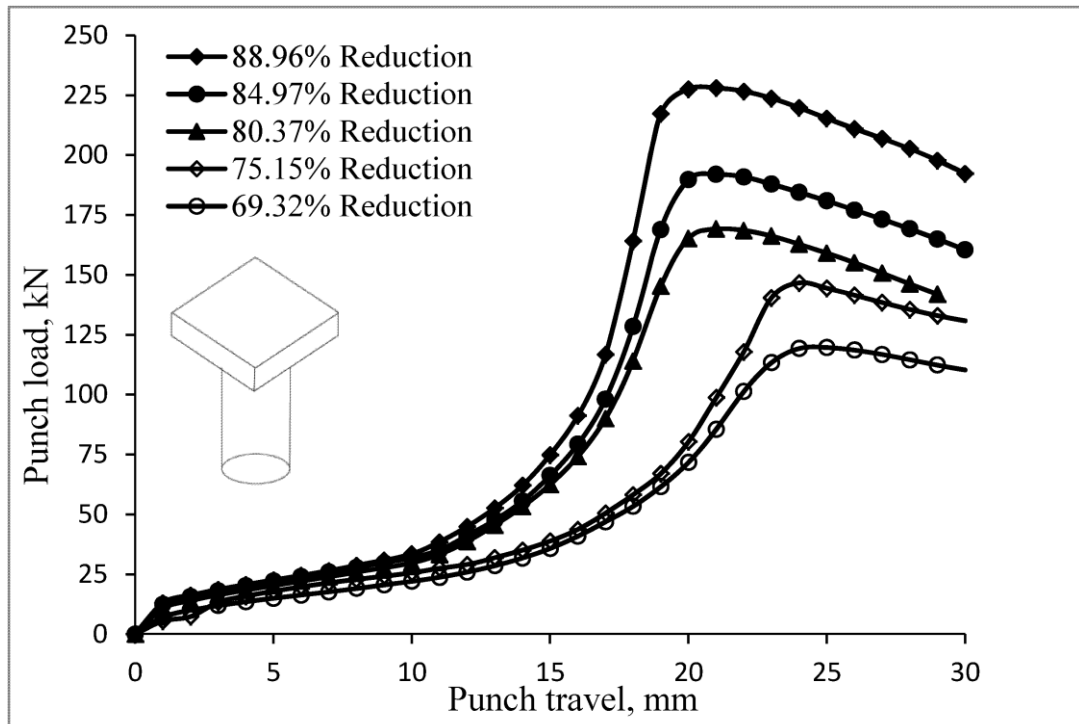


Figure 5.15 Variation of punch load with punch travel of experimental analysis of forward extrusion-forging process of square section

The load corresponding to the peak load, where steady state extrusion starts, considered as the extrusion load and is tabulated in the Table 5.2. This table provides the value of the mean extrusion pressure P_{av} , the value of the uniaxial yield stress in compression σ_0 , and the non-dimensional mean extrusion pressure P_{av}/σ_0 . The theoretical value of P_{av}/σ_0 computed with the help of proposed SERR technique, are also provided in the Table 5.2 for a comparison.

Table 5.2 Computation of non-dimensional average extrusion pressure for forward extrusion-forging process

% Reduction	Extrusion load(kN)	P_{av} MPa	σ_o MPa	P_{ave}/σ_o (Experiment)	P_{ave}/σ_o (Theoretical)
88.96	224.04	140.02	23.428	5.977	6.1
84.97	187.94	117.46	23.475	5.004	5.147
80.37	165.16	103.22	23.521	4.389	4.506
75.15	142.62	89.14	23.567	3.782	3.908
69.32	114.64	71.65	23.613	3.034	3.189

Figure 5.16 shows the complete process at different punch movement, for forward extrusion-forging process, for both FEM simulations and experiment at 77.31 percentage area reduction and at particular intervals of punch movement. It explains that combined extrusion-forging process takes place till the die cavity is completely filled. Then only pure extrusion process takes place.

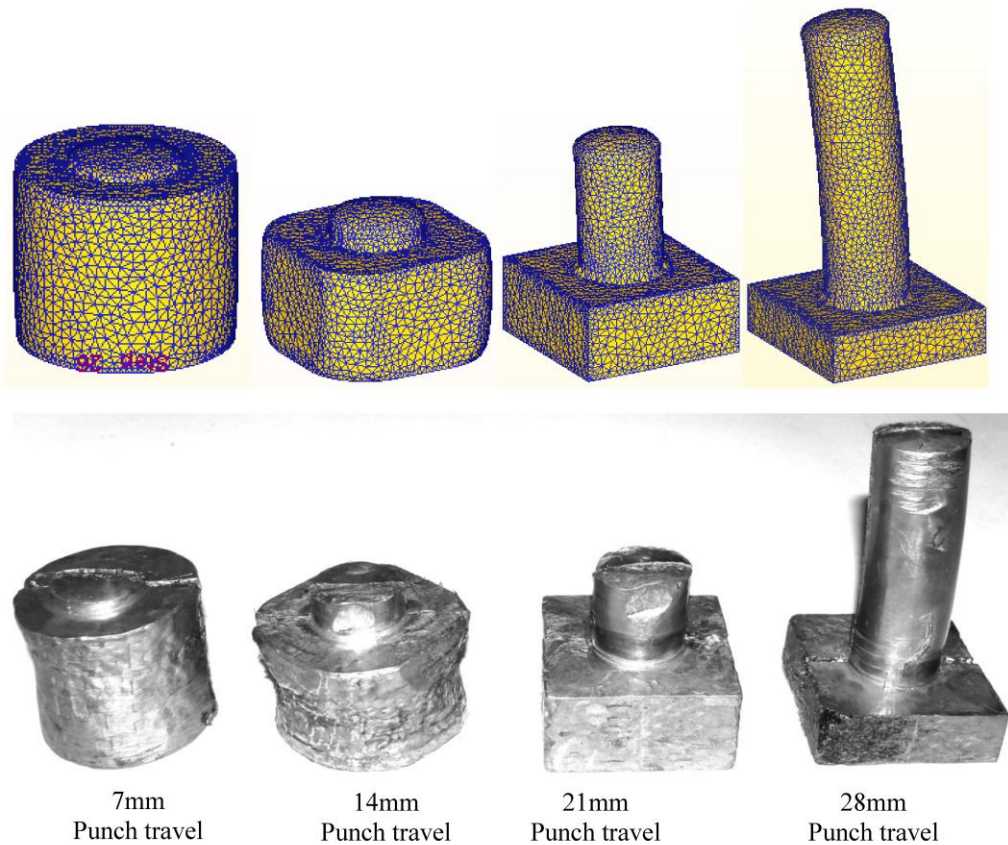


Figure 5.16 Die filling at different punch movement

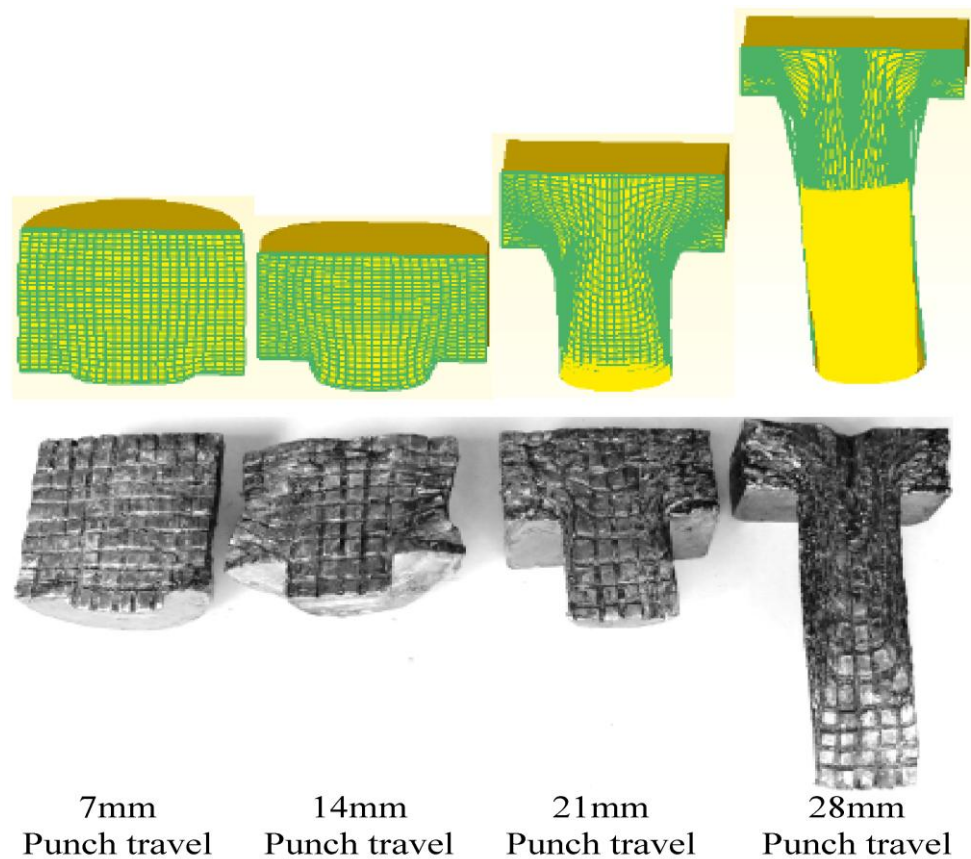


Figure 5.17 Flow pattern at different punch movement

As an illustration, Figure 5.17 shows the photograph of the show pattern for a 77.31 percentage area reduction of forward extrusion-forging process at different punch movement for both in FEM analysis and experimental investigation. The grid line distortion indicates that the process utilizes the maximum amount of redundant work to create flanges of the square.

Experiments are carried out for forward-backward extrusion-forging process. Three different area reduction dies (75.17%, 64.61%, 51.14%, reduction) are used for forward extrusion-forging. Figure 5.18 represents the variation of punch load with punch movement.

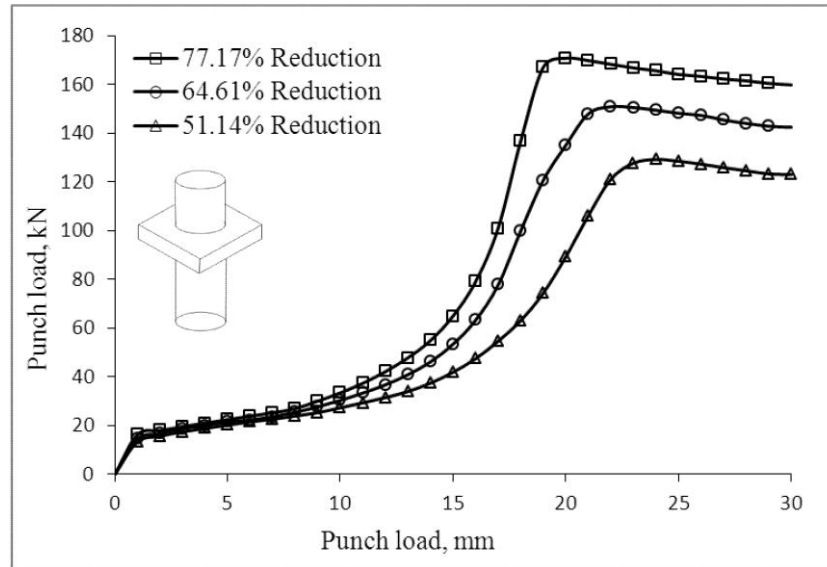


Figure 5.18 Experimental variation of punch load with punch travel

The load corresponding to the peak load, where steady state forward–backward extrusion starts, considered as the extrusion load and is tabulated in the Table 5.3. This table provides the value of the mean extrusion pressure P_{av} , the value of the uniaxial yield stress in compression σ_0 , and the non-dimensional mean extrusion pressure P_{av}/σ_0 . The theoretical value of P_{av}/σ_0 computed with the help of proposed SERR technique, are also provided in the Table 5.3 for a comparison.

Table 5.3 Computation of non-dimensional average extrusion pressure for forward-backward extrusion-forging process

% Reduction	Extrusion load(kN)	P_{av} MPa	σ_0 MPa	P_{ave}/σ_0 (Experiment)	P_{ave}/σ_0 (Theoretical)
75.17	170.71	119.94	23.567	5.09	5.56
64.61	150.80	110.92	23.648	4.69	4.94
51.14	129.16	100.45	23.739	4.23	4.59

As an illustration, Figure 5.19 shows the photograph of the flow pattern for a 75.17% area reduction of forward extrusion-forging process at a particular punch movement for both in FEM and experimental. The grid line distortion indicates that the process utilizes the maximum amount of redundant work to create flanges of the square.



Figure 5.19 Flow pattern for forward-backward extrusion-forging process

5.6 Comparison of result and discussion

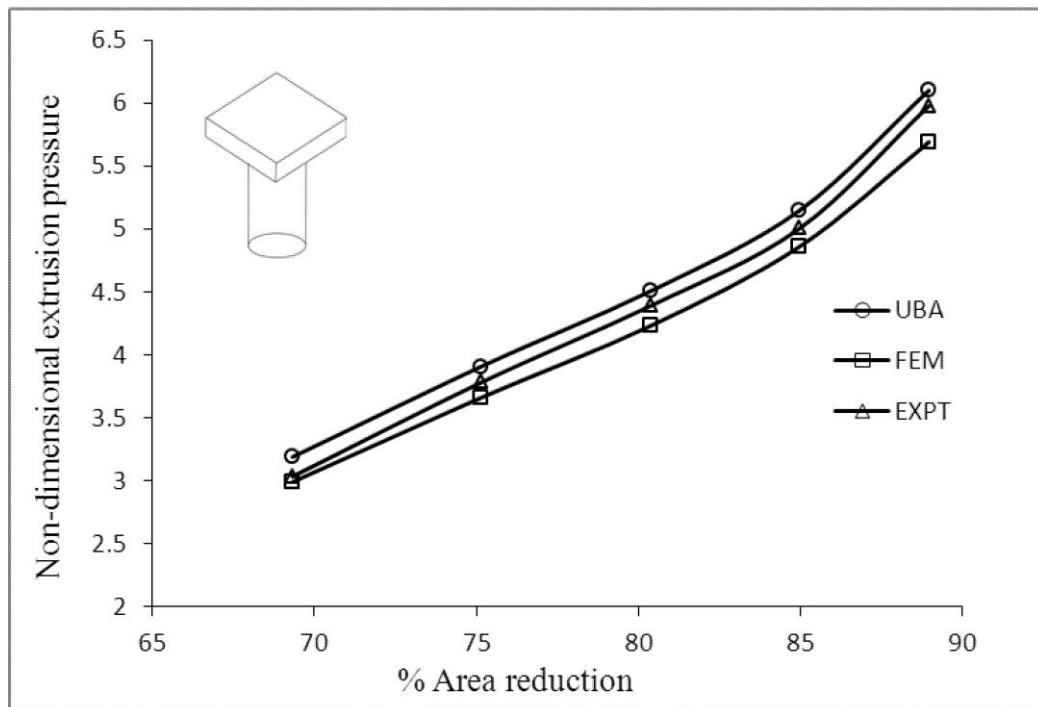


Figure 5.20 Comparison of non-dimensional extrusion pressure without friction for forward extrusion-forging process

Figure 5.20 gives the comparison of P_{av}/σ_0 for upper bound analysis, experimental analysis and finite element analysis. The percentage variation of the three formulations is summarized in Table 5.4. The difference between FEA and UBA are within 7.0%.error. The variance between UBA and expterial analysis are within 5%. The results seem to confirm the suitability of the proposed technique for the combined extrusion-forging processes studied in the present work.

Table 5.4 Variations of non-dimensional extrusion pressure for different formulations without friction for forward extrusion-forging process

% Reduction	% Difference UBA~FEM	% Difference UBA~EXPT
88.96	6.70	2.02
84.97	5.51	2.78
80.37	6.09	2.61
75.15	6.27	3.21
69.32	6.14	4.85

Considering friction for upper bound analysis the variation of P_{av}/σ_0 for FEM, UBA and experimental analysis are shown in Figure 5.21. From the graph we observe that initially when steady-state extrusion starts, FEM and experimental results are closer. As extrusion continues the variation increases because of more redundant work.

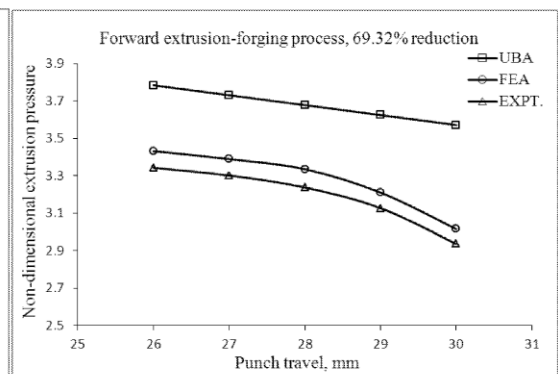
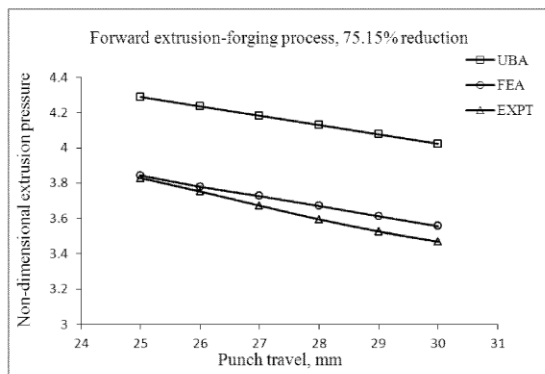
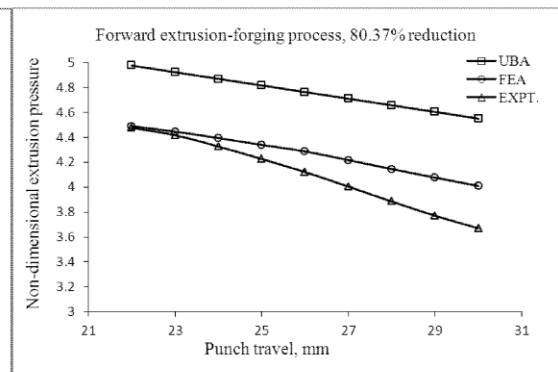
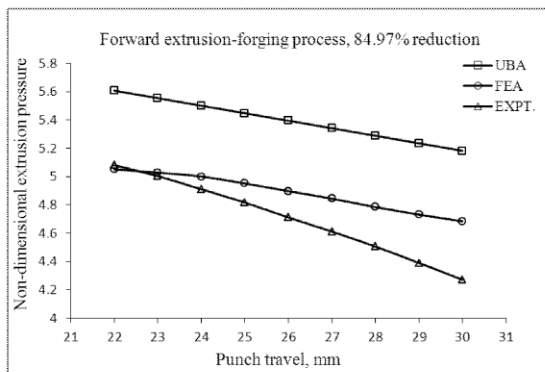
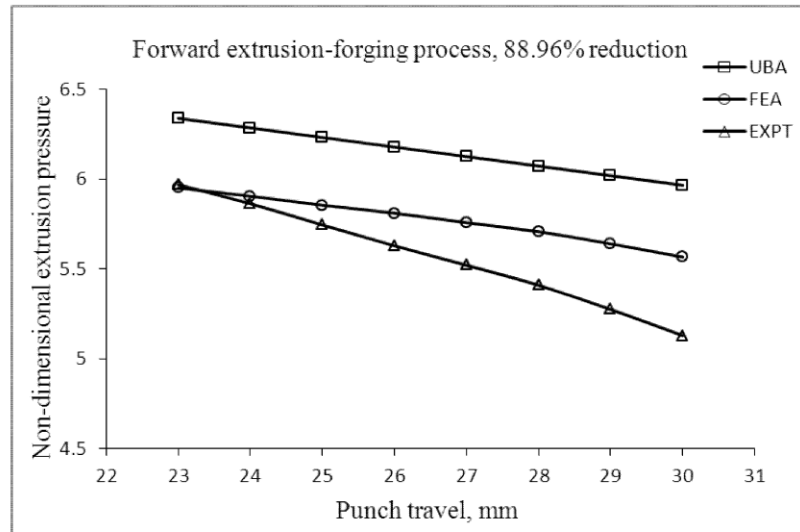


Figure 5.21 Variation of non-dimensional extrusion pressure with friction for forward extrusion forging process for different reduction

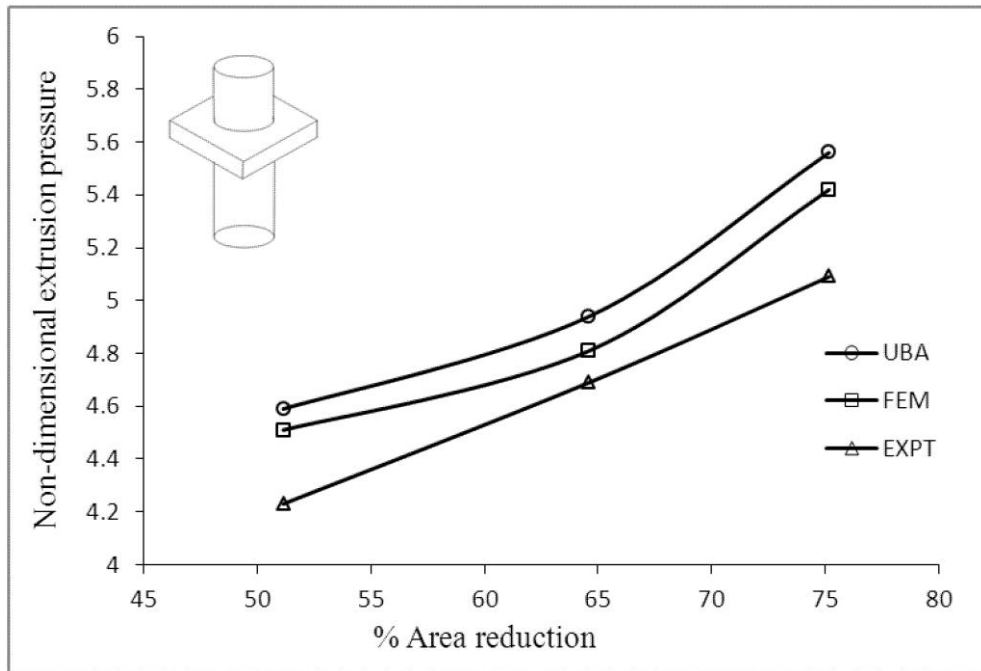


Figure 5.22 Comparison of non-dimensional average extrusion pressure without friction for forward-backward extrusion-forging process

Figure 5.22 gives the comparison of P_{av}/σ_0 for upper bound analysis, experimental analysis and finite element analysis. The percentage variation of the three formulations are summarized in Table 5.5. The difference between UBA and FEM are within 3.0%. Whereas the difference between UBA and EXPT. 10%. It indicates that the proposed method of analysis is also suitable for the forward-backward combined extrusion-forging process.

Table 5.5 Comparison of non-dimensional average extrusion pressure without friction for forward-backward extrusion-forging process

% Reduction	% Difference UBA~FEM	% Difference UBA~EXPT
75.17	2.49	8.38
64.61	2.71	5.09
51.14	1.89	7.88

5.7 Closure

5.7.1 Forward extrusion-forging process

1. The experimental non-dimensional extrusion pressure P_{av}/σ_0 , agrees with the theoretical value computed with the help of proposed SERR technique to within 7% for the range of reduction studied. The results validate and convey the suitability of the proposed technique for the combined extrusion-forging process.
2. Among the three SERR formulation carries out in this study, double-point formulation gives the lowest upper bound to the extrusion pressure for the square section. . It is evident that by increasing the floating point, more than the optimized number, we may incorporate more redundancy (long flow path).
3. The obtained variation of punch load with respect to stroke by proposed technique is also well validated with FE analysis and experiment. It is also observed that with the increase of reduction variation of FE analysis with experimental results increases marginally with the addition of redundant work.
4. The experimental die filling and flow pattern agrees with the FEM analysis.
5. The proposed upper-bound analysis using discontinuous velocity field (modified SERR technique) provides a better method of analysis for this type of section extrusion.

5.7.2 Forward-backward extrusion-forging process

1. The experimental non-dimensional extrusion pressure P_{av}/σ_0 , agrees with the theoretical value computed with the help of proposed SERR technique to within 10% for the range of reduction studied.
2. Among the six SERR formulation carries out in this study, three-point formulation gives the lowest upper bound to the extrusion pressure for the extrude section.
3. The obtained variation of punch load with respect to stroke by proposed technique is also well validated with FE analysis and experiment.
4. The experimental flow pattern agrees with the FEM analysis.
5. The proposed upper-bound analysis using discontinuous velocity field (modified SERR technique) provides a better method of analysis for this type of section extrusion.

3D Analysis of Combined Extrusion-Forging Process for Round-Pentagon-Round Sections

6.1 Theoretical Analysis

The present chapter provides the upper bound solutions for extrusion-forging of pentagon section head with circular shaft through the flat dies from round section billets. Analyses are made for both forward and forward-backward extrusion-forging process for different percentage area reductions. Same assumptions are taken for the present analysis as mentioned in section 4.1.

Following the same procedure described in section 4.2.1 one tenth of the deformation zone (Figure 6.1) is considered for the pentagon section (because of its symmetry about five planes with respect to billet cross-section). The circular cross-section of the shaft is approximated by a 40 sided regular polygon (Figure 6.2).

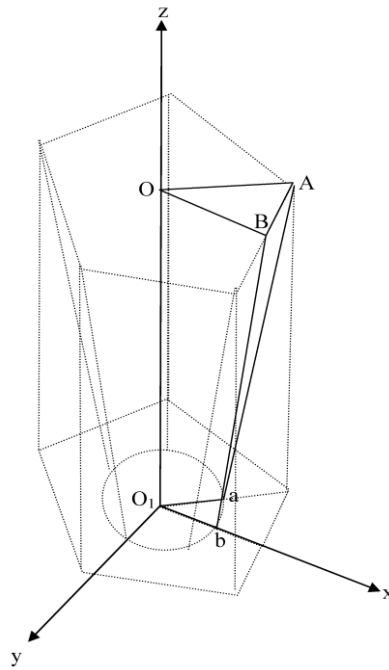


Figure 6.1 Domain of interest A-O-B-O₁-a-b (one tenth of zone of deformation)

Three formulations are considered, which acknowledge one, two and three floating points respectively. For single floating point formulation, an arbitrary point is taken on the extrusion axis. For double point formulation two floating points are taken in the domain of interest, one on the extrusion axis as before and the second on the plane of symmetry at an arbitrary position. Finally, the triple-point formulation, three floating

points are taken, one on the extrusion axis, the second on the plane of symmetry and the third in an arbitrary position in the domain of interest.

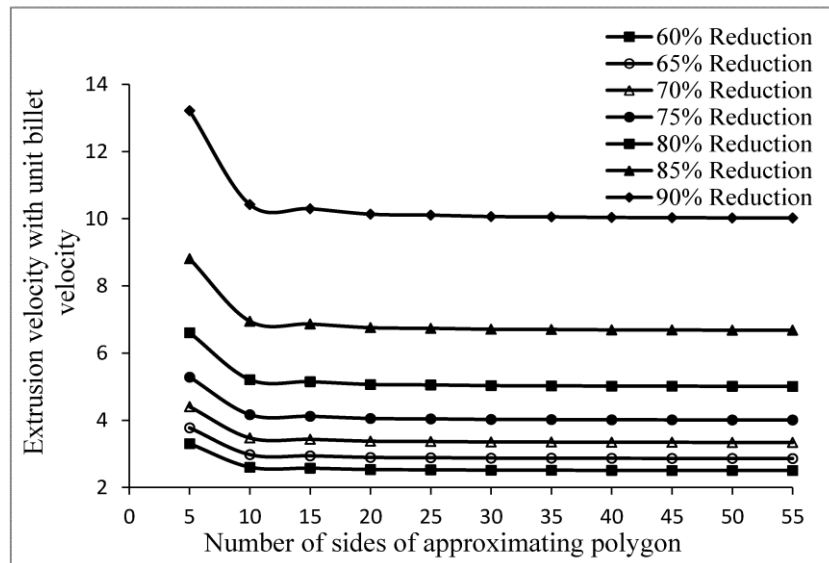


Figure 6.2 Extrusion velocities with number of sides of approximating polygon

The discretization of the forward-backward extrusion-forging process of the pentagon elements with circular shaft on both face of the element is analyzed on the same procedure as followed by the forward extrusion-forging process. Six formulations are considered, which acknowledge one, three, five, seven, nine and eleven numbers of floating points respectively. It was observed that three numbers of floating point formulation give the optimal solution.

FORTTRAN code is used to prepare a comprehensive computational model for forward and forward-backward extrusion-forging process with and without considering friction by incorporating all special features of the proposed cross section. Three formulations for forward extrusion-forging process and six formulations for forward-backward extrusion-forging process is considered.

Computations for all floating point formulations for forward extrusion-forging process are carried out and optimal configuration are considered. Figure 6.3 gives the comparison of the computed results of the three formulations for their respective optimal configurations. It is obvious from the Figure 6.3 that the double-point formulation gives the best results. Therefore, this formulation only is used for further computation and comparison.

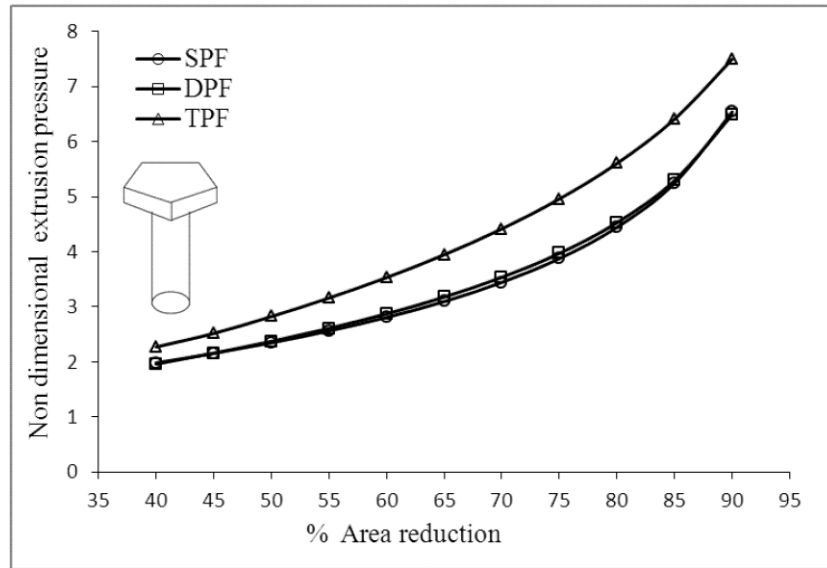


Figure 6.3 Comparison of results for different formulations (N=40)

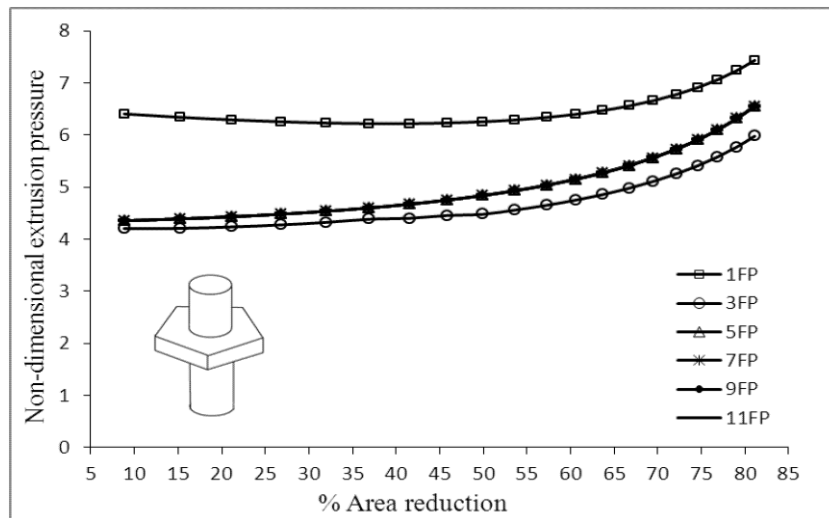


Figure 6.4 Comparison of results for different formulation (N=40)

Figure 6.4 summarize the non-dimensional extrusion pressure of one, three, five, seven, nine and eleven floating point formulations optimal results. Out of this formulation, three floating point formulation gives optimum result and is used for further computation and comparison. It is observed from the graph that increasing the number of floating point after five floating there is a negligible change in the computed value. So, five, seven, nine eleven floating point computed results seem to overlap on the graph.

6.2 Finite Element Analysis

Simulation of forward and forward-backward extrusion-forging of pentagon-round shape product from cylindrical billet is carried out using DEFORM-3D® code.

The detail formulations are presented in previous chapters. Die-punch sets of different percentage area reductions for forward and forward-backward extrusion-forging processes are designed according to the specification and import the STL file for analysis purpose. Simulations are carried out with initial 25000 mesh elements.

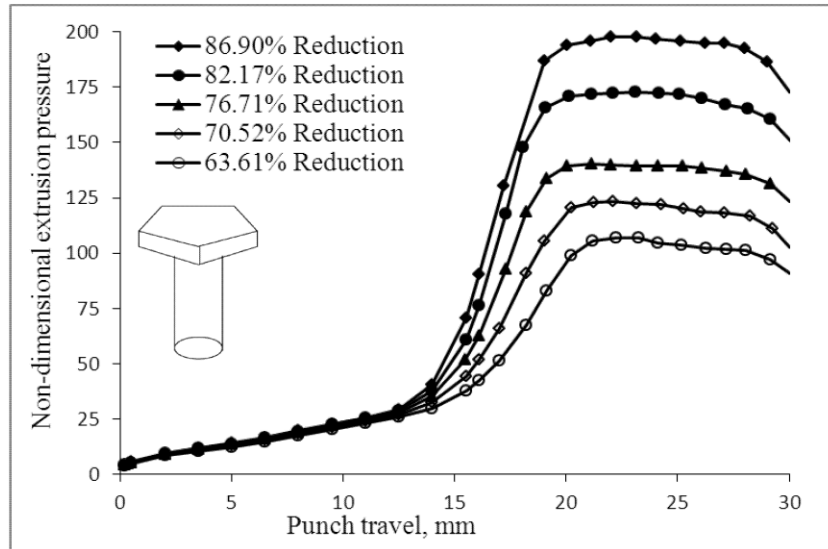


Figure 6.5 Variation of punch load with punch travel

The specimens used in this simulation are 40mm billet length and 35mm billet diameter. Five different area reduction dies (86.90%, 82.17%, 76.71%, 70.52% and 63.61% reduction) are used in this series of experiments. Figure 6.5 gives comparison of punch load with ram movement for different percentage area reductions.

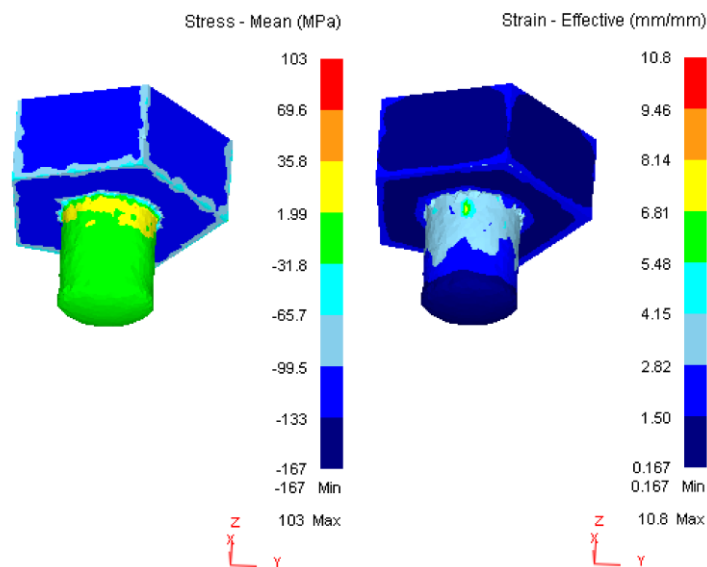


Figure 6.6 Mean stress and effective strain at particular reduction and punch movement for forward extrusion-forging process

Figure 6.6 shows the mean stress distribution and effective strain in terms of solid profile for the reduction of 76.71%; at a ram speed of 1mm/min and ram displacement of 20 mm for forward extrusion-forging process. From the figure it is observed that at the die land and dies corners the material attains a higher compressive stress. Maximum compressive stresses reaches near die walls and die surfaces. The effective strain is large immediate after the extrusion through flat die and gradually decreases.

Three different area reduction dies (69.85%, 59.6061% and 39.27%reduction) for forward-backward extrusion-forging process are used in this series of experiments. Figure 6.7 gives comparison of load with ram movement for different percentage reductions of area.

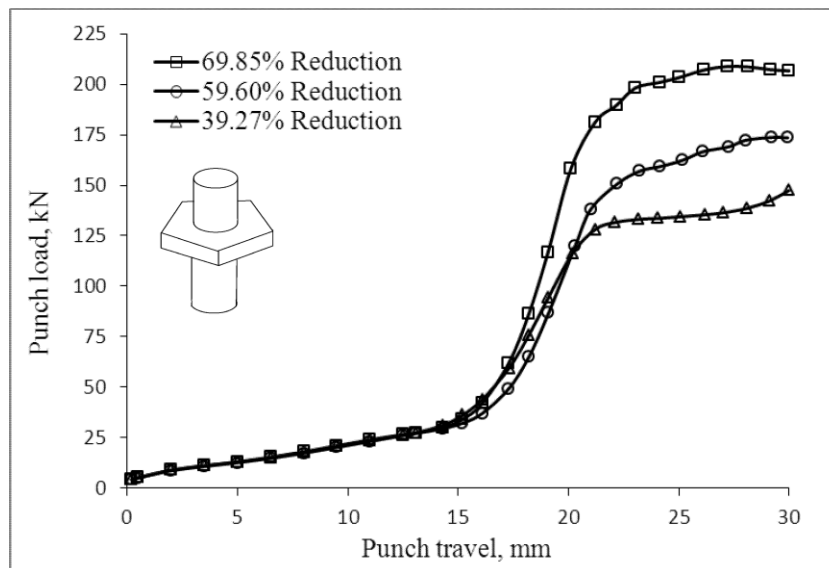


Figure 6.7 Variation of punch load with punch travel

Figure 6.8 shows the mean stress distribution and effective strain in terms of solid profile for the reduction of 59.60%, at a ram speed of 1mm/min and ram displacement of 25mm for forward-backward extrusion forging process. The positive stress signifies the tensile component of stress. From the figure, it is observed that at the die wall the material attains a maximum tensile stress. At the die land the stress is found higher. Maximum compressive stresses reach near die walls. The effective strain is large after the extrusion through flat die and gradually decreases.

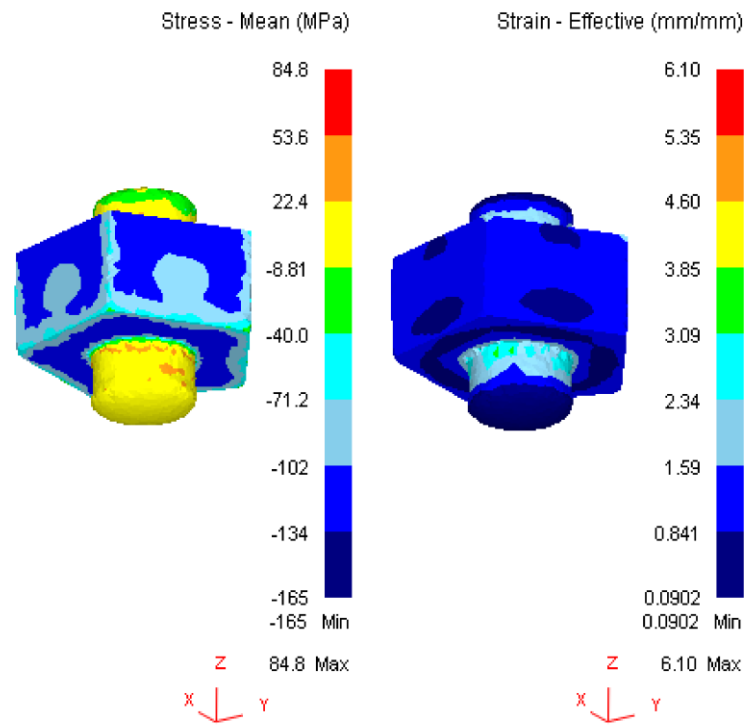


Figure 6.8 Mean stress and effective strain at particular reduction and punch movement for forward backward extrusion-forging process

6.3 Experimental Analysis

Experimental studies are carried out with a view to compare the experimental results with the theoretical ones obtain from proposed method of analysis, and finite element analysis. Experiments are performed on an INSTRON® 600KN Universal testing machine for extrusion-forging of round-pentagon-round sections with square/flat dies. Experiments are carried out for both forward and forward-backward extrusion-forging process. Commercially available lead is used for above mentioned purpose. An extrusion-forging setup for laboratory experimentation is designed and fabricated.

The apparatus, in the main, consists of five parts; namely, the container having a circular chamber, the extruding punch, the forging die holder, extrusion die holder and the supporting block for the assembly. The details about the apparatus are furnished in chapter 4.

Forging and extrusion dies, made of D2 steel hardened up to HRC 50-55 are used for the present experiment. Five sets of forward extrusion die (at different percentage area reduction), and three sets of backward extrusion die (at different percentage area reduction) are employed for experimentation. The details of the forging die and extrusion dies are presented in Figures 6.9 - 6.11.

Specimens of 33mm diameter and 40mm lengths are prepared from commercially available lead. All specimens before use are annealed in boiling water for a period of two hours.

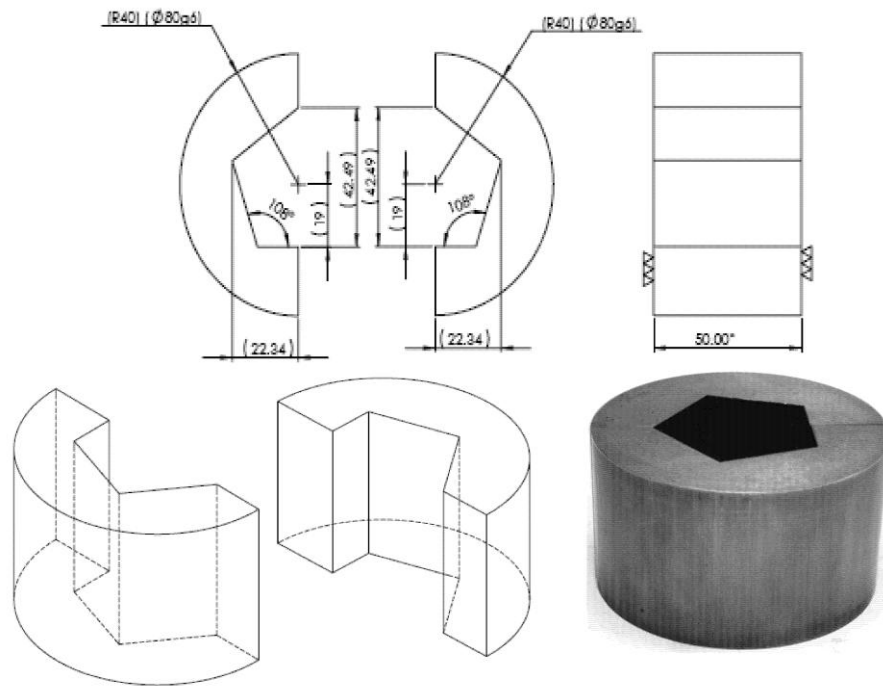


Figure 6.9 Pentagon split type forging die

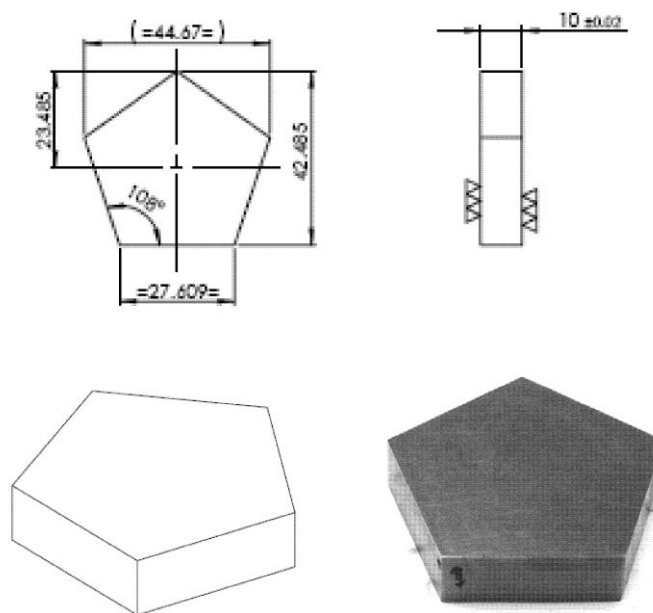


Figure 6.10 Pentagon punch plate

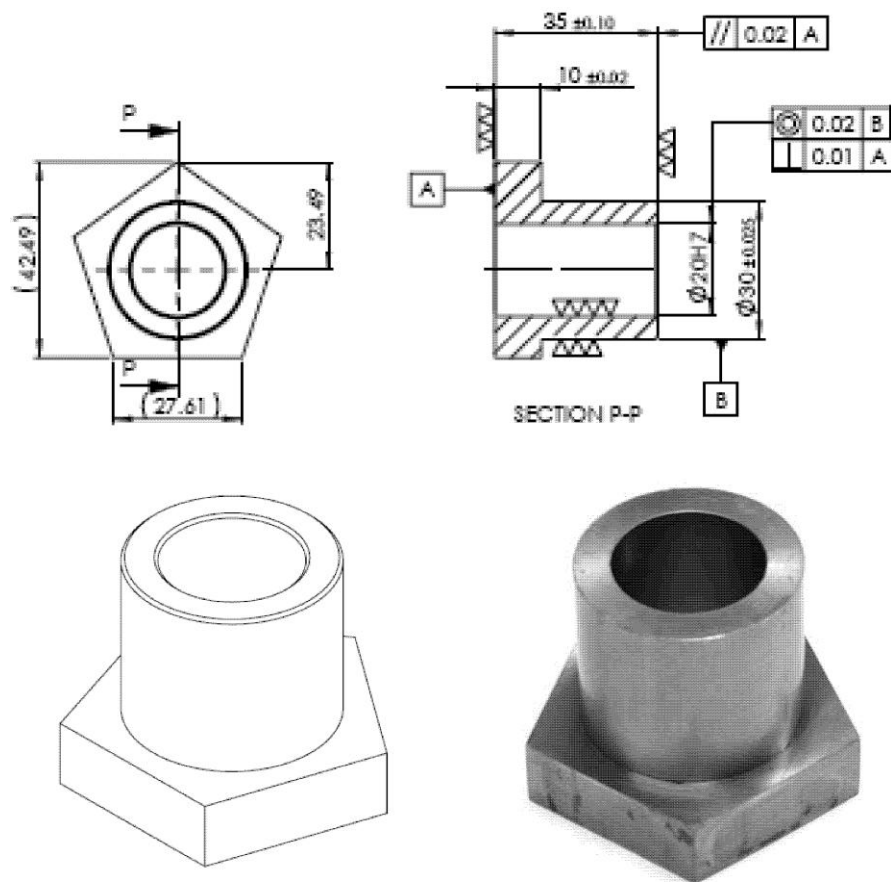


Figure 6.11 Pentagon backward extrusions die

Experiments are conducted on universal testing machine (INSTRON[®] 600KN). To avoid rate affect the movement of the punch being adjusted to approximately 1 mm per minute. Experiments are conducted for all reductions and for both forward and forward-backward, extrusion-forging process. Figure 6.12 and Figure 6.13 gives the output product photography for different percentage area reduction.

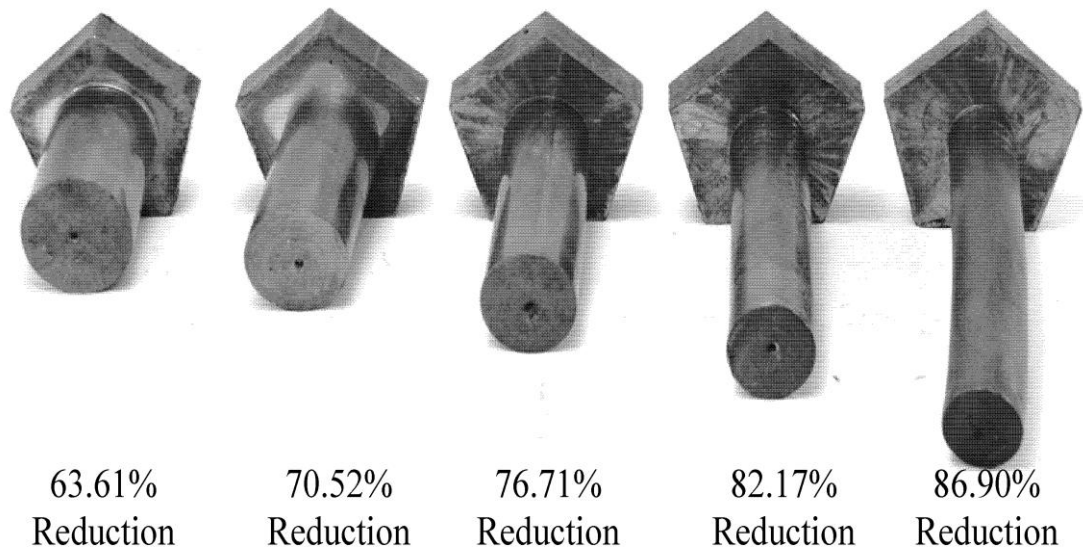


Figure 6.12 Extruded forward extrusion-forging pentagonal head shaped product

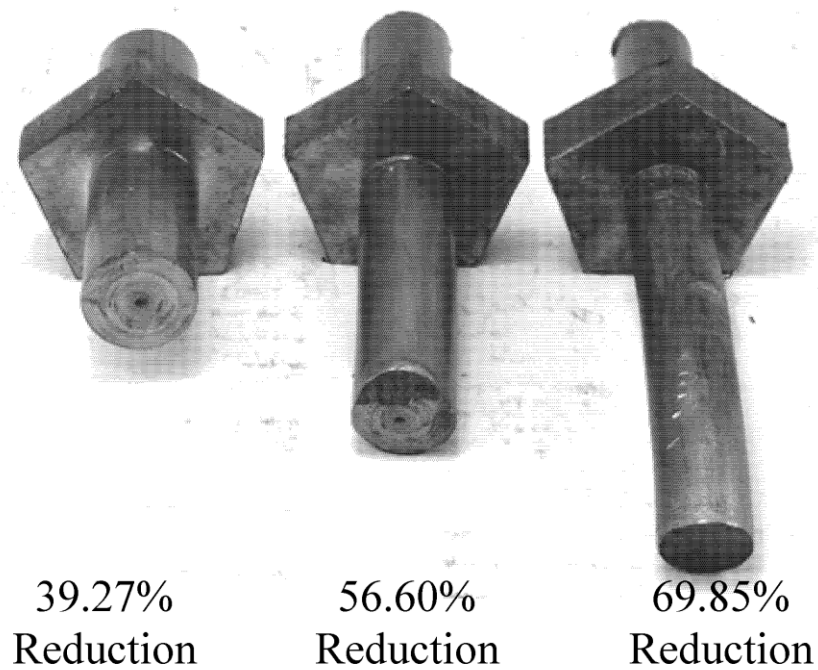


Figure 6.13 Extruded forward-backward extrusion-forging pentagonal head shaped product

6.3.1 Summary

Experiments are carried out for forward extrusion-forging process. Five different area reduction dies (86.90%, 82.17%, 76.71%, 70.53% and 63.61% reduction) are used for forward extrusion-forging. Figure 6.14 represent the variation of punch load with punch movement.

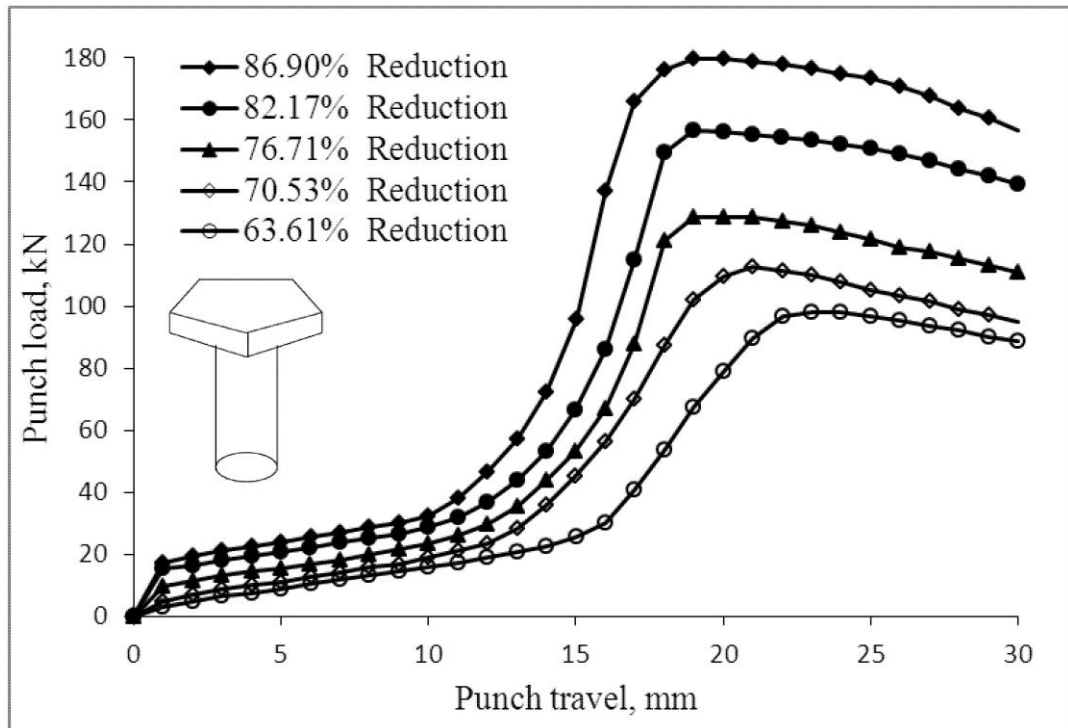


Figure 6.14 Variation of punch load with punch travel of experimental analysis

The load corresponding to the peak load, where steady state extrusion starts, considered as the extrusion load and is tabulated in the Table 6.1. This table provides the value of the mean extrusion pressure P_{av} , the value of the uniaxial yield stress in compression σ_0 , and the non-dimensional mean extrusion pressure P_{av}/σ_0 . Theoretical value of P_{av}/σ_0 computed with the help of proposed SERR technique, are also provided in this table for comparison.

Table 6.1 Computation of non-dimensional average extrusion pressure for forward extrusion-forging process

% Reduction	Extrusion load(kN)	P_{av} MPa	σ_o MPa	P_{ave}/σ_o (Experiment)	P_{ave}/σ_o (Theoretical)
86.90	174.83	129.61	23.454	5.526	5.691
82.17	151.71	112.48	23.504	4.785	4.942
76.71	122.86	91.08	23.554	3.867	4.057
70.52	108.54	80.47	23.604	3.409	3.513
63.61	94.09	69.76	23.655	2.949	3.057

6.3.1.1 Die filling and flow pattern

Figure 6.15 shows the complete process at different punch movement, for forward extrusion-forging process, for both FEM simulations and experiment at 76.71% area reduction and at particular intervals of punch movement. It explains that combined extrusion-forging process takes place till the die cavity is completely filled. Then only pure extrusion process takes place.

As an illustration, Figure 6.16 shows the photograph of the flow pattern for a 76.71% area reduction of forward extrusion-forging process at different punch movement for both in FEM and experimental. The grid lines distortion indicates that the process utilizes the maximum amount of redundant work to create flanges of the pentagon.

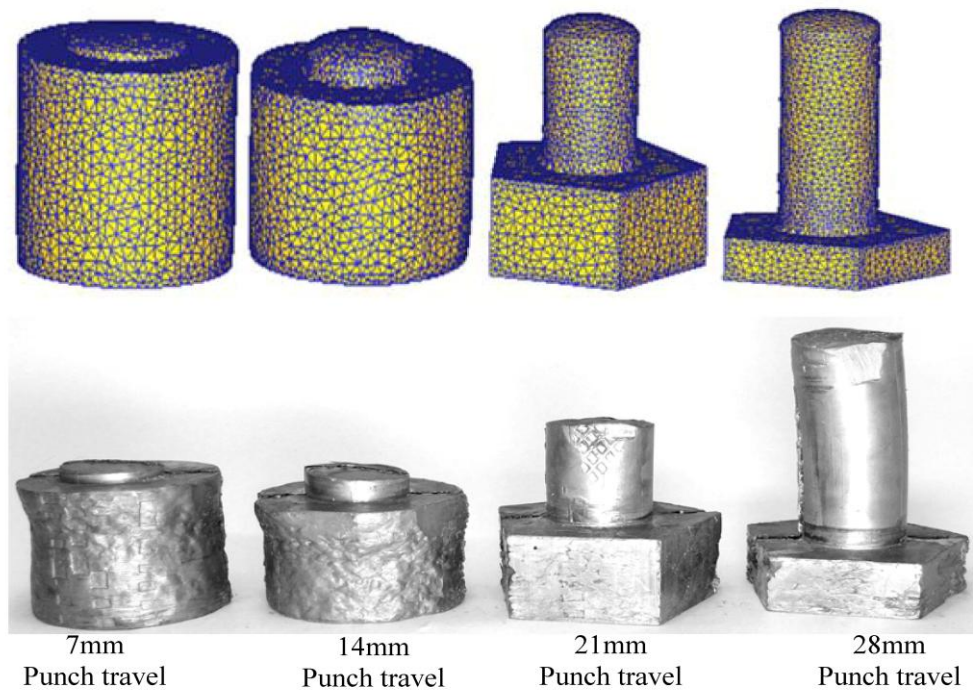


Figure 6.15 Die filling at different punch movement

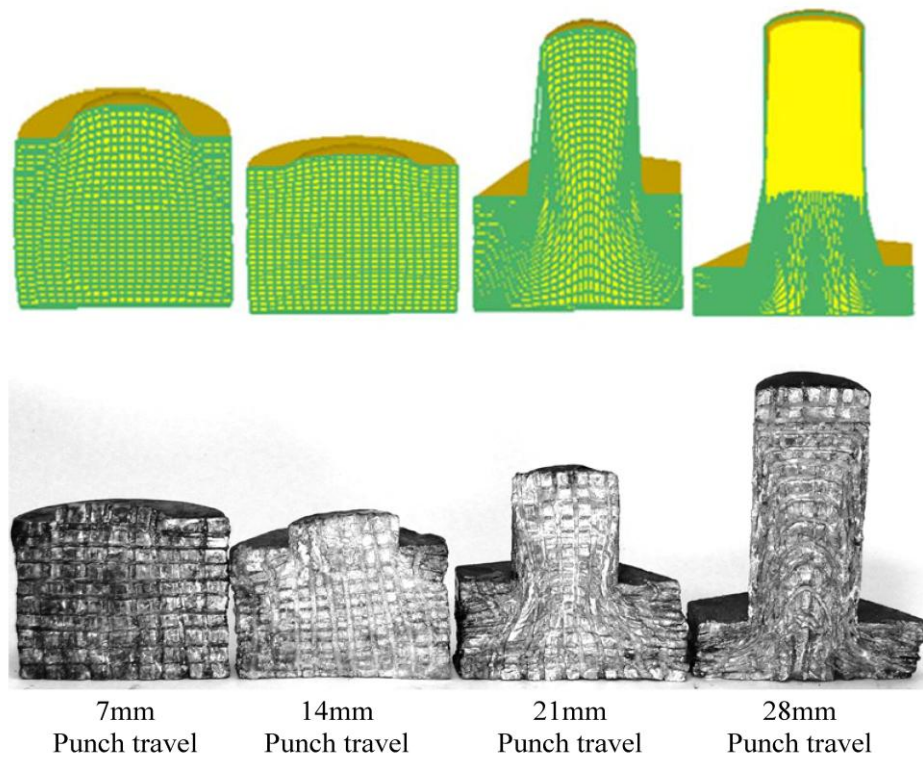


Figure 6.16 Flow pattern at different punch movement

Experiments are carried out for forward-backward extrusion-forging process. Three different percentage area reduction dies (69.85%, 56.60%, 39.27%, area reduction) are used for forward extrusion-forging process. Figure 6.17 represent the punch load versus punch movement. Table 6.2 furnishes the non-dimensional extrusion pressure for theoretical and experimental analysis.

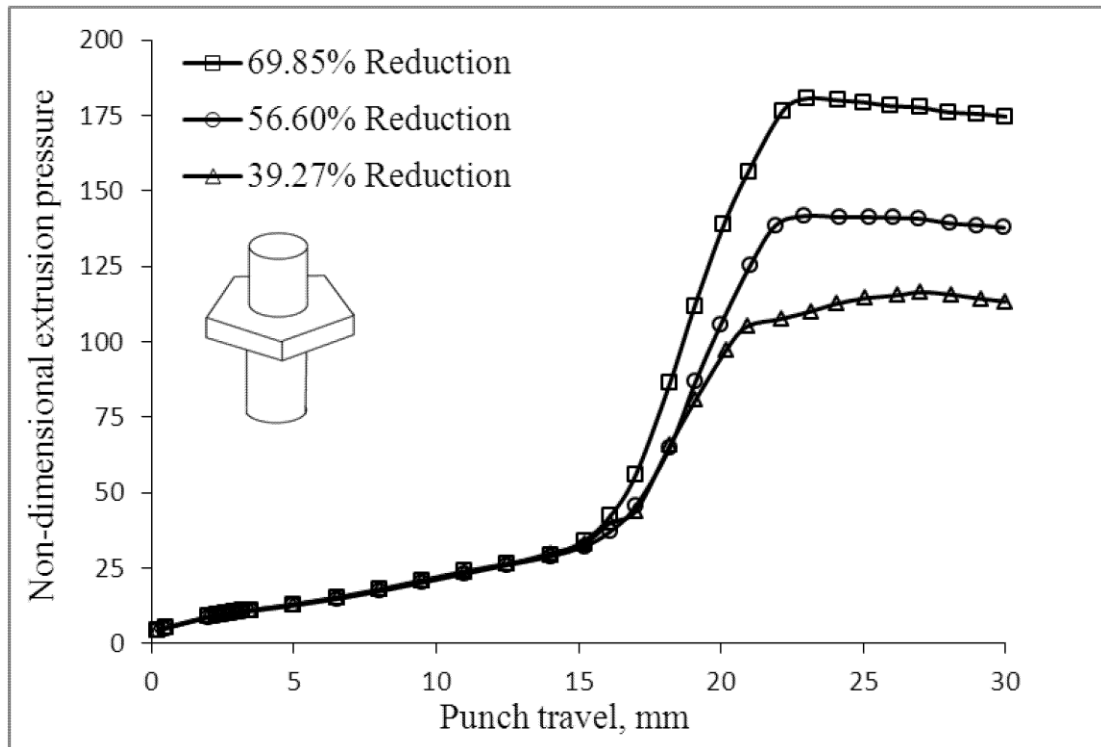


Figure 6.17 Variation of punch load with punch travel of experimental analysis

Table 6.2 Computation of non-dimensional average extrusion pressure for forward-backward extrusion-forging process

% Reduction	Extrusion load(kN)	P_{av} MPa	σ_o MPa	P_{ave}/σ_o (Experiment)	P_{ave}/σ_o (Theoretical)
69.85	137.64	117.43	23.609	4.97	5.12
56.60	11.67	100.76	23.703	4.25	4.64
39.27	98.43	95.13	23.816	3.99	4.39

6.3.1.2 Flow pattern

As an illustration, Figure 6.18 shows the photograph of the flow pattern for a 56.60% area reduction of forward-backward extrusion-forging process at different punch movement for both in FEM analysis and experimental investigation. The grid lines distortion indicates that the process utilizes the maximum amount of redundant work to create flanges of the pentagon.

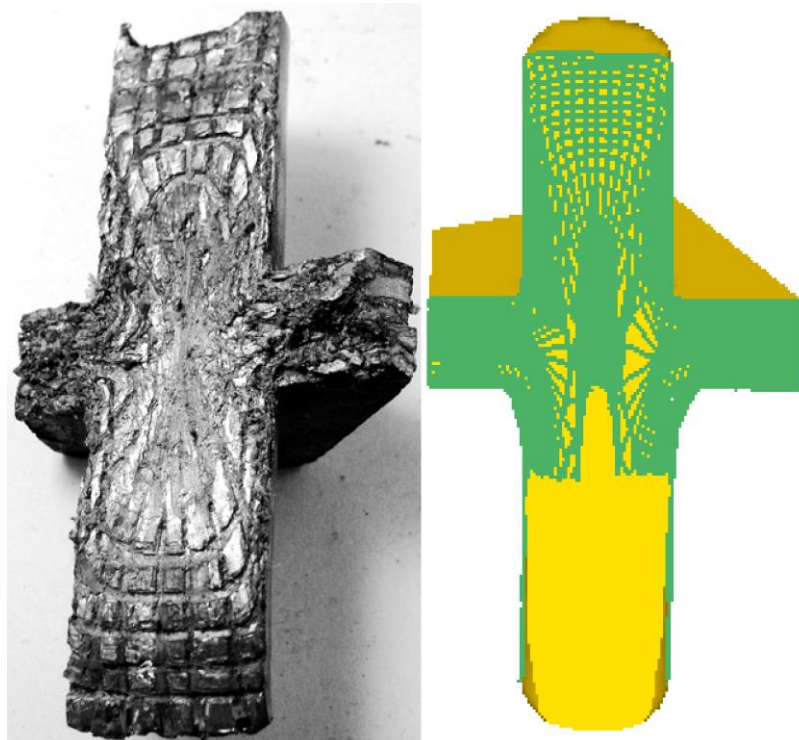


Figure 6.18 Flow pattern at 28mm of punch travel

6.4 Comparison of Results and Discussion

6.4.1 Forward extrusion-forging process

Figure 6.19 gives the comparison of P_{av}/σ_0 for upper bound analysis, experimental analysis and finite element analysis. The percentage variations of the three formulations are summarized in Table 6.3. The difference between UBA and FEM are within 2.0%. Whereas the difference between UBA and Expt. is 5%. The proposed technique appears to provide good prediction of the load requirement for the combined extrusion-forging processes studied in the present work.

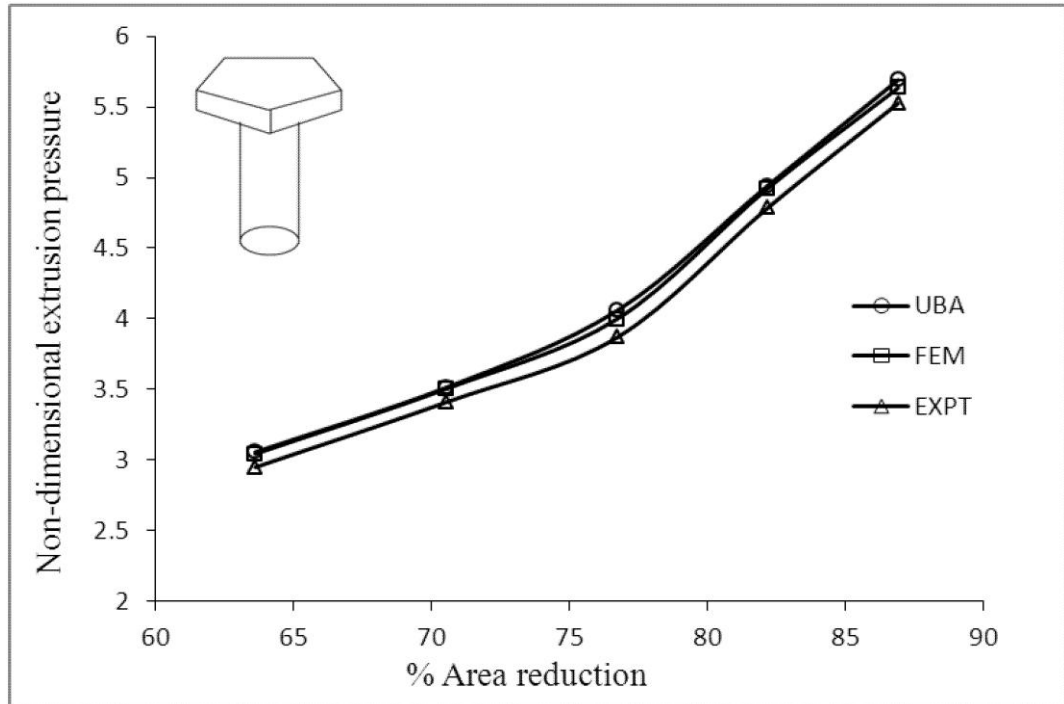


Figure 6.19 Comparison of non-dimensional extrusion pressure without friction for forward extrusion-forging process

Table 6.3 Variation of non-dimensional extrusion pressure without friction for forward extrusion-forging process

% Reduction	% Difference UBA~FEM	% Difference UBA~EXPT
86.9	0.98	2.90
82.17	0.38	3.18
76.71	1.45	4.68
70.52	0.26	2.96
63.61	0.43	3.53

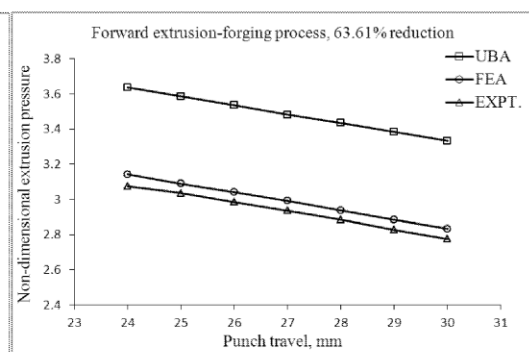
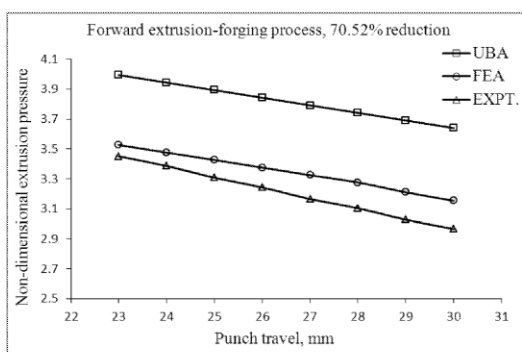
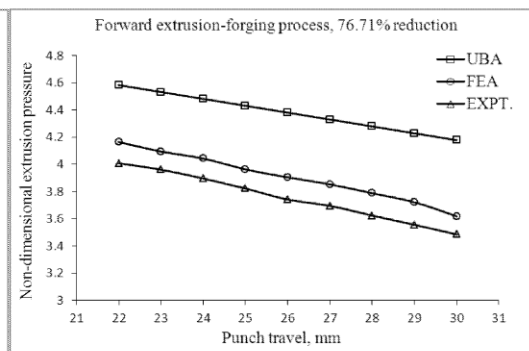
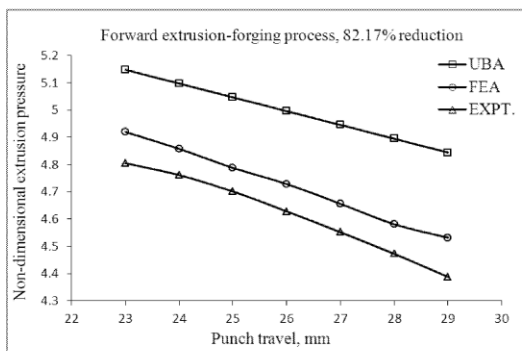
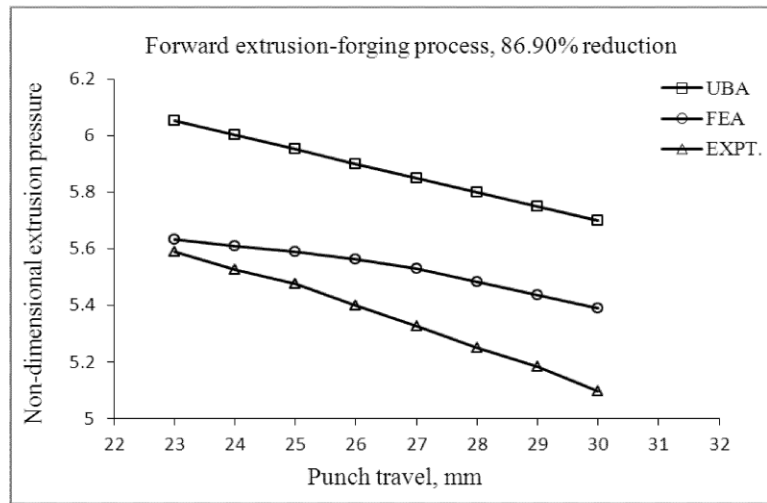


Figure 6.20 Variation of non-dimensional extrusion pressure with friction for forward extrusion forging process for different reductions

Considering friction for upper bound analysis the variation of P_{av}/σ_0 with punch travel for FEM, UBA and Expt. analysis is shown in Figure 6.20 . From Figure 6.20 it is observed that as punch travel forward friction reduces, decreases the non-dimensional extrusion pressure.

6.4.2 Forward-Backward Extrusion-Forging Process

Figure 6.21 gives the comparison of P_{av}/σ_0 for upper bound analysis, experimental analysis and finite element analysis for forward-backward extrusion-forging process. The percentage variations of the three formulations are summarized in Table 6.4. The difference between UBA and FEM are within 11.0%. Whereas the difference between UBA and expt. 9%. The increase of difference with reduction may be attributed to increase of redundant work with friction.

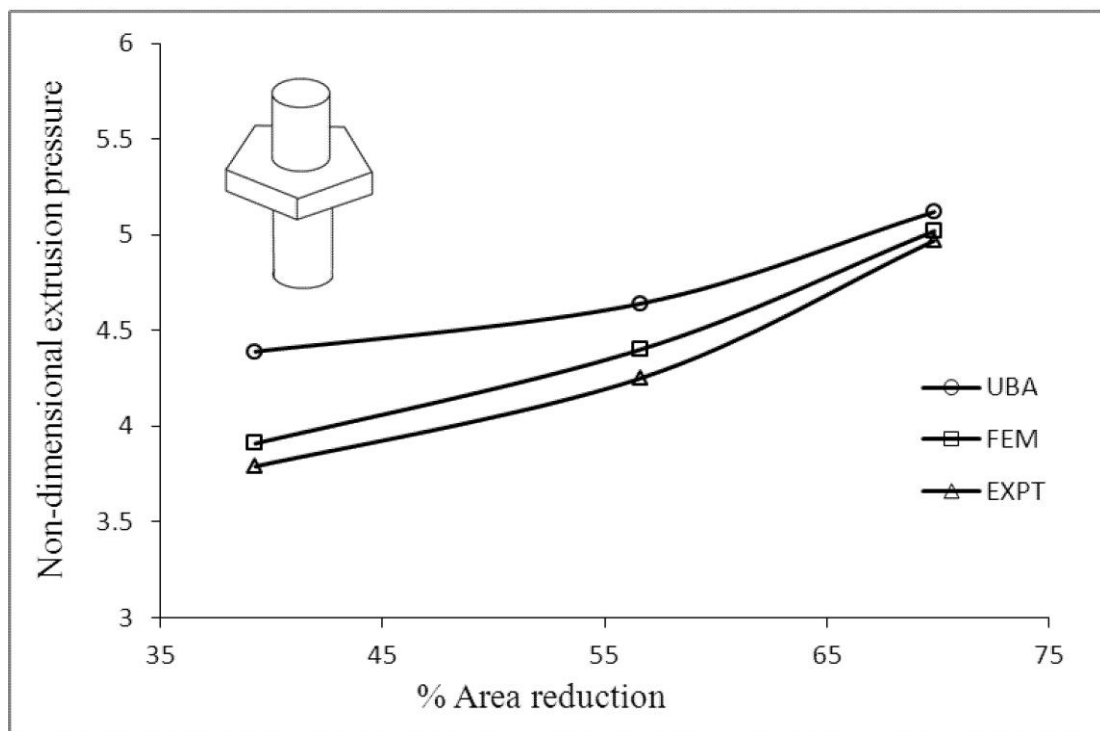


Figure 6.21 Comparison of non-dimensional extrusion pressure without friction for forward-backward extrusion-forging process

Table 6.4 Comparison of non-dimensional average extrusion pressure without friction for forward-backward extrusion-forging process

% Reduction	% Difference UBA~FEM	% Difference UBA~EXPT
69.85	1.82	2.81
56.60	0.82	8.40
39.27	10.91	9.09

6.5 Closure

6.5.1 Forward extrusion-forging process

1. The experimental non-dimensional average extrusion pressure P_{av}/σ_o , agrees with the theoretical value computed with the help of proposed SERR technique to within 5% for the range of reduction studied. The result approves the proposed technique for the combined extrusion-forging process.
2. Among the three SERR formulation carries out in this study, double-point formulation gives the lowest upper bound to the extrusion pressure for the section. It indicates that there is an optimum number of discretization of the deformation zone to get best result.
3. The obtained variation of punch load with respect to stroke by proposed technique is also well validated with FE analysis and experiment. It is also observed that with increase of reduction variation of FE analysis with experimental results increases marginally because of redundancy.
4. The proposed upper-bound analysis using discontinuous velocity field (modified SERR technique) provides a better method of analysis for this type of manufacturing process.
5. The experimental die filling and flow pattern agrees well with the FEM analysis.

6.5.2 Forward-backward extrusion forging process

1. The experimental non-dimensional average extrusion pressure P_{av}/σ_o , agrees with the theoretical value computed with the help of proposed SERR technique to within 10% for the range of reduction studied. It indicates that the proposed method of analysis is also suitable for the forward-backward combined extrusion-forging process.
2. Among the six SERR formulation carries out in this study, three-point formulation gives the lowest upper bound to the extrusion pressure for the

extrude section. It is evident that by increasing the floating points, more than the optimized number, we may incorporate more redundancy.

3. The obtained variation of punch load with respect to stroke by proposed technique is also well validated with FE analysis and experiment.
4. The experimental flow pattern agrees with the FEM analysis.
5. The proposed upper-bound analysis using discontinuous velocity field (modified SERR technique) provides a better method of analysis for the forward-backward extrusion-forging also.

3D Analysis of Combined Extrusion-Forging Process for Round-Hexagon-Round Sections

7.1 Theoretical Analysis

Considering the assumptions described in section 4.1 the present chapter provides the upper bound solution for extrusion-forging of hexagon sections head with circular shaft through the square dies from round section billets. Analyses are made for both forward and forward-backward extrusion-forging process for different reductions.

7.1.1 Forward extrusion-forging process

Following the same procedure described in section 4.2.1 one twelfth of the deformation zone (Figure 7.1) is considered for the pentagon section (because of its symmetry about five planes with respect to billet cross-section). The circular cross-section of the shaft is approximated by a 48 sided regular polygon (Figure 7.2).

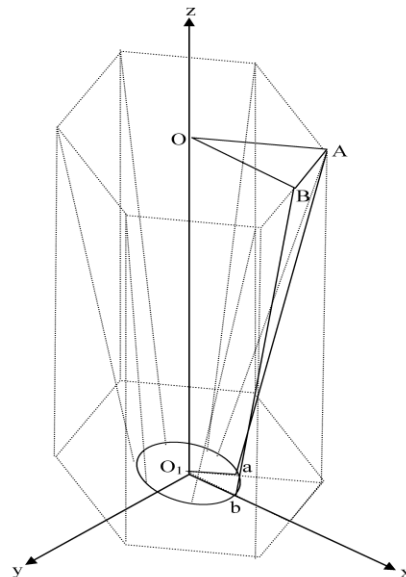


Figure 7.1 Domain of interest A-O-B-O₁-a-b (one tenth of zone of deformation)

Three formulations are considered, which acknowledge one, two and three floating points respectively. For single floating point formulation, an arbitrary point is taken on the extrusion axis. For double point formulation two floating points are taken in the domain of interest, one on the extrusion axis as before and the second on the plane of symmetry at an arbitrary position. Finally, the triple-point formulation, three floating points are taken, one on the extrusion axis, the second on the plane of symmetry and the third in an arbitrary position in the domain of interest.

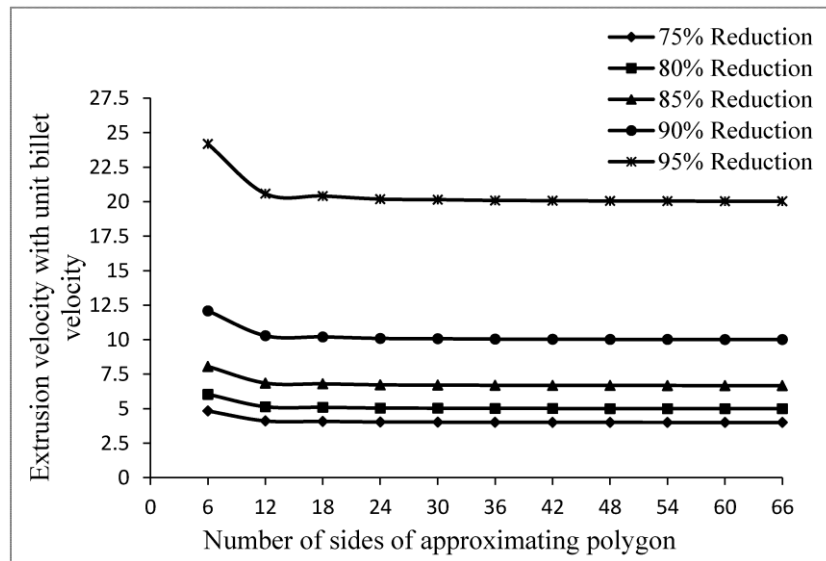


Figure 7.2 Extrusion velocities with number of sides of approximating polygon

7.1.2 Forward backward extrusion-forging process

The discretization of the forward-backward extrusion-forging process of the hexagon elements with circular shaft is proposed in the same manner as followed by the forward extrusion-forging process. Six formulations are considered, which acknowledge one, three, five, seven, nine and eleven numbers of floating points respectively.

FORTTRAN code is used to prepare a comprehensive computational model for forward and forward-backward extrusion-forging process with and without considering friction by incorporating all special features of the hexagon. Three formulations for forward extrusion-forging process and six formulations for forward-backward extrusion-forging process is considered.

7.1.3 Summary

Computations for all floating point formulations are carried out and optimal configuration are considered. Figure 7.3 gives the comparison of the computed results of the three formulations for their respective optimal configurations for forward extrusion-forging process. It is obvious from the Figure 7.3 that the double-point formulation gives the best results. Therefore, this formulation only is used for further computation and comparison.

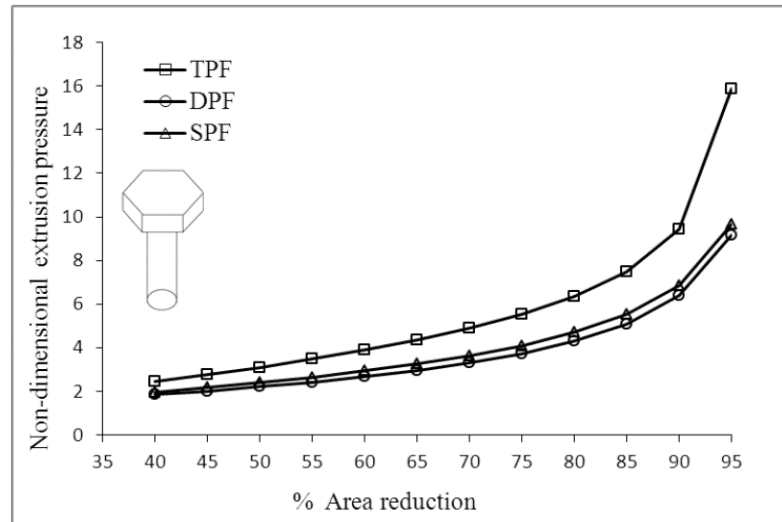


Figure 7.3 Comparison of results for different formulation without friction (N=48)

7.1.4 Forward-backward extrusion-forging process

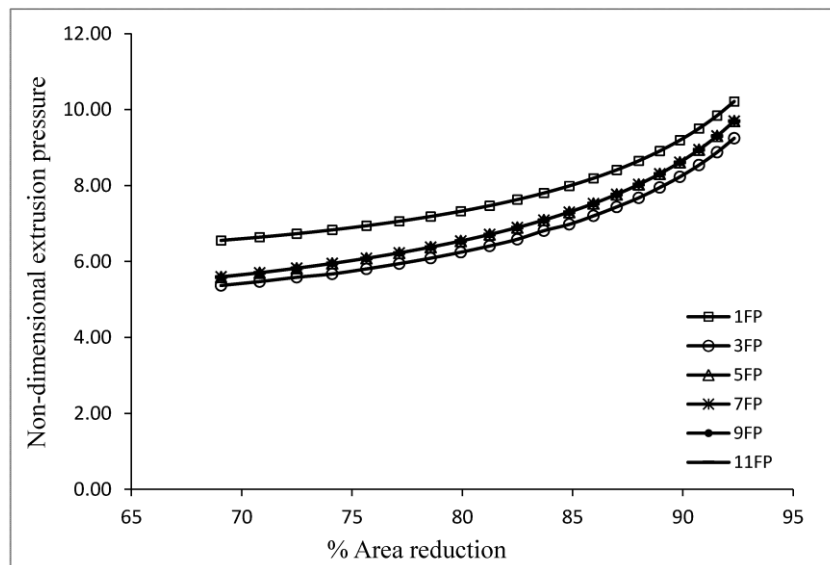


Figure 7.4 Comparison of results for different formulation

Figure 7.4 summarize the non-dimensional extrusion pressure of one, three, five, seven, nine and eleven floating point formulations optimal results for forward-backward extrusion-forging process. Out of this formulation, three floating point formulation gives optimum result and is used for further computation and comparison. It is observed from the graph that increasing the number of floating point after five floating there is a negligible change in the computed value. So, five, seven, nine eleven floating point computed results seem to overlap on the graph.

7.2 Finite Element Analysis

Simulations of forward and forward-backward extrusion-forging of hexagon-round shape product from cylindrical billet are carried out using DEFORM[®]-3D code. The detail formulations are presented in previous chapters. A die-punch set of different area reduction for forward and forward-backward extrusion-forging process is designed according to the specification and import the STL file for analysis purpose. Simulations are carried out with initial 25000 mesh elements.

7.2.1 Summary

7.2.1.1 Forward extrusion-forging process

The billet of 40mm length and 45mm diameter are used in this simulation. Five different area reduction dies (92.44%, 89.71%, 86.56%, 83.00% and 79.01% reduction) are used for forward extrusion-forging process. The dies and punch plate used for simulation is same as that of experimental sets. Figure 7.5 gives comparison of punch load with ram movement for different % reductions of area.

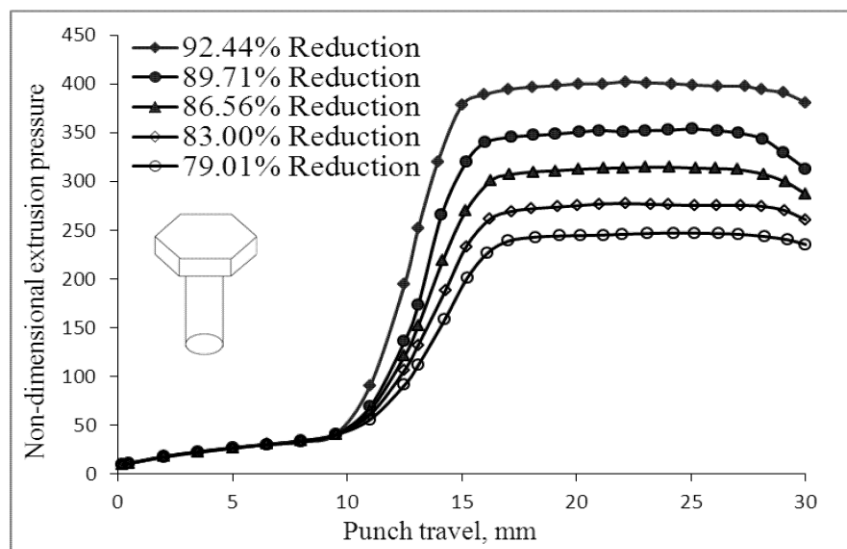


Figure 7.5 Variation of punch load with punch travel

Mean stress and effective strain Figure 7.6 shows the mean stress distribution and effective strain in terms of solid profile for the reduction of 86.56%; at a ram speed of 1mm/min and ram displacement of 25 mm for forward extrusion-forging process. The positive stress signifies the tensile component of stress. From the figure it is observed that at the die land and die corners mean stress are at a range of 89.6-53.5 MPa. At die face and die walls the material attain a maximum compressive

stress. The effective strain is large immediate after the extrusion through flat die and gradually decreases. Maximum effective strain is at die corners and die lands.

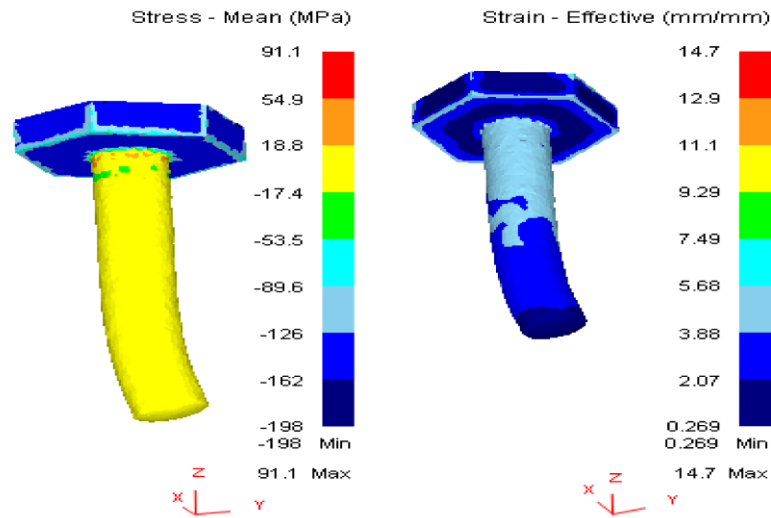


Figure 7.6 Mean stress and effective strain at particular reduction and punch movement for forward extrusion-forging process

7.2.1.2 Forward backward extrusion-forging process

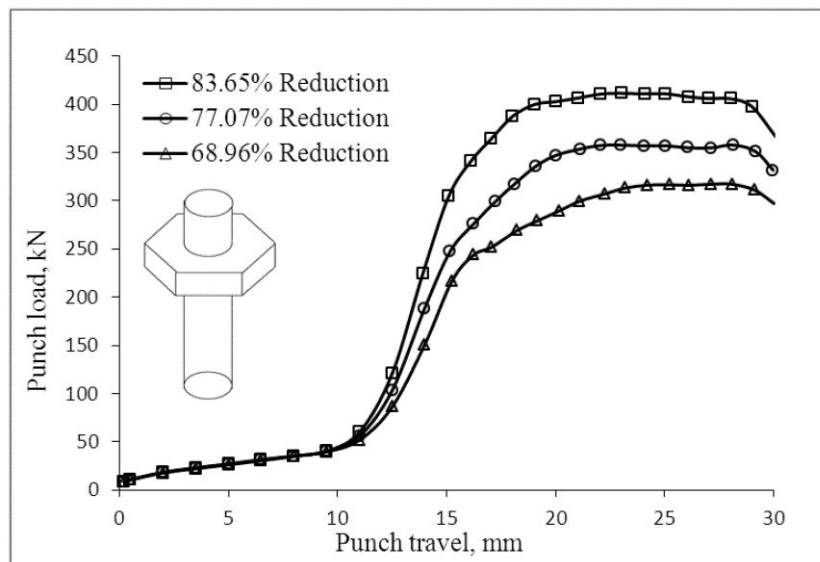


Figure 7.7 Variation of punch load with punch travel

Three different area reduction dies (83.65%, 77.07% and 68.96% reduction) are for forward backward extrusion-forging process. The dies and punch plate used for

simulation is same as that of experimental sets. Figure 7.7 gives comparison of punch load with ram movement for different % reductions of area.

Figure 7.8 shows the mean stress distribution and effective strain in terms of solid profile for the reduction of 77.07%, at a ram speed of 1mm/min and ram displacement of 25mm for forward-backward extrusion forging process. The positive stress signifies the tensile component of stress. From the figure it is observed that at the die faces and at die walls the materials attain a maximum compressive stress. At the die land the stress is found higher. The effective strain is large after the extrusion through flat die and gradually decreases.

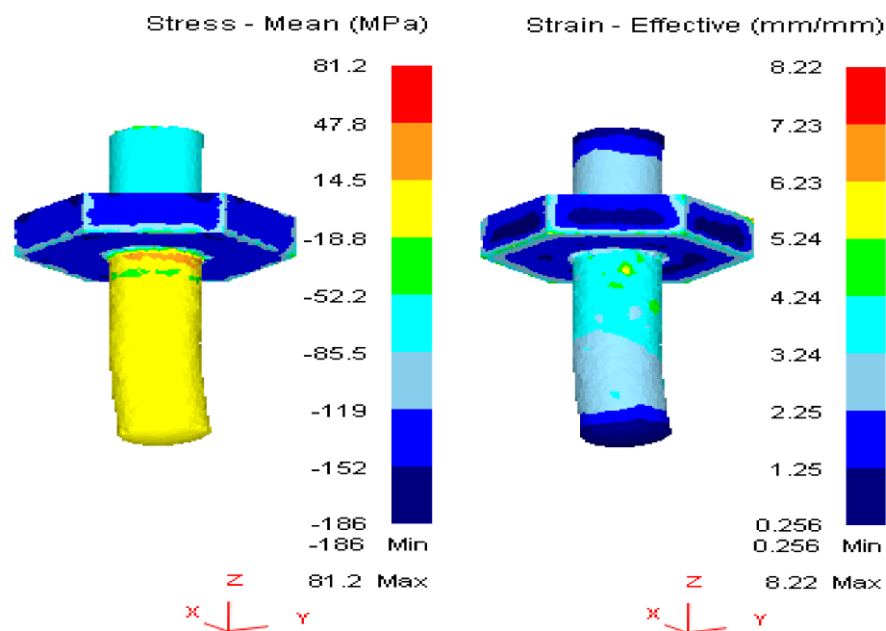


Figure 7.8 Mean stress and effective strain at particular reduction and punch movement for forward backward extrusion-forging process

7.3 Experimental Analysis

Experiments are carried out for both forward and forward-backward extrusion-forging process. Commercially available lead is used for above mentioned purpose. An extrusion-forging setup for laboratory experimentation is designed and fabricated.

The apparatus, in the main, consists of five parts; namely, the container having a circular chamber, the extruding punch, the forging die holder, extrusion die holder and the supporting block for the assembly. The details about the apparatus are furnished in chapter 4.

The setup used in previous section extrusion is used here. The forging and extrusion dies are made of two split halves for easy removal of product after extrusion cycles. These dies are manufactured from D2 steel, hardened up to HRC 50-55. Five sets of forward extrusion die (at different reduction in the area), and three sets of forward-backward extrusion die (at different reduction in area) are employed for experimentation. The details of the forging die and extrusion dies are presented in Figures 7.9 – 7.11.

Specimens of 45mm diameter and 40mm lengths are prepared from commercially available lead. All specimens before experimentation are annealed in boiling water for a period of two hours.

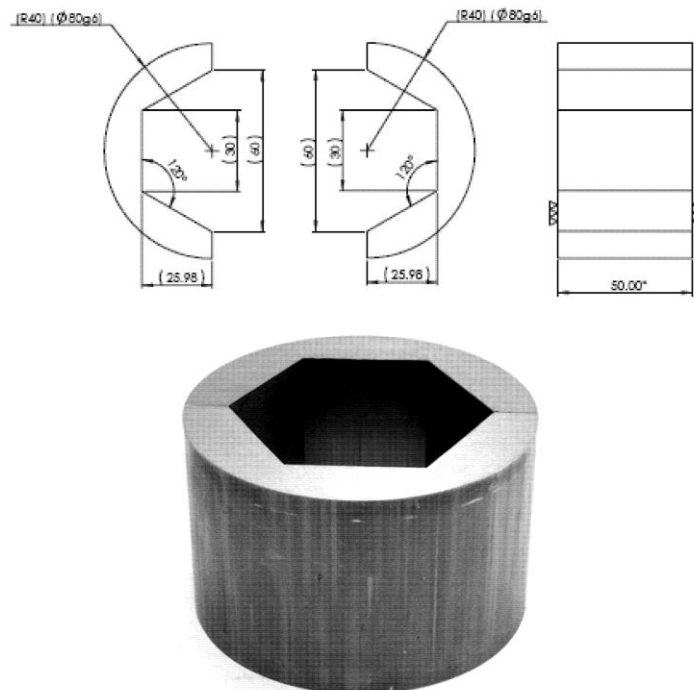


Figure 7.9 Hexagon split type forging die

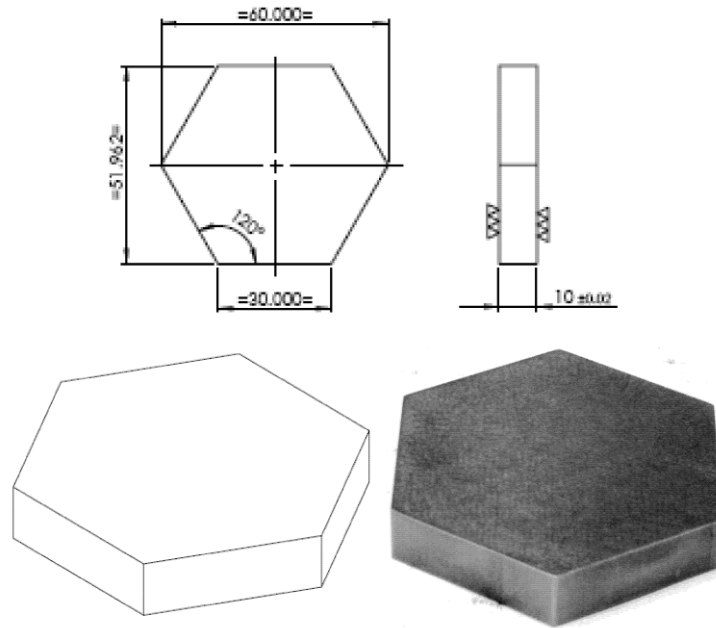


Figure 7.10 Hexagon punch plate

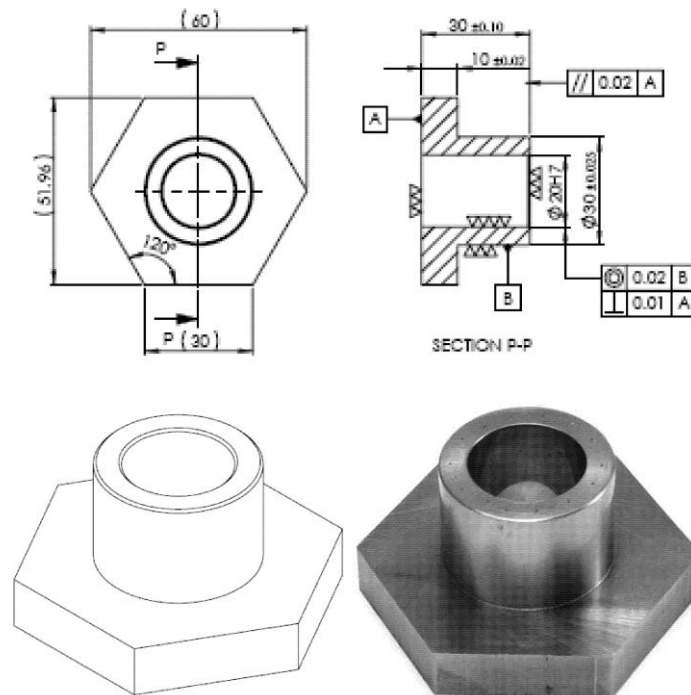


Figure 7.11 Hexagon backward extrusions die

Experiments are conducted on universal testing machine (INSTRON[®] 6000KN). To avoid rate affect the movement of the punch is being adjusted to approximately 1 mm per minute. Experiments were conducted for all reductions and for both forward and forward-backward extrusion-forging process. Figure 7.12-7.13 gives the output products photography for different percentage reduction in area.

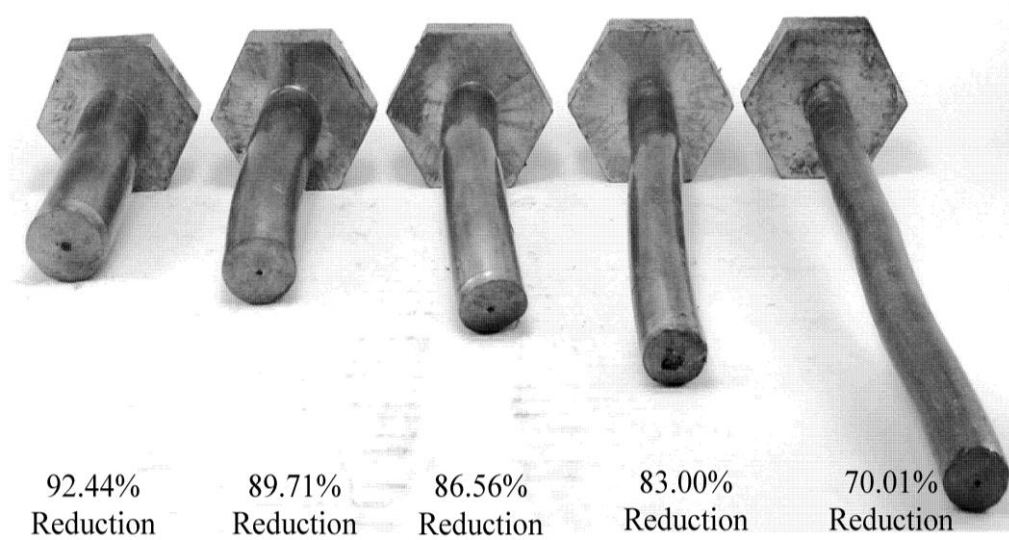


Figure 7.12 Extruded forward extrusion-forging triangular head shaped product

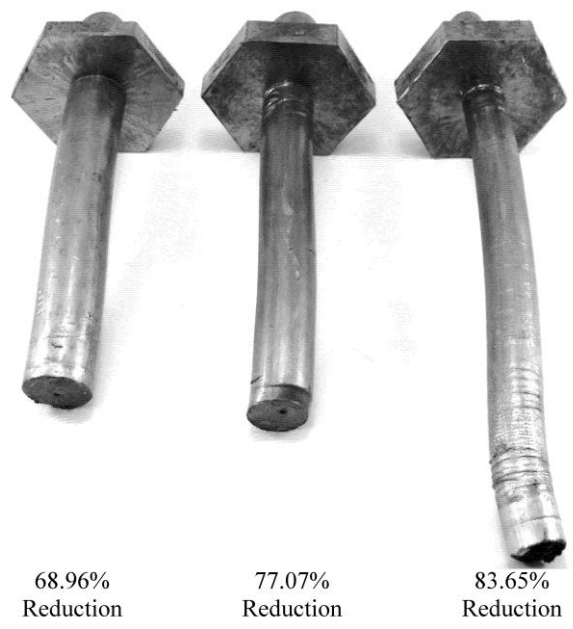


Figure 7.13 Extruded forward-backward extrusion-forging hexagon head shaped product

7.3.1 Summary

Experiments are carried out for forward extrusion-forging process. Five different area reduction dies (92.44%, 89.71%, 86.56%, 83.00% and 79.01% reduction) are used for forward extrusion-forging. Figure 7.14 represent the variation of punch load with ram movement.

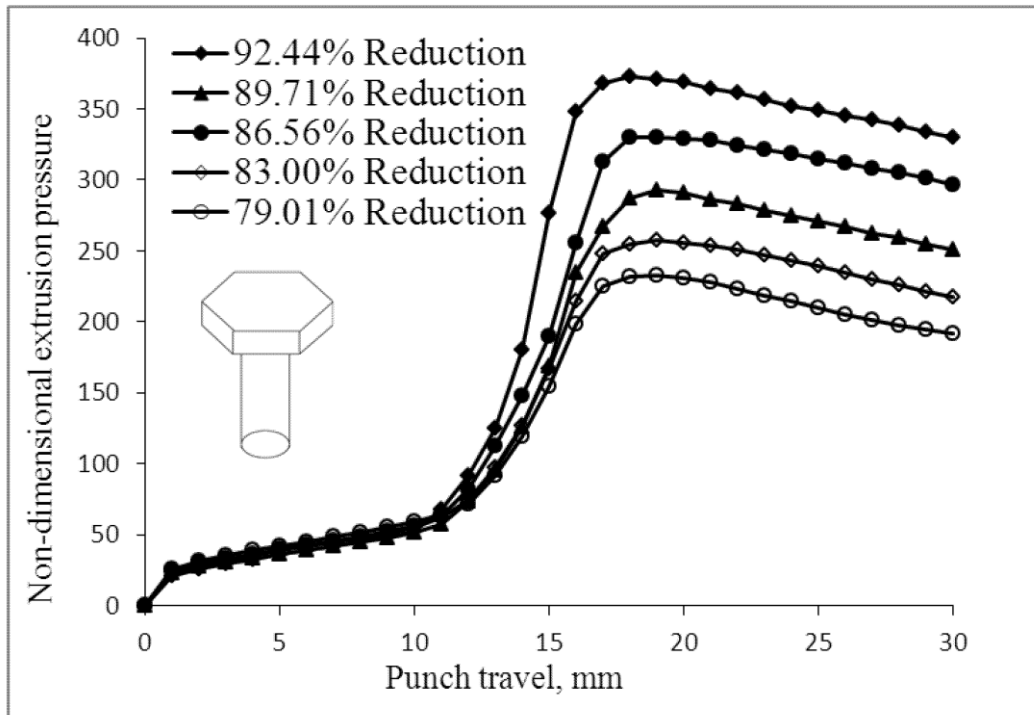


Figure 7.14 Variation of punch load with punch travel of experimental analysis

The load corresponding to the peak load, where steady state extrusion starts, considered as the extrusion load and is tabulated in the Table 7.1. This table provides the value of the mean extrusion pressure P_{av} , the value of the uniaxial yield stress in compression σ_0 , and the non-dimensional mean extrusion pressure P_{av}/σ_0 . Theoretical value of P_{av}/σ_0 computed with the help of proposed SERR technique, are also provided in this table for comparison.

Table 7.1 Computation of non-dimensional average extrusion pressure for forward extrusion-forging process

% Reduction	Extrusion load(kN)	P_{av} MPa	σ_0 MPa	P_{ave}/σ_0 (Experiment)	P_{ave}/σ_0 (Theoretical)
92.44	368.75	157.70	23.377	6.746	6.850
89.71	324.43	138.75	23.418	5.925	6.081
86.56	287.02	122.75	23.457	5.233	5.377
83.00	254.47	108.83	23.496	4.632	4.706
79.01	219.97	94.07	23.534	3.997	4.200

Figure 7.15 shows the complete process at different punch movement, for forward extrusion-forging process, for both FEM simulations and experiment at 86.56% area reduction and at particular intervals of punch movement. It explains that combined extrusion-forging process takes place till the die cavity is completely filled. Then only pure extrusion process takes place.

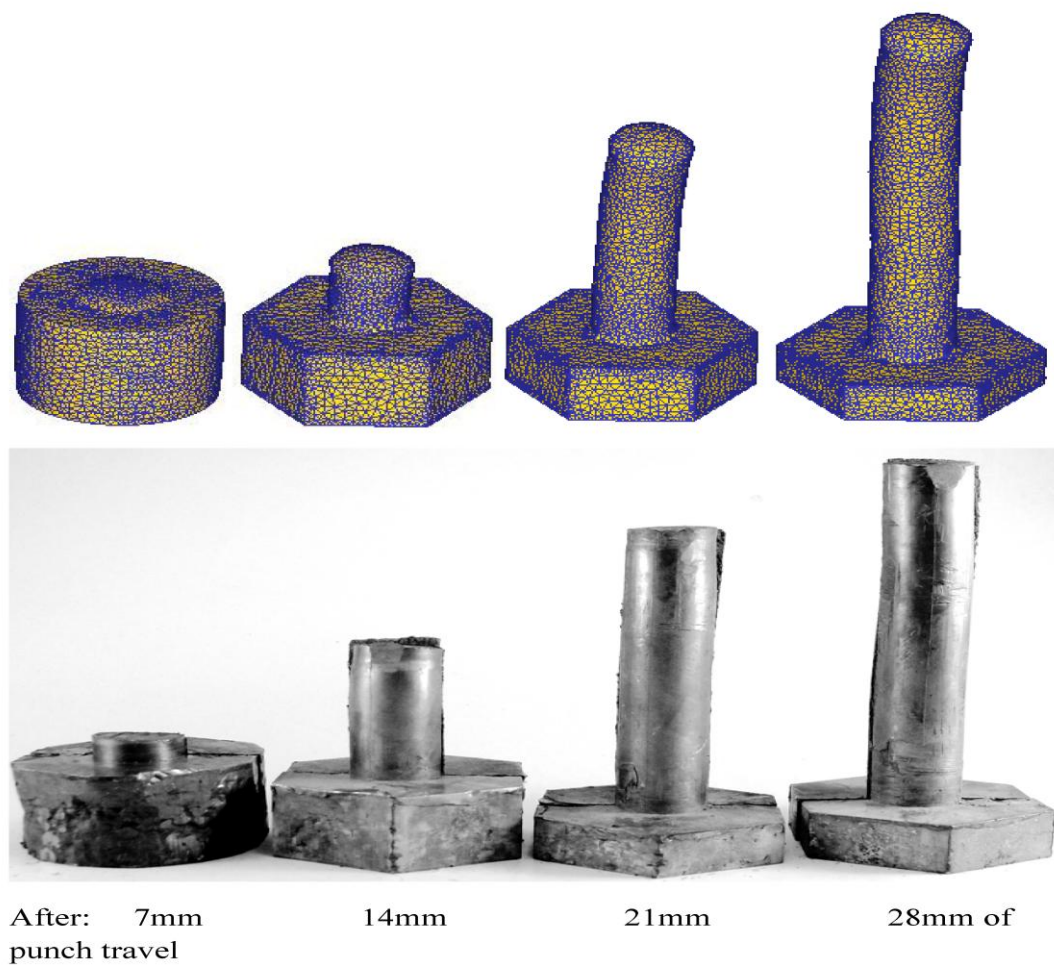


Figure 7.15 Die filling at different punch movement

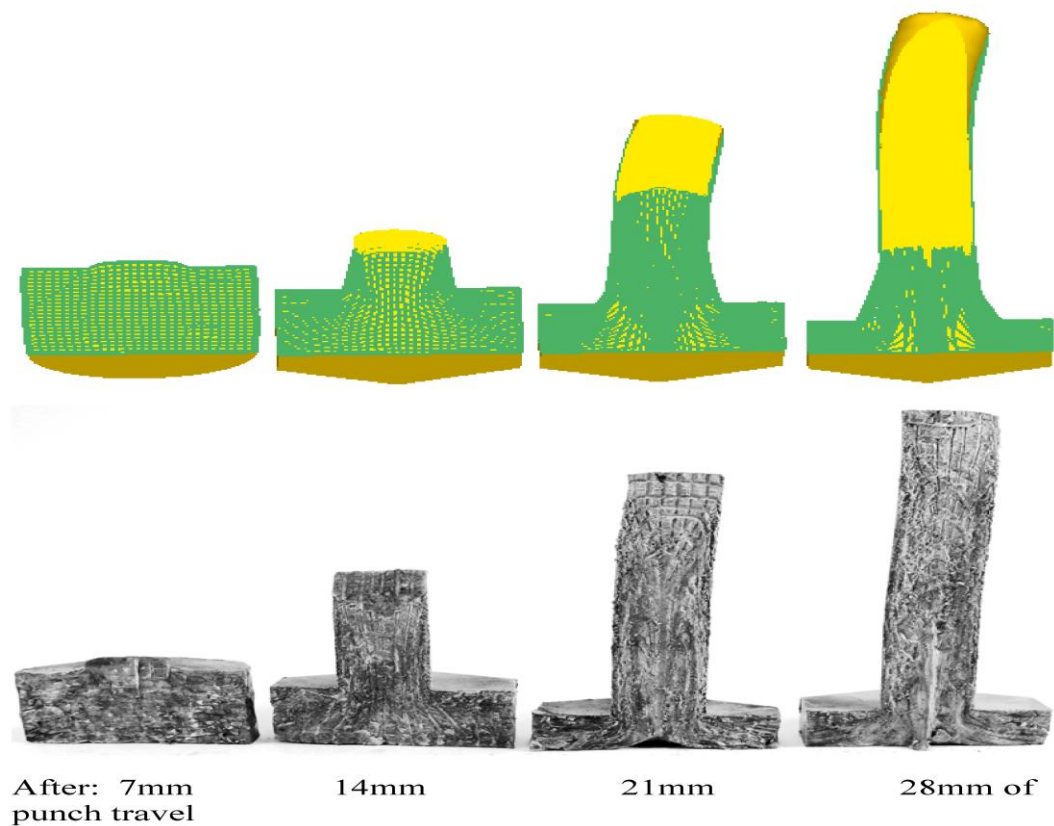


Figure 7.16 Flow pattern at different punch movement

As an illustration,

Figure 7.16 shows the photograph of the flow pattern for a 76.71% area reduction of forward extrusion-forging process at different punch movement for both in FEM and experimental. The grid lines distortion indicates that the process utilizes the maximum amount of redundant work to create flanges of the hexagon.

Experiments are carried out for forward-backward extrusion-forging process. Three different area reduction dies (88.65%, 77.07%, 68.96%, reduction) are used for forward-backward extrusion-forging. Figure 7.17 represent the punch load versus punch movement. Table 7.2 provides the non-dimensional extrusion pressure for theoretical and experimental analysis.

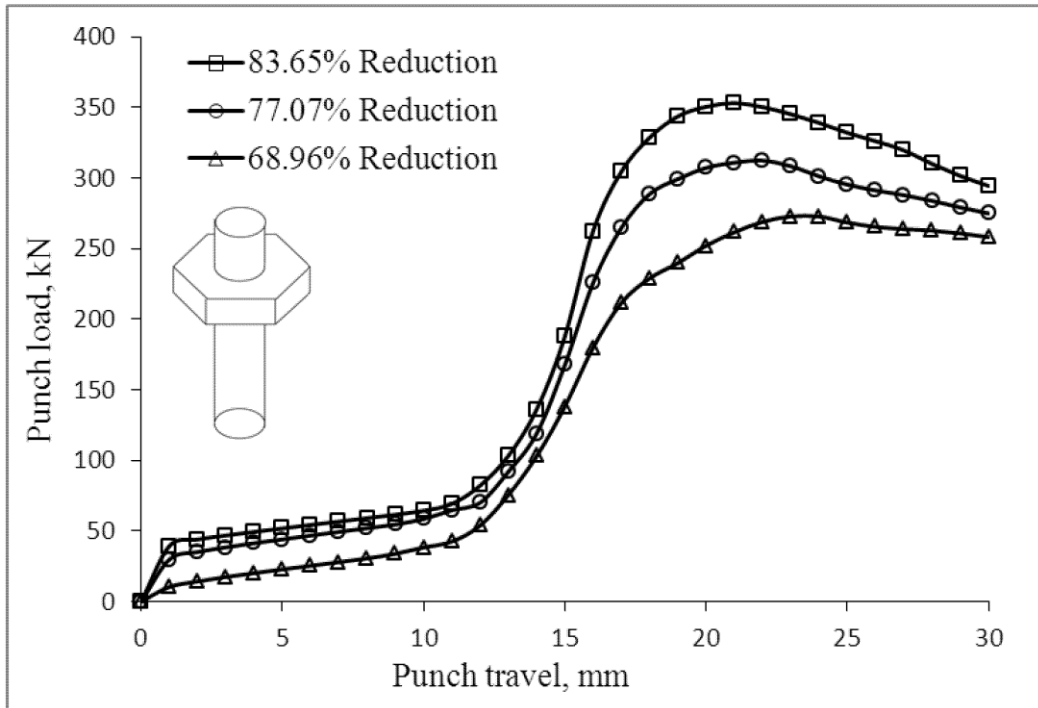


Figure 7.17 Variation of punch load with punch travel of experimental analysis

Table 7.2 Computation of non-dimensional average extrusion pressure for forward-backward extrusion-forging process

% Reduction	Extrusion load(kN)	P_{av} MPa	σ_o MPa	P_{av}/σ_o (Experiment)	P_{av}/σ_o (Theoretical)
83.65	333.04	154.07	23.489	6.56	6.78
77.07	286.37	136.51	23.551	5.80	5.93
68.96	242.82	119.96	23.616	5.08	5.35

7.4 Comparison of Results and Discussion

7.4.1 Forward extrusion-forging process

Figure 7.18 gives the comparison of P_{av}/σ_0 for upper bound analysis, experimental analysis and finite element analysis with considering friction. The percentage variations of the three formulations are summarized in Table 7.3. The difference between FEM and UBA are within 8.0%. Whereas the difference between UBA and EXPT. 3%. The findings entrust the proposed model.

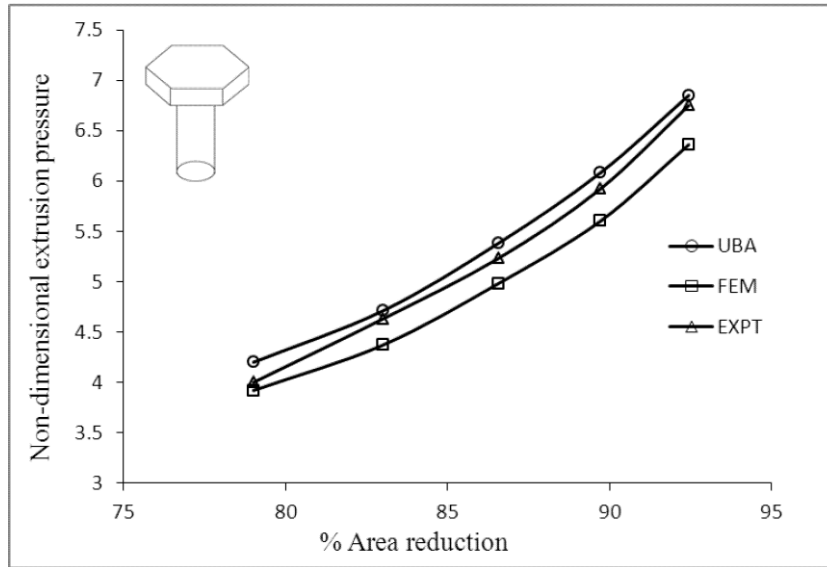


Figure 7.18 Comparison of non-dimensional extrusion pressure without friction for forward extrusion-forging process

Table 7.3 Comparison of non-dimensional extrusion pressure without friction for forward extrusion-forging process

% Reduction	% Difference UBA~FEM	% Difference UBA~EXPT
92.44	7.21	1.52
89.71	7.87	2.57
86.56	7.35	2.68
83.00	7.12	1.58
79.01	6.78	4.82

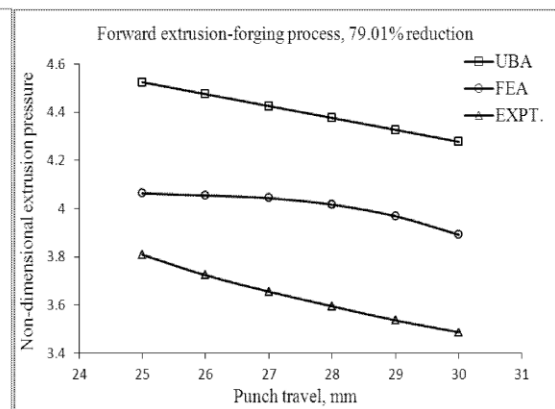
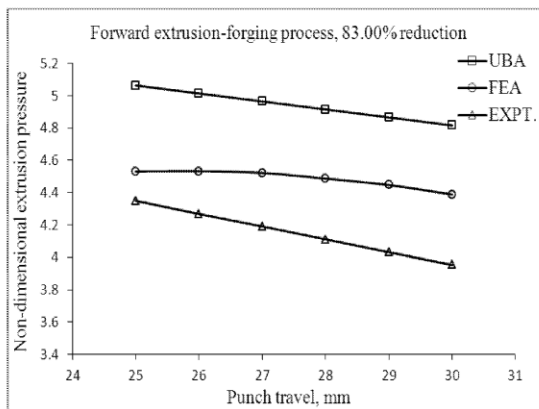
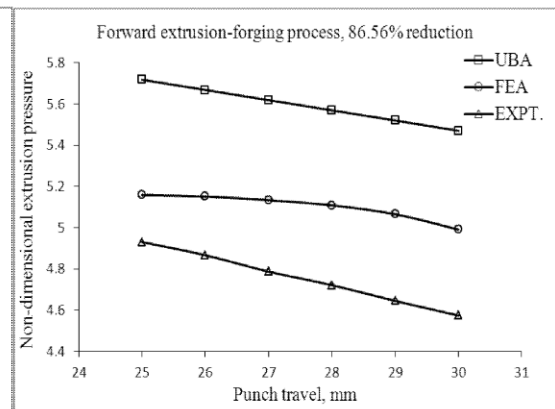
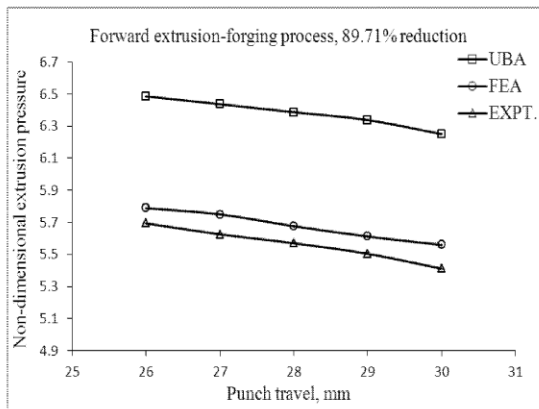
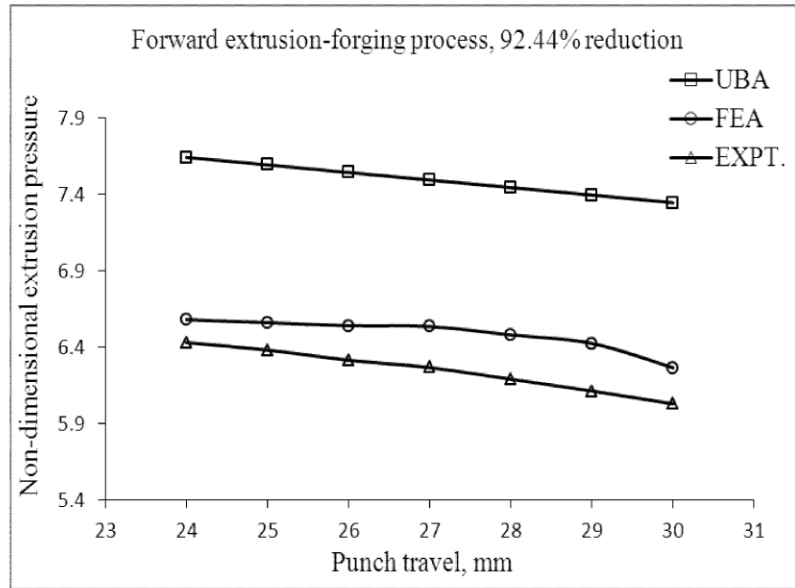


Figure 7.19 Variation of non-dimensional extrusion pressure with friction for forward extrusion forging process for different reduction

Considering friction for upper bound analysis the variation of P_{av}/σ_0 with punch travel for FEM, UBA and Expt. analysis is shown in Figure 7.19. From figure it is observed that as punch travel forward friction reduces, decreases the non-dimensional extrusion pressure.

7.4.2 Forward-backward extrusion-forging process

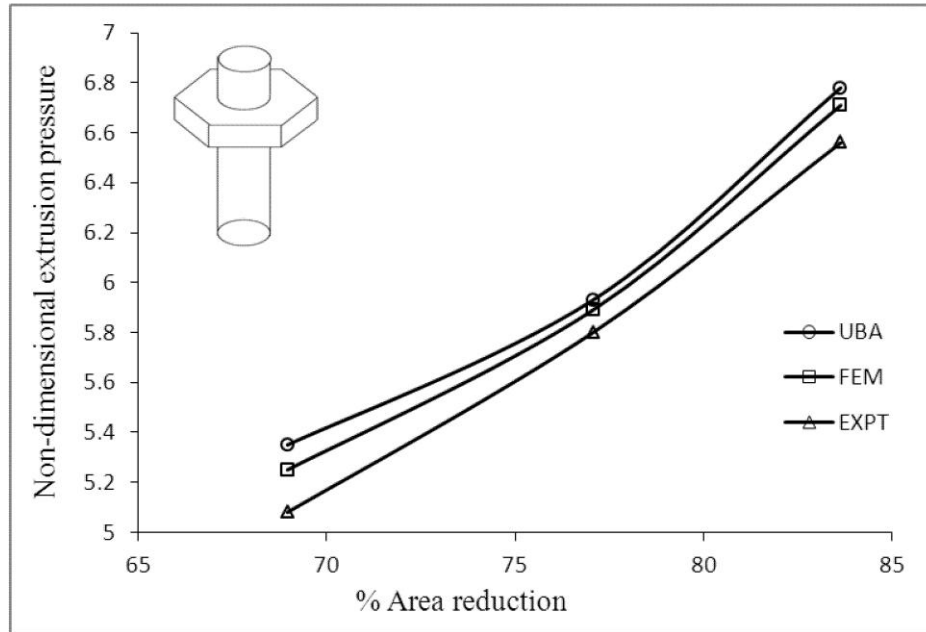


Figure 7.20 Comparison of non-dimensional extrusion pressure without friction for forward-backward extrusion-forging process

Figure 7.20 gives the comparison of P_{av}/σ_0 for upper bound analysis, experimental analysis and finite element analysis. The percentage variations of the three formulations are summarized in Table 7.4. The difference between UBA and FEM are within 2.0%. Whereas the difference between UBA and EXPT. 4%. The findings also entrust the proposed model for the forward-backward extrusion-forging process.

Table 7.4 Comparison of non-dimensional average extrusion pressure without friction for forward-backward extrusion-forging process

% Reduction	% Difference UBA~FEM	% Difference UBA~EXPT
83.65	0.98	3.27
77.07	0.58	2.22
68.96	1.86	4.99

7.5 Closure

7.5.1 Forward extrusion-forging process

1. The experimental non-dimensional average extrusion pressure P_{av}/σ_o , agrees with the theoretical value computed with the help of proposed SERR technique to within 2% for the range of reduction studied, which, entrust the proposed model.
2. Among the three SERR formulation carries out in this study, three-point formulation gives the lowest upper bound to the extrusion pressure for the section.
3. The obtained variation of punch load with respect to stroke by proposed technique is also well validated with FE analysis and experiment. It is also observed that with increase of reduction variation of FE analysis with experimental results increases marginally. The results obtained by the proposed model well in line with the practical observed situation.
4. The findings ensure that proposed upper-bound analysis using discontinuous velocity field (modified SERR technique) provides a better method of analysis for this type of production process.

7.5.2 Forward-backward extrusion-forging process

1. The experimental non-dimensional average extrusion pressure P_{av}/σ_o , agrees with the theoretical value computed with the help of proposed SERR technique to within 10% for the range of reduction studied. The results ensure the model for the forward-backward combined extrusion-forging process also.
2. Among the six SERR formulation carried out in this study, three-point formulation gives the lowest upper bound to the extrusion pressure for the extrude section. The results point out the requirement of minimum path to decrease the redundancy.
3. The obtained variation of punch load with respect to stroke by proposed technique is also well validated with FE analysis and experiment.
4. The experimental flow pattern agrees with the FEM analysis.
5. The proposed upper-bound analysis using discontinuous velocity field (modified SERR technique) provides a better method of analysis for this type of section extrusion-forging.

3D Analysis of Combined Extrusion-Forging Process for Round Gear-Round Sections

I. THEORETICAL ANALYSIS

8.1 Introduction (Theoretical Analysis)

Spur gears are most commonly used machine elements in engineering industries. Spur gears can be manufactured either by cutting and then assembling with shaft or by forming process with integrated shaft. Forming gear with shaft has an advantage of greater utilization of raw material and high productivity, less failure, etc. rate over conventional method. The present chapter provides the upper bound solutions for extrusion-forging of gear like sections head with circular shaft through the square dies from round section billets. Analyses are made for both forward and forward-backward extrusion-forging process for different percentage area reductions and also for the different number of teeth. Figure 8.1 shows the dead-metal zones proposed in such a manner that a deformation cavity is formed in which the gears tooth section of the billet gradually forms into the round section of the product. The dead metal zones have been assumed to cover the die faces, and the upper bound loads have been computed using discontinuous velocity fields. The discontinuous velocity fields have been obtained by discretizing the deformation zone into tetrahedral blocks using the reformulated SERR technique. Spur gears with involutes profile and $14\frac{1}{2}^{\circ}$ pressure angle are considered for the present analysis.

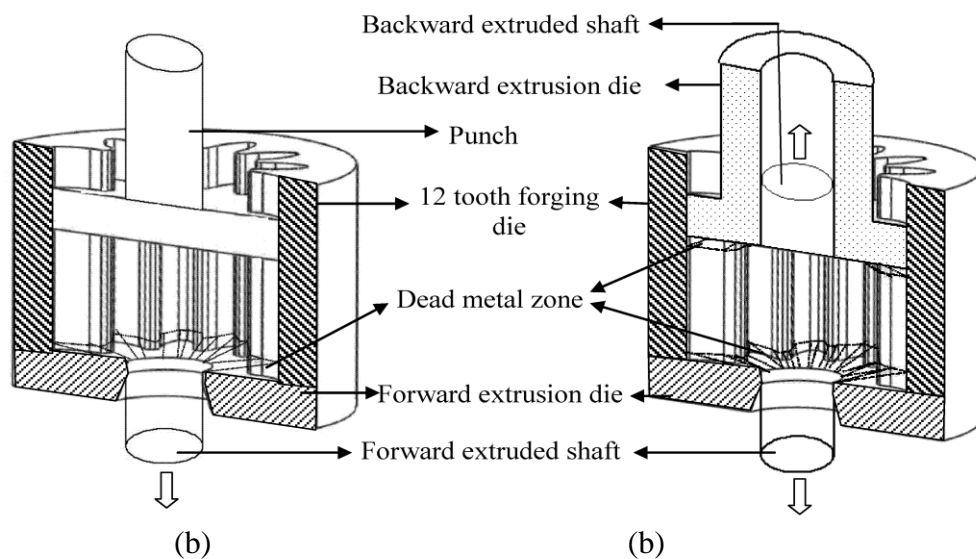


Figure 8.1 Cavity formed by the dead metal zone for 12-tooth spur gear (a) forward and (b) forward-backward extrusion-forging process

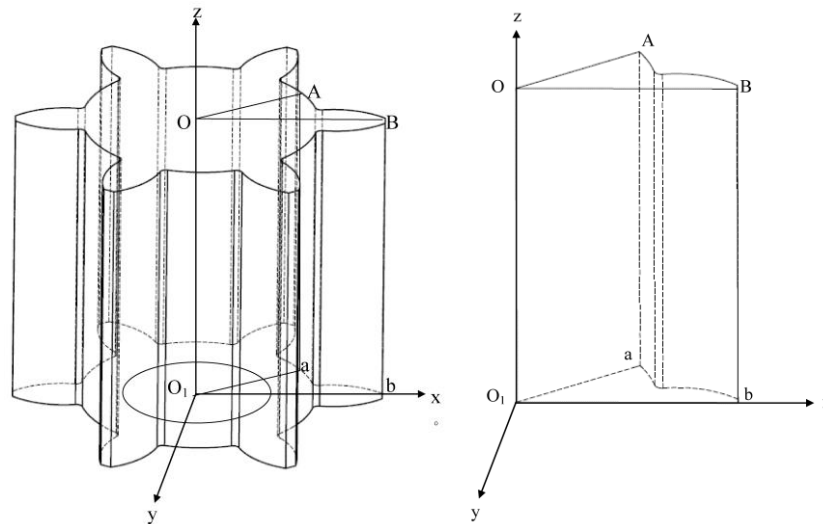


Figure 8.2 Domain of interest A-O-B-O₁-a-b (one twelfth of zone of deformation)

8.2 SERR Method of Analysis

8.2.1 Forward extrusion-forging process

In the present analysis, the circular product (shaft) outlet has been approximated to a regular polygon of 32 sides. The spur gear (with involutes profile and $14\frac{1}{2}^{\circ}$ pressure angle) outer profile of 4-tooth into 80 sides, 6-tooth into 120 sides, 8-tooth into 160 sides and 12-tooth into 240 sides approximating polygon are considered (as there is a negligible change of final computed values by further increasing the number of sides of approximating polygon). The dead metal zones are proposed in such a manner so that a deformation cavity is formed in which the gear section of the billet gradually forms into the circular sections of the product. It is appropriate to mention here that the dead metal zones are a part of the proposed velocity field (being zones of zero velocities), and the upper bound theorem admits any velocity fields as long as it is kinematically admissible. The cavity formed by the dead metal zones, called the domain of interest hereafter (Figure 8.2 as an illustration), for one-eighth of the deformation geometry of 4-tooth spur gear section (because of its symmetry about four planes with respect to billet cross-section). Analyses are also made for six, eight, twelve tooth gear profile for forward extrusion with circular shaft. The domains of interest hereafter are one twelfth, one sixteenth and one twenty-fourth of the deformation geometry of six, eight and twelve tooth gear profile respectively. The subzones of deformation are delineated in the domain of interest by taking suitably located floating points. Three formulations are considered, which acknowledge one, two and three floating points

respectively. For single floating point formulation, an arbitrary point is taken on the extrusion axis. For double point formulation, two floating points are taken in the domain of interest, one on the extrusion axis as before and the second on the plane of symmetry at an arbitrary position. Finally, the triple-point formulation, three floating points are taken, one on the extrusion axis, the second on the plane of symmetry and the third in an arbitrary position in the domain of interest. Figure 8.3 (point 20 is the floating point), Figure 8.4 (point 20 and 21 are the two floating point) and Figure 8.5 (point 20, 21 and 23 are the three floating point) refer to the single, double and triple floating point formulation respectively.

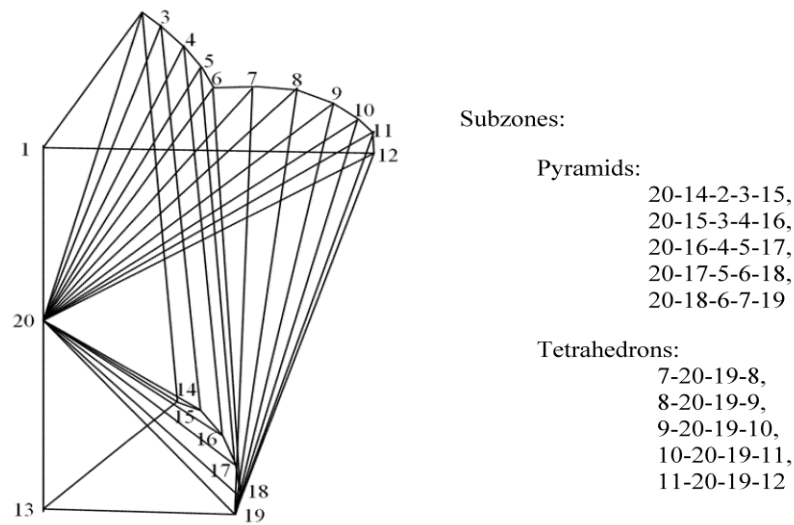


Figure 8.3 Deformation zone with single-point formulation

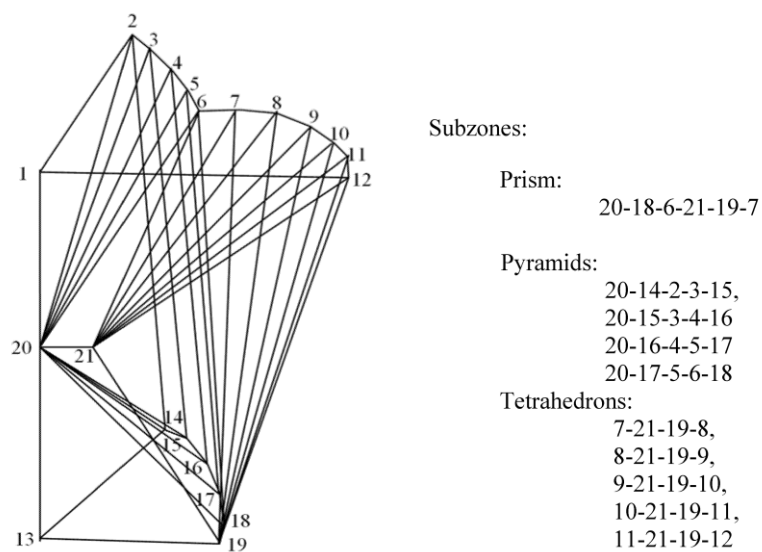
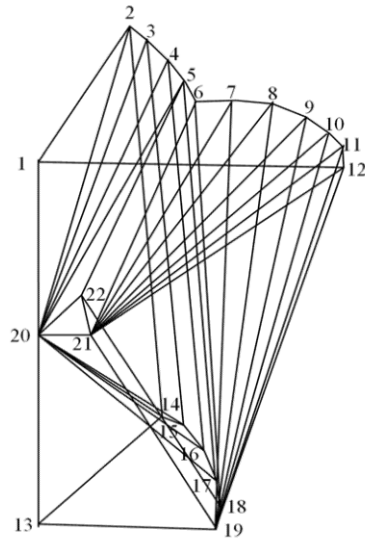


Figure 8.4 Deformation zone with double-point formulation



Subzones:

Prism:

20-17-5-22-18-6,
22-18-6-21-19-7

Pyramids:

20-14-2-3-15,
20-15-3-4-16,
20-16-4-5-17

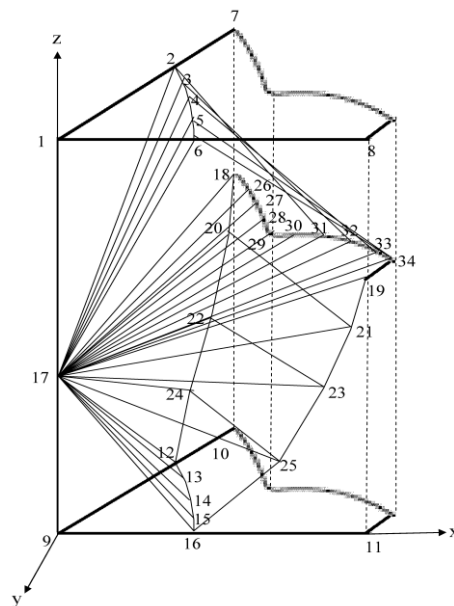
Tetrahedrons:

7-21-19-8,
8-21-19-9,
9-21-19-10,
10-21-19-11,
11-21-19-12

Figure 8.5 Deformation zone with triple-point formulation

8.2.2 Forward-backward extrusion-forging process

The discretization of the forward-backward extrusion-forging process for four, six, eight, twelve tooth spur gear forms with circular shaft are proposed as explained in detail in chapter 4. Six floating formulations (which acknowledge one, three, five, seven, nine and eleven number of floating points) for forward-backward extrusion-forging are considered. As an illustration deformation zone of 12-tooth gear (one twenty-fourth subzone) with nine floating point formulation is shown in Figure 8.6.



Subzones:

Tetrahedrons: 18-17-2-26
26-17-2-27
27-17-2-28
28-17-2-29
29-17-2-30
30-17-2-31

Pyramids: 17-2-31-32-3
17-3-32-33-4
17-4-33-34-5
17-34-5-6-19

Tetrahedrons: 18-17-20-26
26-17-20-27
27-17-20-28
28-17-20-29
29-17-20-30
30-17-20-31
31-17-20-32
32-17-20-33
33-17-20-34

Pyramids: 17-20-34-19-21
17-22-20-21-23
17-24-22-23-25
17-12-24-25-13

Tetrahedrons: 13-17-25-14
14-17-25-15
15-17-25-16

Figure 8.6 Deformation zone of 12-tooth gear (one twenty-fourth subzone) with nine floating point formulation

8.3 Computation

A comprehensive computational model using FORTRAN code is developed for forward and forward-backward extrusion-forging process with and without considering friction by incorporating all special features of the gear. Three formulations for forward extrusion-forging process and six formulations for forward-backward extrusion-forging process is considered.

8.4 Summary

8.4.1 Forward extrusion-forging process

Computations for all floating point formulations and for all teeth, gears are carried out and the optimal configuration is considered. Table 8.1 summarizes the zone of interest into different subzones.

Figure 8.7 gives the comparison of the computed results of the three formulations for their respective optimal configurations. It is obvious from the Figure 8.7 that the single-point formulation gives the best results for all the cases Therefore, this formulation is used for further computation and comparison.

Table 8.1 Summary of discretization schemes for forward extrusion-forging process

Item	Single floating point formulation	Double floating point formulation	Triple floating point formulation
Subzones	5 Pyramids, 5 Tetrahedrons	1 Prism 4 Pyramids, 5 Tetrahedrons	2 Prisms, 3 Pyramids, 5 Tetrahedrons
Total No. of SERR blocks	15	16	17
No. of discretization schemes	$2 \times 2 \times 2 \times 2 \times 2$ =32	$6 \times 2 \times 2 \times 2 \times 2$ =96	$6 \times 6 \times 2 \times 2 \times 2$ =288
Total No. of triangular faces	46	49	52
No. of Velocity Component	15x3=45for SERR + 1 at exit velocity, total=46	16 x 3=48 for SERR + 1 at exit velocity, total=49	17x 3=51 for SERR + 1 at exit velocity, total=52
No of optimizing parameters	3	5	8

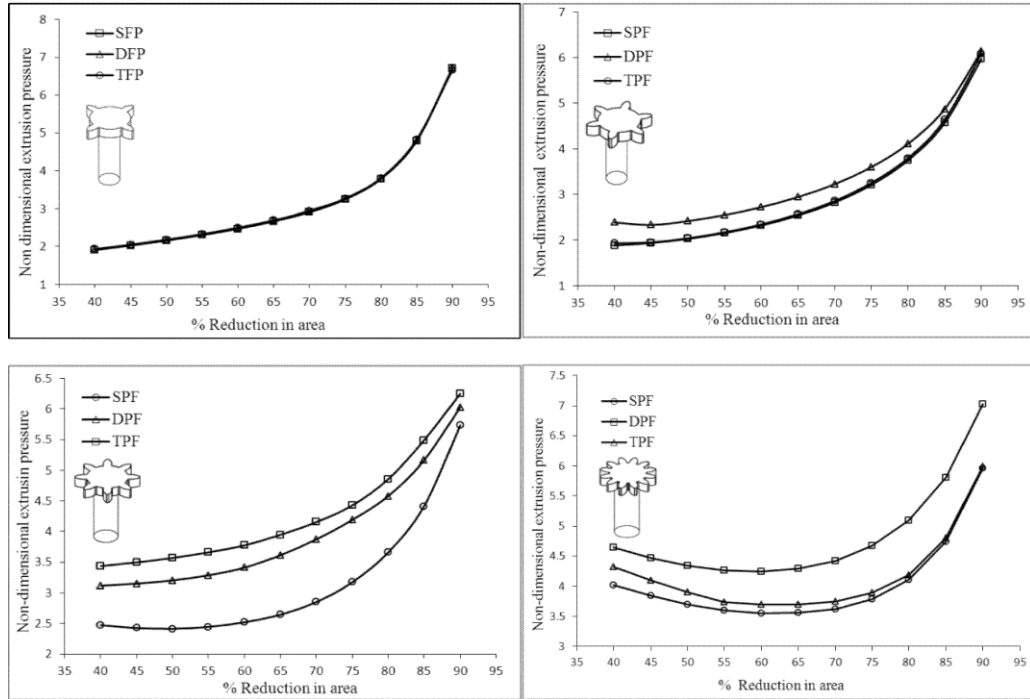


Figure 8.7 Comparison of non-dimensional extrusion pressure with percentage area reduction for different tooth gear

8.4.2 Forward-backward extrusion-forging process

Figure 8.8 summarize the optimal non-dimensional extrusion pressure for four, six, eight and twelve tooth gear profile. Three-floating point formulation in all the cases gives the optimal result for all the gear shape profiles. Therefore, this formulation only is used for computation and comparison.

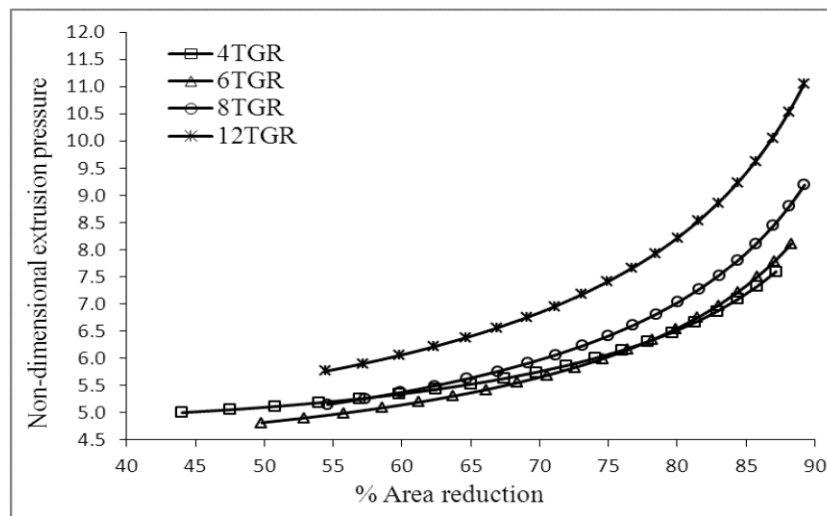


Figure 8.8 Comparison of optimal results for different tooth gear

II. FINITE ELEMENT ANALYSIS

8.5 Introduction (Finite Element Analysis)

Simulations of forward and forward-backward extrusion-forging of four, six, eight and twelve tooth gear (spur gears with involutes profile and $14\frac{1}{2}^{\circ}$ pressure angle) with circular shaft from cylindrical billet are carried out using DEFORM[®]-3D code. Analysis was made for forward and forward-backward extrusion-forging process. The detail formulations are presented in chapter 4. A die-punch set of different reduction area is designed according to the specification and import the STL file for analysis purpose. Simulations are carried out with initial 25000 mesh elements.

8.6 Summary

8.6.1 Forward Extrusion-forging process

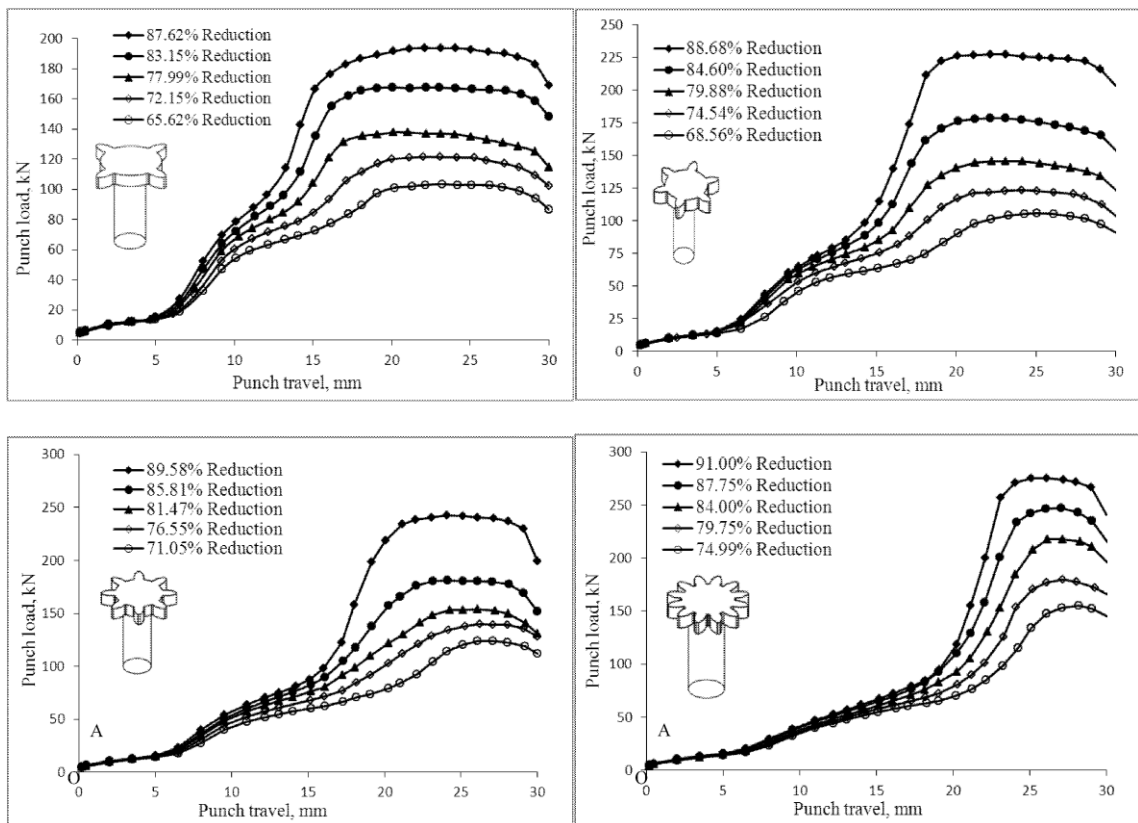


Figure 8.9 Variation of punch load with punch travel for different tooth gears

The process parameters used in this simulation is 35 mm diameter and 40mm length billet, simulation run at ambient conditions, ram speed 1mm/min, friction factor 0.23 and flow stress of chosen material is 0.0233kN/mm^2 . Five different area

reductions for forward extrusion-forging of four, six, eight and twelve tooth gear are used in this series of analysis. The dimension of dies and punch plate used for simulation are same as that of experimental sets. Figure 8.9 gives comparison of punch load with punch movement for different percentage area reductions of and different number of teeth.

From the above graph it is observed that as the number of tooth increases

- i. The steady state extrusion load increases with increasing.
- ii. Die filling time (i.e., punch travel) increases.
- iii. As the percentage reduction increases the steady state extrusion load increases.

8.6.1.1 Mean stress and effective strain analysis

Figure 8.10 shows the mean stress distribution and effective strain in terms of solid profile for the reduction of 80.37%; at a ram speed of 1mm/min and ram displacement of 20 mm for forward extrusion-forging process. The positive stress signifies the tensile component of stress.

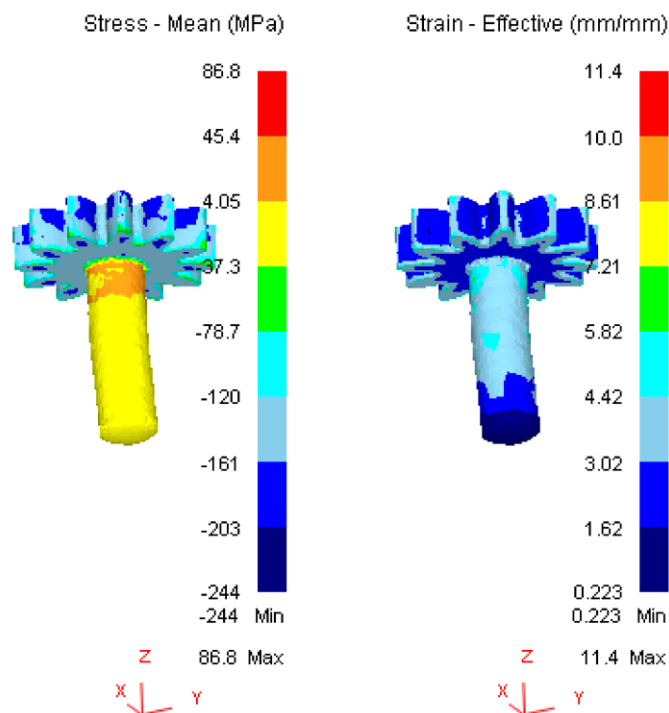


Figure 8.10 Mean stress and effective strain at particular reduction and punch movement for forward extrusion-forging process

8.6.2 Forward backward extrusion-forging process

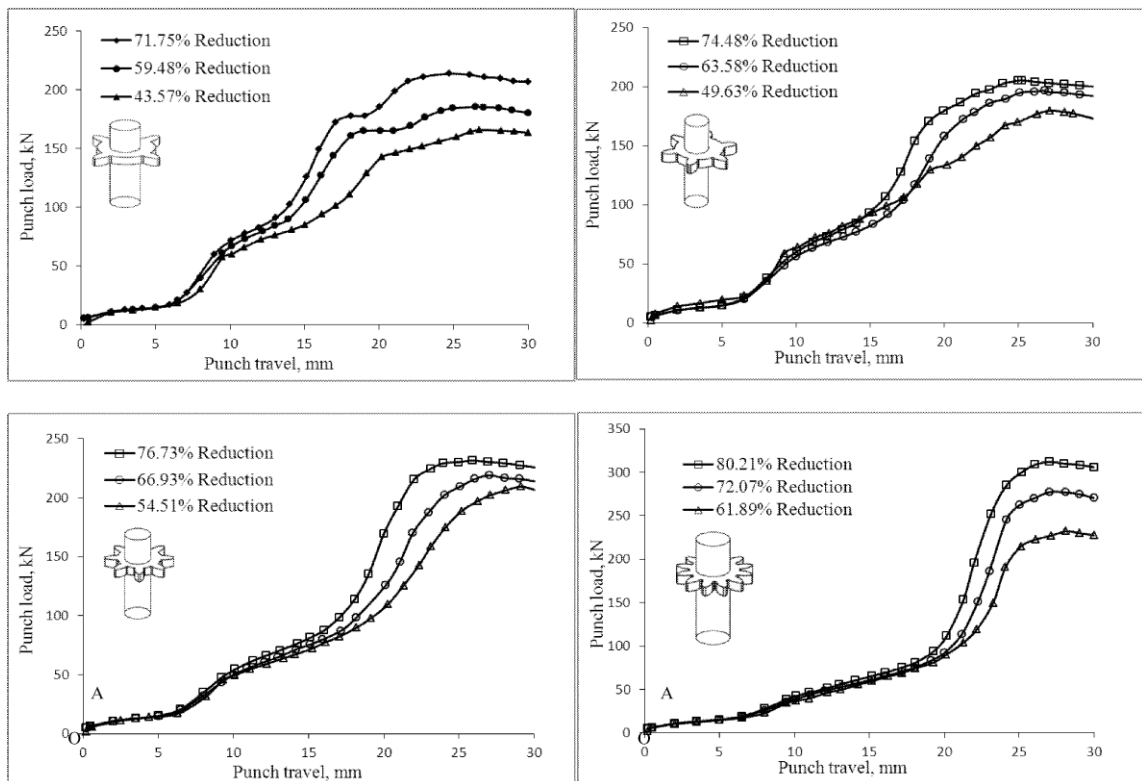


Figure 8.11 Variation of punch load with punch travel of four, six, eight and twelve tooth spur gear fem simulation

Three different area reduction dies for all four, six, eight and twelve tooth gears are used in this series of analysis. The dies and punch plate used for simulation was same as that of experimental sets. Figure 8.11 gives comparison of punch load with punch movement for different percentage area reductions and different tooth gear.

From the above graph it was observed that as the number of tooth increases

- i. The steady state extrusion load increases with increasing.
- ii. Die filling time (i.e., punch travel) increases.
- iii. As the percentage reduction increases the steady state extrusion load increases.

For six teeth forward-backward simulation it was observed that 49.43% reduction simulation gives some erroneous result at initial stage which may be due to some unknown factors.

8.6.2.1 Mean stress and effective strain analysis

Figure 8.12 shows the mean stress distribution and effective strain in terms of solid profile for the reduction of 51.14%, at a ram speed of 1mm/min and ram displacement of 25mm for forward-backward extrusion forging process. The positive stress signifies the tensile component of stress. From the figure it is observed that at the die land the material attain a maximum tensile stress. At the die land the stress is found higher Maximum compressive stresses reaches near die walls. From the figure it is observed that there is a large stress concentration (0.0797 – 0.0341kN/mm²) round the die entrance. The effective strain is large after the extrusion through flat die and gradually decreases.

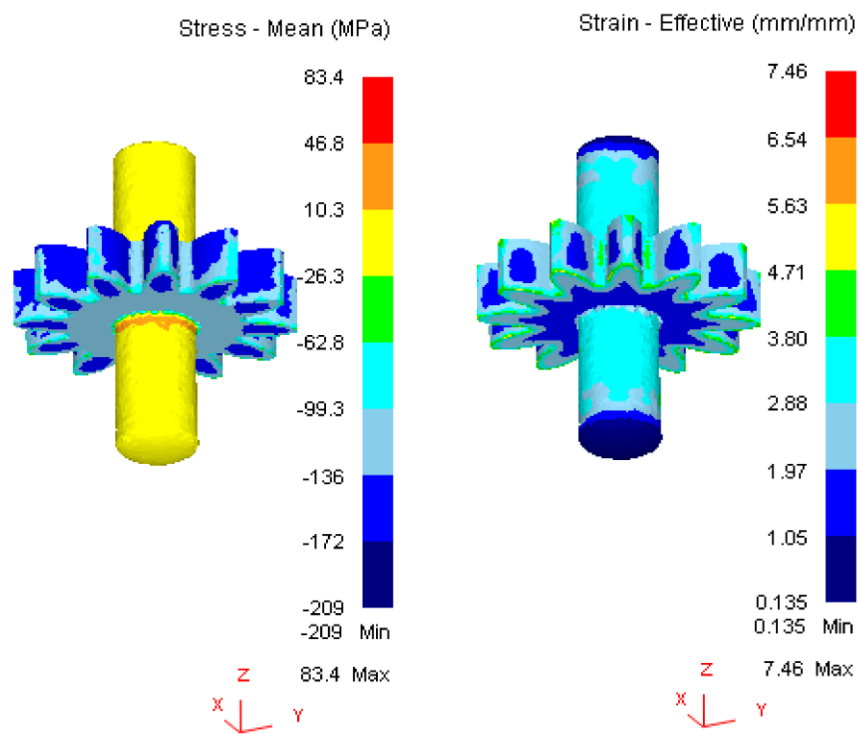


Figure 8.12 Mean stress and effective strain at particular reduction and punch movement for forward-backward extrusion-forging process

III. EXPERIMENTAL ANALYSIS

8.7 Introduction (Experimental Analysis)

Experimental studies are carried out with a view to compare the experimental results with the theoretical ones obtain from proposed method of analysis, and finite element analysis are carried out from commercially available DEFORM[®]-3D software. Experiments are performed on an INSTRON[®] 600KN Universal testing machine for extrusion-forging of round-gear-round sections with square/flat dies. Experiments are done for both forward and forward-backward extrusion-forging process. Commercially available lead is used for experiment. An extrusion-forging setup for laboratory experimentation is designed and fabricated.

8.8 Apparatus

The apparatus, in the main, consists of five parts; namely, the container having a circular chamber, the extruding punch, the forging die holder, extrusion die holder and the supporting block for the assembly. The details about the apparatus are furnished in chapter 4.

8.8.1 Dies

Five sets of forward extrusion die (at different percentage area reduction), and three sets of backward extrusion die (at different percentage area reduction) are employed for experimentation. Spur gears with involutes profile and $14\frac{1}{2}^{\circ}$ pressure angle having four, six, eight and twelve number of teeth are employed for present analysis. The details of the forging die and extrusion dies are presented in Figures 8.13– 8.18.

8.8.2 Billet specification

Rectangular billets of commercially available lead (98% purity) are taken as work material for the above purpose. These are prepared from commercially available 75mm square blocks by casting to approximate size. The specimens then finish to size by lathe machine using kerosene as cutting fluid. Specimens 35mm diameter and 40mm lengths are used for experimental analysis. All specimens before use are annealed in boiling water for a period of two hours.

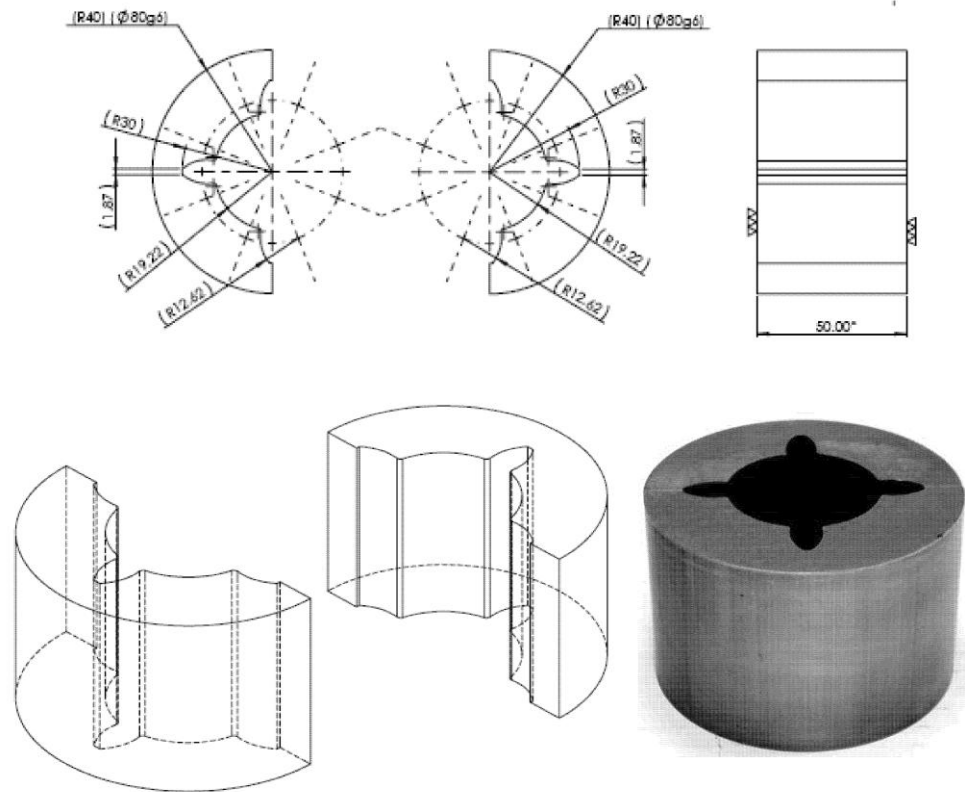


Figure 8.13 4-tooth gear split type forging die

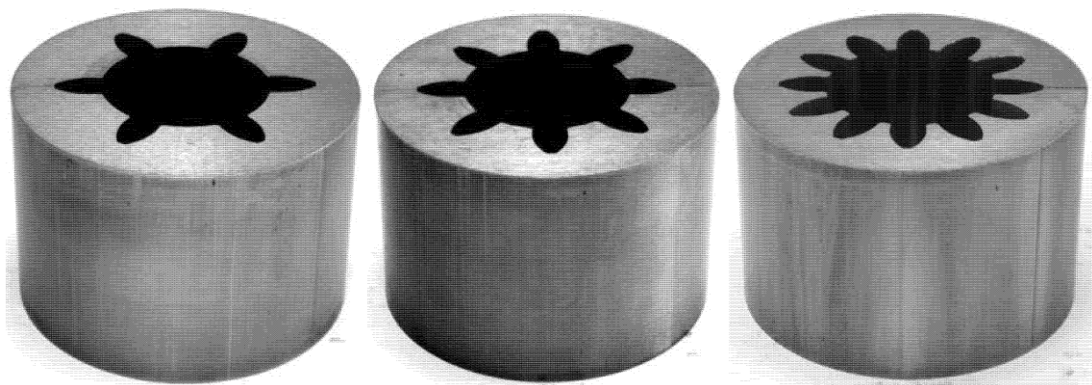


Figure 8.14 6-, 8-, 12- tooth gears forging dies

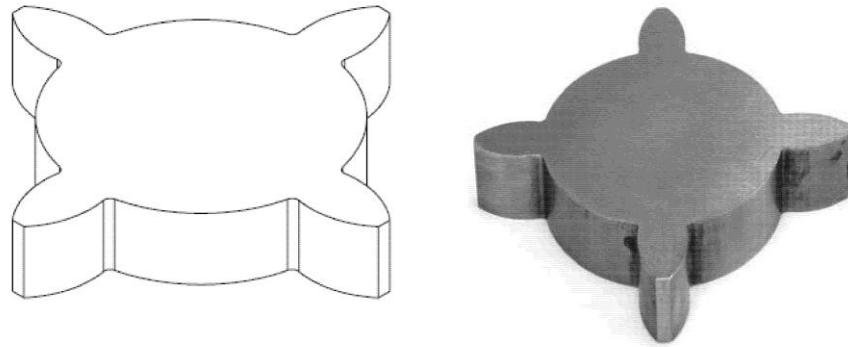
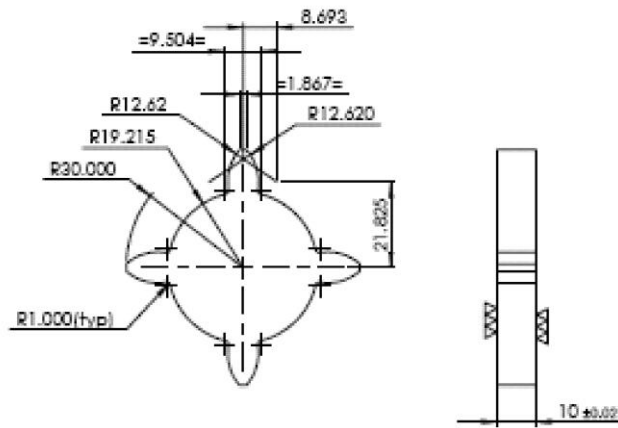


Figure 8.15 4-tooth spur gear punch plate



Figure 8.16 6-, 8-, 12-tooth spur gears punch plate

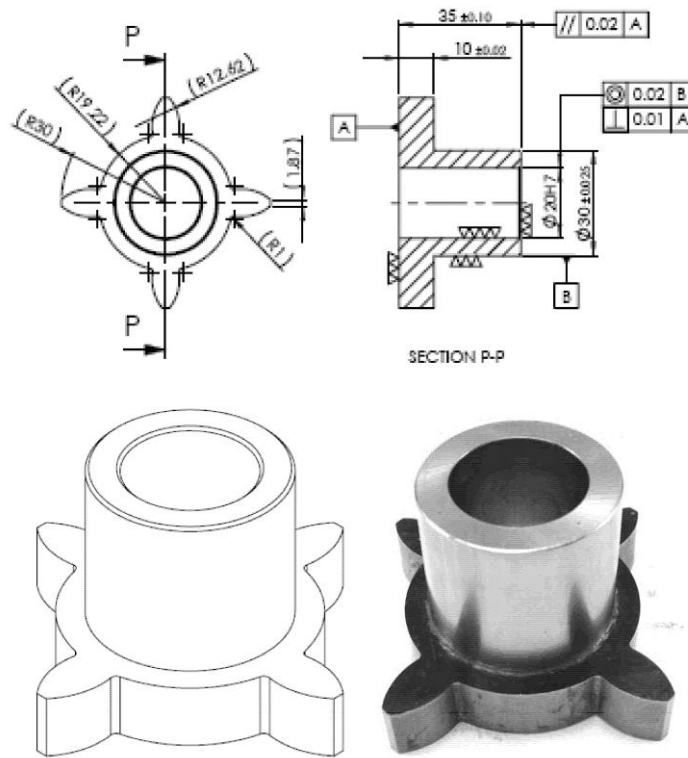


Figure 8.17 4-tooth gear backward extrusions die

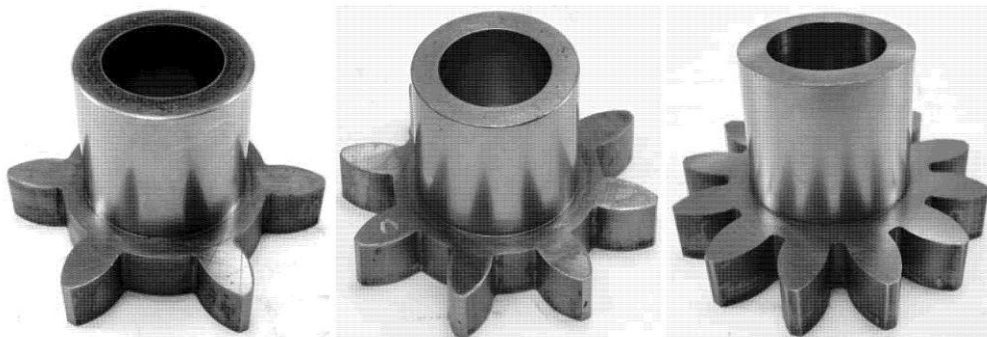


Figure 8.18 6-, 8-, 12-tooth gears backward extrusions dies

8.9 Experimental Procedure

Following the standard procedure (described in section 4.16) experiments are conducted on universal testing machine (INSTRON[®] 6000KN). To avoid rate affect the movement of the punch is being adjusted to approximately 1 mm per minute. Experiments were conducted for all reductions and for both forward and forward-backward extrusion-forging process. Figure 8.19- 8.26 gives the output products photography for different percentage reduction in area, different number of tooth and forward and forward-backward extrusion-forging process.

From the photography, it was observed that 59.48% and 43.57% reductions of four tooth forward-backward gear shape product shaft are curved. This may be due to the mismatch of the center of the cylindrical billet with machine axis, and extrusion die axis. All other products are fairly straight shaft extruded.

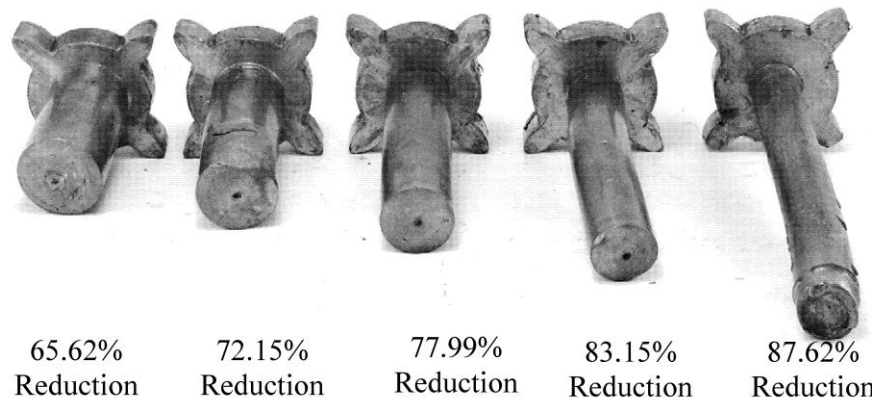


Figure 8.19 Extruded forward extrusion-forging 4-tooth gear head shaped product

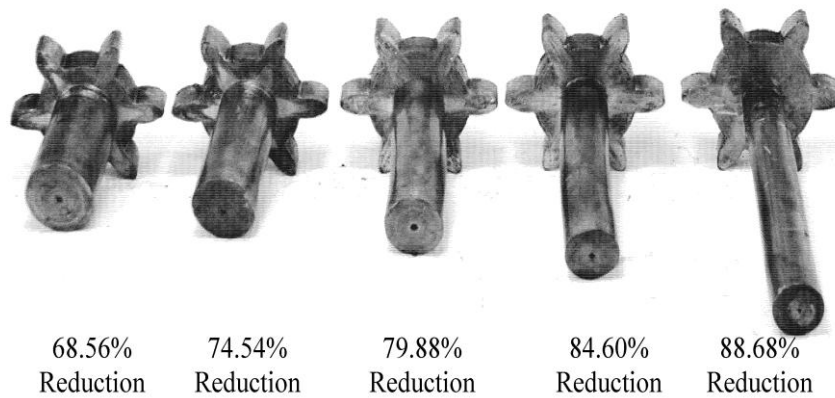


Figure 8.20 Extruded forward extrusion-forging 6-tooth gear head shaped product

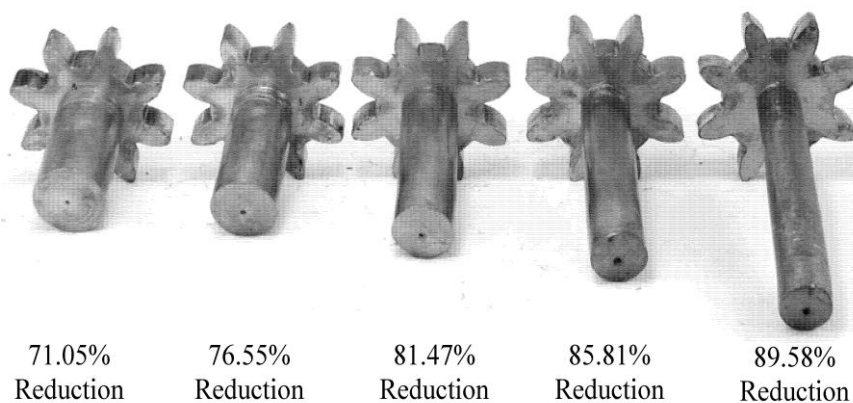


Figure 8.21 Extruded forward extrusion-forging 8-tooth gear head shaped product

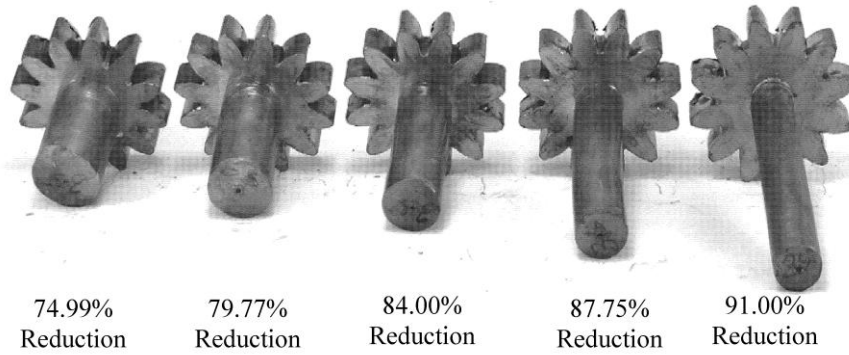


Figure 8.22 Extruded forward extrusion-forging 12-tooth gear head shaped product

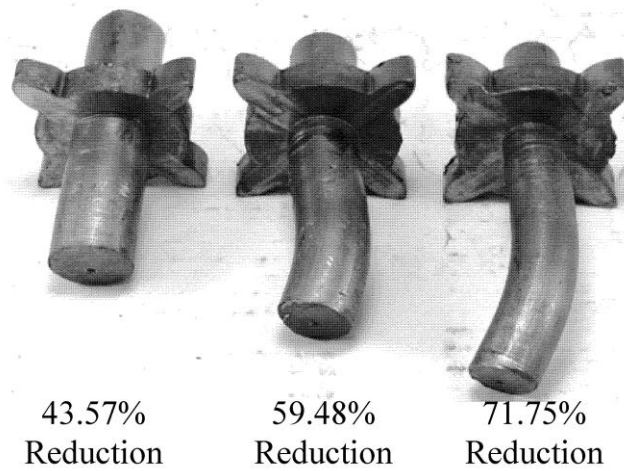


Figure 8.23 Extruded forward-backward extrusion-forging 4-tooth gear head shaped product

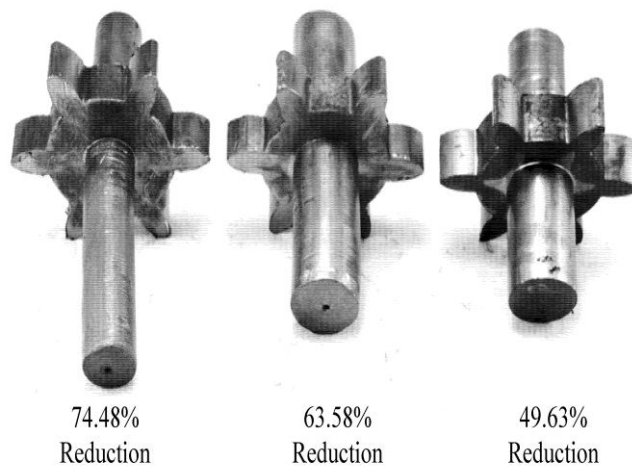


Figure 8.24 Extruded forward-backward extrusion-forging 6-tooth gear head shaped product

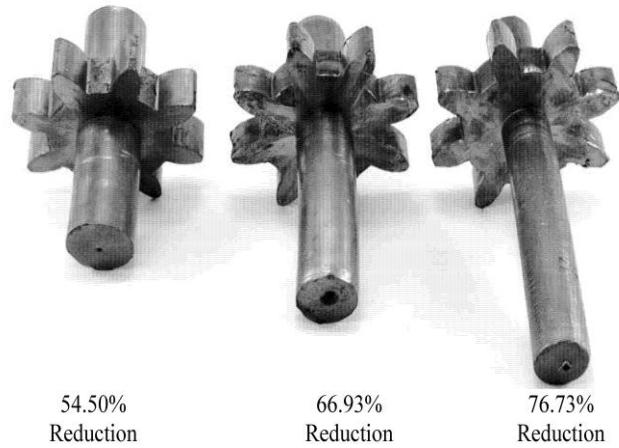


Figure 8.25 Extruded forward-backward extrusion-forging 8-tooth gear head shaped product

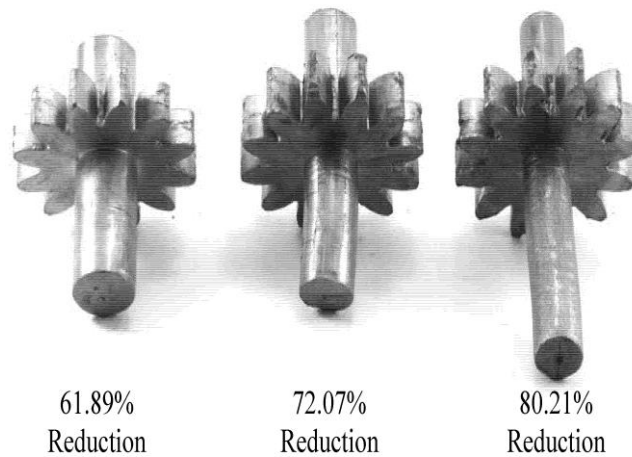


Figure 8.26 Extruded forward-backward extrusion-forging 12-tooth gear head shaped product

8.10 Summary

8.10.1 Forward extrusion-forging process

Experiments are carried out for forward extrusion-forging process of spur gear. Five different percentage area reduction dies, and four different numbers of teeth are used to investigate the process. Figure 8.27 represents the punch load with punch travel. Referring to the above diagram (six tooth gear), it is seen that the whole process consists of five major stages: namely (i) a coining stage in which initial compression (O to A) of the billet takes place. The second stage refers to forging stage (A to B) where the billet forged till it touches the die wall (dedendum circle). In this stage, load increase slowly with respect to punch movement. In the third stage, material starts entering the tooth

cavity (B to C). In this stage, load increase with respect to punch movement. In the fourth stage dies tooth corners are filled up (C to D), where the maximum load reaches. In this stage, there is an increase in load with respect to punch movement followed by a steep rise. There is no fixed distinguish region on the load-moment curve for die filling/corner filling stages. Above all the process simultaneous extrusion, process is accomplished. After the die completely filled, in fifth stage (D to E) the steady-state extrusion process takes place. There is a drop in load in this stage, due to continuous decrease of billet length thereby decreasing the frictional force between billet and extrusion chamber. However, the drop in load from the peak value is found to be minimal, which may be due to adequate lubrication between the billet and the extrusion chamber.

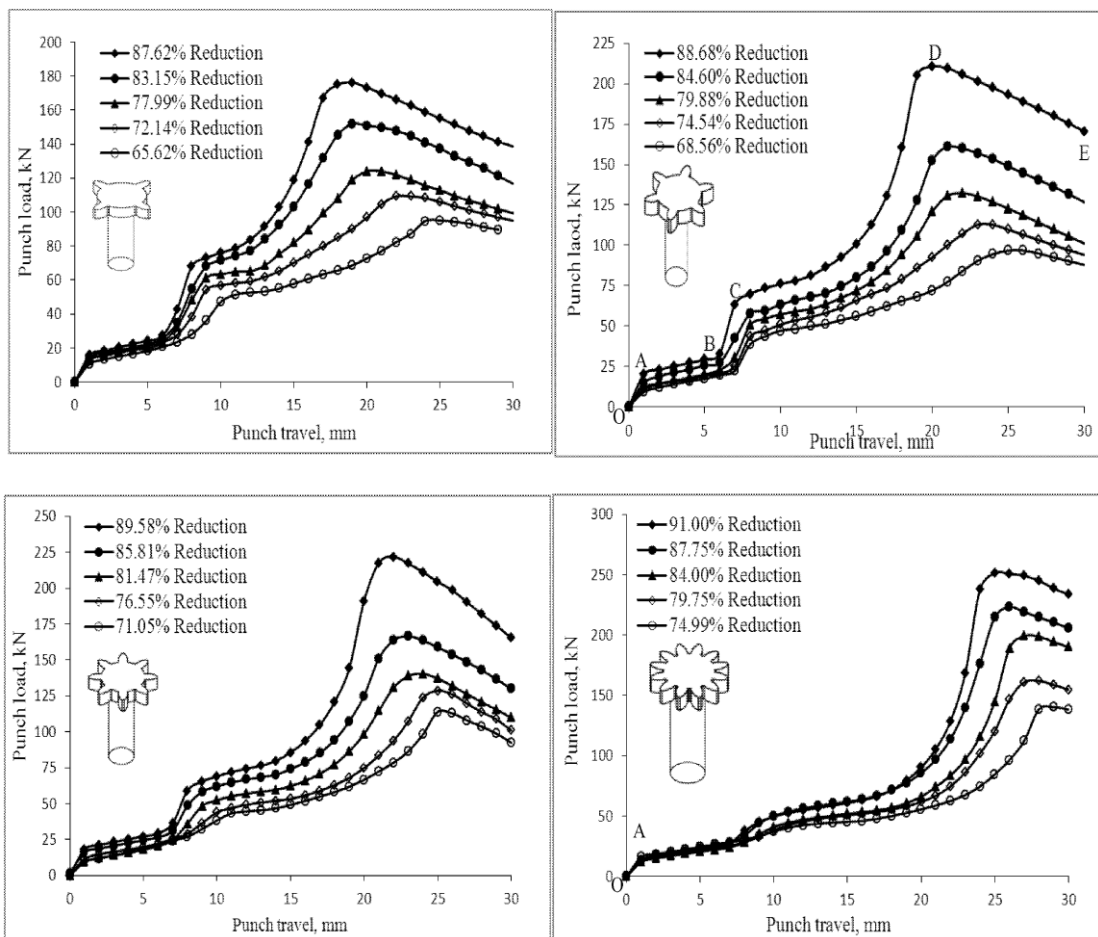


Figure 8.27 Variation of punch load with punch travel of experimental analysis of four, six eight and twelve tooth spur gear

8.10.1.1 Die filling and flow pattern

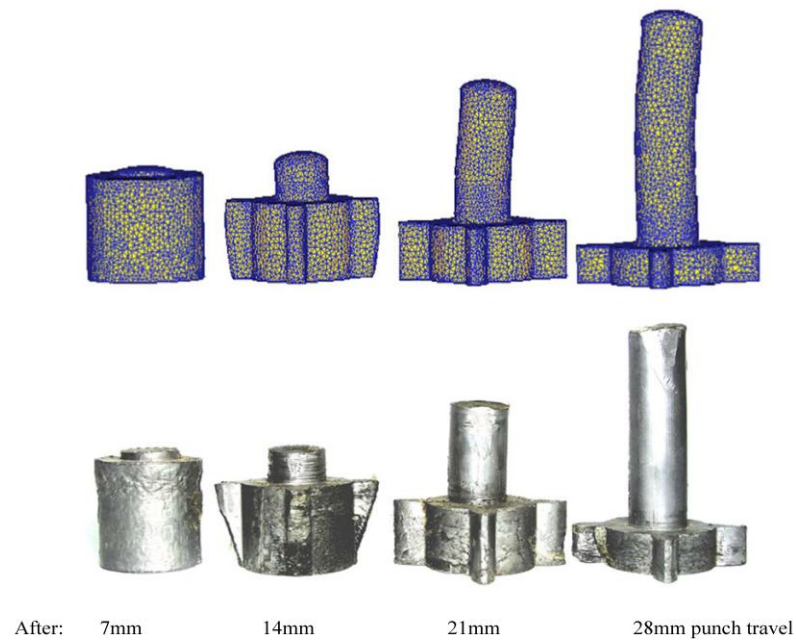


Figure 8.28 Die filling at different position of punch travel

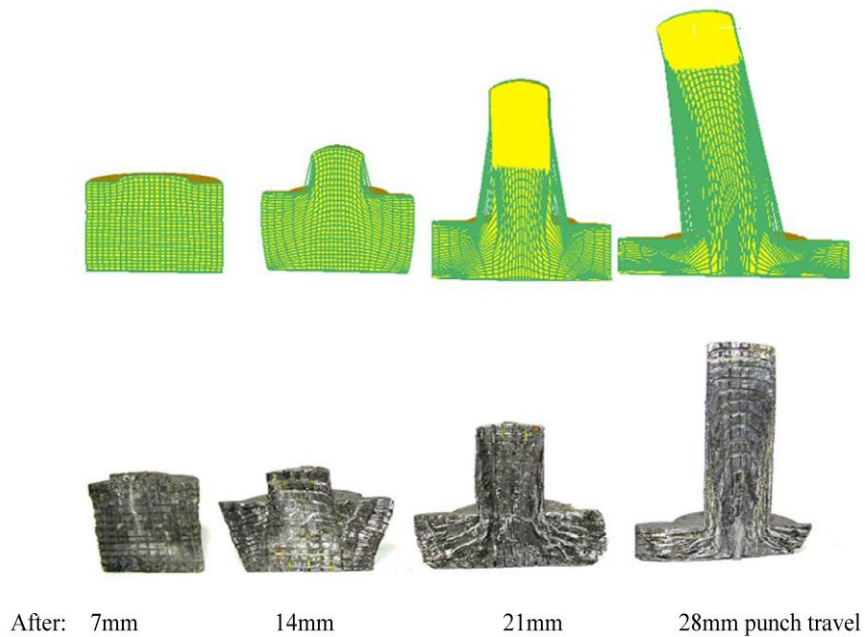


Figure 8.29 Flow pattern at different punch movement

Figure 8.28 shows the complete process for four tooth gear at different punch movement, for forward extrusion-forging process, for both FEM simulations and experiment at 77.99 percentage area reduction and at particular intervals of punch movement. It explains that combined extrusion-forging process takes place till the die cavity is completely filled. Then only pure extrusion process takes place.

Table 8.2 Computation of non-dimensional average extrusion pressure for forward extrusion-forging process of 4, 6, 8, 12-tooth spur gear

% Reduction	Extrusion load(kN)	P_{av} MPa	σ_o Mpa ²	P_{av}/σ_o (Experiment)	P_{av}/σ_o (Theoretical)
4-tooth spur gear					
87.62	174.34	122.12	23.445	5.21	5.38
83.15	151.89	106.39	23.494	4.53	4.68
77.99	124.01	86.86	23.543	3.69	3.79
72.15	109.32	76.57	23.591	3.25	3.34
65.62	95.01	66.55	23.641	2.82	2.89
6-tooth spur gear					
88.68	210.59	134.87	23.432	5.76	5.85
84.60	161.00	103.11	23.479	4.39	4.51
79.88	132.25	84.70	23.526	3.60	3.74
74.54	112.82	72.25	23.572	3.07	3.20
68.56	96.74	61.95	23.619	2.62	2.73
8-tooth spur gear					
89.58	221.82	130.84	23.420	5.59	5.72
85.81	166.65	98.30	23.466	4.19	4.41
81.47	140.49	82.87	23.511	3.52	3.70
76.55	128.65	75.88	23.555	3.22	3.31
71.05	112.84	66.56	23.600	2.82	2.94
12-tooth spur gear					
91.00	251.36	128.05	23.400	5.47	5.71
87.75	223.20	113.70	23.443	4.85	5.07
84.00	199.19	101.47	23.486	4.32	4.42
79.75	162.05	82.55	23.527	3.51	3.65
74.99	140.33	71.49	23.568	3.03	3.07

As an illustration, Figure 8.29 shows the photograph of the flow pattern for a 77.99% area reduction of forward extrusion-forging process at different punch movement for both in FEM and experimental. The grid lines distortion indicates that the process utilizes the maximum amount of redundant work to create flanges of 4-tooth spur gear.

The load corresponding to the peak load, where steady state extrusion starts, considered as the extrusion load and is tabulated in the Table 8.2. This table provides the value of the mean extrusion pressure P_{av} , the value of the uniaxial yield stress in compression σ_0 and the non-dimensional extrusion pressure (P_{av}/σ_0) for different tooth gear. Theoretical value of P_{av}/σ_0 computed with the help of proposed SERR technique, are also furnished in the table for a comparison.

8.10.2 Forward-backward extrusion-forging process

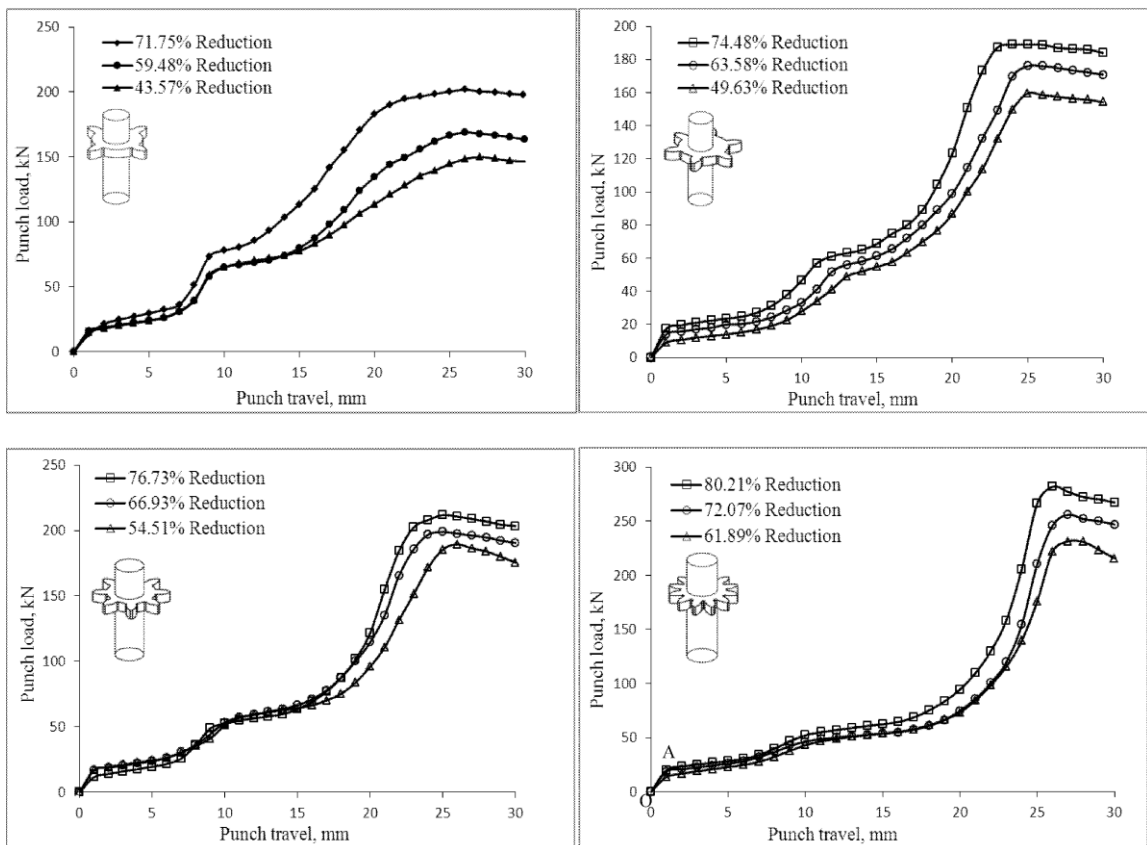


Figure 8.30 Variation of punch load with punch travel of experimental analysis for forward-backward extrusion of four, six, eight and twelve tooth spur gear shape

Experiments are carried out for forward-backward extrusion-forging process for four, six, eight and twelve tooth gear profile. Figure 8.30 represent the punch load with punch movement. Some deviations are observed in some reduction from graph which may be due to defect in samples. Table 8.3 furnishes the non-dimensional extrusion pressure for theoretical and experimental analysis for forward-backward of different tooth gear profile.

Table 8.3 Computation of non-dimensional average extrusion pressure for forward-backward extrusion-forging process of 4, 6, 8, 12-tooth spur gear

% Reduction	Extrusion load(kN)	P_{av} MPa	σ_o Mpa ²	P_{av}/σ_o (Experiment)	P_{av}/σ_o (Theoretical)
<i>4-tooth spur gear</i>					
71.75	168.68	134.84	23.595	5.72	5.84
59.48	145.92	122.92	23.684	5.19	5.33
43.57	129.93	116.69	23.788	4.91	5.00
<i>6-tooth spur gear</i>					
74.48	179.14	129.37	23.573	5.49	5.97
63.58	146.02	110.56	23.655	4.67	5.29
49.63	129.56	103.87	23.749	4.37	4.81
<i>8-tooth spur gear</i>					
76.73	221.85	146.09	23.554	6.20	6.59
66.93	191.89	131.90	23.631	5.58	5.75
54.51	161.51	116.93	23.717	4.93	5.13
<i>12-tooth spur gear</i>					
80.21	317.18	178.01	23.523	7.57	8.24
72.07	256.00	148.62	23.592	6.30	7.05
61.89	231.43	146.36	23.667	5.93	6.17

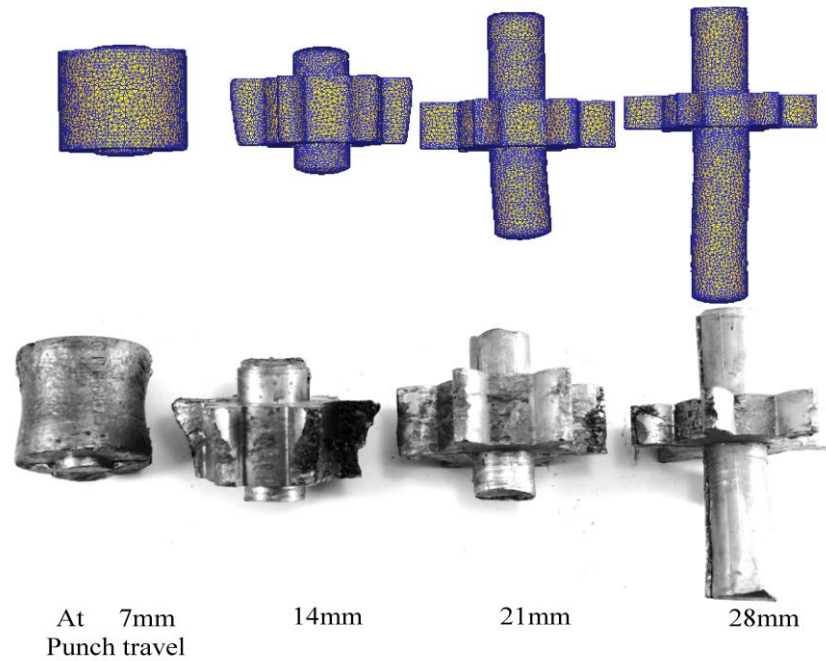


Figure 8.31 Die filling at different position of punch travel (a comparison between FEA and experimental analysis)

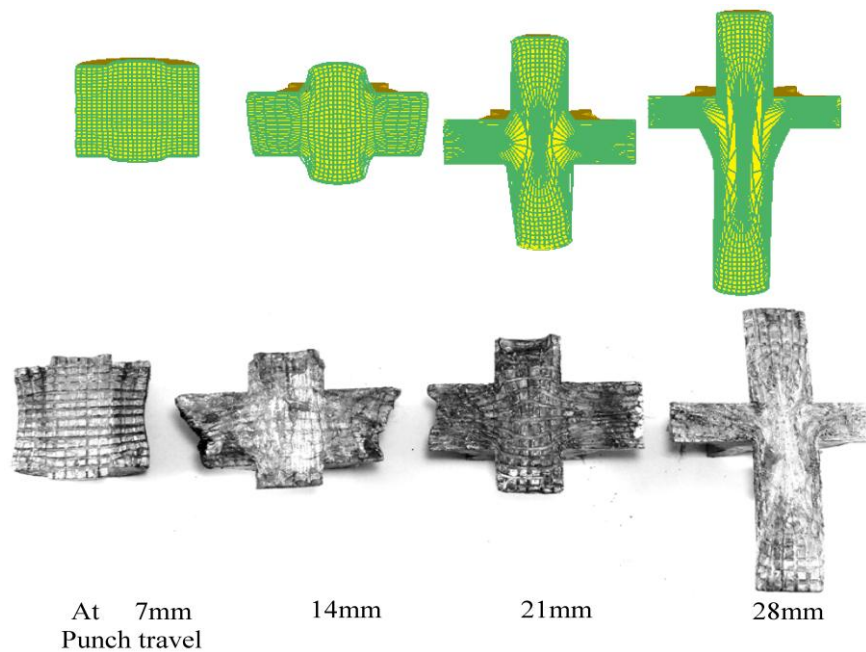


Figure 8.32 Comparison of flow pattern between FEM and experiment at different punch travel movement

Figure 8.31 shows the complete process for four tooth gear at different punch movement, for forward extrusion-forging process, for both FEM simulations and experiment at 77.99 percentage area reduction and at particular intervals of punch

movement. It explains that combined extrusion-forging process takes place till the die cavity is completely filled. Then only pure extrusion process takes place.

As an illustration, Figure 8.32 shows the photograph of the flow pattern for a 77.99% area reduction of forward extrusion-forging process at different punch movement for both in FEM and experimental. The grid lines distortion indicates that the process utilizes the maximum amount of redundant work to create flanges of 4-tooth spur gear.

8.11 Comparison of Results and Discussion

8.11.1 Forward extrusion-forging process

8.11.1.1 Without considering friction

Figure 8.33 gives the comparison of non-dimensional extrusion pressure (P_{av}/σ_0) for upper bound analysis, experimental analysis and finite element analysis for different tooth gear at different percentage of reduction (forward extrusion-forging process). The variations of different formulation are highlighted in Table 8.4. The difference between FEM and UBA are within 3.0% error. The difference between UBA and Expt. analysis are within 5% error.

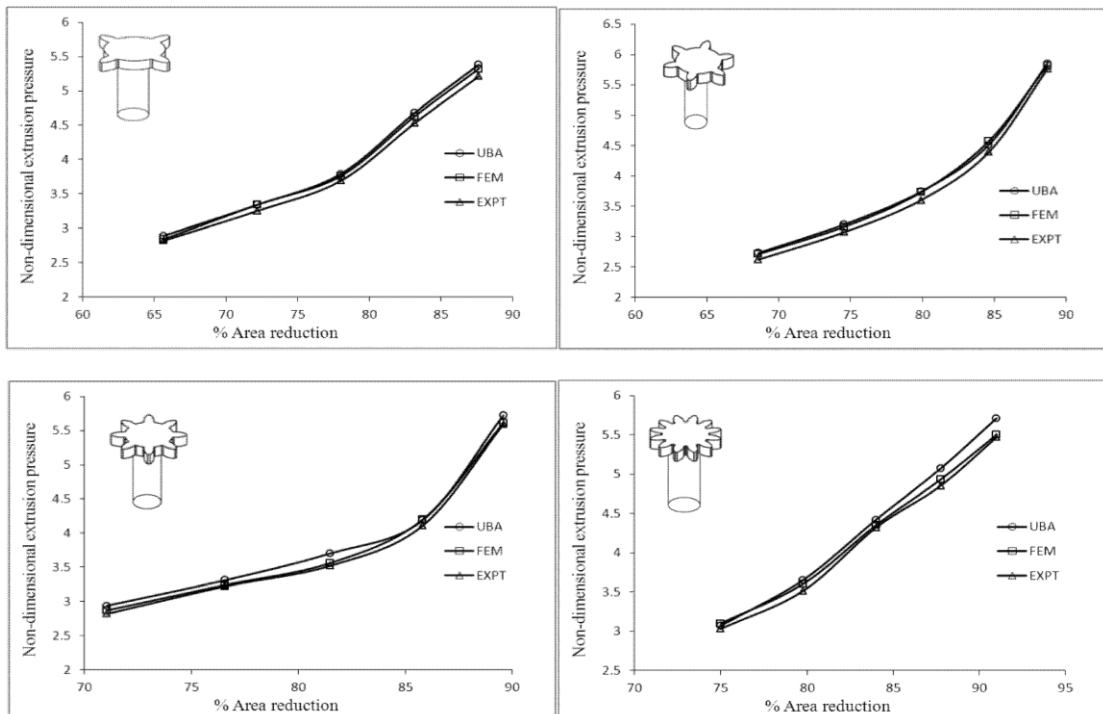


Figure 8.33 Comparison of non-dimensional extrusion pressure without friction for forward extrusion-forging process of 4, 6, 8, 12-tooth spur gear

Table 8.4 Comparison of non-dimensional extrusion pressure without friction for forward extrusion-forging process of 4, 6, 8, 12-tooth spur gear

% Reduction	% Diff. UBA~FEM	% Diff. UBA~EXPT	% Reduction	% Diff. UBA~FEM	% Diff. UBA~EXPT
4-tooth gear			8-tooth gear		
87.62	1.12	3.16	89.58	1.92	2.27
83.15	1.07	3.21	85.81	-0.24	1.91
77.99	0.79	2.64	81.47	3.78	4.86
72.15	0.00	2.69	76.55	2.11	2.72
65.62	1.73	2.42	71.05	2.38	4.08
6-tooth gear			12-tooth gear		
88.68	0.51	1.54	91.00	3.68	4.20
84.60	-1.33	2.66	87.75	2.76	4.34
79.88	0.27	3.74	84.00	1.58	2.26
74.54	1.25	4.06	79.75	1.37	3.84
68.56	0.73	4.03	74.99	-0.98	1.30

8.11.1.2 Considering friction

Figure 8.34 – 8.37 shows the comparison graph of different tooth gear and for different reductions for every tooth gear. It is observed that the variation between UBA and FEA are within 18% whereas the difference between UBA and Experimental results are within 15%. Some cases it is observed that the last result of the FEA analysis decrease suddenly due to the drop in load at the last step of the FEA simulation load.

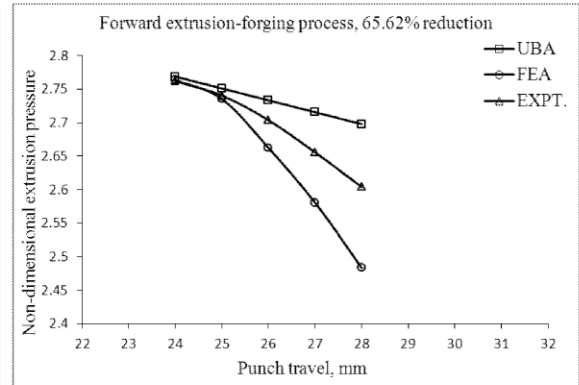
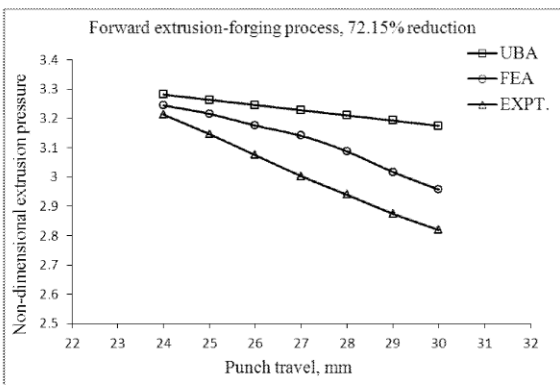
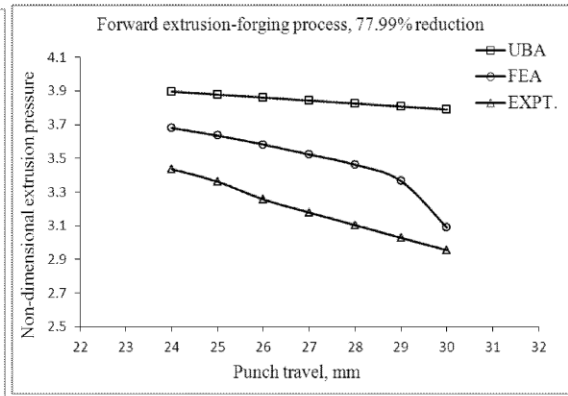
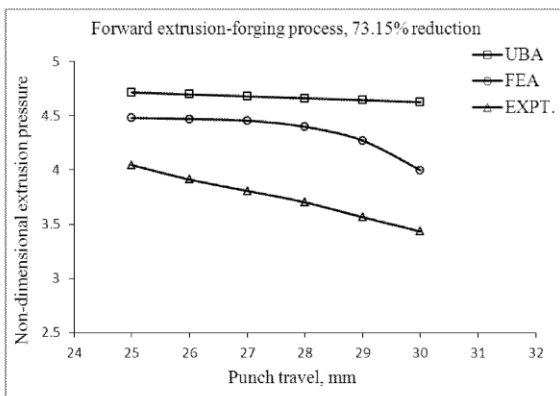
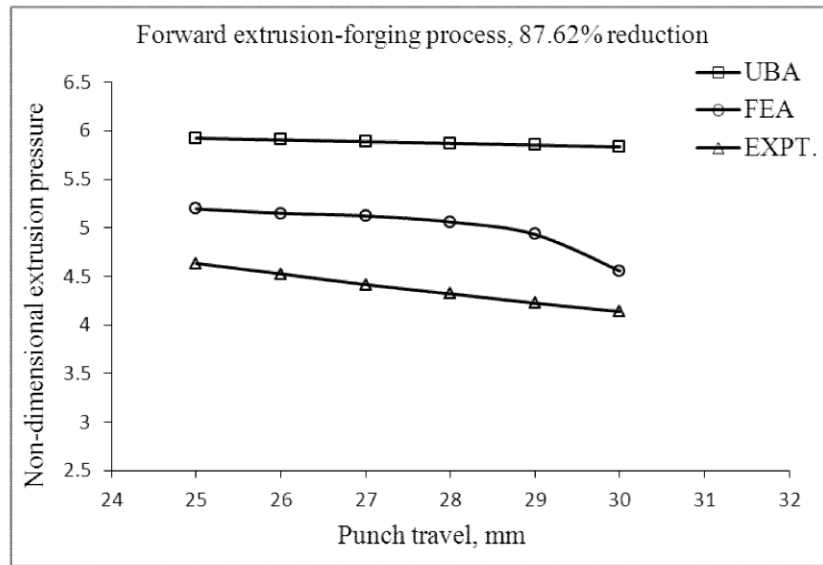


Figure 8.34 Variation of non-dimensional extrusion pressure with friction for forward extrusion forging process of 4-tooth spur gear for different reductions

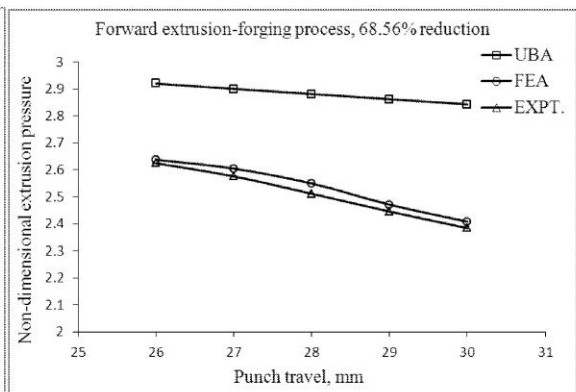
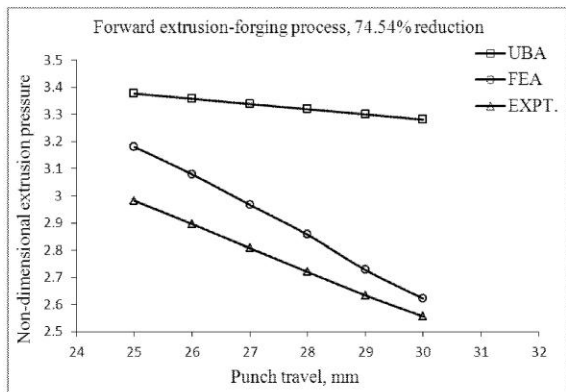
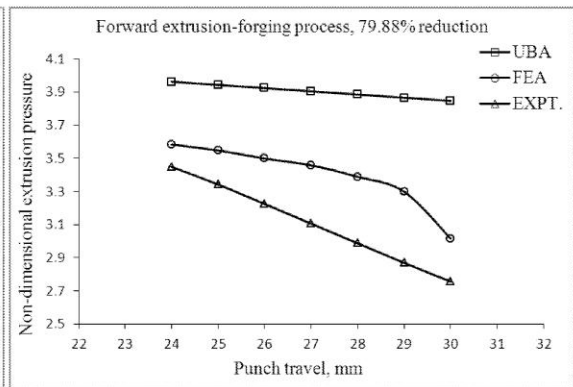
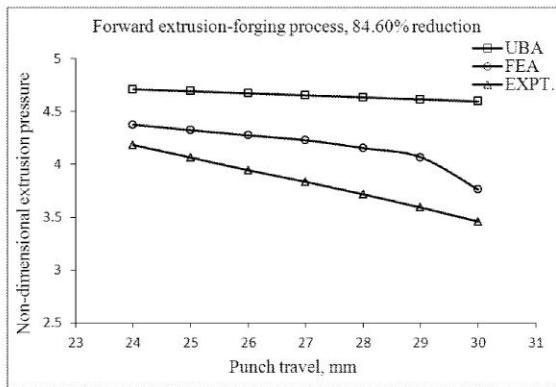
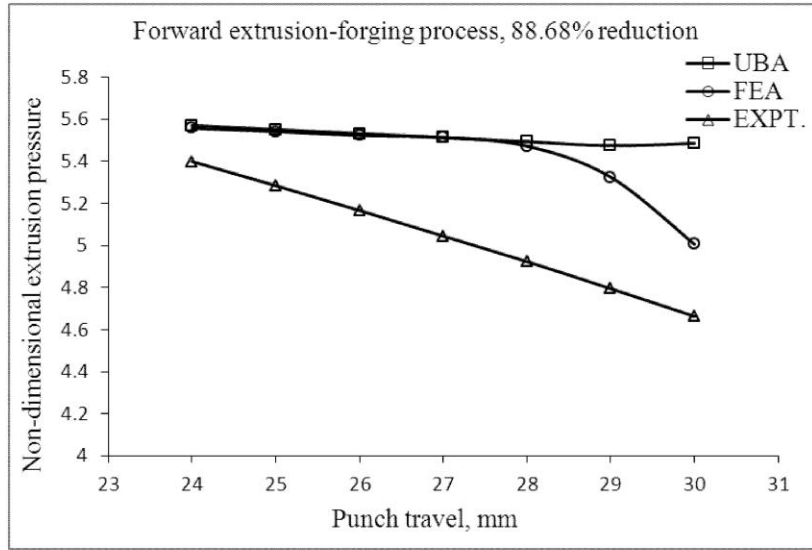


Figure 8.35 Variation of non-dimensional extrusion pressure with friction for forward extrusion forging process of 6-tooth spur gear for different reductions

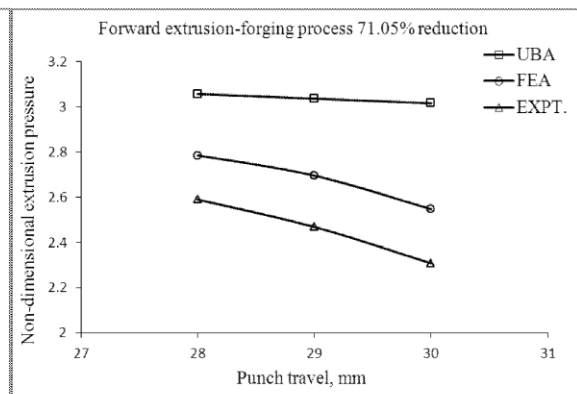
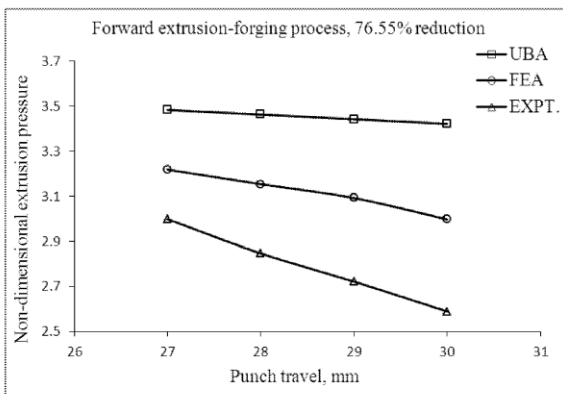
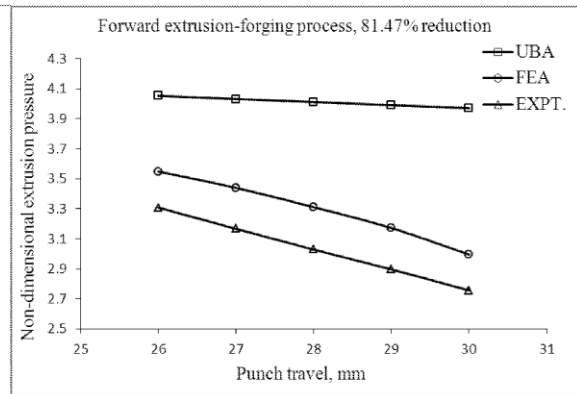
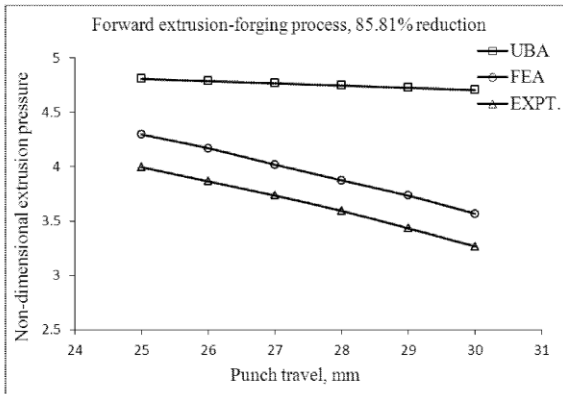
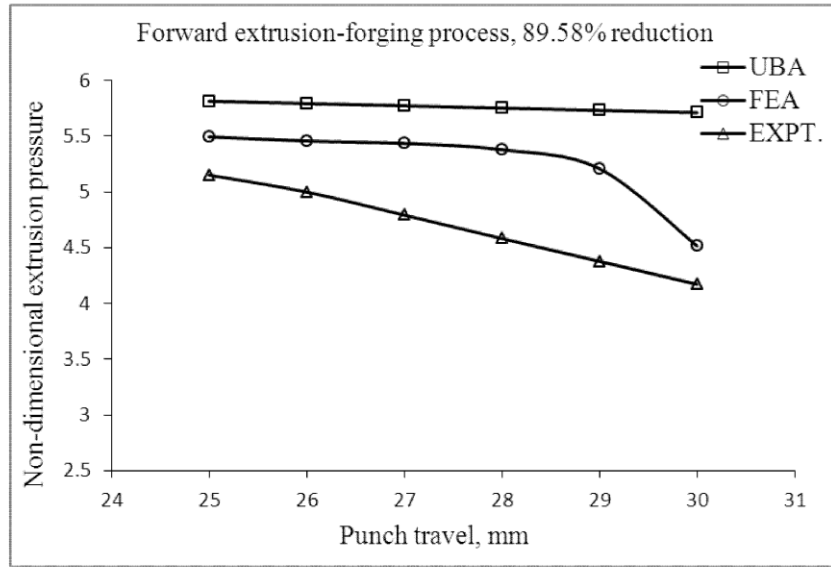


Figure 8.36 Variation of non-dimensional extrusion pressure with friction for forward extrusion forging process of 8-tooth spur gear for different reductions

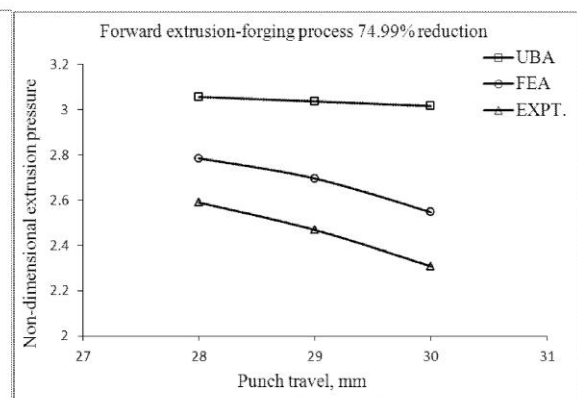
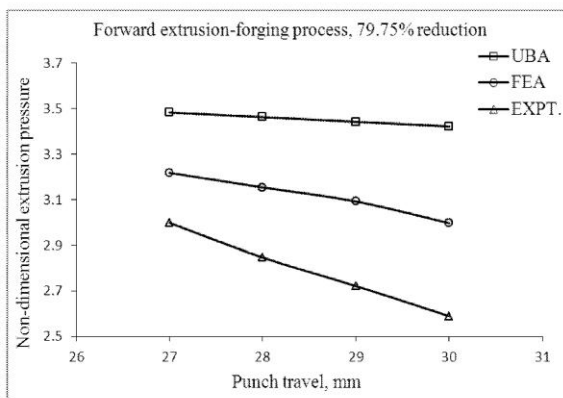
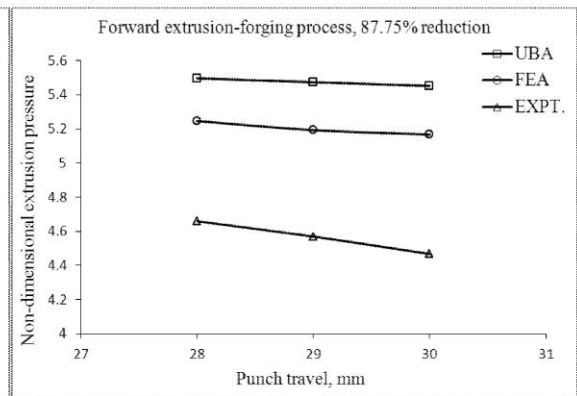
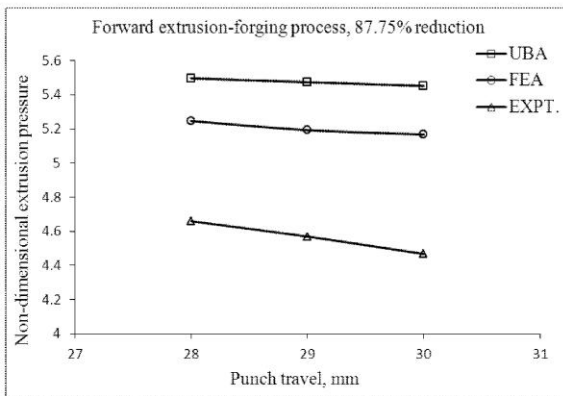
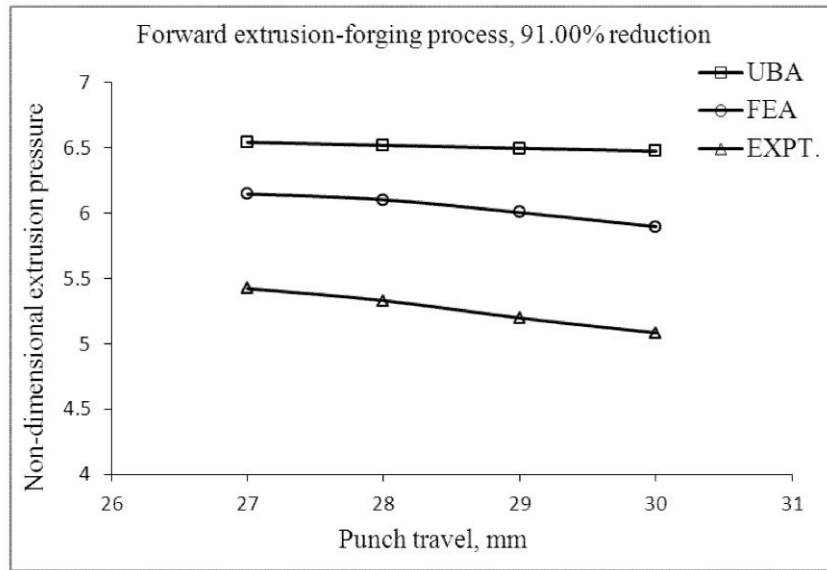


Figure 8.37 Variation of non-dimensional extrusion pressure with friction for forward extrusion forging process of 12-tooth spur gear for different reductions

8.11.2 Forward-backward extrusion-forging

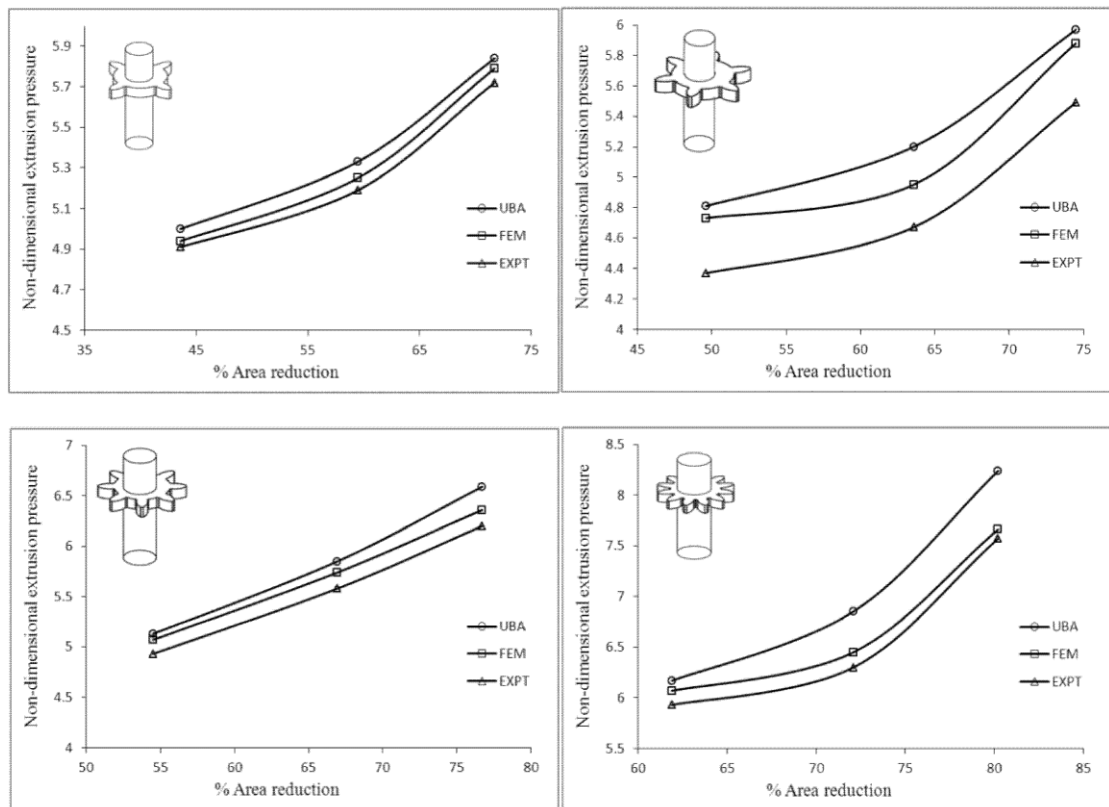


Figure 8.38 Comparison of non-dimensional extrusion pressure for forward-backward extrusion-forging process of 4, 6, 8, 12-tooth spur gear

Table 8.5 Comparison of non-dimensional average extrusion pressure for forward-backward extrusion-forging process of 4, 6, 8, 12-tooth spur gear

% Reduction	% Diff. UBA~FEM	% Diff. UBA~EXPT	% Reduction	% Diff. UBA~FEM	% Diff. UBA~EXPT
4-tooth gear			8-tooth gear		
71.75	0.87	2.17	76.73	3.62	5.94
59.48	1.46	2.65	66.93	0.14	2.92
43.57	1.07	1.82	54.51	1.16	3.91
6-tooth gear			12-tooth gear		
74.48	1.53	8.06	80.21	7.00	8.13
63.58	6.43	11.71	72.07	8.51	10.66
49.63	1.49	9.00	61.89	1.60	3.83

Figure 8.38 gives the comparison of non-dimensional extrusion pressure (P_{av}/σ_0) for upper bound analysis, experimental analysis and finite element analysis for different tooth gear at different percentage of reduction (forward extrusion-forging

process). The variations of different formulation are highlighted in Table 8.5. The difference between FEM and UBA are within 10 % error, whereas, it is 11 % between UBA and experiments.

8.12 Clouser

8.12.1 Forward extrusion-forging process

1. The experimental non-dimensional average extrusion pressure P_{av}/σ_o , agrees with the theoretical value computed with the help of proposed SERR technique to within 5% for the range of reduction studied.
2. Among the three SERR formulation carries out in this study, double-point formulation gives the lowest upper bound to the extrusion pressure for the extrude section.
3. The obtained variation of punch load with respect to stroke by proposed technique is also well validated with FE analysis and experiment. It is also observed that with increase of reduction variation of FE analysis with experimental results increases marginally.
4. The proposed upper-bound analysis using discontinuous velocity field (modified SERR technique) provides a better method of analysis for this type of section extrusion.
5. The experimental die filling and flow pattern agrees with the FEM analysis.

8.12.2 Forward-backward extrusion-forging process

1. The experimental non-dimensional average extrusion pressure P_{av}/σ_o , agrees with the theoretical value computed with the help of proposed SERR technique to within 10% for the range of reduction studied.
2. Among the six SERR formulation carries out in this study, three-point formulation gives the lowest upper bound to the extrusion pressure for the extrude section.
3. The obtained variation of punch load with respect to stroke by proposed technique is also well validated with FE analysis and experiment.
4. The proposed upper-bound analysis using discontinuous velocity field (modified SERR technique) provides a better method of analysis for this type of section extrusion.
5. The experimental flow pattern agrees with the FEM analysis.

Executive Summary, Conclusions and Future Recommendations

9.1 Introduction

In the simplest form of the combined extrusion-forging process, the forging to fill the die cavity and the extrusion through the orifice take place simultaneously; this is performed in one station only. This tooling arrangement permits the simultaneous lateral spread due to forging, and backward/forward extrusion or both forward and backward extrusion simultaneously through the hole in the platen. The flow pattern of the material is dependent on a number of factors, including the frictional conditions at the work piece/tooling interface; the geometry of the dies, particularly the size of the dies hole; material type; and the percentage area reductions. Due to the complexity of the process, and because of the large number of process variables, it is difficult to estimate the forming force required to manufacture a given component. In this direction, the present work emphasize on estimation of forming load for forward and forward-backward extrusion-forging process of regular shapes and different tooth spur gear shapes.

9.2 Summary of Findings

Because of the industrial significance of the combined extrusion/forging process the proposed research work not only attempt to develop and optimize the process, but also make an effort to understand the flow stress of the material, frictional conditions and mode of flow of the material.

1. Computational model for forward and forward-backward extrusion-forging process with and without considering friction is developed by incorporating all special features for the sections. Three formulations for forward extrusion-forging process and six formulations for forward-backward extrusion-forging processes are analyzed and the optimal solution for non-dimensional extrusion pressure is found out for further computation. Among all formulations carries out in this study, in the most of the cases, double-point formulation gives the lowest upper bound for forward extrusion-forging situations, and it is the three-point formulation for forward-backward extrusion-forging. It is evident that by increasing the floating points, more than the optimized number, we may incorporate more redundancy.

2. The model is self-developed using FORTRAN code. The results validate and convey the suitability of the proposed model for the combined extrusion-forging processes.
3. Experimental studies are carried out with a view to compare some of the theoretical results predicated using upper bound method in general, modified SERR technique in particular, with that obtained from the experiment. SERR technique is used to analysis the last stage of the combined extrusion forging process (which requires maximum load). Both forward and forward-backward extrusion-forging processes are analyzed. The results obtained by the proposed model well in line with the practically observed results.
4. Experiments are performed for triangle, square, pentagon, hexagon, 4-tooth, 6-tooth, 8-tooth and 12-tooth spur gear form (with involutes profile and $14\frac{1}{2}^{\circ}$ pressure angle) using flat/square die. Both forward and forward-backward extrusion-forging processes are carried out.
5. FEM based commercial package code is used for finite element analysis of the processes. The experimental die filling, flow pattern and load requirements agree well with the FEM analysis.
6. The results obtained from experimental investigation are found to be in good agreement with the similar one predicted by theoretical analysis using the proposed modified SERR technique and finite element analysis. The difference between UBA and FEM are within 7.0%. Whereas the difference between UBA and experiment is 10%. The proposed technique appears to provide good prediction of the load requirement for the combined extrusion-forging processes studied in the present work..

9.3 Contribution of the Research Work

- The first and foremost contribution of the present work is to replace ‘Thumb rules’ or ‘designer’s intuition’ based design, which are still prevalent in the industry, by a methodical analysis process when installing and deciding on capacity of a machine/ equipment/tool/die and production of complex parts.
- Design and fabrication of a laboratory purpose experimental setup for the combined extrusion-forging process is carried out to look after the process behavior and validation of the proposed model of analysis.

- Preparation of sample by casting, machining and annealing from commercially available lead ingot.
- Performing exhaustive experiments for forward and forward-backward extrusion-forging process at different percentage area reductions (for all the manufactured dies). Experimental results are also checked for repeatability.
- Computational models are developed for forward and forward-backward extrusion-forging process considering with and without friction by incorporating special features for all the section extrusion and forging.
- FEM analyses using commercially available package DEFORM[®]-3D codes.
- The most important is to transform basic knowledge about extrusion & forging and the subsequent manufacturing process into a form that is useful in product design.

9.4 Limitation of the Study

In spite of several advantages achieved through proposed study, followings may be treated as limitations of the study since they have not been addressed.

- Computational models are developed only for steady-state extrusion process where only extrusion takes place and the processes attain the peak value of load.
- The gear shapes are designed empirically; convenient point of view of fabricating dies. Not to the point of view of design analysis. Only one type of gear (spur), gear profile (involute) and pressure angle ($14\frac{1}{2}^\circ$) is considered.

9.5 Scopes for future work

The present work will inspire the future investigators and have a wide scope for to explore many aspects of combined extrusion-forging processes. Some recommendations for future research include:

- This method can be extended to analyse section extrusion of other shapes.
- The analysis can be extended for the extrusion of sections through converging, and curve dies.
- The proposed technique can be applied to predict metal flow.
- FEM analysis can be done by own code incorporating special conditions.
- Computational models can be developed for all stages of the processes

REFERENCES

- [1] K. Osakada, "History of plasticity and metal forming analysis," *Journal of Materials Processing Technology*, vol. 210, no. 11, pp. 1436-1454, Aug. 2010.
- [2] L Prandtl., "Über die Härte plastischer Körper, Nachrichten von der Königlichen Gesellschaft der Wissenschaften zu Göttingen," *Math.-physik. Kl.* 1920, 74-85.
- [3] H. Hencky, "Über einige statisch bestimmte Fälle des Gleichgewichts in plastischen Körpern," *Z. Angew. Math. Mech.*, vol. 3, pp. 241-251, 1923.
- [4] H. Geiringer, "Beit zum Vollständigen ebenen plastizität problem," *Proc. 3rd Int. Congr. Appl. Mech., Stockholm*, vol. 2, pp. 185-190, 1930.
- [5] Hill, R: *The Mathematical Theory of Plasticity*, Oxford at the Clarendon Press, 1950.
- [6] W. Prager, and P.G. Hodge, "Theory of perfectly plastic solids," Wiley, New York, 1951.
- [7] W. Johnson, R. Sowerby, and J. B. Haddow, *Plane-strain Slip-line Fields. Theory and Bibliography*, E. Arnold, London, 1970.
- [8] Johnson, W., Extrusion through square dies of large reduction. *J. Mech. Phys. Solids*. 4, 194-209, (1956).
- [9] Johnson, W., Extrusion through wedge-shaped dies, Part-I and Part-II, *J. Mech. Phys. Solids*. 3, 218-249, (1955).
- [10] W. Johnson, P. B. Mellor, and D. M. Woo, "Extrusion Through Single Hole Staggered And Unequal Multi-Hole Dies," *Journal of the Mechanics and Physics of Solids*, vol. 6, pp. 203-222, 1958.
- [11] L. Dodeja and W. Johnson, "On The Multiple Hole Extrusion Of Sheets Of Equal thickness," *Journal of the Mechanics and Physics of Solids*, vol. 5, pp. 267-280, 1957.
- [12] A. P. Green, "On Unsymmetrical Extrusion In Plane Strain," *Journal of the Mechanics and Physics of Solids*, vol. 3, pp. 189-192, 1955.
- [13] W. A. Green, "Extrusion Through Medium Smooth Square Dies Of Medium Reduction," *Journal of the Mechanics and Physics of Solids*, vol. 10, pp. 225-233, 1962.

- [14] D. J. F. Ewing, "A Series-Method For Constructing Plastic Slip line Fields," *Journal of the Mechanics and Physics of Solids*, vol. 15, no. 2, pp. 105-114, Mar. 1967.
- [15] I. F. Collins, "The Algebraic-Geometry of Slip Line Fields with Applications to Boundary Value Problems," *Proceedings of the Royal Society A: Mathematical, Physical and Engineering Sciences*, pp. 03-317, Mar. 1968.
- [16] N. S. Das, N. R. Chitkara, and I. F. Collins, "The computation of some slip-line field solutions for asymmetric extrusion." vol. 11, pp. 1379-1392, 1977.
- [17] N. R. Chitkara, N. S. Das, and W. Johnson, "A class of slip-line field solutions for unsymmetrical extrusion and some experimental results," *Proc. 17th M.T.D.R. Int. Conf. McMillon*, 1977.
- [18] P. Dewhurst, I. F. Collins, and W. Johnson, "A class of slip-line field solutions for the hot rolling of strip.," *Journal of Mechanical Engineering Science*, vol. 15, pp. 439-451, 1975.
- [19] I. F. Collins and P. Dewhurst, "A slip-line field analysis of asymmetrical hot rolling of strip.," *Int. J. Mech. Engg. Sci.*, vol. 17, pp. 643-663, 1975.
- [20] B. I. Bachrach and S. K. Samanta, "A Numerical Method for Computing Plane Plastic Slip-Line Fields," *ASME, Journal of Applied Mechanics*, vol. 43, no. 1, pp. 97-101, 1976.
- [21] N. Das and, K.P. Maity "A class of slipline field solutions for extrusion through wedge shaped dies with slipping friction," *Materials & Design*, vol. 28, no. 2, pp. 380-386, 2007.
- [22] D. G. Christopherson, W. B. Palmer, and P. L. B. Oxley, "Orthogonal cutting of work hardening materials.," *Trans. ASME, J. Appl. Meek.*, vol. 186, pp. 113-134, 1958.
- [23] L. Chenot, L. Folgeres, B. Lavarenne, and J. Salencon, "A numerical application of the slip-line field method to extrusion through conical dies.," *Int. J. Engg Sci.*, vol. 16, no. 4, pp. 263-273, 1978.
- [24] I. F. Collins and B. K. Williams, "Slip-line field analysis of axisymmetric tube drawing.," *Int. J. Mech Sci.*, vol. 27, no. 4, pp. 199-223, 1985.

- [25] N. Das and W. Johnson, "Slip-line fields of indirect type for end extrusion through partly rough square dies," *International Journal of Mechanical Sciences.*, vol. 30, no. 1, pp. 61-69, 1988.
- [26] K. Abrinia and R. Tahriri Mossuleh, "An approximate load estimation method for three dimensional metal forming problems," *International Journal of Mechanical Sciences*, vol. 51, no. 11-12, pp. 774-781, Nov. 2009.
- [27] E. Siebel, "Untersuchungen über bildsame Formänderung unter besonderer Berücksichtigung des Schmiedens," *Maschinenbau/Betrieb*, vol. 9, pp. 307-312, 1923.
- [28] H. Lippmann and O. Mahrenholts, "Plastomechanik der Umformung metallischer Werkstoffe," *Springer-Verlag*, 1967.
- [29] K. Lange, *Handbook of metal forming*. McGraw-Hill, 1985.
- [30] Kaneko. et al., "Study on the biaxial forming of polymers(application of the slab method to the backward extrusion of high-density polyethylene," *Nippon Kikai Gakkai Ronbunshu. A HenTransaction of the Japan Society of Mechanical Engineers, Part A*, vol. 52, no. 483, pp. 2552-2558, 1986.
- [31] W. Shichun, D. Zhen, and L. Miaoquan, "Prediction of corner-cavity formation during backward extrusion by the modified slab method," *Journal of Materials processing Technology*, vol. 31, pp. 113-118, 1992.
- [32] C.S. Yih, "Stream functions in three-dimensional flow." *La Houille Blanche*, Vol.12, pp99-107, 1957
- [33] N. Chitkara and A. Aleem, "Extrusion of axi-symmetric bi-metallic tubes: some experiments using hollow billets and the application of a generalized slab method of analysis," *International Journal of Mechanical Sciences*, vol. 43, no. 12, pp. 2857-2882, Dec. 2001.
- [34] H.-H. Hsu and G.-Y. Tzou, "Two analytical models of double-layer clad sheet compression forming based on the upper bound and the slab methods," *Journal of Materials Processing Technology*, vol. 140, no. 1-3, pp. 604-609, Sep. 2003.
- [35] M. Bakhshi-Jooybari, M. Saboori, M. Noorani-Azad, and S. J. Hosseinipour, "Combined upper bound and slab method , finite element and experimental study

- of optimal die profile in extrusion,” *Materials & Design*, vol. 28, pp. 1812-1818, 2007.
- [36] A. Samadi Ghoshchi, A. S. Ghoshchi, S. M. Bazargani, and S. Emami, “Slab Method of Analysis for Three Dimensional Forward Extrusion of Squared End Section,” in *ASME 2010 10th Biennial Conference on Engineering Systems Design and Analysis, Volume 4*, 2010, vol. 4, pp. 491-495.
- [37] D. N. Kamble and V. M. Nandedkar, “Slab Method Modification and Its Experimental Investigation for Hot Forming Process,” *Materials and Manufacturing Processes*, vol. 26, no. 5, pp. 677-683, May. 2011.
- [38] R. Hill, *The Mathematical Theory of Plasticity*,. Oxford at the Clarendon Press, 1950.
- [39] A. P. Green, “The compression of a ductile material between smooth dies,” *Phil. Mag.*, vol. 42, pp. 9000-918, 1951.
- [40] H. Kudo, “Some analytical and experimental studies of axi-symmetric cold forging and extrusion—I,” *International Journal of Mechanical Sciences*, vol. 2, no. 1-2, pp. 102-127, Oct. 1960.
- [41] H. Kudo, “An Upper-Bound Approach To Plane-Strain Forging And Extrusion—I, II, III,” *Int. J. Mech. Sci.*, vol. I, pp. 57-83, 1960.
- [42] W. Johnson, “Estimation of Upper Bound Loads for Extrusion and Coining Operations,” *Proc. Inst. Meek Engrs*, vol. 173, no. 1, pp. 61-72, 1957.
- [43] W. Johnson and H. Kudo, *The Mechanics of Metal Extrusion*. Manchester University Press, Manchester, 1962.
- [44] J. Adie and J. Alexander, “A graphical method of obtaining hodographs for upper-bound solutions to axi-symmetric problems,” *International Journal of Mechanical Sciences*, vol. 9, no. 6, pp. 349-357, Jun. 1967.
- [45] R. Avitzur, *Metal Forming processes and Analysis*. McGraw Hill, New York, 1968.
- [46] J. Frisch and E. G. Thomsen, “Stresses and strains in cold extruding 28-0 Aluminium,” *Trans. ASME*, vol. 77, pp. 1343-1362, 1955.

- [47] A. Shabaik and E. G. Thomsen, "A theoretical method for the analysis of metal-working problems.," *Trans. ASME, J. of Engng. for Industry*, vol. 90, pp. 343-359, 1968.
- [48] R. Hill, "General Metal method of Analysis For Metal working Processes," *J. Mech. Phys. Solids*, vol. II, pp. 305-326, 1963.
- [49] Y.-maw Hwang, H.-hsiou Hsu, and Y.-lin Hwang, "Analytical and experimental study on bonding behavior at the roll gap during complex rolling of sandwich sheets," *International Journal of Mechanical Sciences*, vol. 42, pp. 2417-2437, 2000.
- [50] N. R. Chitkara and A. Aleem, "Extrusion of axi-symmetric bi-metallic tubes: some experiments using hollow billets and the application of a generalised slab method of analysis," *International Journal of Mechanical Sciences*, vol. 43, no. 12, pp. 2857-2882, Dec. 2001.
- [51] N. R. Chitkara and M. A. Bhutta, "Dynamic Heading of Triangular, Hexagonal, and Octagonal Shaped Heads at Low Impact Velocities : Some Experiments and an Analysis," *Mechanical Engineering*, vol. 1, pp. 332-347, 2001.
- [52] W. Johnson, "Experiments in plane-strain extrusion," *Journal of the Mechanics and Physics of Solids*, vol. 4, no. 4, pp. 269-282, Aug. 1956.
- [53] K. F. Celik and N. R. Chitkara, "Extrusion of non-symmetric U- and I-shaped sections through ruled-surface dies: numerical simulations and some experiments," *International Journal of Mechanical Sciences*, vol. 44, pp. 217-246, 2002.
- [54] W. A. Gordon, "Extrusion through Spherical Dies—An Upper Bound Analysis," *Journal of Manufacturing Science and Engineering*, vol. 124, no. 2, pp. 92-97, 2002.
- [55] H. R. Darani and M. Ketabchi, "Simulation of 'L' section extrusion using upper bound method," *Journal of Engineering for Industry*, vol. 25, pp. 535-540, 2004.
- [56] B. S. Altan, G. Purcek, and I. Miskioglu, "An upper-bound analysis for equal-channel angular extrusion," *Journal of Materials Processing Technology*, vol. 168, pp. 137-146, 2005.

- [57] A. R. Eivani and A. K. Taheri, "An upper bound solution of ECAE process with outer curved corner," *Journal of Materials Processing Technology*, vol. 182, pp. 555-563, 2007.
- [58] J. S. Ajiboye and M. B. Adeyemi, "Effects of die land on the cold extrusion of lead alloy" *Journal of Materials Processing Technology*, vol. 171, pp. 608-611, 2006.
- [59] J. S. Ajiboye and M. B. Adeyemi, "Upper bound analysis for extrusion at various die land lengths and shaped profiles" *International Journal of Mechanical Sciences*, vol. 49, pp. 335-351, 2007.
- [60] J. S. Ajiboye, "Upper bound analysis of extrusion from square billets through circular and square / rectangular dies," *Journal of Mechanical Science and Technology*, vol. 23, pp. 461-474, 2009.
- [61] D. Y. Yang, C. H. Han, and M. U. Kim, "A Generalized Method for Analysis of Three- Dimensional Extrusion of Arbitrarily-Shaped Sections," *Int. J. Mech. ScL*, vol. 28, no. 8, pp. 517-534, 1986.
- [62] M. Bakhshi-Jooybari, "A theoretical and experimental study of friction in metal forming by the use of the forward extrusion process," *Journal of Materials Processing Technology*, vol. 125-126, pp. 369-374, 2002.]
- [63] S. O. Onuh, M. Ekoja, and M. B. Adeyemic, "Effects of die geometry and extrusion speed on the cold extrusion of aluminium and lead alloys," *Journal of Materials Processing Technology*, vol. 132, pp. 274-285, Jan. 2003.
- [64] K. Abrinia and M. Makaremi, "A new three-dimensional solution for the extrusions of sections with larger dimensions than the initial billet," *Journal of Materials Processing Technology*, vol. 205, no. 1-3, pp. 259-271, Aug. 2008.
- [65] M. K. Sinha, S. Deb, and U. S. Dixit, "Design of a multi-hole extrusion process," *Materials & Design*, vol. 30, no. 2, pp. 330-334, Feb. 2009.
- [66] L. Brayden and J. Monaghan, "An analysis of closed-die extrusion/forging," *Journal of Materials Processing Technology*, vol. 26, no. 2, pp. 141-157, Jun. 1991.

- [67] J. Vickery and J. Monaghan, "An upper-bound analysis of a forging-extrusion process," *Journal of Materials Processing Technology*, vol. 55, pp. 103-110, 1995.
- [68] H. I. Lee, B. C. Hwang, and W. B. Bae, "A UBET analysis of non-axisymmetric forward and backward extrusion," *Journal of Materials Processing Technology*, vol. 113, pp. 103-108, Jun. 2001.
- [69] B. C. Hwang, S. J. Hong, and W. B. Bae, "An UBET analysis of the non-axisymmetric extrusion / forging process," *Journal of Materials Processing Technology*, vol. 111, pp. 135-141, 2001.
- [70] H. Yamin, L. Zhouyi, and Z. Yucheng, "The study of cup-rod combined extrusion processes of magnesium alloy (AZ61A)," *Journal of Materials Processing Technology*, vol. 187-188, pp. 649-652, 2007.
- [71] R. Narayanasamy, K. Baskaran, and D. Muralikrishna, "Materials & Design Some studies on stresses and strains of aluminium alloy during extrusion-forging at room temperature," *Materials and Design*, vol. 29, pp. 1623-1632, 2008.
- [72] R. Narayanasamy, K. Baskaran, S. Arunachalam, and D. Muralikrishna, "An experimental investigation on barreling of aluminium alloy billets during extrusion forging using different lubricants," *Materials & Design*, vol. 29, no. 10, pp. 2076-2088, Dec. 2008.
- [73] F. Gatto and A. Giarda, "The characteristics of the three-dimensional analysis of plastic deformation according to the SERR method," *International Journal of Mechanical Sciences*, vol. 23, no. 3, pp. 129-148, 1981.
- [74] N. R. Chitkara and M. B. Adeyemi, "Working Pressure and Deformation Modes in Forward Extrusion of I and T shaped Sections from square Slugs," *Proceedings of the 18th IMTDR Conference, London, 1977*
- [75] P. K. Kar, N. S. Das, and T. N. Subramanian, "Upper Bound Analysis of Extrusion of Square Sections Using Square Dies," *Journal of Institute of Engineers(India)*, vol. 66, pp. 88-91, 1985.
- [76] S. K. Sahoo, P. K. Kar, K. C. Singh, and S. P. Mohapatra, "Upper Bound Analysis of Extrusion of Hexagonal Section Bars from Rectangular Billets

- through the Square Dies,” *Journal of Institute of Engineers(india)*, vol. 77, pp. 164-168, 1996.
- [77] P. K. Kar and R. K. Sahoo, “Application of the SERR Technique to the Analysis of Extrusion of Section from Round Billets,” *Journal of Institute of Engineers (India)*, vol. 78, pp. 151-154, 1997.
- [78] S. K. Sahoo, P. K. Kar, and K. C. Singh, “Three-Dimensional Analysis using SERR Technique for Extrusion of Triangular Section Bars from Square/Rectangle Billets through Square Dies,” *Journal of Institute of Engineers(India)*, vol. 78, pp. 45-48, 1997.
- [79] S. K. Sahoo, P. K. Kar, and K. C. Singh, “Upper-bound analysis of the extrusion of a bar of channel section from square / rectangular billets through square dies,” *Journal of Materials Processing Technology*, vol. 75, pp. 75 - 80, 1998.
- [80] P. K. Kar, S. K. Sahoo, and N. S. Das, “Upper bound analysis for Extrusion of T-section Bars from Square Billets Through Square Dies,” *International Journal of Mechanical Sciences*, vol. 35, pp. 339-410, Aug. 2000.
- [81] S. Sahoo, “Comparison of SERR analysis in extrusion with experiment,” *Journal of Materials Processing Technology*, vol. 103, no. 2, pp. 293-303, Jun. 2000.
- [82] S. K. Sahoo, P. K. Kar, and K. C. Singh, “A numerical application of the upper-bound technique for round-to-hexagon extrusion through linearly converging dies,” *Journal of Materials Processing Technology*, vol. 91, pp. 105 - 110, 1999.
- [83] S. K. Sahoo and P. K. Kar, “Round-to-hexagon drawing through straightly converging dies: an application of the SERR technique,” *International Journal of Mechanical Sciences*, vol. 42, no. 3, pp. 445-449, Mar. 2000.
- [84] S. Sahoo, “An analysis of plastic flow through polygonal linearly converging dies: as applied to forward metal extrusion,” *Journal of Materials Processing Technology*, vol. 132, no. 1-3, pp. 286-292, Jan. 2003.
- [85] R. K. Sahoo, P. K. Kar, and S. K. Sahoo, “3D upper-bound modeling for round-to-triangle section extrusion using the SERR technique,” *Journal of Materials Processing Technology*, vol. 138, pp. 499-504, 2003.
- [86] R. K. Sahoo, P. R. Samantaray, S. K. Sahoo, B. Sahoo, and P. K. Kar, “Round-to-channel section extrusion through linearly converging die: a three-dimensional

- analysis,” *The International Journal of Advanced Manufacturing Technology*, vol. 41, no. 7-8, pp. 677-683, May. 2008.
- [87] N. R. Chitkara and M. A. Bhutta, “Near Net Shape Spline Forging: An Experimental Investigation and A Simple Upper Bound Analysis,” *International Journal of Mechanical Science*, vol. 37, no. 12, pp. 1247-1268, 1995.
- [88] J. C. Choi, Y. Choi, K. D. Hur, and C. H. Kim, “A Study on the Forging of Spur Gears,” *International Journal of Mechanical Science*, vol. 38, no. 12, pp. 1333-1347, 1996.
- [89] N. R. Chitkara and M. A. Bhutta, “Near-Net Shape Forging of Spur Gear Forms : An Analysis and Some Experiments,” *International Journal of Mechanical Science*, vol. 38, no. 8-9, pp. 891-916, 1996.
- [90] N. R., Chitkara, and Y. Kim, “An Analysis of External Spline Gear Forming by an Upper Bound Energy Method,” *International Journal of Mechanical Science*, vol. 38, no. 7, pp. 777-789, 1996.
- [91] H. Cho, J. Choi, G. Min, Y. Choi, and J. Choi, “An upper-bound analysis of the closed-die forging of spur gears,” *Journal of Materials Processing Technology*, vol. 67, pp. 83-88, May. 1997.
- [92] H.-hsiou Hsu, “A study on precision forging of spur gear forms and spline by the upper bound method,” *International Journal of Mechanical Sciences*, vol. 44, pp. 1543 - 1558, 2002.
- [93] T. Altinbalik and Y. Can, “An experimental study of lateral extrusion of splines,” *Materials & Design*, vol. 27, pp. 727-734, 2006.
- [94] O.C.Zienkeiwicz, and Y. C. Cheung, “The finite element method in structural and continuum mechanics,” *Mc-Graw-Hill*, New York, 1967.
- [95] P. V. Marcal, and I. P. King, “Int. J. Mech. Sci.,” Elastic-Plastic Analysis of Two-Dimensional Stress Systems by the Finite Element Method,” vol. 9, pp.143-145, 1967.
- [96] D.J Hayes, P. V. Marcal,”Determination of upper bounds for problems in plane stress using finite element techniques,”*Int. J. Mech. Sci.*, vol.9, pp. 245-251. 1967.

- [97] G. Maccarini, C. Giarelini, A. Bugini, and D. I. Meccanica, "Extrusion Operation: F.E.M. Approach and Experimental Results," *Journal of Materials Processing Technology*, vol. 24, pp. 395-402, 1990.
- [98] S. I. Oh, W. T. Wu, and J. P. Tang, "Simulations of cold forging processes by the DEFORM system," *Journal of Materials Processing Technology*, vol. 35, pp. 357-370, 1992.
- [99] M. Meidert, M. Knoerr, K. Westphal, and T. Altan, "Numerical and physical modelling of cold forging of bevel gears," *Journal of Materials Processing Technology*, vol. 33, pp. 75-93, 1992.
- [100] T. Reinikainen, K. Andersson, S. Kivivuori, and A. S. Korhonen, "Finite-element processes analysis of copper extrusion," *Journal of Materials Processing Technology*, vol. 34, pp. 101-108, 1992.
- [101] M. Knoerr, J. Lee, and T. Altan, "Application of the 2D finite element method to simulation of various forming processes," *Journal of Materials Processing Technology*, vol. 33, pp. 31-55, 1992.
- [102] H. Kim, K. Sweeney, and T. Altan, "Application of computer aided simulation to investigate metal flow in selected forging operations," *Journal of Materials Processing Technology*, vol. 46, pp. 127-154, Oct. 1994.
- [103] C.-Y. Wu and Y.-C. Hsu, "The influence of die shape on the flow deformation of extrusion forging," *Journal of Materials Processing Technology*, vol. 124, pp. 67-76, Jun. 2002.
- [104] H. Y. Cho, G. S. Min, C. Y. Jo, and M. H. Kim, "Process design of the cold forging of a billet by forward and backward extrusion," *Journal of Materials Processing Technology*, vol. 135, pp. 375-381, Apr. 2003.
- [105] J. Zhou, L. Li, and J. Duszczuk, "3D FEM simulation of the whole cycle of aluminium extrusion throughout the transient state and the steady state using the updated Lagrangian approach," *Journal of Materials Processing Technology*, vol. 134, pp. 383-397, 2003.
- [106] Y.-Lang Yang and S. Lee, "Finite element analysis of strain conditions after equal channel angular extrusion," *Journal of Materials Processing Technology*, vol. 140, pp. 583-587, 2003.

- [107]G. Fang, J. Zhou, and J. Duszczyc, “FEM simulation of aluminium extrusion through two-hole multi-step pocket dies,” *Journal of Materials Processing Technology*, vol. 209, pp. 1891-1900, 2008.
- [108]A. Farhoumand and R. Ebrahimi, “Analysis of forward – backward-radial extrusion process,” *Materials and Design*, vol. 30, pp. 2152-2157, 2009.
- [109]S. Z. Qamar, “Shape Complexity, Metal Flow, and Dead Metal Zone in Cold Extrusion,” *Materials and Manufacturing Processes*, vol. 25, no. 12, pp. 1454-1461, Dec. 2010.
- [110]H. Jafarzadeh and M. Zadshakoyan, “Numerical and Experimental Studies of Splines Produced by Injection Forging Process,” *Materials and Manufacturing Processes*, vol. 26, no. 5, pp. 703-712, May. 2011.
- [111] B. Basily and D. Sansome, “Some theoretical considerations for the direct drawing of section rod from round bar,” *International Journal of Mechanical Sciences*, vol. 18, no. 4, pp. 201-208, Apr. 1976.
- [112] B. Juneja and R. Prakash, “An analysis for drawing and extrusion of polygonal sections,” *International Journal of Machine Tool Design and Research*, vol. 15, no. 1, pp. 1-18, May. 1975.
- [113] V. Nagpal and T. Altan, “Analysis Of The Three-Dimensional Metal Flow In Extrusion Of Shapes With The Use Of Dual Stream Functions.,” *North Am Metalwork Res Conf, 3rd, Proc; Pittsburgh, PA, USA;*, vol. 5, 1975.
- [114] D. Yang and C. Lee, “Analysis of three-dimensional extrusion of sections through curved dies by conformal transformation,” *International Journal of Mechanical Sciences*, vol. 20, no. 9, pp. 541-552, 1978.
- [115] R. Hill, “Theoretical analysis of stresses and strains in extrusion and piercing ,” *J. Iron and Steel Institute*, vol. 158, pp. 177-185, 1948.
- [116] V. Nagpal, “On the three-dimensional metal-forming processes.”, *Trans ASME, Sec.99*, pp. 624-632, 1977.
- [117]D.Y. Yang and K. Lange, “Analysis of hydrofilm extrusion of three-dimensional shapes from round billets.”, *Int. J. Mech. Sci.*, vol. 26, pp. 1-19, 1979..
- [118] S. Kobayashi, S. I. Oh, and T. Altan, *Metal Forming and Finite Element Method*. Oxford University Press, 1989.

- [119] W. Johnson and P. B. Mellor, “*Engineering Plasticity English*,” Van-Nostrand Reinhold, London , 1973.
- [120] H. Kudo, “Some analytical and Experimental studies of axisymmetrical cold forging and extrusion- II.,” *International Journal of Mechanical Sciences*, vol. 3, no. 1-2, pp. 96-106, 1961.
- [121] J. L. Kluster and J. H. Mize, *Optimization Techniques with FORTRAN*, McGraw Hil. 1973.
- [122] W. Johnson, “Experiments In The Cold Extrusion of Rods of Non-Circular Section,” *Journal of Mechanics and Physics of Solids*, vol. 7, pp. 37-44, 1958.
- [123] S. Guruswamy, *Engineering Properties and Applications of Lead Alloys*, Dekker, 2000.

BIO-DATA

Name Mr. Laxmi Narayan Patra
Date of Birth June 07, 1969 (Berhampur, Orissa, India)
Nationality Indian
Designation Research Scholar (PhD Candidate)
National Institute of Technology Rourkela
Present Address C/o Dr. Susanta Kumar Sahoo
Department of Mechanical Engineering
National Institute of Technology Rourkela
Rourkela(Orissa) – 769 008, INDIA
Tel: +91(0)-9437204005,
E-mail: lnpatra@gmail.com

Academic qualifications:

- ❖ *Ph.D. – N.I.T, Rourkela, India.(Expected date of thesis submission: Mar-2012)*
- ❖ M. Tech. (MP&S) – K.I.I.T, Bhubaneswar (Odisha), India, 2006 (CPGA 8.71/10).
- ❖ B. E. (Mechanical Engineering) - Kuvempu University, (Karnataka), India, 1994(First class-65.15%).
- ❖ Diploma (Mechanical Engineering) – S.C.T.E.T, Odisha, India, 1989(Second division-53.33%).
- ❖ H.S.C – B.S.E, Odisha, India, 1984(First division-63%)

Fields of interest:

Manufacturing process, Non-Conventional processes, Metal cutting and Robotics

Membership of professional Organizations:

Member, The Institution of Engineers (India): Membership Grade and Number: M-139734-0

Industry experience:

- ❖ 2 years (as a maintenance engineer, Mudra foundry Pvt. Ltd.)

Teaching experience:

- ❖ 3 years 6 month at N.I.T. Rourkela (as Senior Research Fellow, DST Grant Project)
- ❖ 2 years at College of Engineering, Bhubaneswar, Odisha
- ❖ 10 years 5 month at Degree engineering college S.M.I.T Chandipader, Odisha.

List of publications

List of Publications in International Journals

- [1] S. K. Sahoo, B. Sahoo, **L. N. Patra**, U. C. Paltasingh, and P. R. Samantaray, "Three-dimensional analysis of round-to-angle section extrusion through straight converging die," *The International Journal of Advanced Manufacturing Technology*, vol. 49, pp. 505-512, Nov. 2009.
- [2] **L. N. Patra**, S. K. Sahoo, and K. P. Maity, "Plastic Flow of Metal through Flat Dies: A Three Dimensional Analysis," *International Journal of Mechanical and Materials Engineering*, vol. 1, no. 3, pp. 160-165, 2010.
- [3] **L. N. Patra**, S. K. Sahoo, and K. P. Maity, "Extrusion-forging of Round Shaft with 8-Tooth Spur Gear Head: A Three-Dimensional Analysis," *International Journal of Advances in Machining and Forming Operations*, vol. 3, no. 2, pp. 153-165, 2011.

List of Publications in International Conferences

- [1] L.N.Patra, S.K.Sahoo, B.Sahoo and K.P.Maity , Triangle-to-round section Extrusion through Flat dies: A three Dimensional Analysis, Proceedings of the International conference on Advances in Mechanical Engineering(ICAME-10), NIT , Surat, PP 448-452, January 4-6, 2010.
- [2] L.N.Patra, S.K.Sahoo and K.P.Maity , Plastic flow of metal through Flat dies: A three Dimensional Analysis, Proceedings of the National conference on Recent Advances in Fluid and Solid Mechanics (RAF&SM), NIT , Rourkela PP 199-203, February 27-28, 2010.
- [3] L.N.Patra, S.K.Sahoo and K.P.Maity, Extrusion-Forging of Circular Shaft with Hexagonal Head: A Three-dimensional Analysis, Proceedings of the 4th International Conference on Advances in Mechanical Engineering(4th ICAME), SVNIT September 23-25, 2010
- [4] L.N.Patra, S.K.Sahoo and K.P.Maity, Extrusion-forging of Round shaft with Square Head: A Three-dimensional Analysis, Proceedings of the 3rd International and 24th AIMTDR-2010, PP 411-415, December 13-14, 2010.
- [4] L.N.Patra, S.K.Sahoo and K.P.Maity, Extrusion-forging of Round shaft with Triangle Head: A Three-dimensional, Proceedings of the 2nd International

- Conference on Production and Industrial Engineering (CPIE-2010), NTI Jalandhar, PP 214-219, December 3-5, 2010.
- [5] L.N.Patra, S.K.Sahoo, B. C. Behera and K.P.Maity, Extrusion-forging of Circular shaft with Pentagonal Head: A Three-dimensional, Proceedings of the International Conference on Innovative Science And Engineering Technology-2011(ICIEST-2011), V.V.P. Engineering College, Rajkot, PP 37-42, April 8-9, 2011.
- [6] L.N.Patra, S.K.Sahoo and K.P.Maity, 3D Analysis for net shape gear production by combined extrusion-forging process, accepted for publication on Proceedings of the International conference on Computational Methods in Manufacturing (ICMM-2011), PP 23-30, IIT Guwahati, December 15-16, 2011.